# Shear Behaviour of Precast/Prestressed Hollow-Core Slabs

**by**

**MAHMUT SAMI CELAL**

A Thesis submitted to the Faculty of Graduate Studies of

The University of Manitoba

in partial fulfillment of the requirements of the degree of

MASTER OF SCIENCE

Department of Civil Engineering

University of Manitoba

Winnipeg, Manitoba, Canada

# ABSTRACT

Shear strength of precast/prestressed hollow-core (PHC) slabs subjected to concentrated or line loads, especially near supports, may be critical and usually is the governing criteria in the design. This study presents the second phase of a research program, undergoing at the University of Manitoba, to calibrate the shear equations in the Canadian code for predicting the shear capacity of PHC slabs. This phase includes both experimental and numerical investigations using a finite element analysis (FEA) software package. The length of bearing, void shape and size, level of prestressing and shear span-to-depth ratio were investigated. The experimental results were compared to the predictions of the Canadian, American and European codes. It was concluded that the Canadian code is unduly conservative. However, the special European code for PHC slabs resulted in better and more consistent predictions. The FEA suggested that the adequate prestressing reinforcement ratio to obtain highest shear capacity ranges between 0.7% and 1.1%.

# ACKNOWLEDGEMENT

I would like to express my deepest and sincere gratitude to my supervisor Dr. Ehab El-Salakawy Ph.D., P.Eng., Professor and Canada Research Chair in Durability and Modernization of Civil Structures in the Department of Civil Engineering at the University of Manitoba, for his guidance, continuous encouragement and unlimited support throughout the course of this research program. The assistance of Dr. Amr El-Ragaby, Ph.D., P.Eng. in the laboratory work is also greatly appreciated.

I would like to express my gratitude and sincere appreciation for the financial support received from the Canadian Precast/Prestressed Concrete Institute (CPCI), the hollow-core slab producers and the hollow-core extruder suppliers who contributed towards this research project, the Natural Science and Engineering Research Council of Canada (NSERC), through Canada Research Chairs program. The equipment funds received from Canada Foundation for Innovation (CFI) is greatly appreciated. The help received from the technical staff of the McQuade Heavy Structural Laboratory in the Department of Civil Engineering at the University of Manitoba is also acknowledged.

I would like to thank my colleagues, Karl Truderung, P.Eng. M.Sc., Dr. Mostafa El-Mogy, Ph.D. and Dr. Mohamed Mady, Ph.D. for their mentoring, support and encouragement.

Finally, I would like to express my deepest gratitude to my parents and my uncle, Mr. Abdullah Özmen, for their invaluable support throughout my academic career.

*M. Sami Celal*

# TABLE OF CONTENTS

# LIST OF TABLES

# LIST OF FIGURES

# CHAPTER 1: INTRODUCTION

## 1.1. General

The design of a floor or a roof system is a common structural engineering challenge. The ideal design should deliver optimum combination of safety, serviceability and economy. This could be achieved by a structural system that minimizes the overall thickness, maximizes the span, safely resists ultimate loads and restricts service-load deflections to allowable limits. Combining the beneficial effects of prestressing together with a structurally efficient cross-section, precast hollow-core (HC) slabs are considered one of the best structural systems capable of covering large spans with minimal overall thickness and weight. Moreover, the ease of manufacturing and installation provides a significant time-saving advantage over most traditional structural systems.

In 1962, the extrusion technology was introduced in Winnipeg for the first time in Canada to produce prestressed hollow-core (PHC) slabs. Since then, the use of PHC slabs has spread all over Canada, current consumption rate reached 1.4 million square meters in 2003 (*fib* 2003; CPCI 2007). In Europe, estimations are more than 25 million square meters per year (Elliott 2000). This excessive use of PHC slabs is mostly accountable for their cost efficiency and excellent structural performance.

It is well known that an I-shaped reinforced concrete cross-section is more efficient than a rectangular cross-section with the same area, since the material layers close to the neutral axis are not as effective as those near the section boundaries in resisting flexural stresses. A PHC slab cross-section typically has 40% to 50% less concrete material than a solid rectangular cross-section. This reduction in self-weight results in a proportional reduction in the required size of supporting beams and columns. This means lighter superstructure and consequently less dead load is transferred to soil and more economical foundation system could be designed given the

fact that foundation usually is one of the most expensive parts of any structure. In addition, the continuous voids in HC slabs improve sound isolation between floors and could be utilized to house mechanical and electrical lines and in some cases air conditioning.

Comparing the amount of reinforcing steel used in a PHC slab with an equivalent typical solid slab, it can be seen that HC slabs have approximately 30% less reinforcement due to the high strength of the used prestressing strands. Moreover, prestressing has a significant effect on reducing deflections which increase the efficiency of the cross-section in terms of spanning capability. For instance, a PHC slab with 300-mm thickness could span up to 15 meters (according to CPCI manual) without violating serviceability limits of codes. The reduced slab thickness increases the clear height per story which enables designers to maximize the effective use of permitted municipal regulations for height of structures. Another advantage of PHC slabs is their superior long lasting durability compared to traditional steel-reinforced structures. A fully prestressed concrete element is designed to be un-cracked under service loads, which provides better protection to the prestressing reinforcement. Ideally, if moisture has no access to the strands, corrosion is not an alarming problem in PHC slabs.

On the economical side, the use of PHC slabs can also be cost efficient in the construction process. Casting concrete on site, scaffolding and formworks are usually expensive and time consuming tasks. Hollow-core slab floors, however, are easier to install, since very limited number of workers is required to lift the prefabricated units and place them over the supports. Furthermore, the floor becomes a safe platform for sub-contractors like electricians and plumbers to commence work right after erection without any delay. In addition, weather conditions have no significant impact on the construction process since HC slabs are already cured in the manufacturing plant.

The main concern for PHC slabs is their relatively low shear resistance. Hollow-core slabs under ideal conditions are usually designed to resist flexural stresses (moments) due to assumed uniformly distributed loads. However, these slabs could be subjected also to concentrated vertical loads which lead to shear failures. Floor slabs in buildings like parking garages and warehouses are the most expected to experience these types of loads, for instance, due to vehicle wheel loads. In residential and office buildings, uniform loads are predominant in most cases except for special cases such as a masonry partition wall supported directly on the slab. In such cases, the shear resistance of slabs is usually critical and accurate shear capacity evaluation becomes very important to arrive at a safe design.

## 1.2. Problem Definition

Despite the widespread usage of PHC slabs in construction, their shear capacity has not been well addressed in the Canadian code CSA-A23.3-04 (CSA 2004). The code has a general design approach used for shear design of all types of elements. In that approach, the procedure for evaluation of concrete shear resistance ($V_c$) is based on the modified compression field theory (MCFT) developed by Vecchio and Collins (1986). The theory is known to be a successful model in predicting shear resistance of diagonally cracked reinforced concrete elements subjected to in-plane shear and normal stresses. Hence, this model deals with shear resistance of already-cracked concrete elements assuming that significant amount of shear resistance is developed after cracking.

The design model of the current CSA code does not take into consideration the significant effect of variation of prestressing forces on shear strength in the transfer zone, unlike the model

proposed in the DIN EN-1168 code (Deutsche Norm 2008). Also the existing CSA model has no methodology to classify the expected mode of shear failure.

In practice, shear behaviour of PHC slabs is different from that of concrete slabs with shear reinforcement. Prestressed HC slabs hardly show any post-cracking resistance after diagonal shear cracks occur within the transfer zone. This is mainly due to the lack of shear (transverse) reinforcement, which usually controls the width of diagonal cracks once initiated and contributes to the ultimate shear strength.

The main differences in shear behaviour between PHC slabs and solid concrete counterparts could be identified based on the four main components of concrete shear resistance, namely, un-cracked concrete in compression, aggregate interlock, dowel action of longitudinal reinforcement and tensile resistance of concrete. Since PHC slabs are usually made of high strength concrete, the crack surface is known to be smooth which reduces aggregate interlock. Also, due to the small support length in PHC slabs structural systems, the anchorage length of prestressed strands is reduced. This increases the probability that strands within the transfer zone experience slippage at high stresses, which would contribute to wider cracks. Another important peculiar shear behaviour exhibited in PCH slabs is the fact that flexural cracks in prestressed elements usually extend from bottom face deeper into the depth making the height of the uncracked region very small. This is the reason why the flexural shear failure after cracking of prestressed element is sooner than those of their non-prestressed counterparts (less ductile failure).

The most critical section of PHC slabs in shear resistance is located in a zone called “transfer zone”. This zone is considered the weakest due to the following reasons:

- Compression normal stresses due to bending moments increase shear resistance, however, because the transfer zone is very close to the support, the bending moment is negligible and pure shear will be governing the design;

- The gradual transfer of prestressing force from the strand to the concrete in this zone generates gradient moment. This moment is going to cause additional internal shear forces that reduce the capacity of sections in the transfer zone. This will be discussed in the following sections in more details.

In cases where shear stresses in PHC slabs are found to be critical based on current code provisions, the prevalent practice is to fill the cores in zones of the floors where vertical shear stresses are expected with fresh concrete. Also, the shear critical zones of the slabs can be strengthened in the field with longitudinal reinforcement using near-surface mounting technique. In fact, all those techniques are penalizing the efficiency characteristics of PHC slabs that were addressed earlier especially those related to mass production and fast construction rate. In addition, lack of confidence in current design methodologies of codes makes manufacturers of PHC slabs increase safety factors or recommend the use of prevalent in-site shear resistance enhancement techniques to avoid brittle shear failure.

This research project is directed to investigate the shear strength of PHC slabs at end zones. It worth mentioning that all design tables and charts provided by PHC slab producers are made for uniformly-distributed loads and not counting for concentrated loads. This indicates lack of information and need for research when concentrated and line loads are involved.

## 1.3. Scope of Work

This project is part of a research program conducted at the University of Manitoba to investigate the shear resistance of PHC slabs at ultimate limit state. The scope of this phase of the research program is to test a series of full-scale PHC slabs with one level of prestressing under concentrated line load to cause shear failure and compare the experimental results with the predicted capacities based on provisions of the current international standards including Canadian, American and European design codes (CSA 2004, ACI 2008, Deutsche Norm 2005). Parameters considered in the experimental stage of this phase include the thickness of slabs, geometry of voids, and length of bearing. The experimental results of the tested slabs was utilized in constructing a verified finite element model (FEM) to simulate the behaviour of PHC slabs. The FEM was used in performing further investigations to better understand the behaviour of PHC slabs at the critical transfer zone.

## 1.4. Research Objectives

Despite its complexity, the main objective of this study is to evaluate the response of PHC slabs under concentrated shearing loads in order to make the design provisions in the codes more representative to actual behaviour. The specific objectives of this work are to:

1. Evaluate the accuracy of the most commonly used design codes (CSA 2004, ACI 2008, Euro Code 2008) when predicting shear capacity of PHC slabs based on tests carried out in this study;

2. Analyze load-strain response at selected specific critical points on the specimens during experiments to establish platform for FEM models verification;

3. Simulate the actual tested slabs using ANSYS (nonlinear finite element modelling software package) to better understand the behaviour at the transfer length zone and to run a parametric study;

4. Verify the effect of support bearing length on the shear capacity of PHC slabs;

5. Verify the effect of non-circular void shapes on the shear capacity of PHC slabs.

## 1.5. Methodology

A total of twelve full-scale PHC slabs are tested using the standard test method suggested by the European Product Standard EN-1168 (EN-1168 2008). The method is typically used by designers and producers as a quality-assurance check for hollow-core slabs.

Limited research performed on PHC slabs investigated the effect of the length of bearing at the support on their shear capacity. In practice, PHC slabs are, in some cases, erected with less than the specified bearing length at the support due to accumulation of construction and production tolerances. One of the goals of this research is to verify experimentally the effect of reducing the bearing length over supports on either the shear capacity or the mode of failure of PHC slabs.

Furthermore, a finite element model is constructed using ANSYS software, release 13 (ANSYS, 2010). The model is verified against the obtained experimental results and then used in a parametric study to expand the range of investigated parameters in this research. The conducted parametric study investigates the effect of three variables: level of prestressing and shear span-to-depth ratio.

## 1.6. Thesis Organization

This thesis consists of eight chapters. The contents of each chapter are as follows:

- Chapter one presents a brief introduction on PHC slabs, as well as the problem definition, scope of work and research objectives and the followed methodology.
- Chapter two provides a literature review on the effect of a list of factors on shear capacity of PHC slabs. Also, some important terminologies related to shear in PHC slabs were explained.
- Chapter three outlines the relevant code provisions for evaluating shear capacity of PHC slabs in Canadian, American and European concrete design codes (CSA A23.3-04, ACI 318-08, EC2 2004, EN 1992-1-1-05, and EN 1168-08). In addition, transfer length estimation provisions in different codes were compared and their expressions were summarised.
- Chapter four provides details of the experimental testing program; variable parameters considered, test specimens' geometric and structural properties, material properties, test set-up details, loading procedure and instrumentation.
- Chapter five provides analysis and discussion of experimental test results in terms of observed shear capacity, mode of failure and cracking profiles, and interpretation of the instrumentation outputs. Also, the shear capacity of tested specimens were predicted using spread sheets, which are programmed according to provisions of the three codes CSA A23.3-04, ACI 318-08 and EN 1992-1-1-05), were presented and compared with experimental results.
- Chapter six provides details of the FEM modeling including constitutive models used in simulation of different element, geometry and boundary conditions, and failure criterion

used to control solution. In addition, a specific section discusses the verification process for the developed model against selected experimental results.

- Chapter seven presents results of parametric study conducted on FEM models in terms of influence of those parameters on shear capacity and their behaviour.
- Chapter eight presents conclusions derived from this research project and recommendations for future research.

.

# CHAPTER 2: LITERATURE REVIEW

## 2.1. General

Wide range of experimental research programs on PHC slabs have been conducted in several countries. In such experiments, specimens were tested under concentrated line loads until failure, and then failure loads were compared to the shear resistance predicted by national and international building or structural design codes. In some cases, the failure loads were less than code predictions, while in other cases they were several times higher. Such conclusions make PHC unit suppliers and designers worry about reliability on the codes and the level of safety required to avoid unpredicted failures.

For example, very recently in North America, Palmer and Schultz (2010) found that tested specimens from one supplier failed at 61% of the shear capacity predicted by ACI 318-05 (had same shear design expressions as current ACI 318-08) while other specimens from a second supplier failed at 91% of the capacity predicted by the same code. They questioned whether the problem with the code predictions is a result of misestimating the transfer length, effect of geometric factors, or tensile strength of the webs. Hawkins and Ghosh (2006) targeted shear capacity of PHC slabs thicker than 300 mm and also found that ACI 318-05 code equations for web-shear were un-conservative. They thought that, most probably, the under prediction is due to the fact that the code model assumes a certain fixed position for critical section while it appeared from test results that geometry of the specimen has an influence on location of critical section for web shear. They suggested that other factors could have effect and need to be identified. On the contrary, Cheng & Wang (2010) reported that the same ACI 318-05 code predicted the shear capacity of the tested 200-mm PHC slabs conservatively by 16.9% less than the experimental

capacity. The underestimation was blamed for negligence of the potential effect of interaction between adjacent webs on the shear capacity.

Also in Europe, Pajari (2005) found that the web-shear design model in EN 1992-1-1-05 code overestimates (unsafe) the shear capacity of majority of PHC slabs especially those with flat webs by approximately 10%; another indication for effect of geometry on shear capacity.

As revealed from those mentioned examples, there is a set of factors or parameters pointed out by researcher to be the source of the problem in shear capacity predictions by codes. Consequently, it would be a good asset to review in this chapter the findings of previous research on the effect of different factors on shear resistance of PHC slabs.

## 2.2. Fundamental Concepts

Prior to getting into discussion of factors affecting shear capacity of PHC slabs, it is essential to understand definition of certain terminology that are used very frequently in the area of subject matter. For instance, there are two main types of shear failure that could be observed in PHC slabs. Definition of each mode of failure in terms of mechanism and appearance is provided in the following sections.

### 2.2.1. Web shear failure

It is failure due to diagonal cracking in the web at a specific point located between the top and bottom flanges of the section. When resultant principle stresses from shear and bending exceeds the tensile strength of concrete, a crack generates at the so-called "critical point" (Yang 1994, Pajari 2009). However, almost instantaneously and without any warning that small principle tensile crack propagates upwards and downwards in a straight inclined form joining the edge of the support with top of the slab and eventually leads to total collapse. The direction of the crack

line forms a 90 degree with the direction of principle tensile stress. Web-shear failure is also called "shear-tension" failure or "un-cracked shear" failure by some researchers and codes. Furthermore, this type of shear failure is mostly expected in members with high flexural resistance capacity like heavily prestressed deep beams, especially when the applied load is concentrated close to the supports.

### 2.2.2. Flexural-shear failure

In slender and lightly prestressed members, when flexural stresses exceed tensile strength of concrete, vertical tensile cracks initiate at the bottom face of slabs. The crack propagates through the cover till it hits the reinforcement. As loading continues to increase, the crack not only widens but also continues to propagate vertically beyond the level of reinforcement (strands) till approximately mid height of the member. With further loading, intensity of shear stress on the remaining un-cracked portion of slab's depth becomes high then crack line tends to take inclined form till reaches the top surface of the slab. As reveals, this is a progressive and ductile failure which makes it more favourable shear failure mode. On the other hand, in case the originally initiated flexural crack in the cover was too close to the end of the slab, limitation of anchorage length could lead to slippage of strands which would be distinguished by extension of a crack line horizontally at the level of strands towards the support, and at the same time inclined cracks propagate upwards from the same point. Other expression used by some researchers and codes to describe flexural-failure is "shear-compression" failure or "cracked shear" failure. According to CTE-73-B4 (1973), flexural-shear commonly occurs in prestressed members under uniform load more than those subjected to concentrated loads.

### 2.2.3. Critical point

It is an expression for the identifiable position of maximum principle tensile stresses on webs of PHC slabs, where theoretically web-shear failure line is expected to explode/initiate. It is important to stress here that critical point is not identified by maximum shear stress point of the cross-section which is usually at level of minimum web thickness, but it is identified by the maximum principle stressed points. Provisions of each code for identification of position or coordinates of critical point could be different. Therefore, those ones for the relevant codes in this research project are discussed in Chapter 3.

## 2.3. Factors Affecting Shear Capacity of Prestressed Hollow Core Slabs

Palmer and Schultz (2010) stated that there are six parameters that may affect web-shear capacity of PHC slabs. However, in a report published by Concrete Technology Associates (Anderson 1976), seven factors were pointed out to influence shear strength of concrete beams in general (prestressed or non-prestressed). Some of the common factors among those two literatures like axial load due to prestressing, shear span-to-depth ratio and different geometric factors, in addition to uncommon ones like transfer length, concrete strength and length of bearing have been in the selected list for review in the following sections. This will help in identifying gaps in the area of research and to build on findings of previous work.

### 2.3.1. Axial stress due to prestressing

The main benefit of prestressing is to delay formation of cracks in concrete In another words, enhancement of tensile resistance of concrete.

#### *2.3.1.1. Effect of variation in prestressing along transfer length*

From structural mechanics, it is known that shear force is the first derivative of moment with respect to the beam length. In other words, a constant bending moment along length of a beam member is an indication of no shear. However, if moment was variable for any reason, it is going to generate shear on the beam. Consequently, as the value of axial force applied by tendons in PHC slabs is different from section to section along the transfer length of strands that means the moment caused by eccentricity of those strands would be variable as well. This was the distinct point in the web-shear capacity expression developed by Yang in 1994, which has taken into account that reducing effect of vertical shear due to prestressing force gradient within the transfer length. He also confirmed the validity of this claimed behaviour by comparing the predictions of the expression with 3D-finite element model (FEM) analysis. In addition, he compared his predictions to 118 test results on slab units collected from 10 different manufacturers and tested at the Technical Research Centre of Finland (VTT) during the period from 1978 to 1987. From such a wide covering investigation, strong evidence was found that PHC slabs suffer from an additional shear forces due to gradation of prestressing at the end zones which causes a reduction of the web-shear capacity of PHC slabs. Considering the negative effect of prestressing gradient by the developed model made calculations of web-shear capacity in better agreement with test results than those made by the traditional method of codes. Pajari (2009 & 2005) also concluded that ignoring this behaviour is a major source of overestimation in ACI 318-05 and Euro-code (EC2 2005) equations that share the same concept of shear design.

Pajari (2009) derived different versions of Yang's formula in an effort to support the success of Yang's expression for web-shear prediction and to include it into the European code. One elaborated version was suitable to account for tendon force gradient effect in slabs with multiple

layer of strands (either more than one tendon in the bottom or if tendons were used in the upper compression flange of PHC slabs). Also, he derived another simplified version of the expression, in case approximation was preferred, by considering the bottom tendons as one layer and assuming a linear shape of prestressing transfer curve.

#### *2.3.1.2. Effect of variation in stress over the cross-section width and height*

This is called "shear lag". It occurs throughout the depth and across the width if the section was not perfectly rigid or when the pre-compression in all webs is not uniform, for example, due to variation in number of strands in some webs. Shear lag could make the shear capacity of individual webs in the same cross-section different from neighbouring webs. Unfortunately, most shear capacity expressions in codes like ACI 318-08 do not account for the shear lag factor which may result in over predictions (Palmer and Schultz 2010).

#### *2.3.1.3. Effect of level of prestressing*

According to traditional expressions used for evaluating the web-shear capacity of prestressed members in Europe and North America, the higher the prestressing level in the concrete, the higher the capacity against shear failure of the web should be. However, this rule does not seem well applying within the transfer zone because the strands are not considered fully anchored close to ends. Yang (1994) performed a 3D-FEM study on I-shaped simply-supported PHC slab strips and found that increasing level of prestressing does not always increase shear capacity as fundamentally assumed by traditional methods. His results (Figure 2.1) indicate that, with non-circular voided slabs, increasing prestressing over a certain level lowered the capacity. There is interference with void shape, so this would be discussed also again in effect of void shapes.

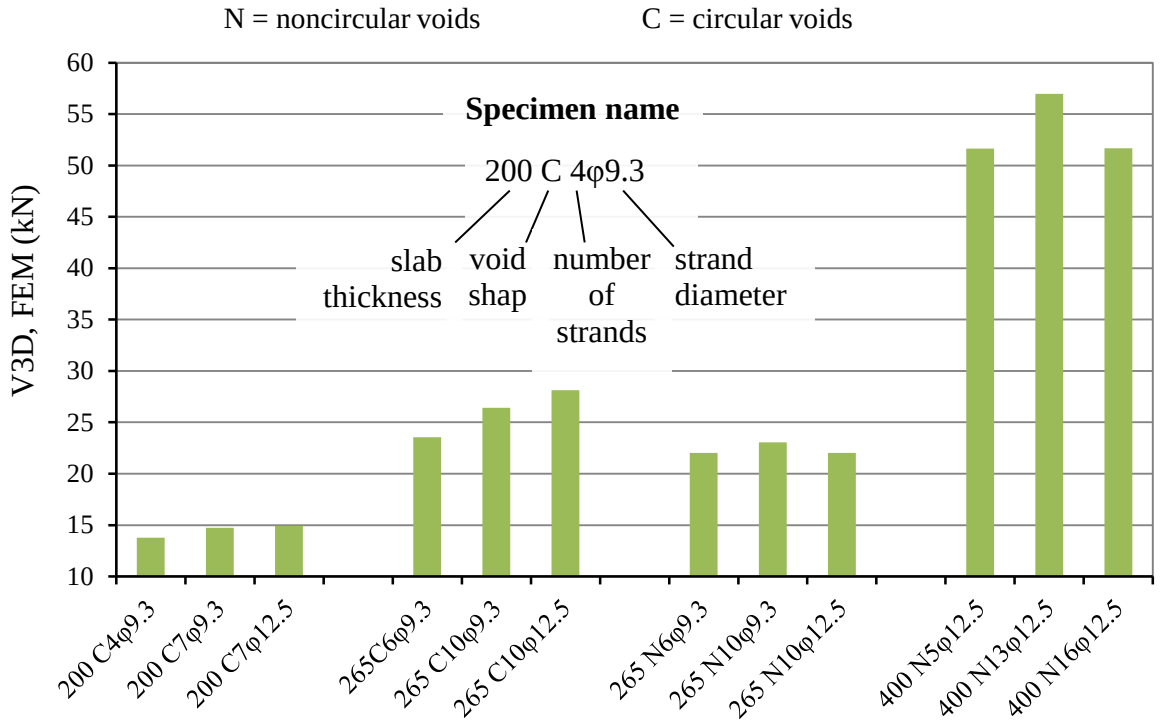


Figure (2.1): Effect of level of prestressing on shear capacity of simulated PHC slabs (reproduced from Table 2 of Yang (1994))

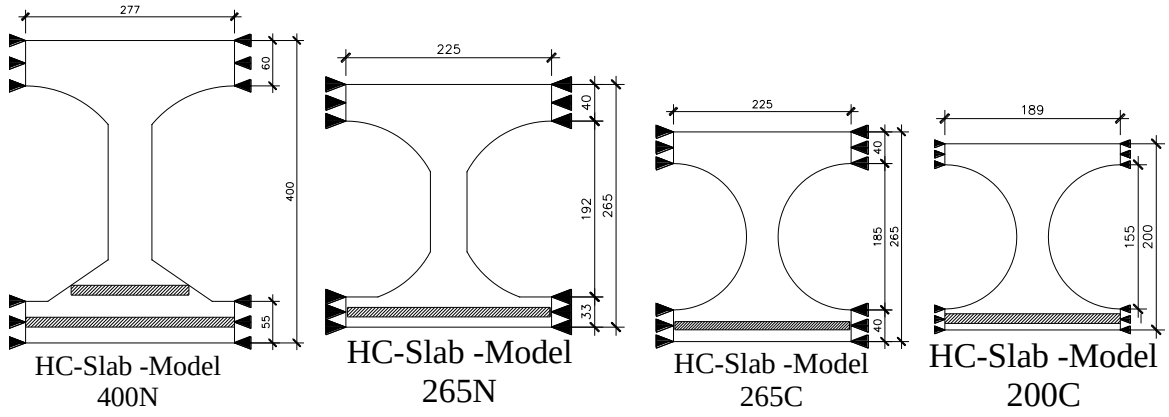


Figure (2.2): Cross-section details of FEM model (reproduced from Yang (1994))

Also, according to results of an experimental study by Becker & Buettner (1985) on 8 in. (203 mm) and 10 in. (254 mm) slabs, increasing the amount of strands (as percentage of the cross section) in the 8-in. slabs from 0.3 to 0.7% and in the 10-in. slabs from 0.27 to 0.6% under same shear span of loading had increased ultimate shear capacity. However, at the same time, the

observed mode of failure changed to a less favourable mode (from flexural-shear to a web-shear). Pisanty (1992) found similar conclusion from results on 300-mm thick slabs. The failure mode was found to be web-shear in middle portions PHC slab units with high prestressing level. However, specimens taken from edge portions of full PHC units with lower prestressing failed in flexural-shear mode.

Walraven and Mercx (1983) tested a series of 200-mm thick slabs. Despite the fact that level of prestressing was increased in the specimen with 11 strands compared to a specimen with 9 strands, both ultimately failed in flexure. That means no effect for level of prestressing observed in those tested 200-mm thick slabs.

In the work conducted by Truderung (2011), the level of prestressing appeared to have a much larger influence on the shear capacity predictions obtained by Canadian code (CSA 2004) compared to the American code (ACI 2008) predictions. In terms of his observed experimental failure loads, increasing the amount of prestressing by a factor of approximately 4 (from slabs 200-01A and 200-01B to slabs 200-20A and 200-20B) increased the failure loads by approximately 12% for slabs with 63-mm of bearing and by about 22% for slabs with 38-mm of bearing.

### 2.3.2. Transfer length

The transfer length is defined as the distance from the end of a pretensioned member to the point where the force in the prestressing strands is fully transferred to the concrete through bond. It is always smaller than the development length. Accurate estimation of the transfer length and transfer-stress distribution of the strands is crucial for the magnitude of the effective prestressing force at the critical point.

Variables that could affect the transfer length are summarised by Palmer and Schultz (2010) as concrete compaction degree, size of strands, spacing, concrete strength, method used in releasing initial prestressing force and type (or surface condition) of the strands.

Applicability of code provisions for transfer length has been questioned because they are mostly based on research outputs performed on precast prestressed concrete girders or small rectangular sections. Even though it is very limited but worth to mention that, up to the author's knowledge, Walraven and Mercx (1983) is the only published work which performed an experiment on a PHC slab unit to evaluate the transfer length. The 6-m long PHC unit was saw-cut along its width into two pieces and strains in concrete were measured before and after cutting at reference points distributed over 1.0 m from each side of the cut. The results showed that because of transfer length effect, the prestressing strains in concrete at each end showed gradual elongation up to 450-550 mm from the cut line and stabilized for the rest of the length of each piece. That indicates that the transfer length for that specific slab, which comprised of 6-No.13-mm strands, was experimentally evaluated and found to range from 35φ to 43φ (450/12.7 to 550/12.7), where φ is diameter of strands. This outcome implied that 50φ provisions of ACI code is conservative and could be safe to apply on PHC units. Moreover, profiles of strain distribution along distance from cut ends suggest that shape of the transfer length curves were almost linear.

Experimental studies to investigate shape of prestress transfer curve in PHC slabs found scarce and most commonly researchers have assumed linear relationship for the transfer of prestressing force while estimating the shear capacity. However, researchers, such as Yang (1994), did not investigate the effect of shape of prestress transfer curve but just adopted a parabolic curve from other literature with its zero point at 5φ from the end point of slabs to account for slippage after cutting. Therefore, the transfer length in his analysis was 55φ. However, he recommended future

researchers to investigate the shape of the transfer curve, for which it could have significant effect on shear capacity predictions. Pisanty (1992) also thinks that it is most appropriate to assume parabolic distribution for the shape of prestress transfer curve in the transfer zone with a reduction factor due to the possible slip after transfer.

### 2.3.3. Geometry of cross section

#### *2.3.3.1. Effect of depth or thickness of slabs on shear capacity*

Popularity of very thick, more than 400 mm, PHC slabs are increasing in North America due to their efficiency in covering long spans. Very possible, that increasing thickness of slabs more than certain size would have negative effect on shear capacity. That is why ACI 318-08 in Clause 11.4.6.1(b) requires providing shear reinforcement in slabs if their depth exceeds 315 mm to prevent failure of thick slabs at ultimate load levels less than expected.

Palmer and Schultz (2010) analysed experimental test data performed on two manufacturers to investigate effect of slab thickness on web-shear capacity. Total number of PHC slabs tests included in this study was 198 with range of thickness ($h$) from 8 in. (203 mm) to 20 in. (508 mm). There were few other variables stated between these large number of specimens such as void shape, concrete strength and prestressing level. Unfortunately, despite an effort was made to separate interference of those variables on the data by categorising, it was not possible to identify a clear evidence of trend for effect of thickness on shear capacity due to large scatter of the web-shear strength data.

Furthermore, Hawkins and Ghosh (2006) analysed the experimental results conducted by three different PHC manufacturers with thickness ranged from 12.5 in. (305 mm) to 16 in. (400 mm). Average test results of the slabs with depth greater than 12.5 in. (305 mm) showed failure

capacities smaller than expected using provisions of ACI 318-05 (unsafe), which raised concerns on capacity of thick slabs. But instead of suggesting unpractical solution, such as addition of shear reinforcement, the authors recommended carrying out further experimental investigation on slabs with sizes deeper than 300 mm with objective of finding an appropriate reduction factor to apply on equations of the code in incidences where thick slabs are used.

Moreover, the thickness of slab seems to govern the mode of failure because most of researches carried out on 200-mm thick PHC slabs indicated that their tendency to fail more in flexural-shear mode while thick slabs (300 mm and more) tend to fail in web-shear mode (Truderung 2011, Cheng and Wang 2010, Walraven & Mercx 1983, Catoia 2011).

#### *2.3.3.2. Effect of size of webs or flanges on shear capacity*

Some suppliers tend to produce PHC units with the two exterior webs thicker than the interior. Well, that could be a source of shear lag since stiffness of webs would be variable relatively to each other in the same slab unit

Palmer & Schultz (2010) stated that even though the traditional method assumes that shear stress is always uniformly distributed on the webs, theoretically the distribution of shear stress across the section of a slab could be dependent on stiffness of the individual webs that make up the slab unit.

As it is well known, there are two types of stiffness: flexural stiffness and axial stiffness. If the load share of individual webs in the section is based on axial stiffness, this means the area of the web should be governing, consequently, thicker webs would be prone to higher shear force than their thinner adjacent counterparts. On the other hand, if distribution of shear was based on flexural stiffness, then inertia of flange, and not the web, will be more governing (Jonnson 1988).

In such a case, webs with large flange width, like interior webs, are expected to be subject to higher shear force than exterior ones. It is important to remind here that uneven distribution of shear force on webs could cause concentration and early failure of those highly stressed webs, which eventually causes reduction of total effective shear resistance of the whole unit. To author's opinion, one symptom for occurrence of uneven shear distribution in experiments could be skewed profile of web shear failure line.

#### *2.3.3.3. Effect of webs interaction on shear capacity*

The traditional shear prediction methods provided by codes treat the unit of PHC slab as an assembly of single web I-beam strips. It is questionable if that assumption is reasonable to be made. Cheng and Wang (2010) compared the resistance of an I-beam portion with resistance of full cross-section of PHC slabs which all had circular shape of voids. They concluded that the conservatism of ACI 318-05 (ACI 2005) code was more noticeable with full slab sections than the single-web concrete I-beams. This is due to the fact that ACI 318-05 (ACI 2005) ignores the interaction between the adjacent webs and their contribution to the shear capacity. However, it is worth to mention that among the tested 4 beams and 4 slab specimens, only one beam specimen was reported to fail due to web-shear. Since no web-shear failure was observed in any of the tested PHC slab specimens, conclusions from this study would be valid for effect of webs interaction on flexural-shear only and would not reflect the effect on the other more significant web-shear failure mode. Actually, that is because only one size of HC slabs unit was considered in this research, 203 mm.

Anderson (1976) investigated reasons, especially geometric factors, and ways to make the ACI 318-71 shear equations efficient because those were found conservatively predicting the capacity of prestressed beams. The main focus in his experimental program was on the effect of width of

flange on shear capacity of the beams, which was not accounted for by the code equations. Experiments were carried on full-scale half double-tee prestressed beams without web reinforcement which were 12.8-m length and subjected to two-point loading at 4.9-m shear span. It was concluded that conservatism in predicted flexural-shear by ACI 318-71 did increase in beams with small width of flange (actual capacity of the beams was higher when width of flange was smaller). Since the author classified PHC slabs as decked bulb-tee beams, which usually have wide thick flanges, it was possible to imply that flexural-shear capacity of PHC slabs could similarly increase if smaller length of flanges were made. That may be accomplished by producing the slab units with more voids instead of few with large diameters. This is quite obvious because for flexural shear the most effective factor is the area of compressed zone which comes above the neutral axis (N.A) that means area of flanges and part of the webs if N.A located in the web. However, if the flange was wide not all the width of flanges will function in shear resistance.

#### *2.3.3.4. Effect of void shape on shear capacity*

The research work performed by Yang (1994) demonstrated that the geometric shape of voids made in the cross-sections can have an impact on the web-shear capacity of HC slab units. Since the void shape affects the location of the maximum principal tensile stress in the slabs, which is the main player in positioning the critical point. Yang (1994), in his 3D-FEM, studied the principle tensile stress results on concrete elements of the I-shaped PHC slabs units that he simulated. Based on that model, he was able to identify a concrete element on the web that reached a stress level equals to tensile strength of concrete. By considering location of that element as the position for the expected critical point, he concluded that position of critical points for non-circular voided slabs was closer to the support at shear loaded end than it is with

similar thickness size but circular voided slabs. The problem is that closer to the end of PHC units, transferred effective prestress force in the strands would be very small which leads to failure at lower shear loads. That implies that probably capacity of slabs with non-circular voids could be more critical than circular ones.

Pajari (2005) has selected 49 shear test results from hundreds of experiments performed at the Technical Research Centre of Finland (VTT) on extruded HC slabs. All of the selected slabs have failed in web-shear when tested in a simply-supported set-up and loaded with a line load. One of the four main variables among the groups of selected specimens was the void shape. There were slabs with circular voids in addition to four different patterns of non-circular void shapes. The objective of the study was to evaluate the European code (EN 1992-1-1-05) and the expression developed by Yang (1994). One of the conclusions was that the code overestimates (unsafe prediction) the majority of slabs especially those with non-circular voids. As a result, he recommended that the uncracked shear design method of EN 1992-1-1-05 should never be used for HC slabs with non-circular webs without a reduction factor, and even though its performance was satisfactory with circular voided slabs, care recommended to be taken.

### 2.3.4. Concrete strength

Precast industry would always look for better efficiency of used materials. High strength concrete is one of the utilized means to realize this improvement. Moreover, high tensile strength is crucial for shear resistance of members without shear reinforcement especially in web-shear resistance where interface shear transfer of concrete is not considered significantly contributing. Yet, at very high strength ($f'c$ > 70 MPa), crack interface could get very smooth that could cause degradation in ductility of flexural-shear failures as it counts for crack interface resistance.

#### *2.3.4.1. Relation of concrete shear strength with $f_c$'*

Pure shear strength of concrete is about half of its compressive strength ($f_c'/2$) (Anderson 1987). However, that high shear resistance value of concrete is not accessible when it is subjected to biaxial state of stresses as in webs of PHC slabs (principle tension combined with transversal principle compression).

Concrete shear resistance in non-prestressed members was given as $V_c = 0.17\lambda\sqrt{f_c'}b_w d$ in ACI 318-08. This empirical relationship suggests that concrete contribution to shear strength should be proportional to depth ($d$) and concrete compressive strength ( $f_c'$). However, Section 1.2.4 of the NCHRP report 549 (Hawkins et al. 2005) investigated the performance of this empirical relationship for evaluation of concrete contribution alone in shear resistance of beams. This was done by performing a comparison with experimental results of two research works; Moody et al. (1954) in US and Angelkos et al. (2001) in Canada. The selected data for comparison were related to the rectangular non-prestressed beams without stirrups and the variables identified between those two researches was size of aggregates used in casting (first one used large aggregate and the second used smaller size aggregates) and depth of beams. The effect of $f_c'$ on shear strength results for both groups plotted against the empirical values of the code. It was observed that results of the beams from the first research, which were 12 in. deep and cast with large aggregates showed that code's empirical relation was safe. However, the results of 2$^{nd}$ research, where beams were 36 in.-deep and used smaller aggregates size, were extremely unsafe. This indicated that size of aggregate is also needed to be considered in the relationship of shear resistance for concrete.

#### *2.3.4.2. Relation of concrete tensile strength with $f_c$'*

There are different types of tensile strength that could be attributed to concrete depending on condition of applied loading. Here are all those types in descending order:

Axial tensile strength, splitting tensile strength ($f_{st}$), flexural tensile strength ($f_{ct}$), and principle tensile strength which is the most interesting one in web-shear resistance.

Theoretically, principle tensile stress is considered the criterion for web-shear failure of PHC slabs. However, there is no direct standard method to measure it such as those for splitting and flexural strengths.

Pisanty (1992) reported that a research conducted on prismatic specimens extracted from webs of PHC slabs showed that flexural strength of web concrete is variable between 8 and 9.5% of $f_c$'. That is also in agreement with recommendation of most codes ($f_{ct}$ = 8 to 10% of $f_c$').

Palmer and Schultz (2010) stated that the potential reason for disparity of shear strength results between the two suppliers (A and B) he studied could have resulted from improper estimation of tensile strength for specimens by each manufacturer. Especially, supplier A for which the researcher assumed a specified constant compressive strength for all tested specimens. While, for supplier B, the reported concrete strength was based on testing 2 cylinders from each unit. They suggested an experimental study to be conducted in future to investigate the impact of concrete tensile strength in the webs on shear strength and also on transfer length. Pisanty (1992) also accepted that concrete strength in extruded HC slabs, especially with thin webs, could be variable from top to bottom. But, that is, unfortunately, inevitably results from casting technique, which also makes representation of actual tensile strength for webs by empirical equations quite a challenge.

### 2.3.5. Shear span to depth ratio

Selection of the right shear span length in the test set-up for evaluation of minimum shear capacity is critical, because shear capacity results from very short shear span tests could be misleadingly high as compression struts form by arching action. On the other hand, application of the test load too far from the support will result in flexural failure, rather than the expected shear failure.

According to MacGregor and Bartlett (2000), the ratio of the shear span to the depth of a beam, $a/d$, can be divided into four classes: very short, short, slender and very slender. Moreover, beams with very short shear span are called deep beams. Each of those categories can be expressed in a range of numbers and have different failure modes summarised in the following bullets:

- Very short shear spans ($0.0 \leq a/d \leq 1.0$)

  In this class, shear crack lines tend to join diagonally between the loaded point and the support. The beam in this class should be analysed instead of beam theory by strut-and-tie model as arching action takes place. Commonly, the failure in such beams ends up by anchorage failure of the longitudinal reinforcement close to loaded end.

- Short shear spans ($1.0 \leq a/d \leq 2.5$)

  Inclined shear cracks can be observed, but the beam would be still capable of carrying more load since redistribution of internal forces occurs to some extent by arching action. Palmer and Schultz (2010) stated that effect of arching diminishes if $a/d$ greater than 2.4 was used. The final failure of such beams will be either due to failure of tensile

reinforcement as result of bond failure, a splitting failure, or a dowel shear failure, or by flexural-shear failure.

- Slender shear spans, ($2.5 \leq a/d \leq 6.0$)

  The inclined shear cracks in this class will be very disruptive to such an extent that the beam fails at the inclined cracking load. Kani (1966) concluded from 2-point loading flexural tests on rectangular beams that diagonal shear cracks occurs if shear span was in the range of this class of slender shear span. Moreover, the lowest critical capacity was attained when *a/d* was around 2.5 in his non-prestressed beams.

- Very slender shear spans ($a/d > 6.0$)

  Usually the beams in this class fail in flexure prior to the formation of inclined cracks.

Probably, provisions of standard testing method in Annex J of EN 1168-08 which suggested to apply the vertical shear load at *a/d* = 2.5 or 600 mm, whichever is greater, is the most appropriate to use with HC slabs testing. However, it appears that there is uncertainty about the shear span range used to attain the minimum shear capacity of PHC slabs. Because despite the standard testing method in EN 1168-08 suggested to apply the vertical shear load at *a/d* = 2.5 or 600 mm, surprisingly there are experimental and FEM results showed that critical shear span value for HC slabs might be different from that well established *a/d* =2.5 value in non prestressed beams. For instance, Figure (2.3) below presents a very recent shear tests and 3D-FEM results carried out on 200-mm deep circular voided PHC slabs by Chen and Wang (2010). The examined *a/d* ranged from 2.5 to 4.3 and it can be implied from the chart that shear strength was 33% lower when *a/d* = 4.3 than at *a/d* = 2.5. It is worth to mention that mode of failure was flexural-shear in all of the range.

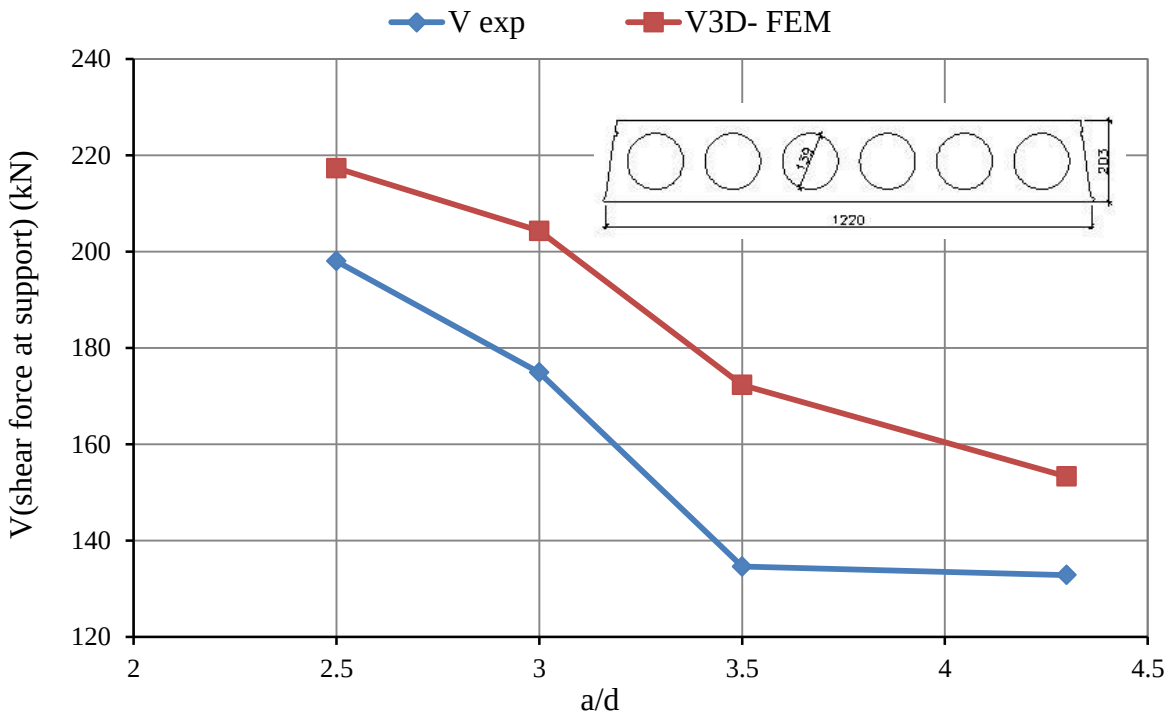


Figure (2.3): Effect of *a/d* on shear capacity of 200-mm PHC slabs (reproduced from Table (1) & Table (4) of Cheng and Wang (2010))

Another research effort to investigate critical shear span in PHC slabs displayed in Figure (2.4) from 3D-FEM study performed by Yang (1994). The represented web-shear data in this chart is only for the 400-mm deep non-circular voided simulated PHC units that shared same level of prestressing and length of bearing. Surprisingly, in this study the observed critical a/d=1.45 for the simulated type of slabs is even lower than 2.5.

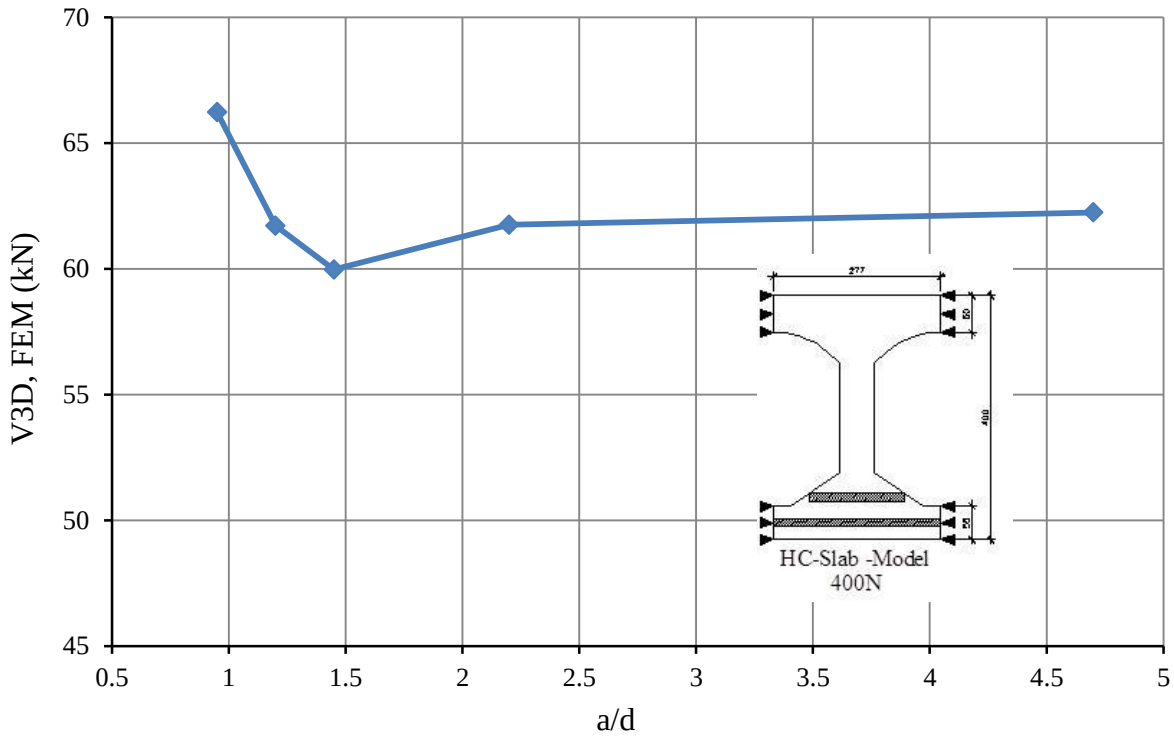


Figure (2.4): Effect of *a/d* on shear capacity of 400 mm modeled PHC slabs (reproduced from Table (2) of (Yang, 1994))

The conclusion is that the effect of shear span requires further investigation because no clear explanation is given for the difference between the critical shear spans of PHC slabs observed in those presented research data.

### 2.3.6. Length of bearing

The significant effect of bearing length (may be called width of supports) on shear capacity of PHC slabs comes from its influence on anchorage capacity of strands and location of critical point. Both anchorage length and distance of the critical section, or as called some time critical point, for web-shear are function of bearing length. Also, theoretically, shear capacity of slabs supported on small bearing length expected to be smaller. Because of limitation of anchorage capacity of the strands and since the critical point is closer to the end, the amount of axial prestressing transferred to concrete would be smaller. That is why Bertagnoli and Mancini

(2009) recommended designers to specify wider bearing length as much as possible and to choose it as a ratio of the slab depth. Also, bearing length is known to be one of the distressing matters faced by manufacturers to deal with unexpected support problems on site.

Definition for length of bearing was different among researchers. For example, Chen and Wang (2010) and Yang (1994) assumed or defined it as the distance from end of the PHC slabs to center line of the supporting plates while others such as Pajari (2005) thought it should extend up to the inner face of bearing pad/plate. The slabs tested by Becker and Buettner (1985) were supported on 76-mm grout pads; however, a portion of the slabs were extending beyond the supports and from an attached photo in the publication, it seems that the extension beyond bearing grouts was as long as width of the grout itself or maybe more. As a result, even though no clarification was provided about their consideration of bearing length for analysis, but according to the 2$^{nd}$ definition mentioned above, the bearing lengths used in this publication was about twice the size of grout width (150 mm).

Research study on effect of bearing length is very scarce and even if some data was found in Yang (1994) the author did not even try to comment or make any conclusion about the effect of bearing length on web-shear capacity results of simulated 400-mm deep slabs. Therefore, it was worth to present these results in the Figure (2.5) below.

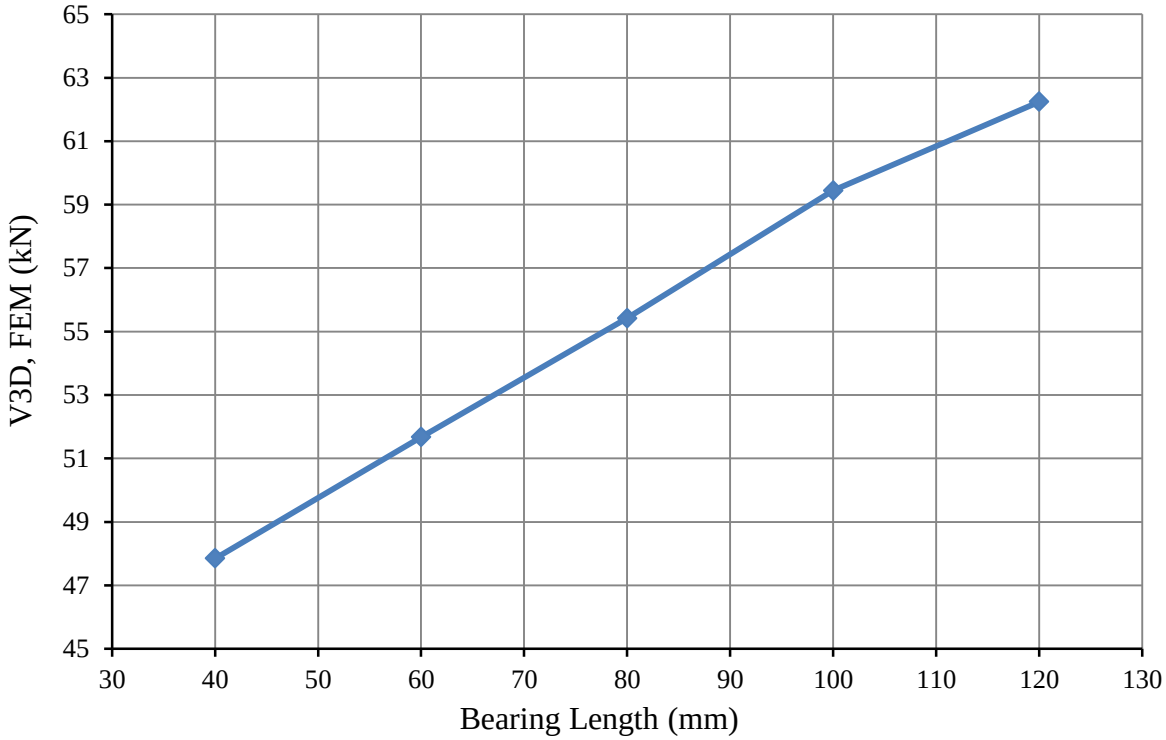


Figure (2.5): Effect of bearing length on shear capacity of 400-mm simulated PHC slabs (reproduced from Table (2) of Yang (1994))

The observation from the chart above is that web-shear capacity was increasing almost linearly in average rate of 19% increase in web-shear capacity for every additional 20 mm bearing length. This conclusion need to be verified in further experimental and FEM study and to make sure if interference of other parameters such as type of void shapes, prestressing level and slab thickness could change percentage of increase in shear capacity. For example, observations in the first phase of this research program performed by Truderung (2011) showed that percentage of increase or decrease in experimental shear capacity for 300-mm slabs has varied with variation of prestressing level. With low level of prestressing, the shear capacity surprisingly increased by 15% compared to small bearing length. On the other hand, when level of prestressing was high the shear capacity did decrease with decreasing bearing length but with only 1%.

Worth to mention that, in practical recommendations CTC (2007) report, suggestion was made that design bearing length should be considered 3 in. (76 mm) long but during installation minimum acceptable bearing length was specified as 2 in. (50 mm).

# CHAPTER 3: SHEAR CAPACITY PREDICTION BY CODES

## 3.1. General

To date, there is no universally accepted model for concrete shear design. This is because there is no full understanding of the shear behaviour of concrete. Almost every structural design code has proposed a distinct methodology for shear design predictions based on certain assumptions made to approximate the problem or ease calculations. However, since it is very significant for manufacturers and design firms to have a simple and dependable design expressions in building codes that would give safe and effective shear design for PHC slabs, many previous researches have expressed concerns and investigated accuracy of code expressions as one of the main objectives in their projects (Becker & Buettner 1985, Yang 1994, Micallef 2005, Pajari 2005, Hawkins & Ghosh 2006, Bertagnoli & Mancini 2009, Cheng & Wang 2010, Palmer & Schultz 2010). Accordingly, for code analysis, presented in Chapter 5 of this research project, three major national codes were selected for comparison with the experimental results as listed below:

- Canadian code for design of concrete structures, CSA A23.3-04 **(CSA)**;
- American code for buildings and structural concrete, ACI 318-08 **(ACI);**
- European code for design of concrete structures, DIN EN 1992-1-1-05 **(EC 2)**;
- Complementary to EC 2; code of hollow core slabs, DIN EN 1168-08 **(EN 1168).**

A detailed review over methods and expressions for shear capacity and transfer length evaluation that is practiced by each of those selected codes is presented in this chapter.

## 3.2. Code Provisions for Transfer Length

Clause 11.2.11 of CSA A23.3-04 states that prestress force may be assumed to vary linearly from zero at the point at which bonding commences to a maximum distance from the end of the

tendon equal to the transfer length, which assumed to be 50 times diameter length for strand and 100 times diameter length for a single wire. However, in Clause 12.9.1 of the commentary code, an expression that considers not only effect of diameter on the transfer length ($\ell_t$) but also prestressing level in the tendons as follows:

$$\ell_t = 0.048 \ f_{pe} \ d_b \qquad [3.1]$$

Where, $f_{pe}$ is the effective stress in prestressing tendons after allowance for all prestress losses. And, $d_b$ is diameter of strand.

Similar to provisions of CSA A23.3-04, Clause 11.3.4 of ACI 318-08 also states that in pretensioned members the prestress force shall be assumed to vary linearly from zero at the end of the prestressing steel, to a maximum at a distance from the end of the prestressing steel equal to the transfer length, assumed to be 50 diameters for strand and 100 diameters for a single wire.

However, an alternative expression for transfer length which could account for also the effect of amount of prestressing on transfer length ($\ell_t$) is provided in Clause 12.9.1 of the code commentary as following:

$$\ell_t = \left( f_{se} / 21 \right) d_b \qquad [3.2]$$

Where, $f_{se}$ (MPa) is the effective stress in prestressing tendons after allowance for all prestress losses.

In EN 1992-1-1-05 - Clause 8.10.2.2 & Clause 8.10.2.2.3.1.2 of Commentary Euro code 2 (2008) value of basic general transfer length ($l_{pt}$) is given by the following equation:

$$l_{pt} = \alpha_1 \alpha_2 \varnothing \sigma_{pm0} / f_{bpt} \qquad [3.3]$$

The above basic general transfer length is more comprehensive than ACI's and CSA's because it considers the effect of 5 factors: method of release ($\alpha_1$), type of tendons ($\alpha_2$), diameter of tendons ($\varnothing$), prestressing stress at release ($\sigma_{pm0}$),

Where, $\alpha_1$ is taken 1.0 for gradual release; as in case of PHC slabs. $\alpha_2$ is equal 0.19 for 7-wire type strands. The bond strength, $f_{bpt}$, is calculated as follows:

$$f_{bpt} = \eta_{p1} \eta_1 f_{ctd}(t) \qquad [3.4]$$

Where, $\eta_{p1}$ is a coefficient that accounts for type of tendon and it is taken 3.2 for 7-wire strands. $\eta_1$ is another coefficient taken as 1.0 if good bond conditions were assumed. The term $f_{ctd}(t)$ is the design value of tensile strength at release of strands.

For safety purposes in design, it is recommended in Clause 8.10.2.2(3) that the basic transfer length should be multiplied by 0.8 or 1.2, whichever is more critical for the case of design. As a result, for case of shear design the higher value was recommended ($l_{pt2} = 1.2 l_{pt}$).

However, one might say that assuming smaller than basic value for transfer length in web shear design could be more critical because prestressing gradient (*dNp/dx*) would be higher which generates more reduction in shear capacity. However, the vision of the code committee could be that longer transfer length makes amount of prestressing smaller in the transfer zone, or because the code was not giving consideration to the effect of prestressing gradient on shear capacity in first place and that is why did not recommend the smaller transfer length.

### 3.3. Critical Sections in Shear

Structural design of members is based on worst cases of loadings and resistance which was ascribed by some guidelines or practical experience. There are two kinds of critical sections of interest in shear design process. First section is called critical section for shear force and it is to identify how close the point of application of vertical concentrated shear force should be to cause the maximum shear force on the member. Second critical section is called critical section for shear resistance which is describable as the territory for most expected section or point for inclined shear cracks. A review of the suggested location for these critical sections provide by different codes is presented in the next sections.

#### 3.3.1. Shear critical sections in CSA code

Clause 11.3.2 states that sections located less than a distance $d_v$ from the face of the support to be designed for the same shear force, $V_f$, as that computed at a distance $d_v$, provided that the reaction force in the direction of applied shear introduces compression into the member and no concentrated load that causes a shear force greater than $0.3\lambda\phi_c\sqrt{f_c'}b_w d_v$ is applied within the distance $d_v$ from face of the support. It is understandable from this clause that the suggested critical section for shear force is identified to be at a distance $d_v$ from inner face of the support.

On the other hand, Clause 11.3.6.4 (d) provides that for sections located closer than $d_v$ to the face of the support, the value of $\varepsilon_x$ calculated at $d_v$ from the face of the support may be used in evaluating $\beta$ factor. This indicates that CSA code is assuming that critical section for shear resistance is located at distance $d_v$ from the face of the support. In more specific terms, coordinates of the critical point, according to CSA code, is measured from inner edge of the

bearing support would be *(z-coordinate = $d_v$)* and (*y-coordinate = d/2*); since $\varepsilon_x$ is calculated at *d*/2.

Where, *dv* is defined in Clause 2.3 as effective shear depth, taken as the greater of 0.9*d*, or 0.72*h* (where, *d* is depth of flexural reinforcement and *h* is the overall height of the member).

### 3.3.2. Shear critical sections in ACI code

Clause 11.1.3.2 permits sections located less than a distance *h/2* from the face of the support in prestressed members to be designed for the same factored shear force, $V_u$, computed at *h/2*, provided that conditions in Clause 11.1.3, which all do apply in case of PHC slab units, are met:

a) Support reaction, in direction of applied shear, introduces compression into the end regions of member;
b) Loads are applied at or near the top of the member.
c) No concentrated load applies between the face of the support and the location of the critical section defined in Clause 11.1.3.2.

It is concluded that critical section for shear force in PHC slabs according to ACI is assumed at distance *h*/2 from inner face of the bearing support.

Regarding the critical section for shear resistance, the code does not explicitly mention that it may be assumed to occur at the same location of *h*/2 from the face of the support. However, this could be concluded from PCI Design Handbook (PCI 2007), since it is similar to ACI 318 based on the same concept of traditional method for shear design. Therefore, it is implied that the critical section for shear force and for shear resistance is both assumed to be at *h*/2 from the edge of the bearing pad for shear prediction by the ACI code.

### 3.3.3. Shear critical sections in EC 2 & EN-1168 code

Provisions for critical section for shear force can be found in Clause 6.2.2 (6) of EC-2, which states that for members with loads applied on the upper side within a distance, $a_v$, more than or equal to 0.5*d* and/or less than 2*d* from the edge of a support, the contribution of this load to the shear force, $V_{Ed}$, may be multiplied by $\beta = a_v/2d$. This reduction may be applied when checking adequacy of uncracked shear capacity. This is only valid provided that the longitudinal reinforcement is fully anchored at the support. More important, it was stated that when the vertical point load is applied at $a_v$ less than or equal to 0.5*d*, the value of shear force at $a_v = 0.5d$ should be used. This implies that EC-2 considers the critical section for shear force to be at 0.5*d*. However, it is important to mention that since tendons of PHC slabs are not considered fully anchored at the support; the reduction factor ($\beta$), suggested by this clause, must not apply on PHC units.

Also, Clause 6.2.2(3) discussed critical section for shear resistance in determination of un-cracked shear by Expression 3.21, presented in Section 3.3.3, and stated that calculation of the shear resistance is not required for cross-sections that are nearer to the support than the point which is the intersection of the elastic centroidal axis and a line inclined from the inner edge of the support at an angle $45^0$. This implies similar assumption of EC-2 of critical section for shear resistance at about *h*/2 since usually thickness of the top and bottom flanges are same for PHC units. In more specific terms, coordinates of critical point according to EC-2 as measured from inner edge of the bearing support would be *(y-coordinate = h/2)*; and (*z-coordinate =h/*2); because $\sigma_{cp}$ is required to be evaluated at the centroidal axis level.

In the complementary code, EN 1168, instead of indicating for a specific fixed section as the critical for shear resistance of PHC slabs, it suggests more general approach to identify it. The

section is identified by calculating the shear resistance at multiple sections, and wherever it was found lowest that is defined as the critical section. However, it is noted that expected position to be at a distance from face of the support not further than $h / \tan 35^0$. This way, the effect of many factors such as void geometry, prestressing level, etc. on position of the critical section for shear resistance is accounted for.

### 3.4. Shear Resistance Equations

The shear capacity equations in all of the three codes, except web-shear expression of EN 1168, were all developed from research work conducted on beams with solid cross-sections. Since no specific expressions exists, the most relevant and most practiced expressions on shear capacity prediction of PHC units in each code is presented in this section with the reference clause number and explanation of terms used.

#### 3.4.1. Shear resistance equations of CSA code

Treating the PHC slabs in a similar way to any other flexural member subjected to shear force, the factored shear resistance of a PHC slab is calculated by the expression in Clause 11.3.3:

$$V_r = V_c + V_s + V_p \qquad [3.5]$$

Where, $V_r$ is the factored shear resistance of the member, $V_c$ is the concrete contribution to shear resistance, based on tensile stresses transmitted across cracks via aggregate interlock, $V_s$ is the shear resistance provided by shear reinforcement, and $V_p$ is the component in the direction of the applied shear of the effective prestressing force. In PHC slabs, there is no shear reinforcement and no vertical component exist for the straight strands profile to counteract the vertical shear, therefore $V_s$ and $V_p$ cross out and the final shear resistance of PHC slabs will be calculated by only $V_c$ from the following empirical relationship found in Clause 11.3.4:

$$V_c = \phi_c \lambda \beta \sqrt{f_c'} b_w d_v \qquad [3.6]$$

Unlike the other two codes, classification for modes of shear failure is not a point of discussion in the CSA code. There is only this general Expression 3.6 to use for estimation of all types of shear resistance.

In design, the material resistance factor, $\phi_c$ is taken as 0.70 for products manufactured in a certified plant, however for the analysis of the laboratory-tested PHC slabs, a value of 1.0 was used for $\phi_c$. The term $\lambda$ is a factor that accounts for low density concrete, which does not apply to any of the test slabs, therefore a value of 1.0 was used for $\lambda$. Equation 3.6 then reduces to:

$$V_c = \beta \sqrt{f_c'} b_w d_v \qquad [3.7]$$

In the above expression, because crack interface in very high strength concrete is smooth which means reduction in aggregate interlock effect, the code suggested in Clause 11.3.4 a limitation to be placed on substituted value of concrete strength ( $f_c' \leq 64MPa$ ) in Expression 3.7 but to observe the effect of variable concrete strength on the predicted value of shear capacity in this project, that limit on $f_c'$ was not applied during code analysis.

In Equation 3.7, $b_w$ is defined as the minimum effective web width in Clause 11.2.10, which in case of PHC slabs would be the sum of minimum web widths across the slab width. The term $d_v$ was defined in Clause 11.2.3 as effective shear depth, taken as the greater of 0.9*d*, or 0.72*h*.

The most important term, $\beta$, in Expression 3.7 has been defined by Clause 11.2.3 as a factor that accounts for shear resistance of cracked concrete. The code provides two methods for evaluation of this $\beta$ factor; one is simplified and the other is general.

For the analysis in this research the general method, which is derived from MCFT, in Clause 11.3.6.4 is used as follows:

$$\beta = \frac{0.40}{(1+1500\varepsilon_x)} \bullet \frac{1300}{(1000+s_{ze})} \qquad [3.8]$$

Where, $s_{ze}$ represents an equivalent value of $s_z$, which allows for the influence of aggregate size. $s_z$ is a crack spacing parameter, that is dependent on the crack control characteristics of the longitudinal reinforcement. The equations for $s_{ze}$ and $s_z$ that are applicable to PHC slabs are presented below.

$$s_{ze} = \frac{35s_z}{(15+a_g)} \geq 0.85s_z \quad [3.9] \text{ where} \qquad s_z = d_v$$

In Equation 3.9, $a_g$ is maximum size of the coarse aggregate used in concrete mix. However, since in high strength concrete bond between aggregate and cement matrix is strong, the aggregate also fails along the crack surface leaving no effect of interlock. That is why Clause 11.3.6.4 requires the value of $a_g$ be reduced to zero, when $f_c' > 70$ MPa. Similarly, $a_g$ shall be linearly reduced to zero, as $f_c'$ goes from 60 to 70 MPa.

$\varepsilon_x$ is the longitudinal strain in concrete at mid-depth of the member due to factored loads and it is determined by transferring strain in the flexural reinforcement at bottom surface of the member to strain in concrete at mid depth with the following expression from clause 11.3.6.4:

$$\varepsilon_x = \frac{M_f / d_v + V_f - V_p + 0.5N_f - A_p f_{po}}{2(E_s A_s + E_p A_p)} \qquad [3.10]$$

Therefore, in the above Equation 3.10, the numerator represents the force in the longitudinal reinforcement at the considered section divided by 2, and the denominator ($E_sA_s$+$E_pA_p$) is the axial stiffness of that reinforcement. The stiffness of concrete is not included here because, principally, this expression assumes that concrete section is cracked already.

The $\beta$ factor in equation 3.8, is inversely proportional to the $\varepsilon_x$ . As the longitudinal strain in the member approaches tensile values, the value of $\beta$ decreases which consequently reduce the estimated concrete shear-resistance, $V_c$. In the contrary, if compressive $\varepsilon_x$ were applied such as due to prestressing the $V_c$ would increase very rapidly. This might cause extra sensitivity of the code method for prestressing levels. If the calculated value of $\varepsilon_x$ by Equation 3.10 found to be negative, that means the considered section is not cracked yet and in that case Clause 11.3.6.4(c) suggests considering axial stiffness of the un-cracked concrete area below centroid level of the section, $E_{ct}\,A_{ct}$, in the denominator.

In Equation 3.10, the terms $M_f$ and $V_f$ are moments due to factored loads and due to applied factored shear force at the considered section, respectively. $d_v$ and $V_p$ same as defined earlier. $N_f$ is the applied factored axial load on the cross-section other than the prestressing (equals zero in simply supported PHC slabs). $E_sA_s$ and $E_pA_p$ stand for axial stiffness of non prestressed reinforcement and prestressed tendons, respectively, but since only prestressed strands are used in PHC slabs the former term will cross out also from the equation.

The term $f_{po}$ is defined per Clause 11.2.3 as the stress in the prestressing tendons when the strain in the surrounding concrete is zero (it is taken as $0.70f_{pu}$ beyond the transfer length, and linear interpolation is used for sections within the transfer zone between zero value at end of the member and $0.70f_{pu}$ at the end point of transfer length).

In conclusion, the expression for evaluation of $\varepsilon_x$ when tailored for PHC slabs would be as following:

$$\varepsilon_x = \frac{M_f / d_v + V_f - A_p f_{po}}{2(E_p A_p)} \quad or \quad \frac{M_f / d_v + V_f - A_p f_{po}}{2(E_p A_p + E_{ct} A_{ct})} \qquad [3.11]$$

When using the above Equation 3.11 there are few conditions stated in Clause 11.3.6.4 need to be followed; those which related to PHC slabs are listed below:

a) $V_f$ and $M_f$ are positive quantities, and $M_f$ shall not be taken less than $(V_f - V_p)\, d_v = V_f\, d_v$.

b) $\varepsilon_x$ shall not be taken as less than $-0.20 \times 10^{-3}$ nor greater than $3.0 \times 10^{-3}$

### 3.4.2. Shear resistance equations of ACI code

Nominal shear capacity of members without shear reinforcement is dependent only on concrete contribution, $V_c$. ACI code also has no specific provisions for shear resistance of PHC slabs and the most appropriate way for determination of $V_c$ is to follow provisions of Clause 11.3 that deals with concrete shear strength in prestressed members in general. However, the code was at least specific with defining two types or modes for concrete shear cracking (web-shear and flexure-shear) and as it was stated in Clause 11.3.3 the smaller of the two types is considered as the governing concrete shear strength, $V_c$. The following paragraphs present the metric form of equations used in determination of each type of shear failure.

Flexural-shear resistance of concrete, $V_{ci}$, is determined from the expression given in Clause 11.3.3.1 as follows:

$$V_{ci} = 0.05\lambda\sqrt{f_c^{'}}\, b_w d_p \; + V_d + \; \frac{V_i M_{cre}}{M_{max}} \geq 0.17\lambda\sqrt{f_c^{'}}\, b_w d \qquad [3.12]$$

Where, $\lambda$ is a modification factor that accounts for density of concrete ( $\lambda = 1$ in this project as normal density concrete was used). The term $b_w$ is the sum of minimum width of webs across the slab section. $d_p$ is taken as the depth measured to centroid of flexural reinforcement, $d$, or $0.80h$, whichever is greatest. $V_i$ and $M_{max}$ are the factored shear force and moment, respectively, at the considered section due to externally applied loads (super-imposed dead loads and live loads). But, $V_d$ is the shear force at the section due to un-factored dead loads only (self-weight only in non-composite members).

$M_{cre}$ is the cracking moment for the considered section due to externally applied loads and is determined as following:

$$M_{cre} = (I / y_t)(0.5\lambda\sqrt{f_c^{'}} + f_{pe} - f_d) \qquad [3.13]$$

In the above Equation 3.13, $(I / y_t)$ is the section modulus, and $f_{pe}$ is the stress caused by effective prestressing (after allowance for all prestress losses) force at the considered section at the level of bottom surface of the slab, where the slab is expected to crack in flexure. Finally, $f_d$ is the stress due to un-factored dead load at the same level where $f_{pe}$ was calculated.

On the other hand, web-shear resistance of concrete, $V_{cw}$, is calculated from the expression given in Clause 11.3.3.2 as follows:

$$V_{cw} = (0.29\lambda\sqrt{f_c^{'}} + 0.3f_{pc})b_w d_p + V_p \qquad [3.14]$$

All those terms in the above Equation 3.14 are same as introduced for Equation 3.12, except the new terms such as $f_{pc}$ is defined as the compressive stress in the concrete due to effective prestressing force at the centroid of considered section, or at the junction of the web and flange if the centroid lies within the flange. Again, $V_p$ is the vertical component of prestressing force which does not apply in case of PHC slabs because strands always have a horizontal profile. Web-shear expression of PHC slabs reduces to:

$$V_{cw} = (0.29\lambda\sqrt{f_c^{'}} + 0.3f_{pc})b_w d_p \qquad [3.15]$$

There are few general conditions provided in the code which need to be considered, while using the shear equations mentioned above, those which apply to PHC slabs are listed below:

a) It was mentioned earlier, that final nominal shear resistance of PHC slab at any section, $V_c$, would be the lesser value of $V_{ci}$ or $V_{cw}$. Yet, in design, nominal resistance has to be multiplied by a strength reduction factor, $\phi$, as implied by Clause 11.1.1. However, since this is an experimental project a value of 1.0 is used.

b) Due to lack of test data and practical experience, Clause 11.2.1 suggested no value greater than 70 MPa to be substituted for concrete compressive strength, $f_c^{'}$, in any of the equations mentioned above. However, during code analysis in this research, actual values from cylinder test results performed on the test date of slabs were used to account for the effect of concrete strength on the predicted slab shear capacity.

c) Even though it is not practical in HC slabs, but as extra precautions against brittle web-shear failures, Clause 11.4.6.1 (b) requests using minimum shear reinforcement in the following two cases:

   1. If thickness of the HC slab unit was bigger than 315 mm, not included topping thickness, or,
   2. if the applied total factored shear force, $V_u$, at any section was greater than $0.5\phi V_{cw}$, where $\phi$ is equal 0.75 for shear.

### 3.4.3. Shear resistance equations of EC 2 code

The European code is more specific and explicit in providing different provisions for shear capacity of members with and without shear reinforcement. Moreover, the design value of shear resistance in members without shear reinforcement, $V_{Rd,c}$, likewise in ACI code is classified into two types: shear resistance of regions un-cracked in bending and shear resistance of sections cracked in bending. Consequently, selection of which shear expression to use in determination of shear capacity at any considered section along the length of the member depends on whether the section is cracked or un-cracked. The following paragraphs are summary of procedures and equations that could be used for evaluating the shear capacity of PHC slabs.

First step is to check whether the considered section is cracked under bending before shear or not. This is achieved by calculating flexural tensile stress on the bottom face of the slab, $f_b(x)$, from the following expression:

$$f_b(x) = -\frac{P_{m,t}(x)}{A_c} - \frac{P_{m,t}(x)\cdot e}{S_b} + \frac{M_{sw}(x) + M_{Ptest}(x)}{S_b} \qquad [3.16]$$

Where is $P_{m,t,}(x)$ is the effective prestress force in the tendons at time $t$ and distance $x$ from the slab end. The term $e$ is the eccentricity of tendons, $A_c$ is area of concrete section, $S_b$ is section modulus and, $M_{sw}(x)$ and $M_{Ptest}(x)$ are moments due to self-weight and applied external load.

It was stated in Clause 6.2.2(2) the considered section is classified as un-cracked only if $f_b(x) < \frac{f_{ctk\,0.05}}{\gamma_c}$, otherwise it is considered cracked. The term $f_{ctk\,0.05}$ is the characteristic axial tensile strength of concrete. Also, $\gamma_c$ is defined as partial factor for concrete (material resistance factor), a value of 1.0 is used within this experimental research project.

The relation between $f_{ctk\,0.05}$ and characteristic compressive cylinder strength of concrete, $f_{ck}$, is derived from empirical equations of Table (3.1) in the EC-2 as following:

$$f_{ctk\,0.05} = 1.484 \ln(1 + \frac{(f_{ck} + 8)}{10}) \quad when \quad f_{ck} > 50MPa$$
$$or \qquad f_{ctk\,0.05} = 0.21(f_{ck})^{2/3} \quad when \quad f_{ck} \le 50MPa \qquad [3.17]$$

The expression for shear resistance of sections cracked by bending (flexural-shear resistance) is found in Clause 6.2.2(1) as follows:

$$V_{Rdc} = \left[ C_{Rd,c} k (100 \rho_l f_{ck})^{1/3} + k_1 \sigma_{cp} \right] b_w d \qquad [3.18]$$

Where, $V_{Rd,c}$ is called the design shear resistance of the member without shear reinforcement; it is measured in units of $N$. The factors $C_{Rd,c}$ and $k_1$ are taken as $\frac{0.18}{\gamma_c}$ and 0.15, respectively. $b_w$ is the sum of smallest web widths of the cross-section in the tensile area. Furthermore, $d$ is called the effective depth or as implied from Figure (6.1) in the code it is the distance from top surface

of cross section to centroid of outermost layer of strands. The term $\rho_l$ is defined as flexural tensile reinforcement ratio and is evaluated as following:

$$\rho_l = \frac{A_{sl}}{b_w d} \leq 0.02 \qquad [3.19]$$

Where, $A_{sl}$ is the area of the tensile reinforcement (strands in PHC slab units), which extends more than a certain anchorage length beyond the considered section.

Also, the term $\sigma_{cp}$ is the axial compressive stress in the cross-section due to effect of prestressing force, $N_{Ed}$ , only as following:

$$\sigma_{cp} = \left( \frac{N_{Ed}}{A_c} \right) < 0.2 f_{cd} \qquad [3.20]$$

Where, $f_{cd}$ is the design value of compressive strength which is taken equal to $f_{ck}$ in this study.

Note that the calculated value of cracked shear strength from Equations 3.18 recommended not be taken less than a minimum strength value calculated as follows:

$$V_{Rd,c} \geq (v_{\min} + k_1 \sigma_{cp}) b_w d \qquad [3.21]$$

Where, the size factor, *k*, and $v_{\min}$ are determined from the following expressions:

$$v_{\min} = 0.035 k^{3/2} \sqrt{f_{ck}} \qquad [3.22] \qquad k = 1 + \sqrt{\frac{200}{d}} \leq 2.0 \qquad [3.23]$$

On the other hand, the expression in EC-2 for shear resistance of sections un-cracked by bending (web-shear resistance) is fundamentally based on the same traditional method concept similar to

ACI code. It is just not assuming that shear distribution over height of the cross-section is uniform, instead using the term (I/S) derived from mechanics of materials, which implies that the distribution of shear stress is parabolic with maximum to occur at the level of centroidal axis. The expression for web-shear provided by EC-2 is as follows:

$$V_{Rdc} = \frac{Ib_w}{S}\sqrt{\left(f_{ctd}\right)^2 + \alpha_\ell \sigma_{cp} f_{ctd}} \qquad [3.24]$$

Where, $I$ is the second moment of area of the whole cross section, $b_w$ is the width of the cross-section at the centroidal axis, $S$ is the first moment of area above and about the centroidal axis. The term $f_{ctd}$ is called design value of concrete tensile strength given as $\frac{f_{ctk\,0.05}}{\gamma_c}$, and $\alpha_l = \ell_x / \ell_{pt2} \leq 1.0$ for pre-tensioned tendons, $\ell_x$ is the distance of section considered from the starting point of the transmission length, and $\ell_{pt2}$ is the upper bound value of the transmission length for the prestressing tendons. $\sigma_{cp}$ same as defined earlier.

It is important to stress that during code analysis with European codes for PHC slabs tested in this research, Expression 3.24 that is provided in EC-2 was not used in prediction of their un-cracked shear capacity. Instead, more specifically oriented un-cracked shear capacity equation for PHC slab units provided in the complimentary code EN 1168 was more preferred. That is presented in the next section.

### 3.4.4. Shear resistance equations of EN 1168 code

One of the most particular aspects of EN 1168 (complementary code for EC-2) is to approve the un-cracked shear design method, that was developed in research works performed by Yang (1994) and Pajari (2005), as a standard expression for estimating web-shear capacity of PHC

slabs. Although it is an iterative process and requires lots of calculations, this method leads to predictions much closer to actual shear capacity than those of CSA and ACI.

Unfortunately, no distinction was made in European codes between denotation used for cracked and un-craced shear; $V_{Rdc}$ is being used for both types of shear resistance.

The expression for un-cracked shear capacity of HC slabs is found in Clause 4.3.3.2.2.1 as follows:

$$V_{Rdc} = \frac{I \cdot b_w(y)}{S_c(y)} \left[ \sqrt{(f_{ctd})^2 + \sigma_{cp}(y) \cdot f_{ctd}} - \tau_{cp}(y) \right] \qquad [3.25]$$

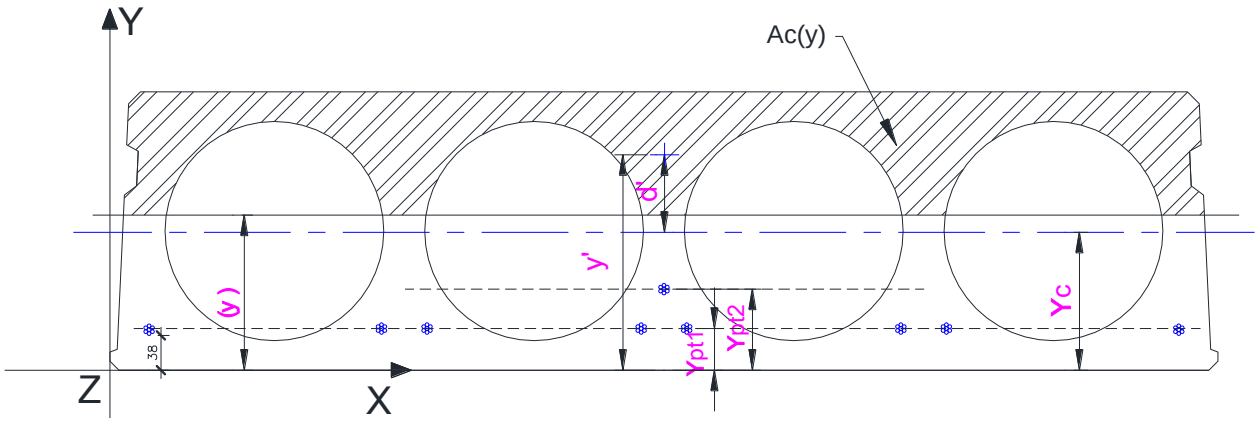


Figure (3.1): Illustration of terms used in Expression 3.25

In the above Equation 3.25, the term (*y*) is not supposed to be substituted by a value; it is just indication that the preceding term needs to be calculated at the height of considered level of critical point as illustrated in Figure (3.1) or in another words, it is y-coordinate of the potential critical point where its x-coordinate is termed by ($l_x$) as will be explained later. Accordingly, $b_w(y)$ is the web width at the height (*y*) and $S_c(y)$ is the first moment of area above the height (*y*) and about the centroidal axis; i.e., the area of hatched zone in Figure (3.1) multiplied by *d'*, which is the distance between centroid of that area and centroid of the whole cross section of the

unit. The term $f_{ctd}$ is the design value of concrete tensile strength as mentioned in the previous section; however since a value of 1.0 is assumed for $\gamma_c$ in this research, $f_{ctd}$ is taken equal to $f_{ctk\,0.05}$.

The variable $\sigma_{cp}(y)$ in Expression 3.25 was defined as compressive stress at the assumed critical point with x-coordinate = ($l_x$) and y-coordinate = ($y$) according to the illustrated position of axes at the left corner of the HC slab unit in Figure (3.1). ($l_x$) is the distance of considered section, over which the assumed critical point lies, from the starting point of the transmission length. In this research, transfer length is assumed to start right from end of the slab.

On the other hand, the variable $\tau_{cp}(y)$ in Expression 3.25 is the concrete shear stress due transfer of prestressing along the transfer length (the additional shear that results from prestressing gradient). This is not accounted for by shear equations of other codes. Values of $\sigma_{cp}(y)$ and $\tau_{cp}(y)$ are estimated from the following expressions:

$$\sigma_{cp}(y) = \sum_{t=1}^{n} \left\{ \left[ \frac{1}{A_i} + \frac{(Y_c - y)(Y_c - Y_{pt})}{I} \right] \cdot P_t(l_x) \right\} - \frac{M_{Ed}}{I} \cdot (Y_c - y) \qquad [3.26]$$

$$\tau_{cp}(y) = \frac{1}{b_w(y)} \sum_{t=1}^{n} \left\{ \left[ \frac{A_c(y)}{A_i} - \frac{S_c(y) \cdot (Y_c - Y_{pt})}{I} + C_{Pt}(y) \right] \cdot \frac{dP_t(l_x)}{d_x} \right\} \qquad [3.27]$$

In the above equations, the term *n* stands for number of tendon layers used on the PHC slab section. Accordingly, *t* is order of the individual layer for which specifically calculation of parameters subscripted by *t* is made. The code defined $A_i$ as fictive cross section surface; however, it can be simply explained as the area of the whole cross-section excluding area of

voids. $M_{Ed}$ is moment due to all loads. The terms $y, Y_c$, and $Y_{pt}$ are height of critical point, height of centroidal axis of the whole unit, and height of the considered tendon layer, respectively. It is worth to mention that all those heights are measured from bottom of the slab and the sign rule is positive for compression. Moreover, $A_c(y)$ is the area above height ($y$) shown hatched in Figure (3.1). Also, $C_{Pt}(y)$ is a factor taken as -1 when ($y$) $\leq Y_{Pt}$ otherwise it is zero.

$P_t(l_x)$ could be called as the effective prestressing force in the considered tendon layer, $t$, at the considered distance of critical point from end of the slab, ($l_x$). And, it can be evaluated from the following expression:

$$\mathrm{P_t}(l_\mathrm{x}) = \alpha_l(l_\mathrm{x})\ \sigma_{\mathrm{m,t}}\mathrm{A_{pt}} \qquad [3.28]$$

Where, $A_{pt}$ is the area of considered tendon layer and $\sigma_{\mathrm{m,t}}$ is the fully transferred prestressing stress in the tendon layer at the end of its transfer length. $\alpha_l(l_\mathrm{x})$ is called the degree of prestressing transmission taken as $\frac{l_\mathrm{x}}{l_{\mathrm{pt2}}} \leq 1.0$; such that $l_{\mathrm{pt2}}$ is the upper value of transmission length which is suggested in clause 8.10.2.2 of EC 2 to be taken as 1.2 times the basic transfer length value, $l_{\mathrm{pt}}$. But, since no factors of safety are applied in experimental studies, $l_{\mathrm{pt2}}$ was taken equal to $l_{\mathrm{pt}}$ during code analysis.

One last significant term to identify in the expression of $\tau_{cp}(y)$ is the $\frac{dP_t(l_x)}{d_x}$. For some reason no definition was found in the code EN 1168. However, after looking at the definition in Pajari (2009), the most appropriate is to call it gradient of prestressing force along the transfer length and estimated as follows:

$$\text{for } 0 < l_x < l_{pt} \quad \rightarrow \quad \frac{dP_t(l_x)}{d_x} = \frac{\sigma_{m,t} A_{pt}}{(l_{pt,t})}$$

$$\text{and } l_x > l_{pt} \rightarrow \frac{dP_t(l_x)}{d_x} = 0 \Rightarrow \tau_{cp}(y) = 0$$

It appears quite cumbersome to evaluate the un-craked shear capacity from Expression 3.25 as identifying the critical point requires lots of iterations. However, to reduce it, the code has suggested trying with points along a line rising from edge of the support and making $35^0$ angle with the horizontal axis. The point on the quoted line where the results of the expression of $V_{Rdc}$ found to be lowest will be the critical point and that is the predicted web-shear resistance of the considered PHC unit. It is worth to mention that EN 1168 does not replace the cracked shear Expression 3.18 provided in EC-2; in fact, reference was made for users to use the same equation in evaluation of flexural shear capacity in cracked regions by bending.

# CHAPTER 4: EXPERIMENTAL PROGRAM

## 4.1. General

Shear behaviour of concrete structures in general is a complex problem, which is not always fully understood. Experimental investigation is one of the most important and reliable ways for better understanding that behaviour. Based on the review performed in Chapter 2 on previous research efforts in the area of shear capacity of PHC slabs and considering the suggestions and demands of two local PHC slab producers, an experimental investigation was conducted in the heavy structures laboratory at the University of Manitoba. The main objective of this experimental program was to verify the influence of a set of variables on actual as-built shear capacity of PHC slabs. The following sections provide details of the tested specimens and the considered parameters for investigation.

## 4.2. Test Specimens

The phase 2 of the research program included full-scale testing of PHC slabs delivered by two local suppliers off their regular production lines. Each supplier provided six specimens, which means in total 12 specimens tested in this study. Both suppliers were using the same dry-cast extrusion method to produce the slabs; a method that utilizes zero-slump concrete to reduce water-to-cement ratio. However, the most noticeable variable among specimens of each supplier was the void shape.

The test specimens were classified into three series, four slabs each, based on their slab thickness. Each series consists of two identical slabs from each supplier; Series-200, Series-250 and Series-300. The designation used for the specimens in this study comprised of three parts; the first three digits denote the nominal slab thickness, the following letter with a digit (P1 or P2)

denote the supplier of the slabs, and the third part is a single letter denotes the length of bearing of the support at loaded end of the slab (A = 63 mm or B = 38 mm). For example, specimen 200-P1-A indicates a 203-mm thick slab, produced by supplier # 1, and the bearing length was 63 mm at the loaded end.

The level of prestressing was aimed to be kept about the same in all specimens. Accordingly, suitable strand configurations that provided a medium level of prestressing in each series were specified to the suppliers. Also, the reason behind the selection of medium level is to complement the test results of Phase 1 of the study, which includes maximum and minimum levels of prestressing (Truderung 2011). Table (4.1) shows the nominal value of level of prestressing in all 12 specimens tested in this phase.

Table (4.1): Levels of prestressing in tested specimens

| Series | Specimen ID | Nominal Slab Depth (mm) | Applied Prestress Jacking Force (kN) | Nominal x-section Area ($mm^2$) | Jacking Force / Area of Slab (MPa) |
|---|---|---|---|---|---|
| Series-300 | 300-P1-A | 305 | 1240 | 180221 | 6.88 |
| | 300-P1-B | | | | |
| | 300-P2-A | | | 180414 | 6.87 |
| | 300-P2-B | | | | |
| Series-250 | 250-P1-A | 254 | 964 | 154897 | 6.22 |
| | 250-P1-B | | | | |
| | 250-P2-A | 254 | 1010 | 154047 | 6.55 |
| | 250-P2-B | | | | |
| Series-200 | 200-P1-A | 203 | 719 | 140194 | 5.13 |
| | 200-P1-B | | | | |
| | 200-P2-A | | | 132887 | 5.41 |
| | 200-P2-B | | | | |

So, three variable parameters are considered in this experimental phase of the project which is slab thickness, shape of voids and length of bearing at the loaded end. Table (4.2) shows a matrix of all 12 tested specimens and the corresponding tested parameters.

Table (4.2): Matrix of studied parameters in the experimental program

| Studied Parameter | Specimen ID | | | | | | | | | | | |
|---|---|---|---|---|---|---|---|---|---|---|---|---|
| | 300-P1-A | 300-P2-A | 300-P1-B | 300-P2-B | 250-P2-B | 250-P2-A | 200-P2-A | 200-P2-B | 200-P1-B | 200-P1-A | 250-P1-A | 250-P1-B |
| Slab thickness (mm) | 300 | | | | 250 | | 200 | | | | 250 | |
| Void Shape | Circular | | | | | | | | Non-circular | | | |
| Length of Bearing | A | | B | | A | | B | | | A | | B |

## 4.3. Slab Geometry

The geometry of the slabs is governed by the type of the extrusion machines. Some manufacturers such as supplier #2 (P2) are utilizing machines with circular voids for all of thickness series they produce, whereas supplier #1 (P1) is utilizing machines with circular voids in production of some thicknesses and non-circular in others. The non-circular void shape could be very versatile and it describes any void shape formed from combination of straight and curved profiles. Figures (4.1 to 4.6) outline the nominal cross-sections for all tested specimens in this program. The actual, as-built, dimensions were measured since code expressions are very sensitive to some dimensions such as web width. The as-built cross-sectional geometry was manually traced at the loaded end of all tested specimens on a drafting paper and transferred to soft copy later on. For reference, all of these as-built cross-sectional drawings are included in Appendix A.

Moreover, nominal sectional properties such as inertia and height of centroid, which are used in code equations for predicting shear capacity, are presented in Figures (4.7 to 4.12) for all tested specimens. The actual as-built slab section properties are provided in Table (4.3) with comparison between the nominal and as-built sectional properties of all tested specimens.

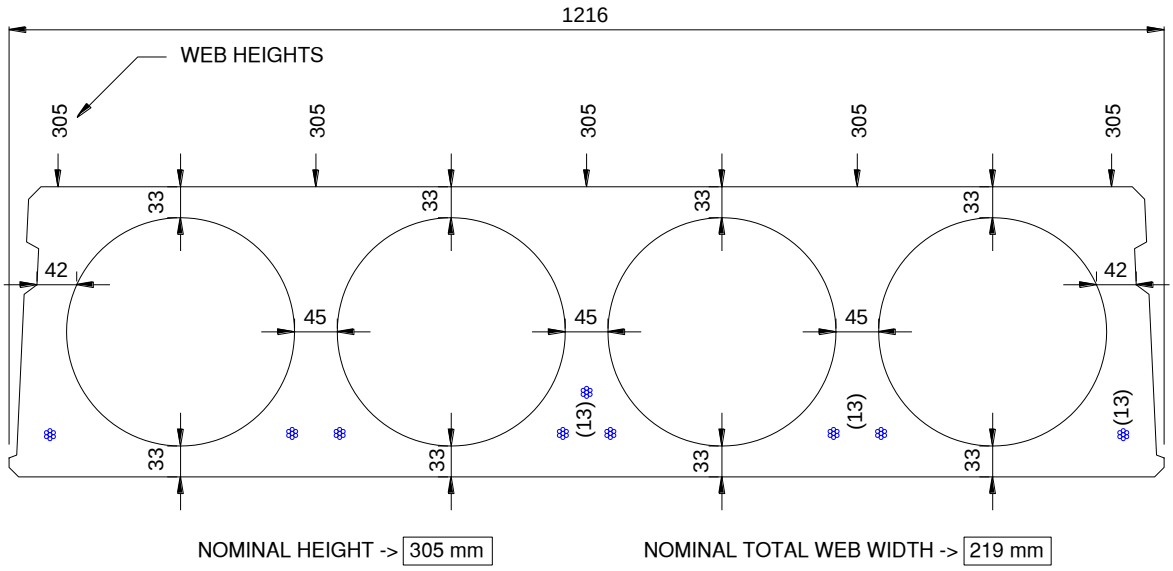


Figure (4.1): Series-300-P1 - nominal slab geometry

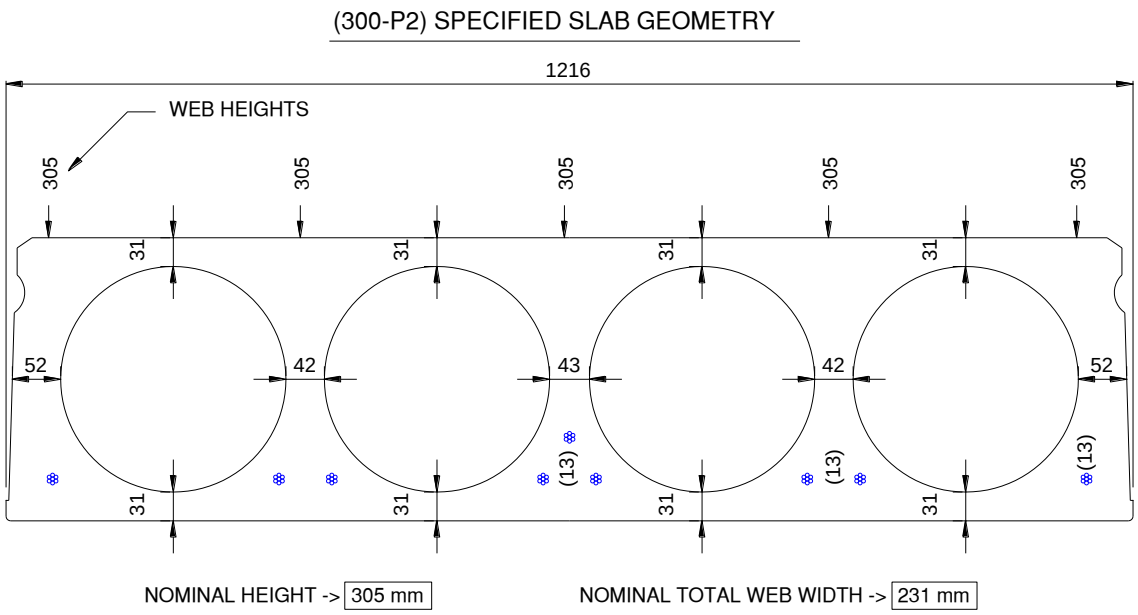


Figure (4.2): Series-300-P2 - nominal slab geometry

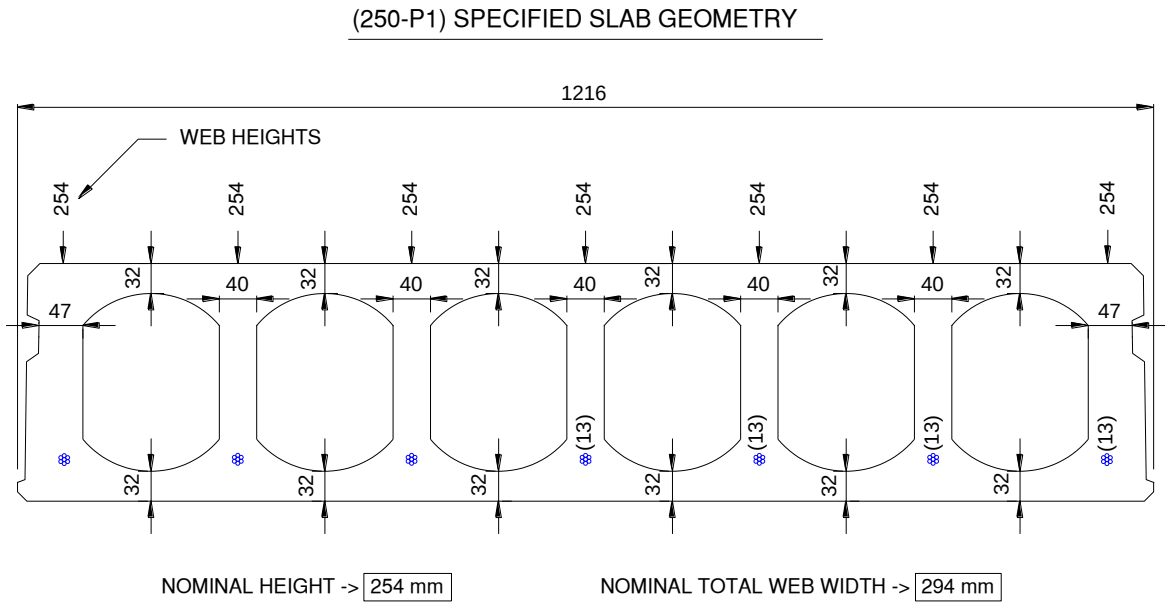


Figure (4.3): Series-250-P1 nominal slab geometry

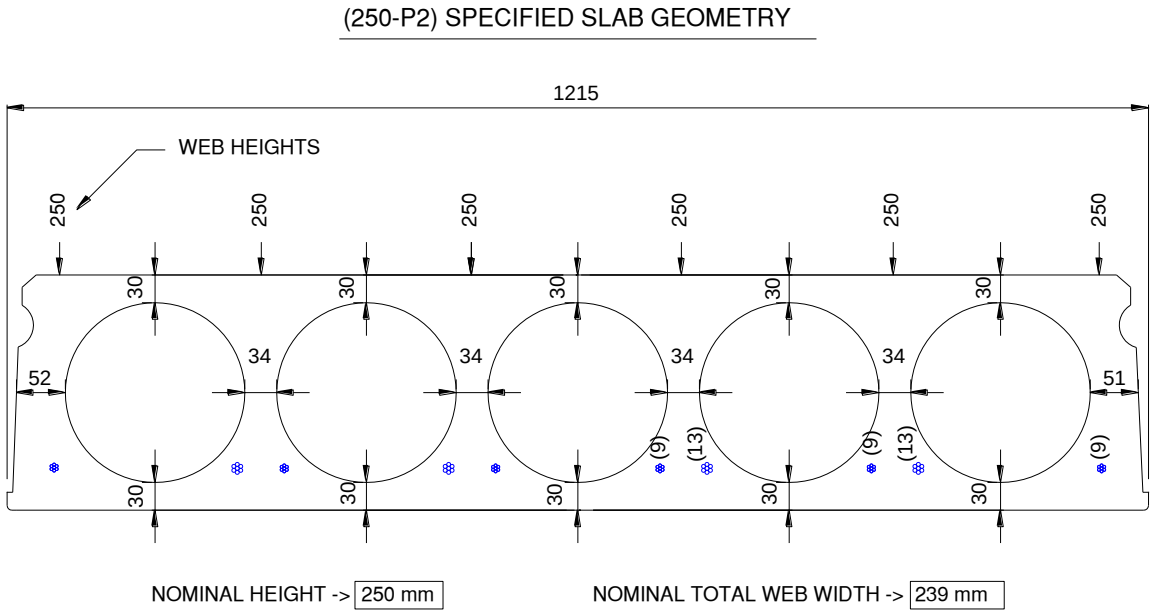


Figure (4.4): Series-250-P2 nominal slab geometry

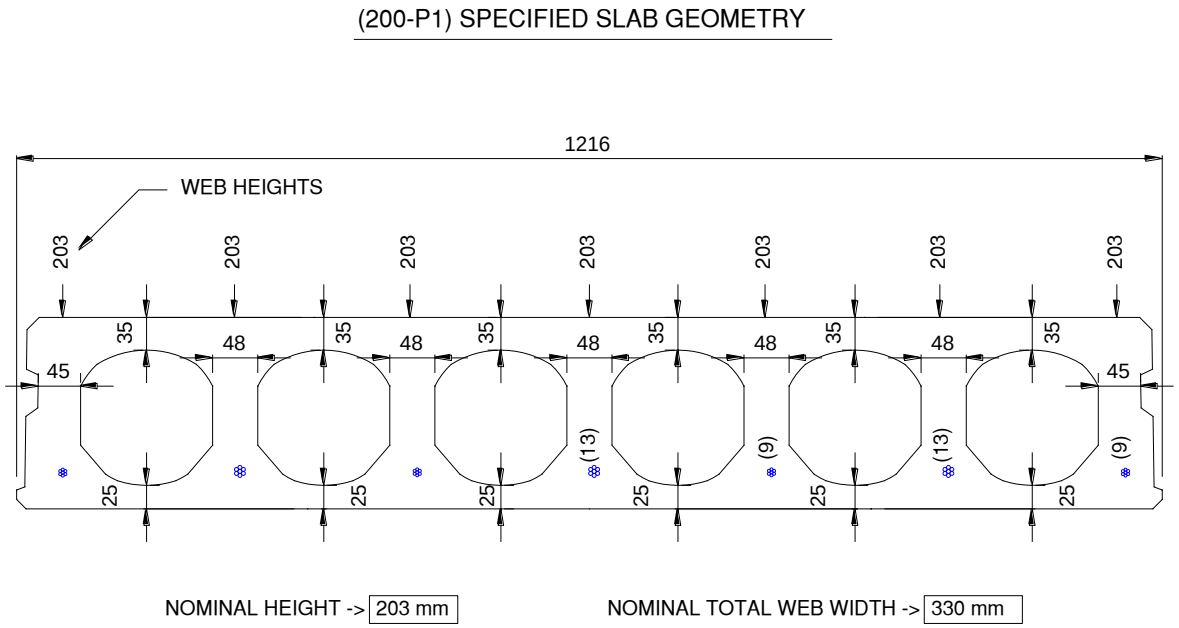


Figure (4.5): Series-200-P1 nominal slab geometry

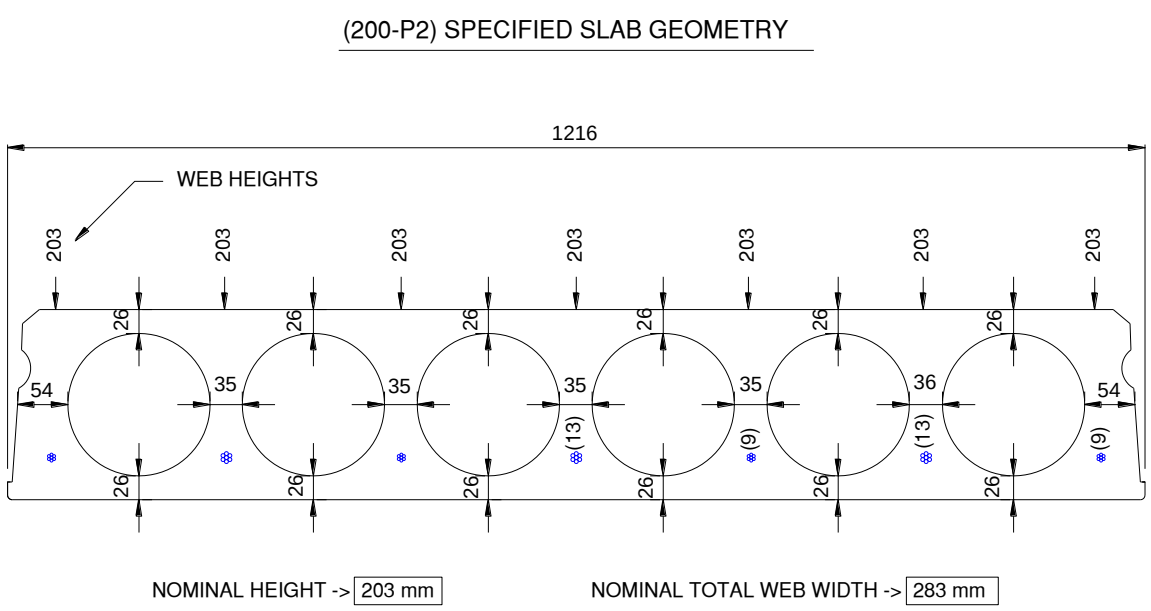


Figure (4.6): Series-200-P2 nominal slab geometry

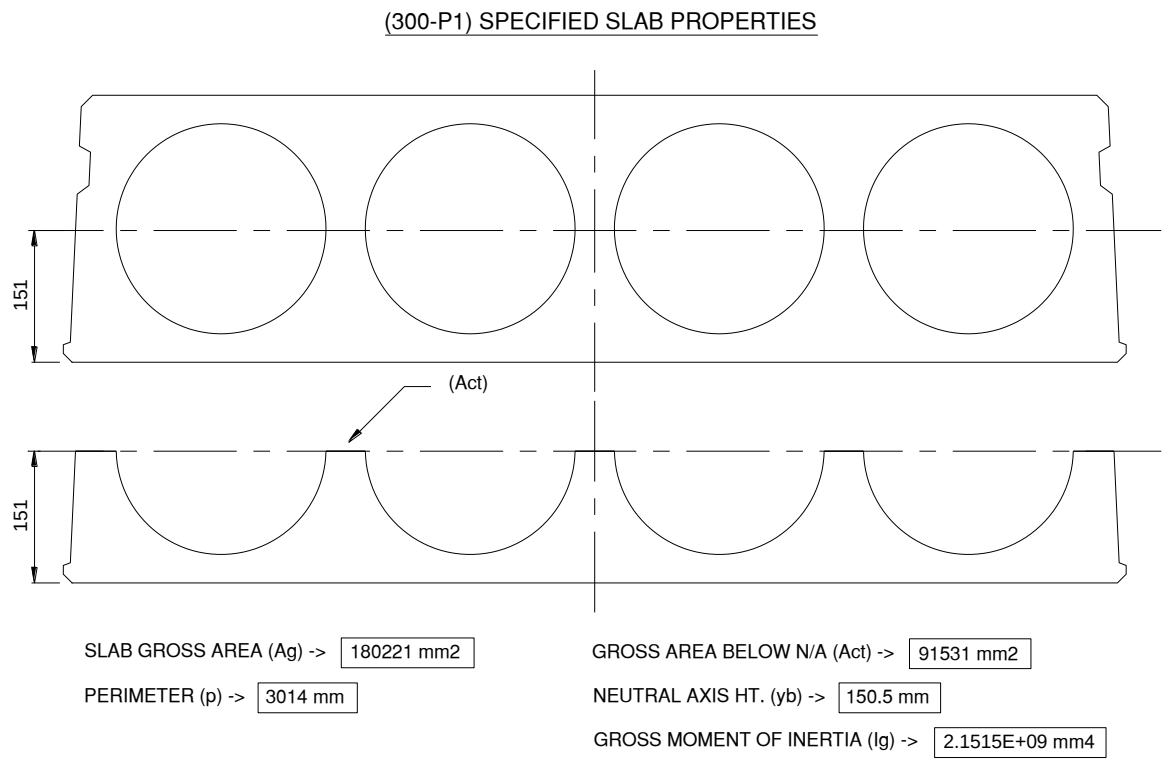


Figure (4.7): Series-300-P1 nominal slab properties

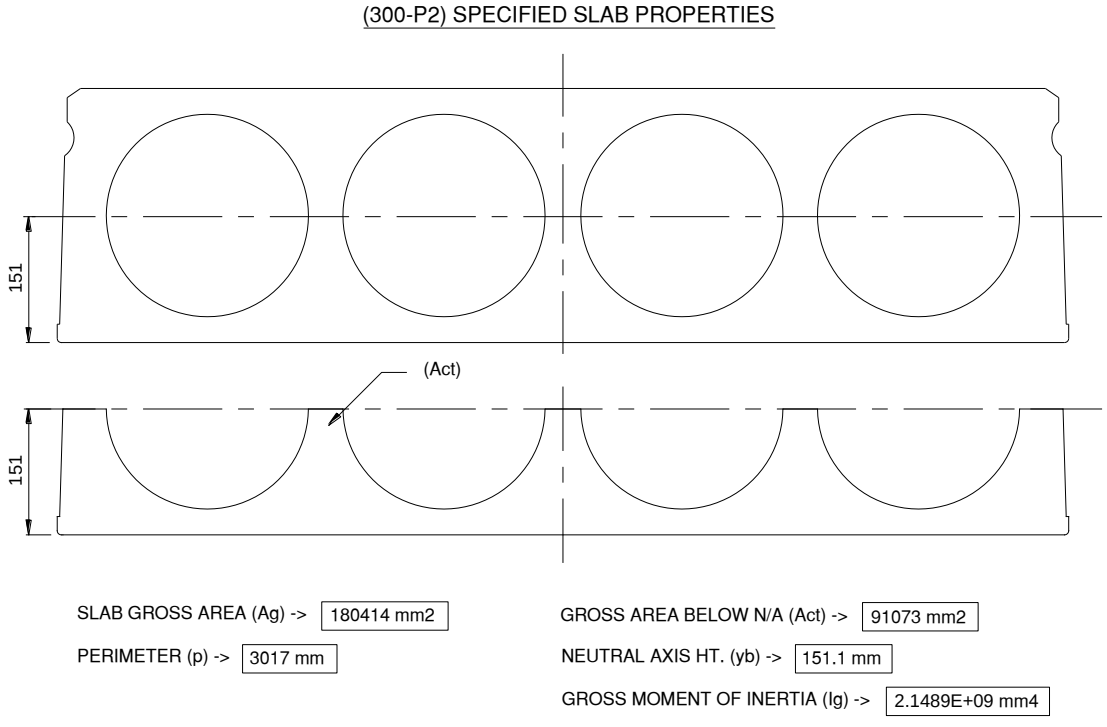


Figure (4.8): Series-300-P2 nominal slab properties

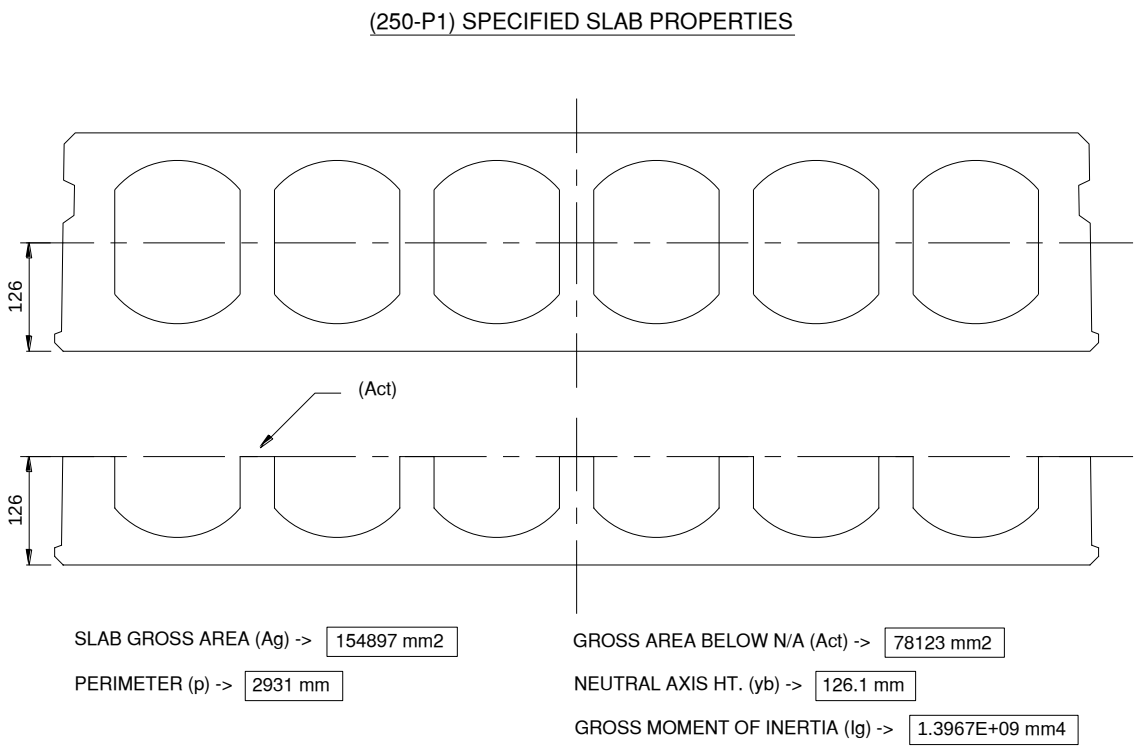


Figure (4.9): Series-250-P1 nominal slab properties

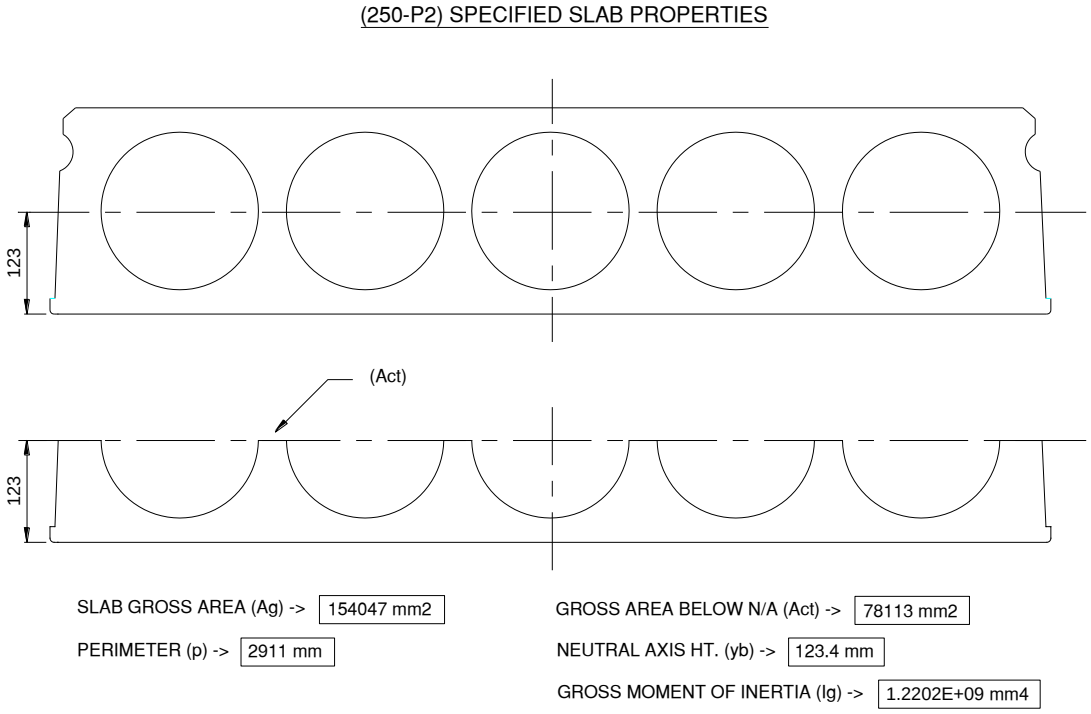


Figure (4.10): Series-250-P2 nominal slab properties

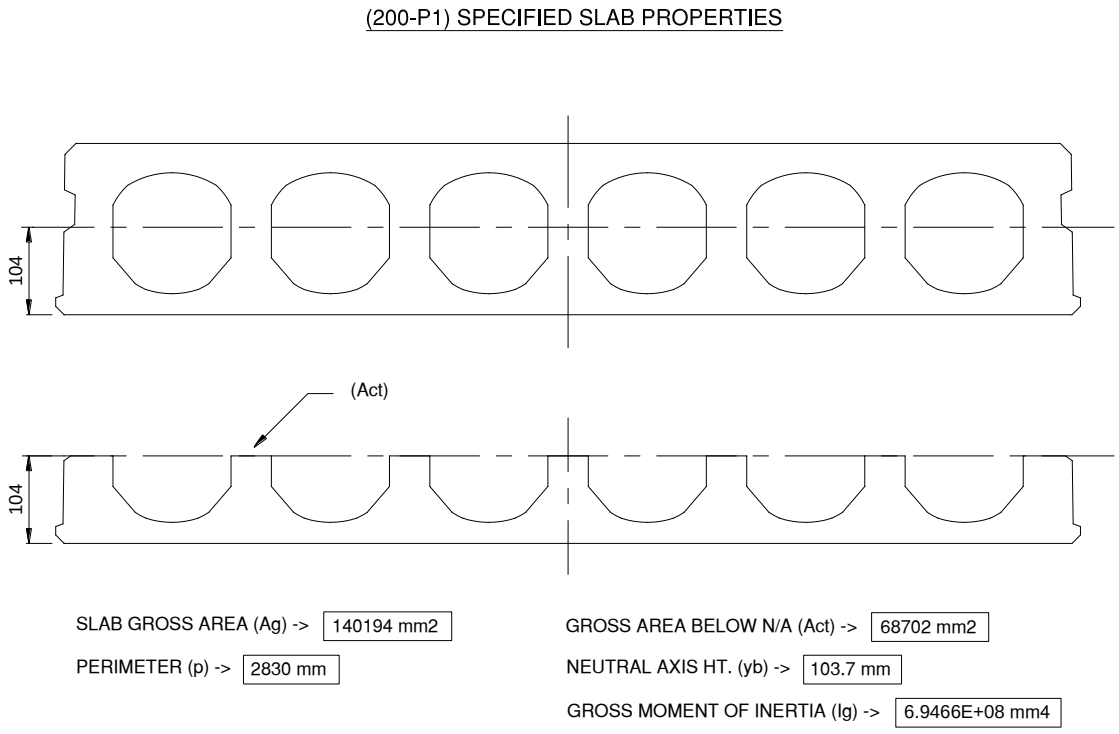


Figure (4.11): Series-200-P1 nominal slab properties

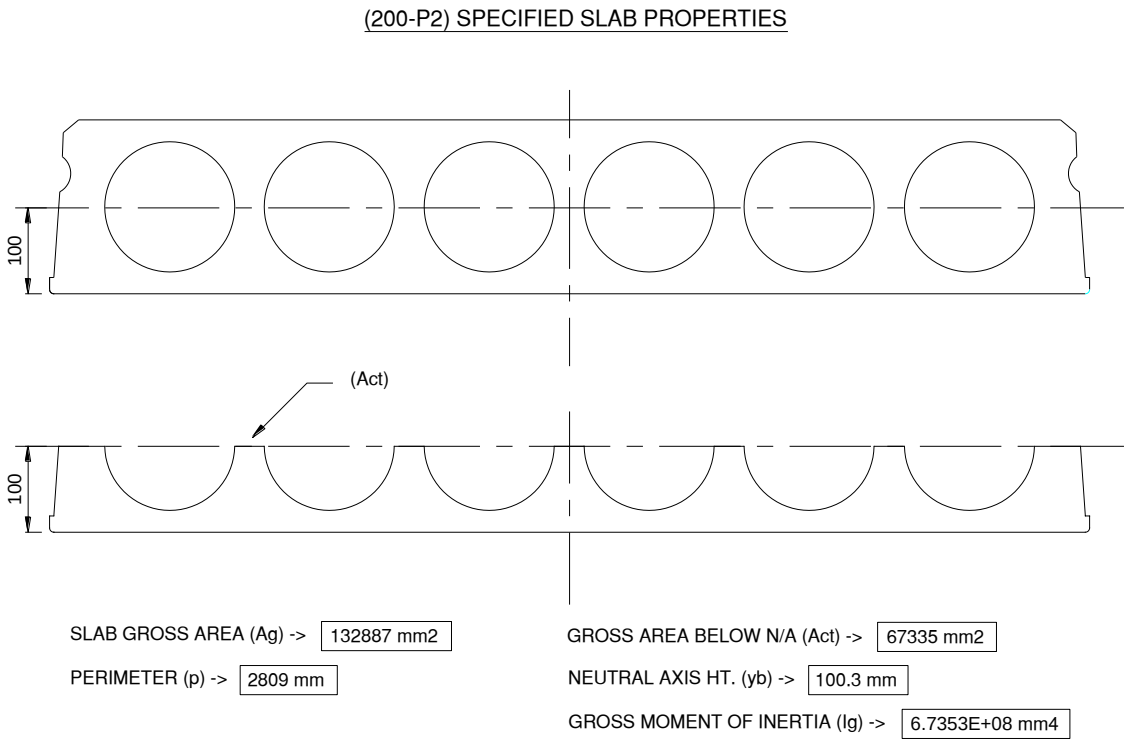


Figure (4.12): Series-200-P2 nominal slab properties

Table (4.3): Nominal vs. experimental sectional properties of tested slabs

| Specimen ID | Average. Height (mm) | Total Web Width (mm) | Slab X-Section Area ($mm^2$) | Flexural Tension Area, $A_{ct}$ ($mm^2$) | Perimeter (mm) | Centre of Gravity Height - $y_{bot}$ (mm) | Gross Moment of Inertia - $I_g$ ($mm^4$) |
|---|---|---|---|---|---|---|---|
| **Series-200** | | | | | | | |
| 200-P1 (Nominal) | 203 | 321 | 140194 | 68702 | 2830 | 104 | 6.9466E+08 |
| 200-P1-A | 201 | 379 | 156179 | 78568 | 2804 | 100 | 7.1463E+08 |
| 200-P1-B | 202 | 388 | 159386 | 80381 | 2809 | 100 | 7.3193E+08 |
| 200-P2 (Nominal) | 203 | 283 | 132887 | 67335 | 2809 | 100 | 6.7353E+08 |
| 200-P2-A | 206 | 313 | 152196 | 75554 | 2820 | 103 | 7.5005E+08 |
| 200-P2-B | 207 | 300 | 150135 | 74839 | 2825 | 103 | 7.5766E+08 |
| **Series-250** | | | | | | | |
| 250-P1 (Nominal) | 254 | 294 | 154897 | 78123 | 2931 | 126 | 1.3967E+09 |
| 250-P1-A | 254 | 338 | 181693 | 89601 | 2912 | 128 | 1.4490E+09 |
| 250-P1-B | 255 | 318 | 179162 | 89249 | 2912 | 127 | 1.4507E+09 |
| 250-P2 (Nominal) | 250 | 239 | 154047 | 78113 | 2911 | 123 | 1.2202E+09 |
| 250-P2-A | 253 | 259 | 175014 | 89189 | 2891 | 124 | 1.3530E+09 |
| 250-P2-B | 254 | 257 | 173778 | 86970 | 2895 | 126 | 1.3588E+09 |
| **Series-300** | | | | | | | |
| 300-P1 (Nominal) | 305 | 229 | 180221 | 91531 | 3014 | 151 | 2.1515E+09 |
| 300-P1-A | 304 | 252 | 206993 | 103107 | 3015 | 151 | 2.3035E+09 |
| 300-P1-B | 302 | 242 | 203193 | 100356 | 3014 | 152 | 2.2839E+09 |
| 300-P2 (Nominal) | 305 | 231 | 180414 | 91073 | 3017 | 151 | 2.1489E+09 |
| 300-P2-A | 303 | 229 | 188725 | 91837 | 2996 | 154 | 2.1798E+09 |
| 300-P2-B | 305 | 234 | 190843 | 93141 | 2995 | 155 | 2.2265E+09 |

## 4.4. Material Properties

### 4.4.1. Concrete

At the production facility, suppliers have taken concrete samples during casting from the same batch used for every set of two slabs of same series to make concrete cylinders. Each supplier prepared 12 standard cylinders (100×150 mm) of which 8 were tested in the manufacturer's facility, 4 at time of release (about 18 hrs) and 4 at 28 days. The last 4 cylinders were shipped with the slabs and tested in the laboratory of the university on the date when each slab unit was tested.

The design concrete strength for the slabs produced by the manufacturers was 28 MPa at 18 hours and 45 MPa at 28 days. The aggregates used in the concrete mix of tested slabs were crushed limestone, with a nominal maximum size of 20 mm. A summary of all concrete strength parameters for each tested specimen can be found in Appendix B.

For the code analysis calculations performed in Chapter 5, the concrete compressive strength at test date was used.

### 4.4.2. Reinforcement

The type of strands used in the tested specimens was seven-wire low-relaxation strands with a design value of tensile strength of 1860 MPa and modulus of elasticity of 196.5GPa. Only two strand sizes were utilized, 9-mm and 13-mm diameter, in the specimens of this experimental program. Actual ultimate strength of strands according to mill certificates was ranging from 1967 to 2075 MPa and their modulus of elasticity from 193 to 200 GPa. However, for the code analysis calculations performed in Chapter 5, a constant average values for strands properties were used for all strands; the ultimate tensile strength ($f_{pu}$) was taken as 2041.4 MPa and the

modulus of elasticity (*E-Value*) was taken as 197.88 GPa. For reference, a summary of the strand properties as retrieved from mill certificates is provided in Appendix C.

## 4.5. Instrumentation

Each slab was instrumented at the loaded end, with strain gauges on two strands, one near the edge and one near the middle. These gauges were mounted directly on the strands by drilling the concrete cover and exposing a small surface of the strand at the specified location. These drilled holes were patched by grout before testing. The steps are also shown by pictures in Figure (4.13) below.

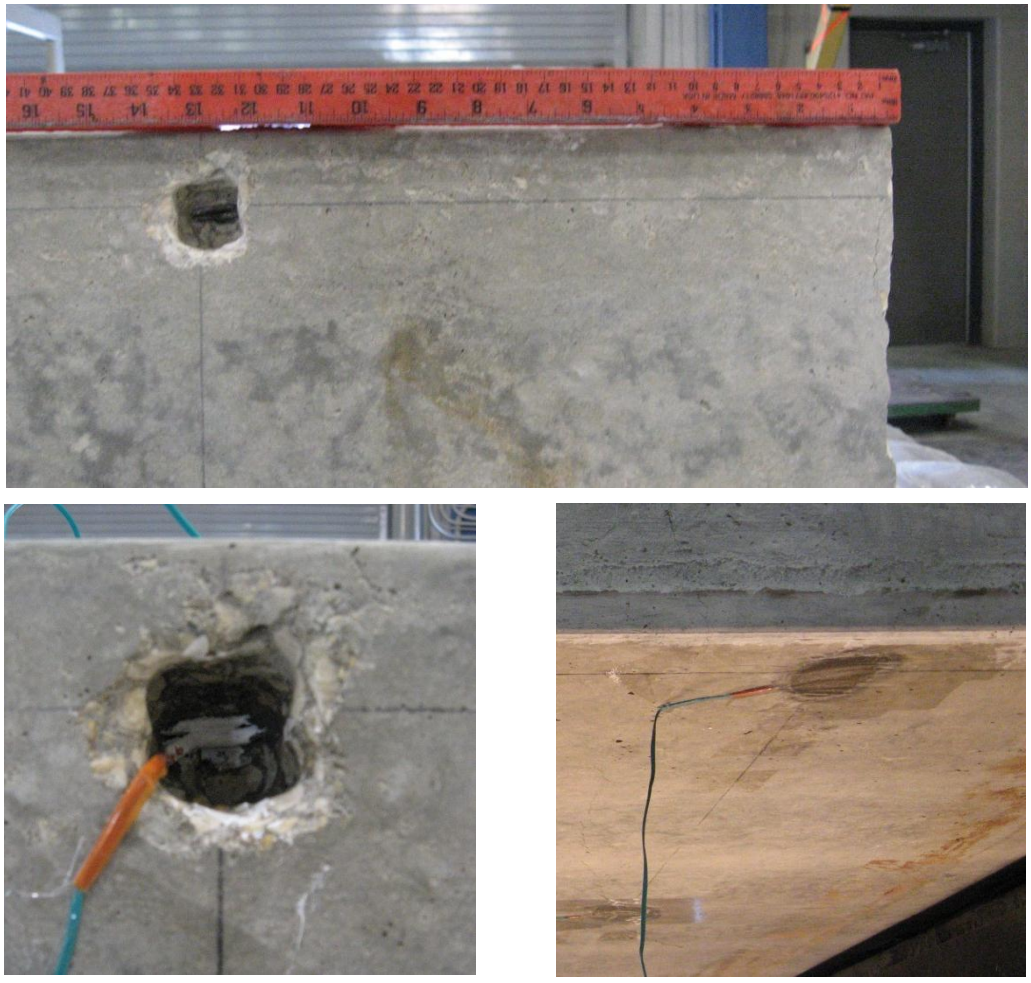

Figure (4.13): Steps used for mounting strain gauges on strands

Also, Four Pi-gauges were installed onto the side of two selected webs (most middle and edge webs) and on the top surface of the same webs. In addition, a linear variable displacement transducer (LVDT) was installed at the end of one strand, which was already instrumented by strain gauge, to measure its end slippage at the loaded end during tests. Figures (4.14 to 4.16) show a sample of those instrumentations used on tested specimens in this project. No instrumentation was used to measure mid-span deflection.

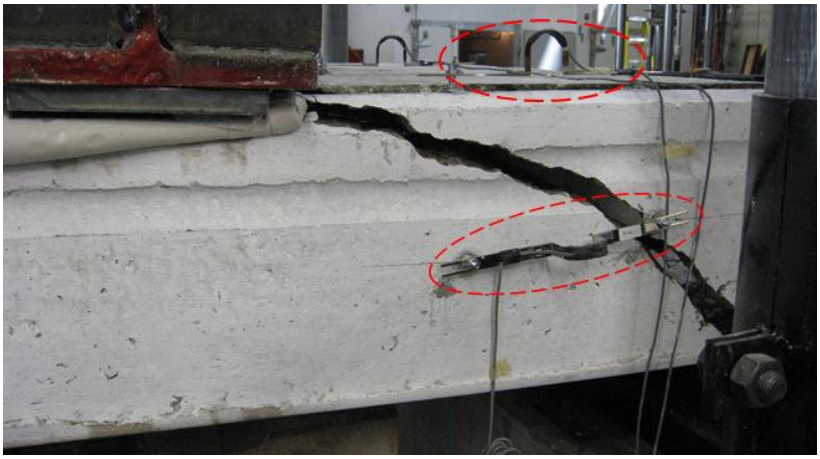

Figure (4.14): Sample view of pi-gauges on edge-web in HC 250-P2-B

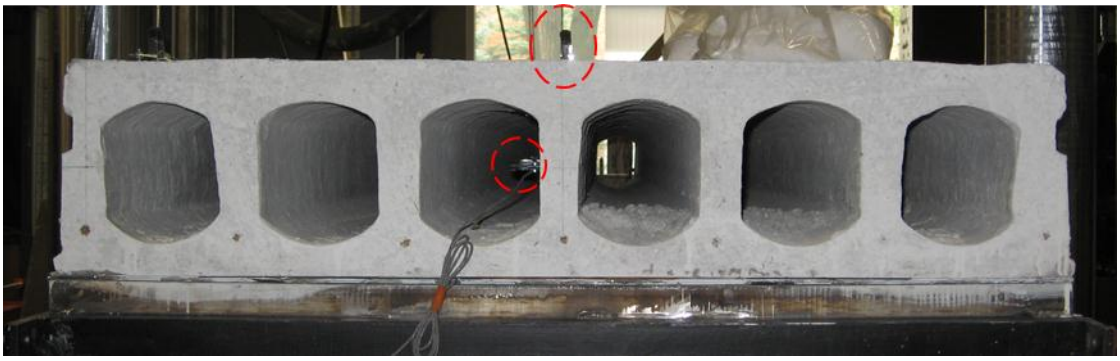

Figure (4.15): Sample view of PI-gauges on mid-web in HC 250-P1-A

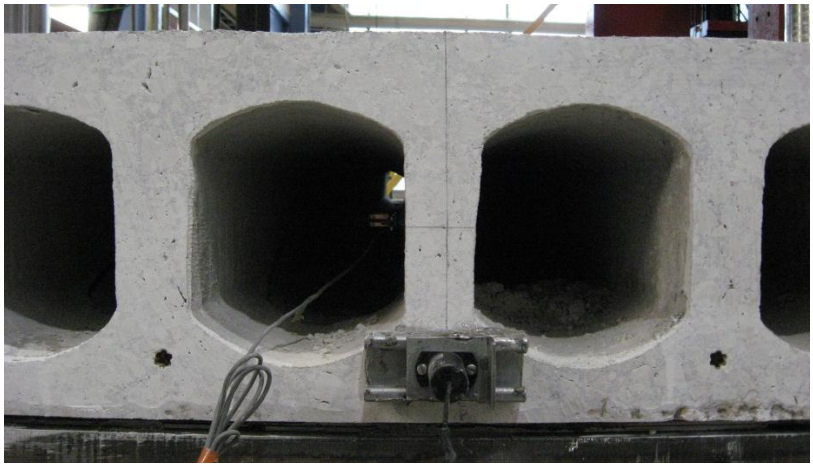

Figure (4.16): Sample view of LVDT for slip measurement in HC 250-P1-A

## 4.6. Test Setup

As there are no guidelines to date in the Canadian or the American codes on full-scale shear testing of PHC slabs, the tests in this experimental program closely followed provisions of the standard shear test method provided in Annex J of the complementary European code for hollow core slabs, EN 1168 (2008). Originally, this standardized test method is being used in Europe as a quality control method for HC slab producers to verify the shear capacity of their slabs in relation to the code-predicted shear resistance. A schematic elevation of the typical test set-up used in this program is outlined in Figure (4.17).

As it is also noticeable in Figure (4.17), the testing standard did not leave the length of test slabs without specification. It has suggested that the span of the test slabs ($L$) shall be 4000 mm or 15$h$, whichever is longer. Consequently, the nominal length for slabs in Series-200 and Series-250 was 4000 mm whereas for slabs in Series-300 it was 4575 mm.

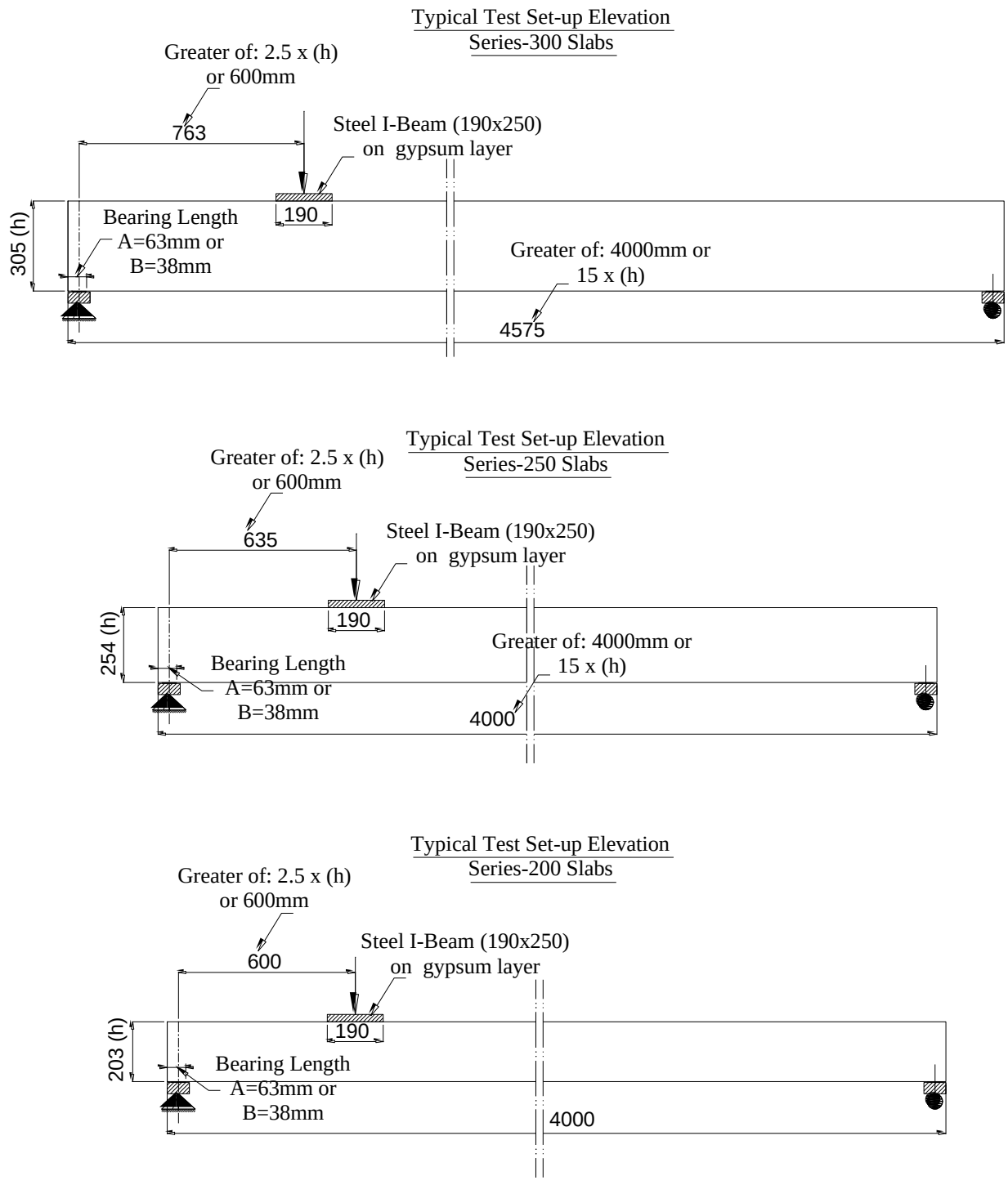


Figure (4.17): Elevation of typical test set-up for full scale shear test

The effect of shear span to depth ratio (*a*/*d*) had been stressed enough during literature review in Section 2.3.5. The suggested position for the load by the standard test method was found to be

very suitable for evaluation of inclined shear carcking resistance as also supported by previous research findings. Accordingly, in this research program, a concentarted line load was applied at *a/d* equal to 2.5*h* or 600 mm, whichever is greater. The selection of concentrated type of loading was again based on the recommendations of the testing method and also since it is the most common approach used by majority of researchers who studied shear capacity in PHC slab. Moreover, unlike uniform loading, concentrated load ensures a constant shear forces value all over the zone from loading point till the supported end, where the weak sections in shear are expected. In case of specimens tested on full bearing length (A), the specified distance of the load was measured from centerline of the support as shown in Table (4.4) and then distance of the load to end of the slab was used as a reference for specimens tested on reduced bearing length (B), where the distance of the load was measured from end of the slabs.

Table (4.4): Ratio of *a/d* for nominal test slab depths with full bearing length at loaded end

| Series | Slab Bearing Length at Test End (mm) | * Nominal Depth to Strands, *d* (mm) | Shear Span, *a* (mm) | Shear Span-to-Depth Ratio *(a/d)* | Shear Span-to-Height Ratio *(a/h)* |
|---|---|---|---|---|---|
| Series-300-P1 | 63 | 255 | 763 | 2.99 | 2.50 |
| Series-300-P2 | | 255 | | 2.99 | 2.50 |
| Series-250-P1 | | 209 | 635 | 3.04 | 2.50 |
| Series-250-P2 | | 207 | | 3.07 | 2.54 |
| Series-200-P1 | | 159 | 600 | 3.77 | 2.96 |
| Series-200-P2 | | 158 | | 3.80 | 2.96 |

** Note: depth of strands is measured to the equivalent centroid of all strand layers*

The support condition was a pin at the end which is nearest to the load and roller on the opposite end, so that no axial forces are generated by rotation and restraint of the slabs at the support. Moreover, the slabs were loaded at the specified distances with a stiffened 254-mm deep by 190-mm wide I-section steel beam across the full width of the cross-section (Fig. 4.18). The width of

the loading beam emulates the width of a load-bearing concrete masonry wall – a common case of partition walls supported on slabs. To prevent load concentration and to ensure that load was uniformly distributed across all webs during loading, a layer of plaster was placed between the slab and the loading I- beam. Figure (4.19) shows how the plaster effectively forms a uniform surface for loading. Also, neoprene pads were placed between the slab and the support steel plates for same purpose.

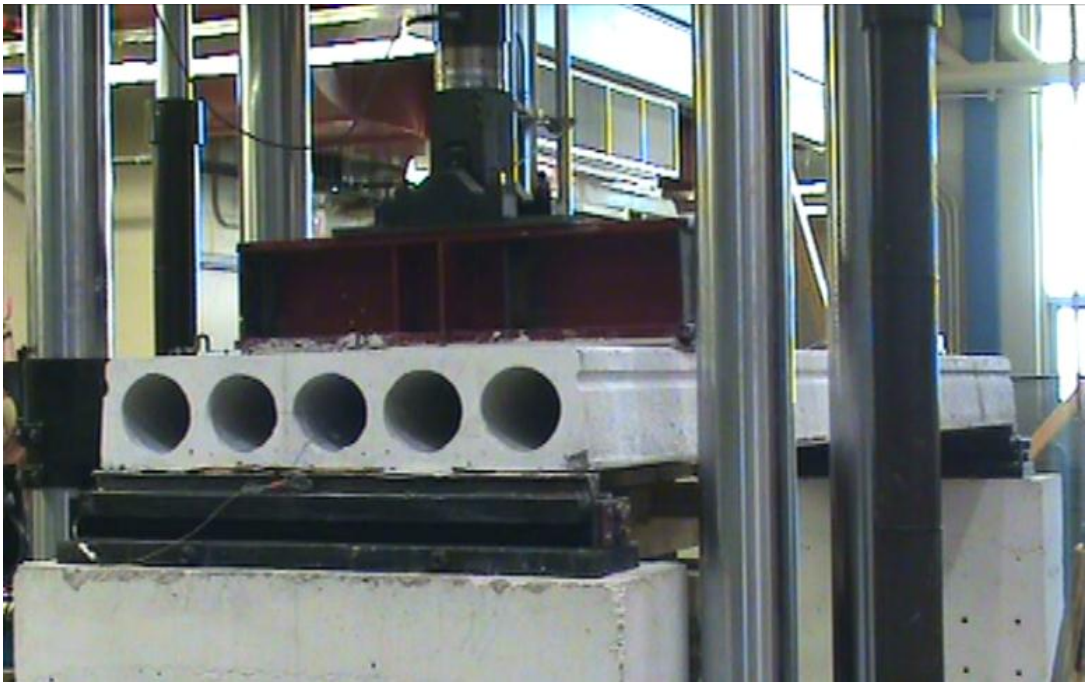

Figure (4.18): Typical view of the test set-up used in experiments

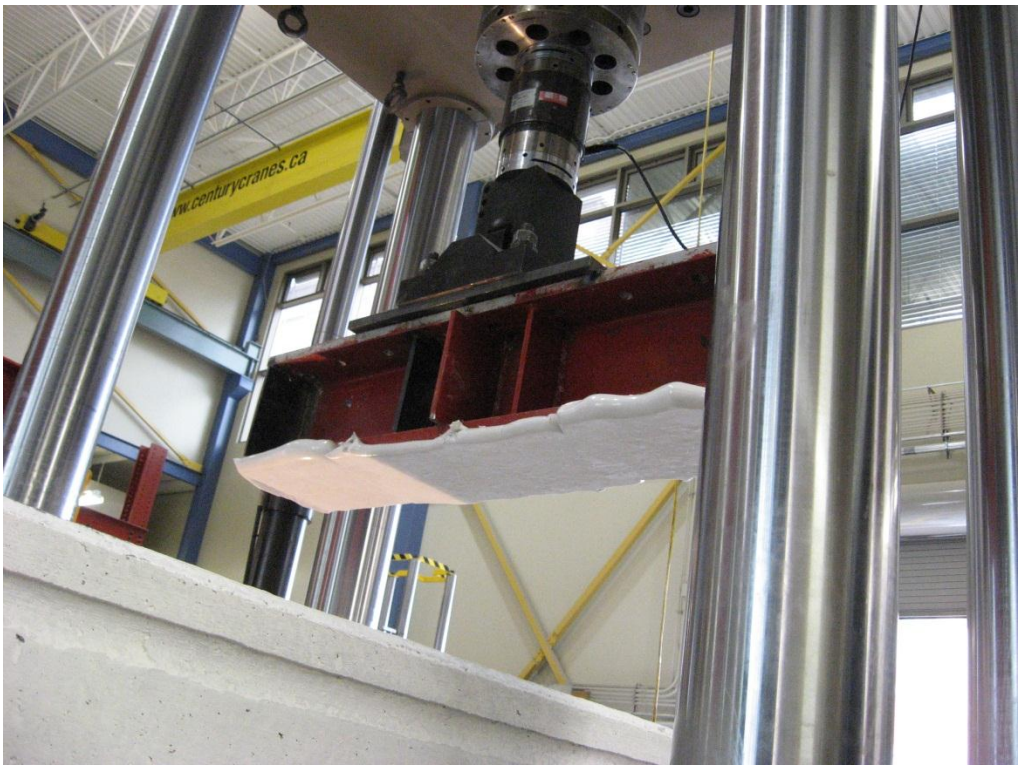


Figure (4.19): View of loading I-beam with plaster layer evenly distributed

The length of bearing in this research program is defined as the distance from the end of the slab to the face of the bearing pad at the loaded end. The full bearing length (A) was 63 mm which represents the standard recommended bearing length while the reduced bearing length (B) was 38 mm and it represents the non-conforming (as-built) site conditions. Figure (4.20) displays close views of the supports at the loaded end. The length of bearing at the other end of the test load was always 63 mm for all cases.

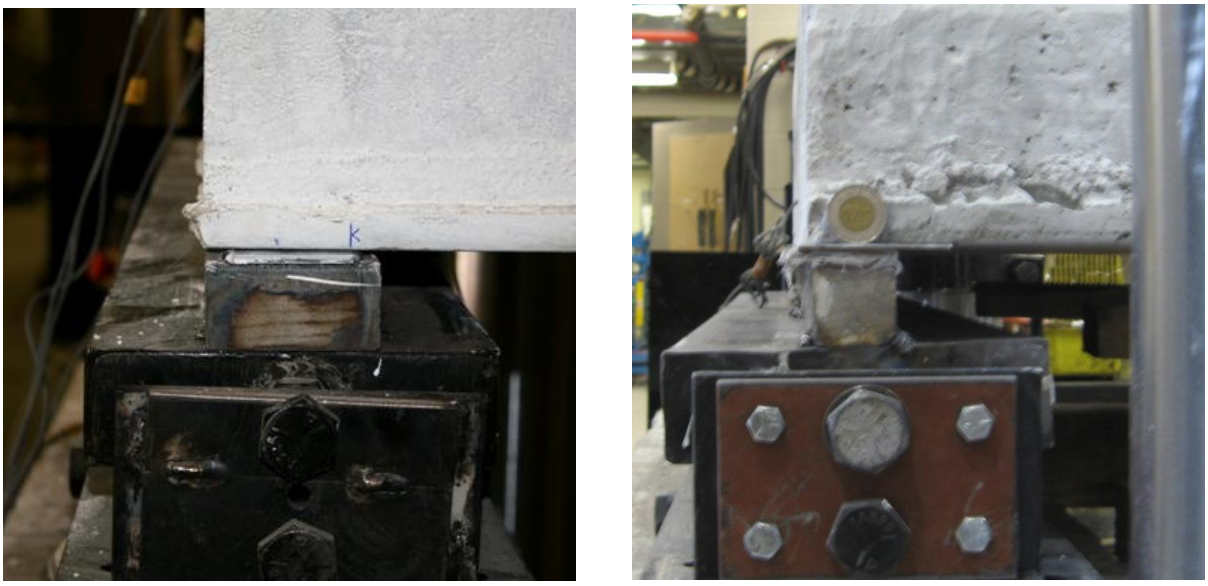

Figure (4.20): Views for loaded end supports (right, full bearing length "A" and left, reduced bearing length "B")

## 4.7. Loading Procedure

The standard shear test method that is followed in this research program suggested that the testing load shall be applied as repeated loading in two cycles. The amplitude of the loading in the first cycle should be at least 70% of the predicted failure load. In the second load cycle, the load should be increased until failure is reached.

Therefore, in this experimental program, the specimens were initially loaded up to 120 kN, which represents about 70% of the predicted failure load. After this first cycle the load was totally released. Then, in the second cycle, the load was increased up to failure. A 5000-kN capacity MTS testing machine was used to apply the load under a load-controlled rate of 20 kN/min.

# CHAPTER 5: EXPERIMENTAL RESULTS AND CODES ANALYSIS

## 5.1. Experimental Results

### 5.1.1. General

The objective of this section is to summarize the experimental results for the tested specimens. The performance of the slabs at different loading stages is assessed and discussed in terms of capacity, mode of failure, crack profile and observed location of critical section for shear. The effect of the experimentally investigated variables on final shear capacity of the tested slabs is also discussed. In addition, typical measurements from instrumentation used on concrete surface and on strands during the third final loading cycle are presented.

### 5.1.2. Crack profiles and the observed location of shear critical section

After testing of each slab, the crushed and spalled concrete of tested end was removed to enable tracing the bottom crack profile on a card board. Also, lines of shear failure for all webs in the slab were accurately measured by vertical and horizontal coordinate points from a certain datum line. Later these measurements and tracings were plotted. In Figures (5.1 to 5.3) the crack profiles of all webs in every tested slab unit in the three series; 200, 250 and 300 were compiled and plotted on one elevation for each slab. In case of the specimens which failed in flexure or flexural-shear, it was difficult to remove the failed end from the slabs and consequently no drawings of crack profile have been made for two specimens, instead a picture of the tested end were shown in Figure (5.3).

Together with the presented web-shear crack profiles, the specified location of critical section for shear failure according to provisions of each code was also highlighted on every slab elevation. The locations of failure predicted by CSA code were typically further from end of the slab than those predicted by ACI code. It is noticeable that the furthest location of web-shear cracking was

observed experimentally in Series-250 in case of the two non-circular voided slabs (250-P1-A and 250-P1-B). In fact, all of the three codes were not successful in predicting the location of failure for these two specimens. Moreover, this experimental observation does not comply with conclusions from FEM study performed by Yang (1994), summarised in Section 2.3.3.4, which stated that slabs with non-circular voids tend to have a lower web-shear capacity than similar circular voided slabs because, as claimed, the shear critical point lies more closer to the support. In general, EN 1168 code was the closest and most realistic in predicting the location of web-shear failure when compared with experimental crack profiles.

It is worth to mention that uneven/scattered web-shear cracking lines could be an indication of shear lag (failure of individual webs before or after other adjacent webs in the same slab) and normally that would be reflected on a discrepancy in level of measured load at which each web cracked.

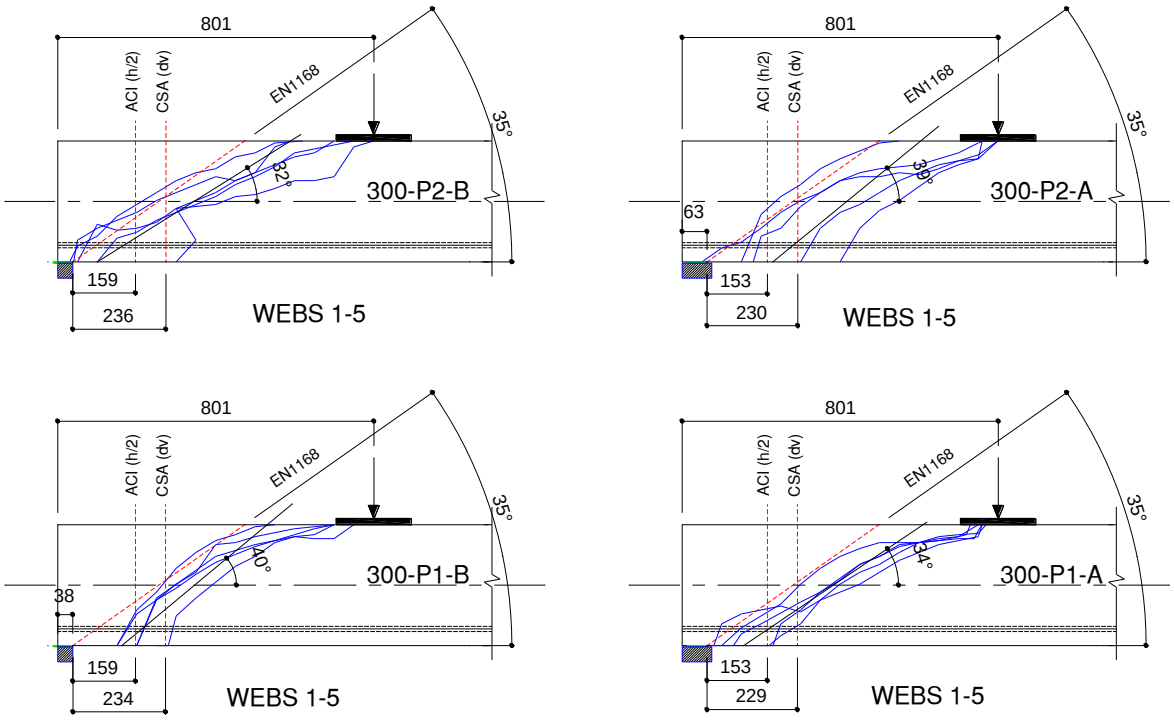


Figure (5.1): Crack profiles and codes predicted location of shear failure in Series-300 slabs

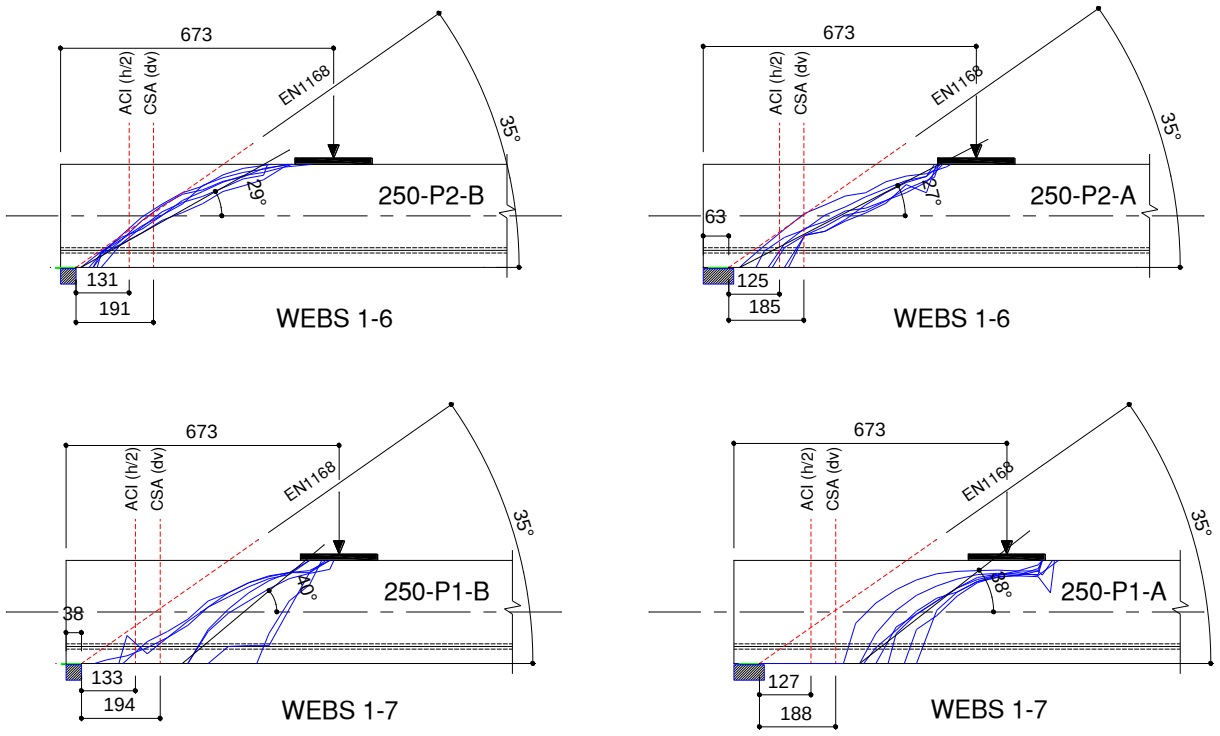


Figure (5.2): Crack profiles and codes predicted location of shear failure in Series-250 slabs

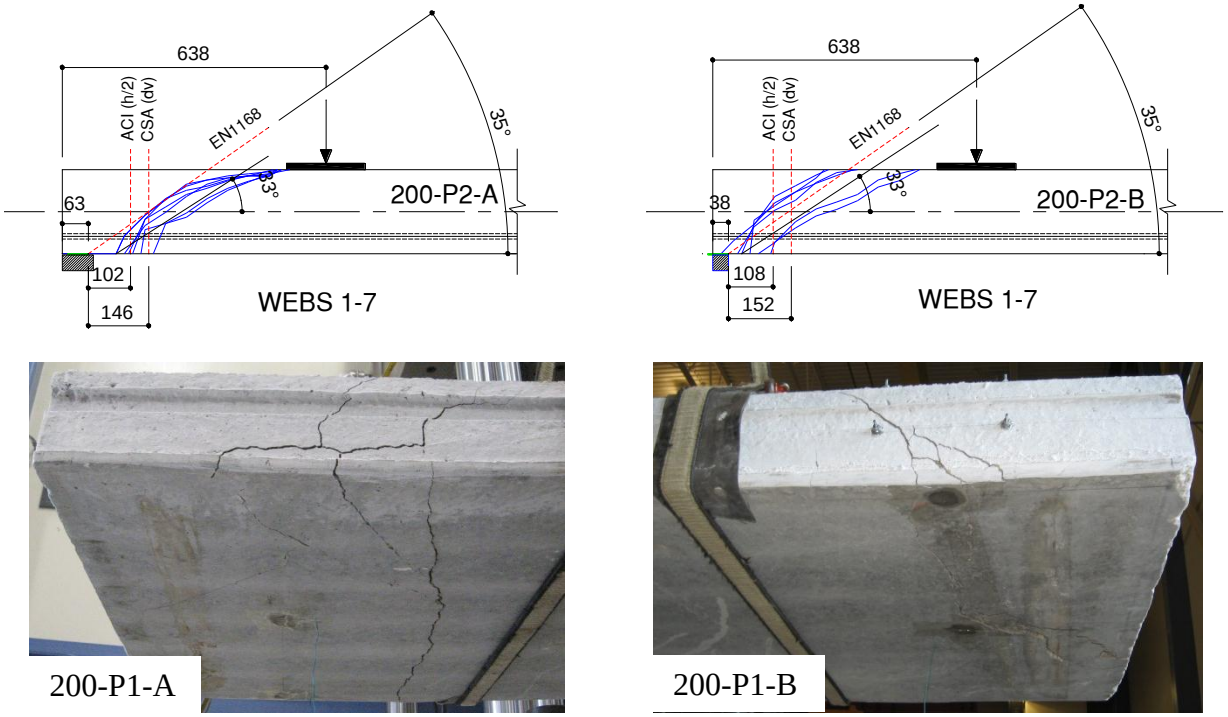


Figure (5.3): Crack profiles and codes predicted location of shear failure in Series-200 slabs

### 5.1.3. Inclination of web-shear cracks

One further useful information which was derived from the crack profiles presented in Figure (5.1) to Figure (5.3), was the observed angle of web-shear failure for each of the tested slabs. The average angles of inclinations were obtained by plotting a straight line from bottom of the slabs that is approximately parallel with the slope of all web crack lines at the mid-height level of the slabs. The angle between the plotted lines and bottom of the slabs were then measured as summarised in Table (5.1) below.

Table (5.1): Experimentally-observed shear crack angles

| Slab ID | Average Experimental Shear Failure Angles (degrees) |
|---|---|
| 300-P1-A | 34 |
| 300-P1-B | 40 |
| 300-P2-A | 39 |
| 300-P2-B | 32 |
| 250-P1-A | 38 |
| 250-P1-B | 40 |
| 250-P2-A | 27 |
| 250-P2-B | 29 |
| 200-P1-A | N/A |
| 200-P1-B | N/A |
| 200-P2-A | 33 |
| 200-P2-B | 33 |

### 5.1.4. Effect of the parameters considered in the experimental program

For sake of easier comparison, the experimental shear capacities (*Vexp*) for each tested specimen as calculated from the applied maximum testing load (*P-test*) by the machine on each specimen before failure are presented in summary tables Table (5.2, 5.3, and 5.4) in Sections 5.2.2 to 5.2.4 for the comparison with each code's prediction. The values of *Vexp* may vary from a table to another since they were calculated specifically for comparison with each code at the same

specified critical location by each considered code; definitions of critical section for shear resistance was reviewed in Section 3.3. However, the ratio between different values of *Vexp* will not be affected since they are derived from the same *P-test* identified for each specimen. In the following sections, the influence of three experimental variables, which were considered in this program, on the observed shear resistances (*Vexp*) of the tested slabs is discussed.

#### *5.1.4.1. Effect of void shape*

Experimental results could imply that non-circularity in void shapes appears to have some positive effect on shear capacity of PHC slabs in Series-200 and Series-250. The enhancement in shear resistance of non-circular voided slabs compared to their counterparts with circular voids was approximately 4% in Series-200. However, in Series-250, this percentage reached 49%. The reason behind the significant influence of void shape observed in Series-250 could be attributed to the differences in the effective concrete area in shear resistance of each slab. Therefore, the influence of void shape was evaluated by calculating the shear stresses at failure load rather than the ultimate shear force. Figure (5.4) shows the effect of void shape on the maximum achieved shear stress at failure. The specimens were divided into four groups to compare slabs with similar thickness and bearing length. It can be seen that the circular void shape in Series-200-P2 slabs improved the capacity compared to the non-circular ones. The highest shear stress was achieved by the non-circular void shape of Series-250-P1 slabs.

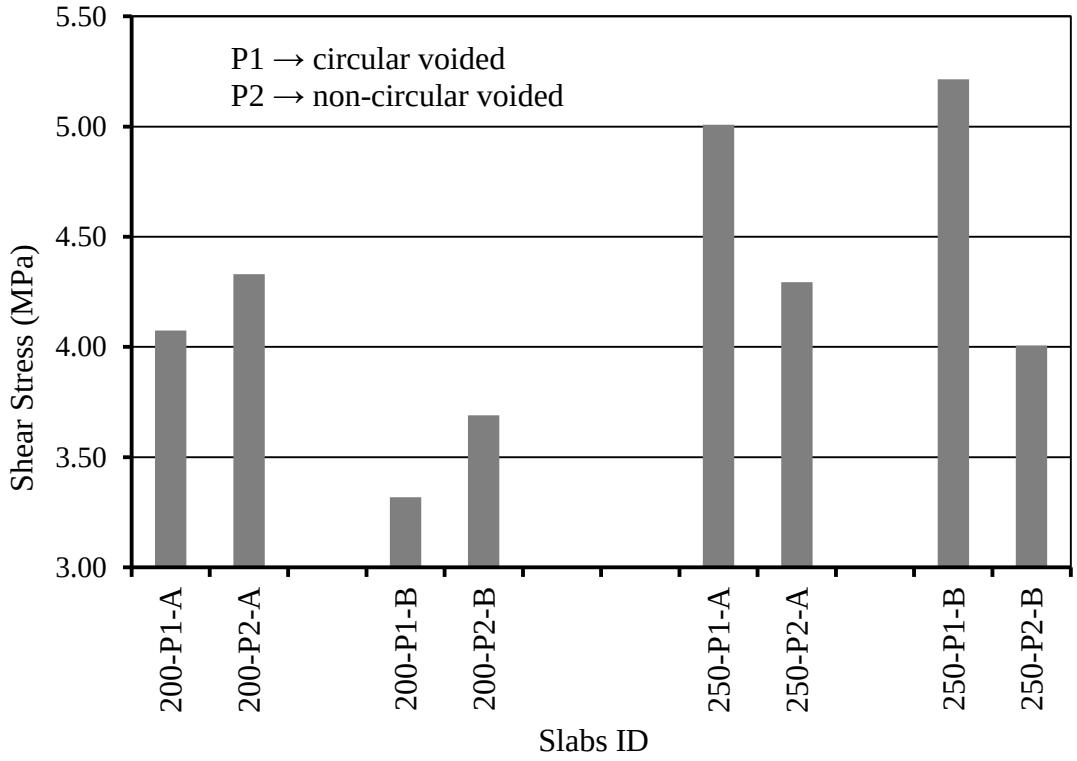


Figure (5.4): Void shape effect on the shear resistance of tested specimens

### *5.1.4.2. Effect of support bearing length*

The experimental shear capacities of tested slabs outlined in (Tables 5.2, 5.3, and 5.4) indicated that a noticeable amount of reduction might actually happen in shear capacity if less than standard bearing length was practiced. By considering the standard full bearing length (*A*) as the control, the observations regarding effect of the bearing length as derived from experimental results could be summarised in the following:

- In Series-200 slabs, the percentage of reduction in shear capacity due to reduced bearing length was in the range of16 % to 17%.
- In Series-250 slabs, the reduction due to reduced bearing length was in the range of 1% to 9%.

- In Series-300 slabs, the percentage of reduction in shear capacity due to reduced bearing length was in the range of 17% to 35%.

In the previous phase of this research program conducted by Truderung (2011), a typical reduction in shear capacity was found to range from 1.0 to 14.0% due to reduction of bearing length from 63 mm to 38 mm. This, along with observations from the current study, raises concerns about the safety of PHC with reduced bearing length due to non-conforming conditions in the construction site.

#### *5.1.4.3. Effect of slab thickness*

To be able to investigate the effect of slab thickness on shear capacity, it was assumed that all slabs have the same prestressing level and concrete strength. These two assumptions seem to be reasonable since the difference in prestressing level among the specimens in this phase of the research program was not very significant (ranged from 5.13 MPa in Series-300 to a maximum value of 6.88 MPa in Series-200) and concrete strength (63 MPa to 78 MPa) is insignificant and can be ignored.

The effect of slab thickness (size effect) on the experimental shear capacity of slabs with circular voids was studied by dividing the specimens into two groups to eliminate effect of bearing length as shown in Figure (5.5). Moreover, the comparison was based on the shear stresses at failure (failure load divided by area of the webs) to eliminate the influence of void shape on the ultimate capacity. It can be seen that in the group of slabs tested with length of bearing A, the size of 300 mm was more efficient for shear resistance. However, the size of 250 mm was found to be better in the second group of slabs tested with length of bearing B. Therefore, more testing is suggested to better investigate this parameter.

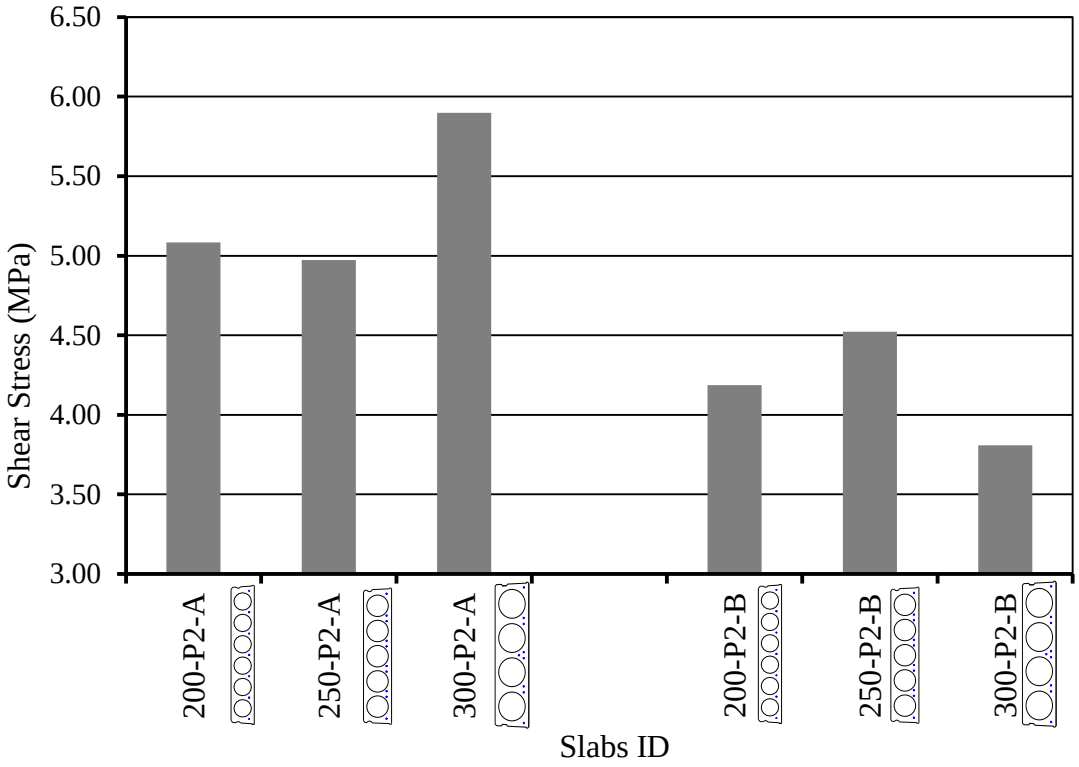


Figure (5.5): Size effect on shear resistance of the tested specimens

### 5.1.5. Load-strain variation in concrete

As discussed in the previous chapter, two sensors of pi-gauge type were attached on the surface of concrete at middle of slabs thickness to monitor strains due to normal stress on webs during loading. Figure (5.6) and Figure (5.7) are showing those typical measured strains in the slab specimens. The distance of the gauge centre from end of slab was decided to be in the mid-point of the shear span. It seems that because the gauge in case of slab 250-P1-A was installed closer to the support, the shear crack occurred outside the gauge length. The gauges showed negative strains instead of tension unlike the other two slabs.

The measured strains in the webs of slab 250-P1-A have linearly increased with load until failure, which was due to web-shear mode. This implies that the slab must have failed instantaneously when cracks started in webs; following, accurately, the theoretical behaviour of

web-shear. However, in strains measured on slab 300-P1-A, which had also failed in web-shear, it can be seen that the edge web of the slab were cracked at approximately 275 kN and the middle web at 255 kN, but yet, the slab was able to resist further shear load even post cracking and finally failed at 315 kN. Another reason for no identifiable cracking symptom in web strains of slab 250-P1-A could be because the crack did not pass through the 200 mm gauge length of the pi-gauge sensor.

To have the inclined cracks forming farther from the support/end as in case of slab 250-P1-A than it was in case of slab 300-P1-A, shown in Figure (5.1) and Figure (5.2), should be an advantage since it provides more anchorage length that is necessary for post cracking web-shear resistance. There is clear evidence that slab 250-P1-A had a higher capacity; however, it is still questionable if that was due to the benefit of longer anchorage length or not.

The sensor readings for the edge web of slab 200-P1-A do not seem very conclusive but strains in the middle web were linear until 188 kN at which flexural cracking occurred.

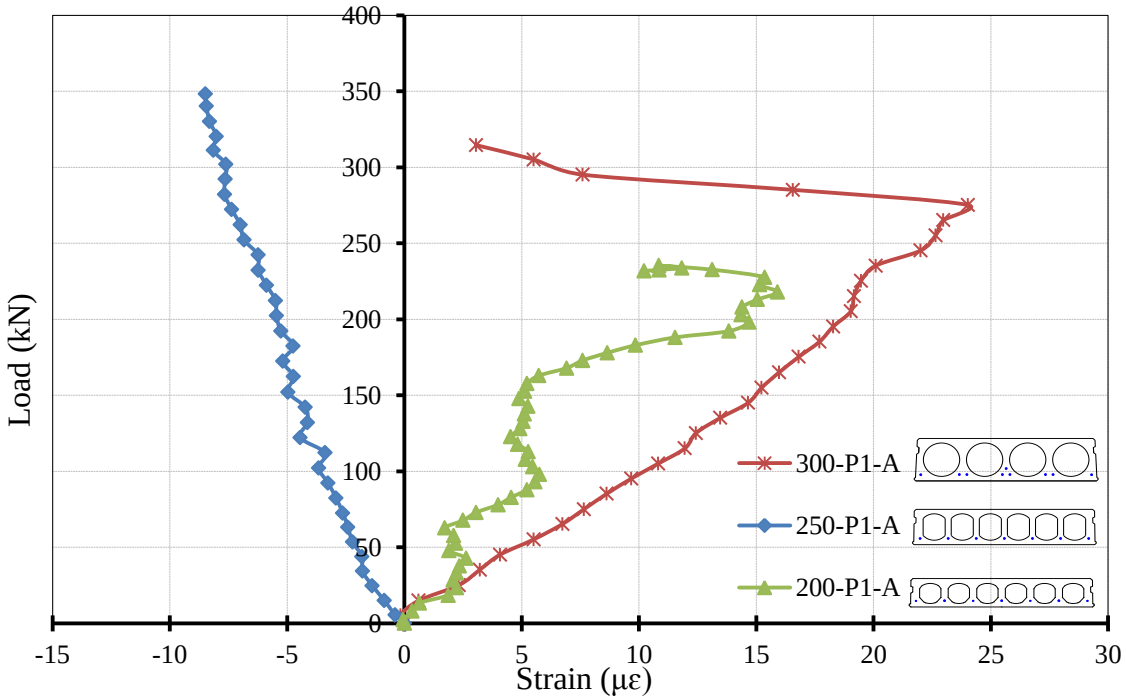


Figure (5.6): Variation of strain with load at edge web (PI#1 Ed-Web)

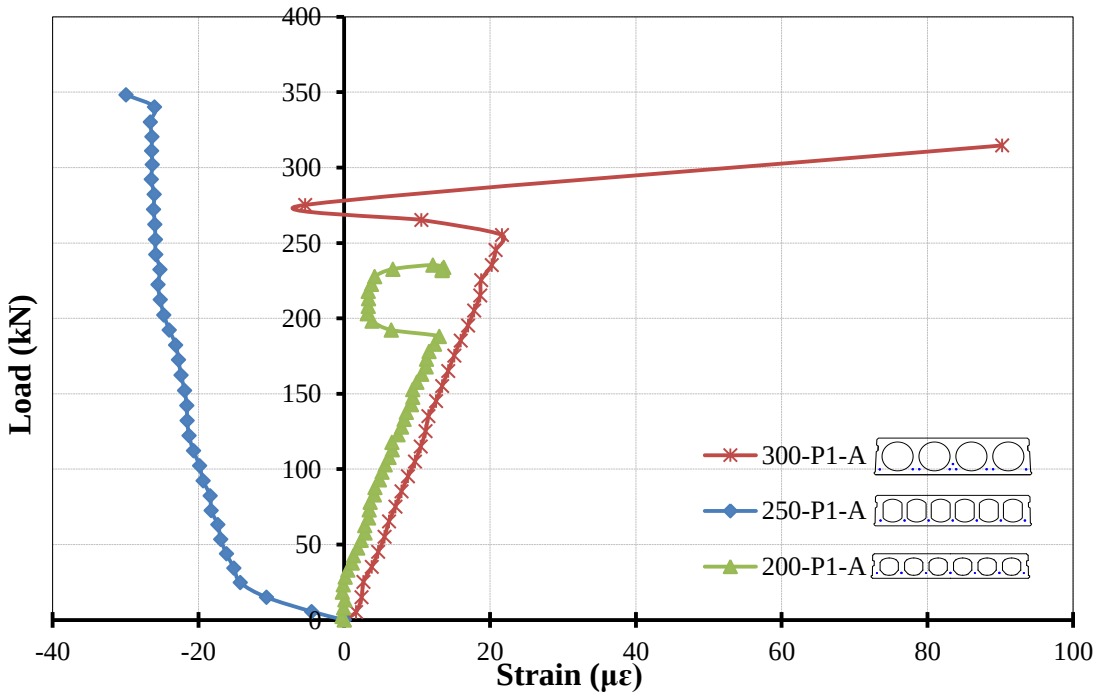


Figure (5.7): Variation of strain with load at middle web (PI#3 Md-Web)

Another two pi-gauge sensors were attached on the upper surface of the slabs; i.e. on the surface of flanges for the same webs which were discussed above. Theses gauges were at the same distance from end of the slabs as specified for the web gauges. The sensors were monitoring the flexural normal strains at upper extreme fibres of the section as shown in Figure (5.8) and Figure (5.9). All strain measurements on the top surface of the slabs were showing compression as expected. Furthermore, the measured values of strains were far from ultimate crushing strain level of concrete in all of the three specimens. This means compression failure of concrete above neutral axis was not the governing factor for the ultimate capacity even in the case of flexural failure of slab 200-P1-A.

The cracking load for the edge web of slab 200-P1-A, which was not recognized from Figure (5.6), is clearly interpretable, now, from Figure (5.8) as 188 kN and that is in agreement with the load concluded from Figure (5.7) for the middle web. This indicates that cracking occurred simultaneously in all webs of this slab without lag as it seems occurred to webs of slab 300-P1-A. For this particular specimen, it was observed that the considered pi-gauge on top of middle web was detached from the specimen when the inclined shear crack initiated. Therefore, once the gauge become free it returned to its initial gauge length while the DAQ (data acquisition system) was still recording the remaining machine load and that would be the explanation for the behaviour seen in Figure 5.9 in the curve of slab 300-P1-A.

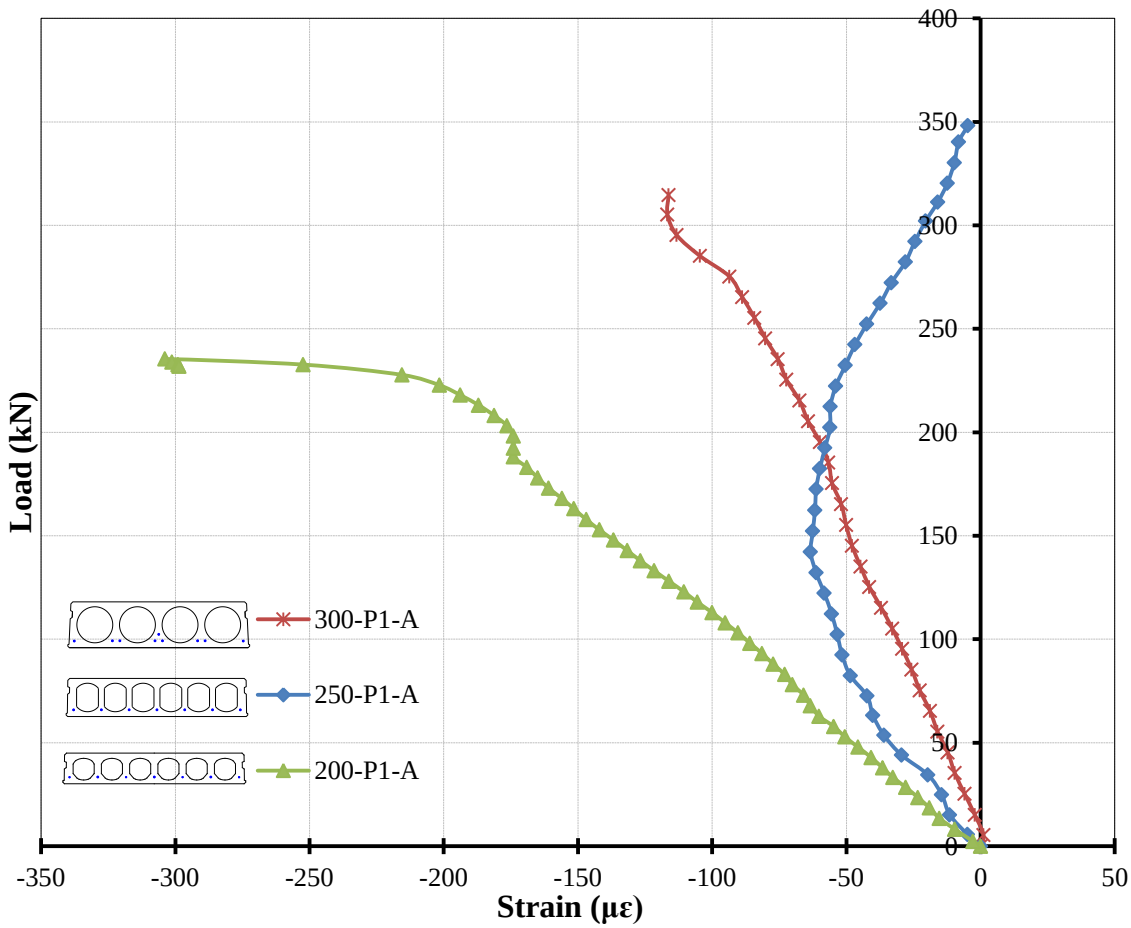


Figure (5.8): Variation of strain with load at top flange of the edge web (PI#2 Ed-Top)

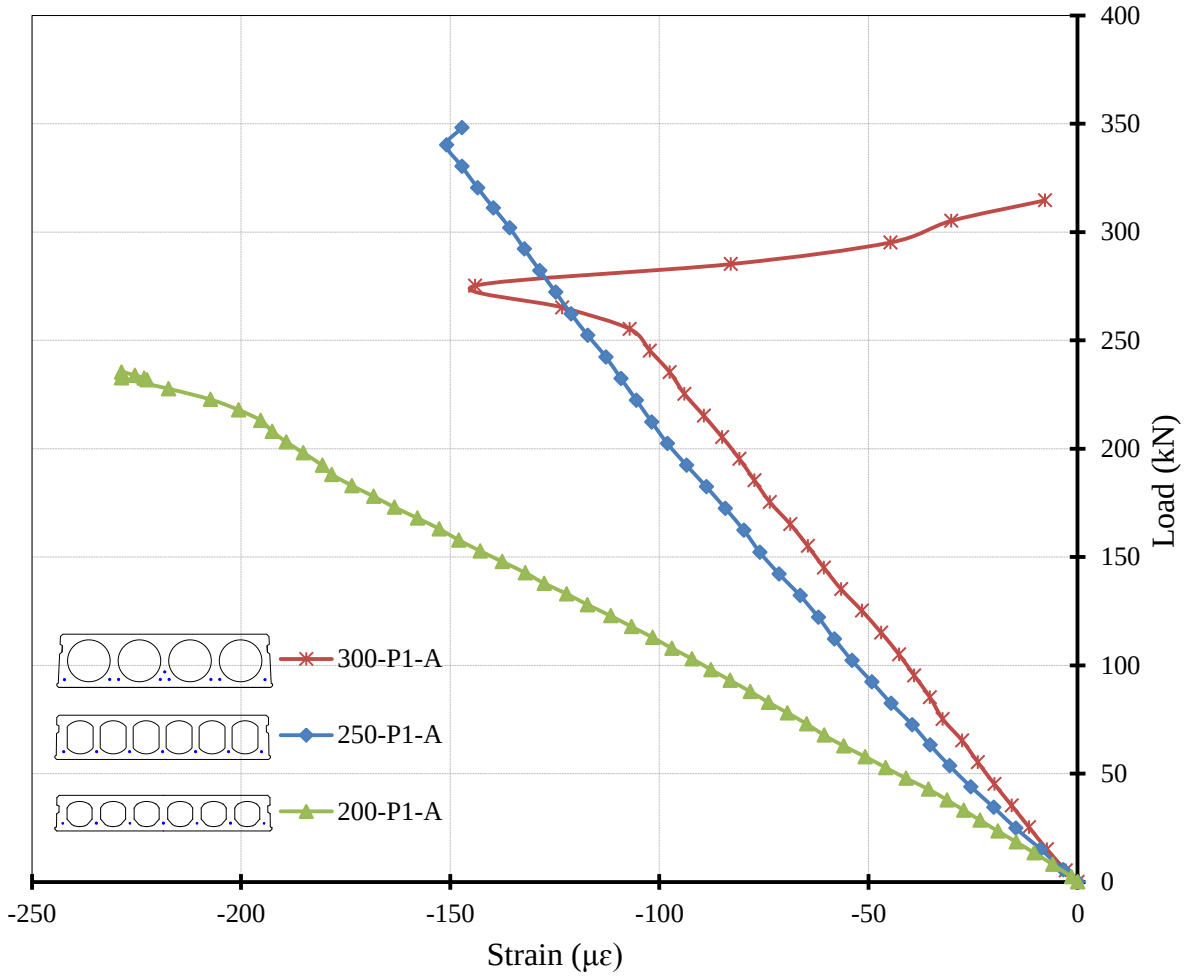


Figure (5.9): Variation of strain with load at top flange of the middle web (PI#4 Md-Top)

### 5.1.6. Load-strain variation in strands

Two strain gauges were mounted on two selected strands as mentioned in the experimental program to monitor the variation of tensile strains in the prestressed strands during shear loading. Unfortunately, the gauge on the edge strand of slab 250-P1-A was malfunctioned during testing, so it was not presented in Figure (5.10).

Because flexural cracks initiate from bottom of the slabs, its effect on strain measurements on strands can be clearly visible by sudden jump in the strain values. That was observed in Figures (5.10 and 5.11) after flexural crack initiated in slab 200-P1-A, the resistance of the slab was

mainly based on the strands. That is appeared by continuous increase in strains of the strands under almost constant load which could be called as the favourable plastic behaviour. However, the ultimate failure seemed to be governed by anchorage failure rather than yielding or rupture of strands. Because the maximum strain that the edge strand experienced was only 883 με and the middle strand only 1103 με which are very low compared to the strain values that a prestressing strand could sustain before yielding/rupture even after considering the initial jacking strain which could be only an additional 6000 με. The remaining strain measurements, after reaching the maximum until failure load, were negative values as load increased while strands continued to slip. It is important to point out that percentage of the post cracking resistance from the ultimate resistance of this slab was about 20%.

Strain measurements on strands of slab 300-P1-A have indicated the same cracking load as found previously from strains on webs. Despite having a web-shear failure in this specimen with bottom edge of the inclined cracks very close to the slab end (Fig. 5.1), surprisingly, there has been still some resistance noticed after cracking. The post cracking resistance of this slab was about 16% of its total ultimate web-shear resistance.

Strain measurements on strands of slab 250-P1-A neither indicated the cracking load nor had any plastic behaviour before failure (Figure 5.11). This is the worst web-shear failure type which could be anticipated from a design point of view even though achieving the highest ultimate shear capacity among the considered slabs. The post cracking resistance with respect to the ultimate resistance of this slab was approximately 0% (absolutely brittle and sudden failure).

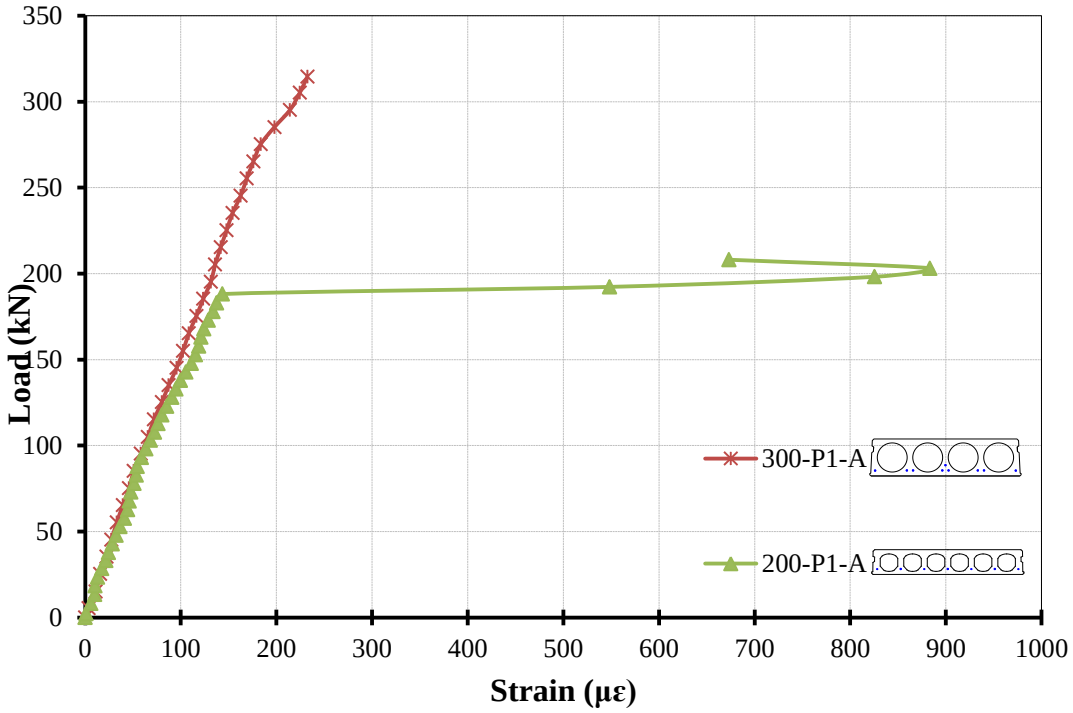


Figure (5.10): Variation of strain with load in a strand at the edge web (SG#1 Ed-Stra)

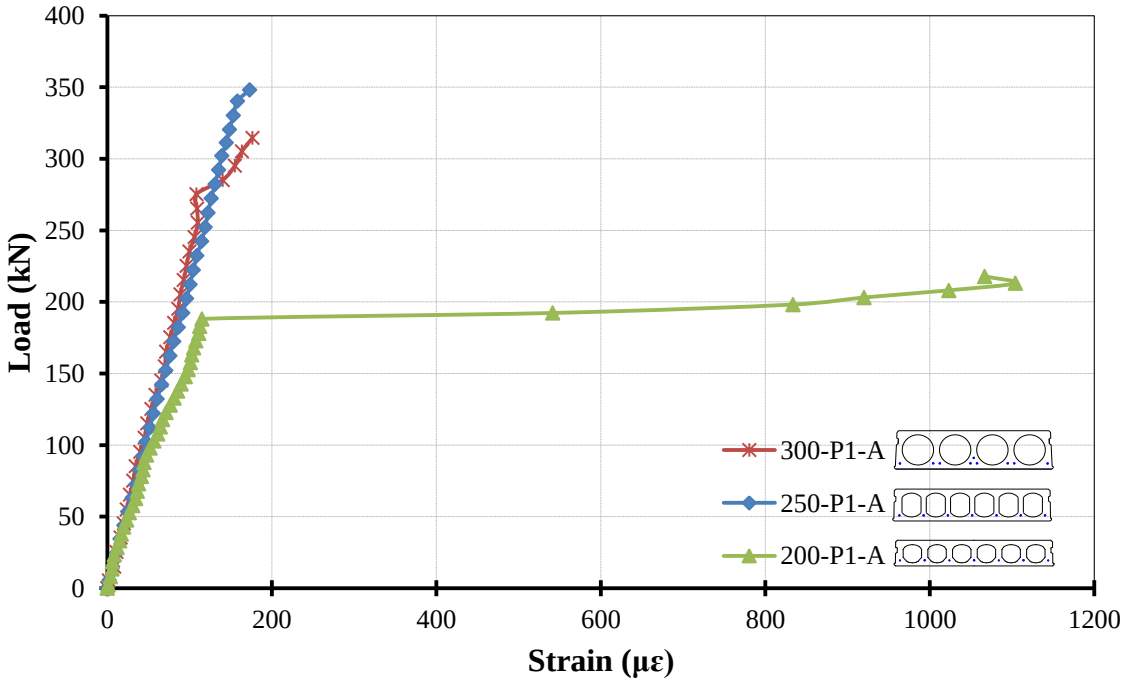


Figure (5.11): Variation of strain with load in a strand at the middle web (SG#2 Md-Stra)

### 5.1.7. Slippage of strands

An LVDT was attached to the exposed end of the middle stand in the cross section of the tested slabs as it was shown in Figure (4.20). The purpose of measuring displacement at the end of the strands was to capture the slippage of strands during loading. It was mentioned earlier that the formation inclined cracks farther from the support is anticipated to enhance the shear capacity of the slab (slab 250-P1-A compared to slab 300-P1-A). In fact, as can be seen from Figure (5.10), when webs of slab 250-P1-A were cracked, the load has already reached very high level (351 kN) that was impossible to resist by any available anchorage length. The vey sudden 0.5-mm jump in displacement of the strand of slab 250-P1-A indicates severe slippage.

Results of 300-P1-A, on the other hand, have showed progressive displacement values for the strand until failure without any sudden jumps. Consequently, the ultimate capacity of the web-shear failure for this specimen, apparently, has been controlled by degradation in resistance of the crack interface due to widening of the crack rather than slippage.

From notes taken during the tests it was found that slab 200-P1-A experienced a significant slippage at failure of this specimen. That was achieved by manually measuring the amount of displacement in strand end by means of a calliper. The average slippage of all 7 stands in the cross section after failure was about 6.2 mm. However, it is worth to mention that this slippage was not sudden to cause a brittle failure like in case of slab 250-P1-A.

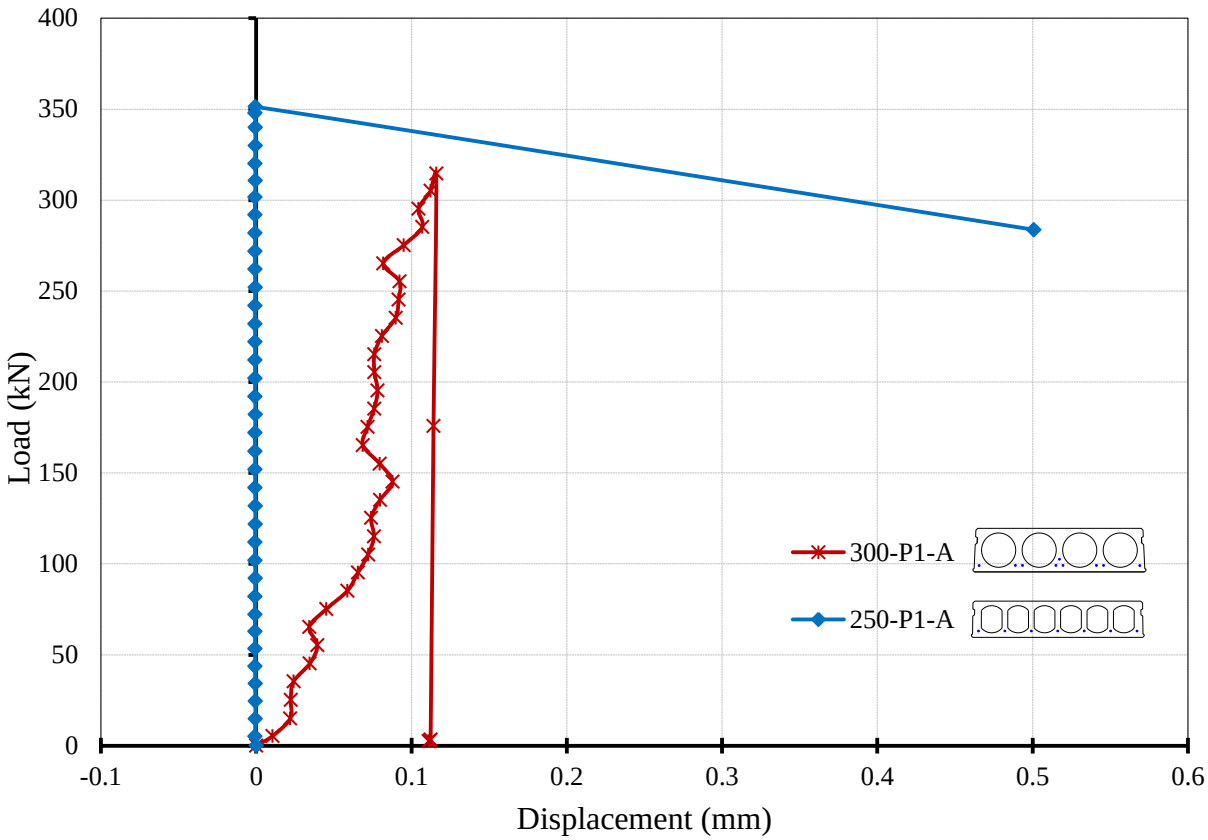


Figure (5.12): Variation of slippage with load in the strand at the middle web

## 5.2. Analysis of Test Specimens Using Different Code Provisions

### 5.2.1. General

During the earlier phase of this research project conducted at the University of Manitoba, Truderung (2011) developed two advanced sets of spreadsheets that adopted the Canadian and American building code provisions, as outlined in Chapter 3, for assessing the shear capacity of PHC slabs. The spreadsheets were designed to predict shear stresses not only at the specified critical sections but over a length of 2.0 m from the loaded end (more than 3 times the shear span). Those spreadsheets were used for the same purpose in this phase of research. In addition, a third set of spreadsheets were developed to predict shear capacity according to the European code, as outlined in Chapter 3.

All input data in these spreadsheets were as much as possible based on actual characteristics of materials. The applied test load was modelled as a distributed 190-mm long line load across the full width of the slab. However, when it comes to geometric properties of specimens, the analysis was conducted twice for each tested slab; once with nominal cross section dimensions and second time with as-built geometric details. This was conducted because expressions of the codes are very sensitive to geometric details such as webs thickness and depth of reinforcement. Prestressing losses were also evaluated according to the provisions of the considered code. Finally, results of analysis by each code were summarised in shear resistance diagrams which are presented in the following sections.

### 5.2.2. CSA code

The concrete shear resistance ($V_c$) according to the general method of CSA code is a function of the applied external loads, which is the test load in case of this project (*P-test*). Since $V_c$ is

estimated based on magnitude of the longitudinal strain in concrete at mid-depth, $\varepsilon_x$ , which is determined from Expression 3.11 stated in Chapter 3. For reference the expression for $\varepsilon_x$ has been repeated here again.

$$\varepsilon_x = \frac{M_f / d_v + V_f - A_p f_{po}}{2(E_p A_p)} \quad or \quad \frac{M_f / d_v + V_f - A_p f_{po}}{2(E_p A_p + E_{ct} A_{ct})} \qquad [3.11]$$

This implies that to predict shear resistance by this code there are two unknowns ($V_c$ & $V_f$), where $V_f$ is derived from *P-test*. To sort it out, a criterion that failure should only happen when shear force is equal to shear resistance at any point between the load and the specified shear critical section from face of support was used. As result, starting with a small value, the *P-test* was increased until first failure point was identified where $V_c$ = $V_f$ and that *P-test* value is identified to be the predicted failure load, of the specific slab unit, according to the code analysis. Plotting the shear-force over shear-resistance diagrams was a very useful tool especially to visualize the process of failure point identification.

In the next Sections 5.2.2.1 to 5.2.2.3, results of analysis according to CSA code for every specimen in the tested three slab series have been presented in a form of shear-force and shear-resistance diagrams. Moreover, for ease of comparison and discussion, the predicted values were summarised in a table format in Section 5.2.2.4

The shear diagrams include the following information:

- $V_{(x)}$ stands for the shear-force, $V_f$, calculated at a considered section with an *x* distance from the loaded-end of the tested slab. That includes effects of the *P-test* and self-weight of the member.

- $V_c$ is the code predicted shear resistance according to relevant provisions of the detailed method for CSA code which was outlined in Section 3.4.1.
- The line ($x = d_v$ from face of support) represents location of the shear critical section as specified by the code from face of the support at the loaded side of the specimen.

#### *5.2.2.1. Shear resistance diagrams for Series-200 slabs*

The variables that should be discussed in this series are void shape and bearing length. It is evident from the diagrams that the CSA code prediction is not affected by shape of voids. For instance, slabs 200-P1-A and 200-P2-A, with P1 was non-circular and P2 circular. Actually, this was quite expected because there is nothing in the code expressions which account for effect of voids geometry. However, there is a little effect for length of bearing noticeable in predicted shear capacity of slab 200-P1-A compared with 200-P1-B or slab 200-P2-A with 200-P2-B. In the first pair of specimens, the CSA code predicted 2% reduction in shear capacity when the bearing length was reduced. While in the second pair the reduction was about 5%. The change in percent of reduction in the second pair was higher probably due to a variation in substituted value of minimum webs thickness for each specimen.

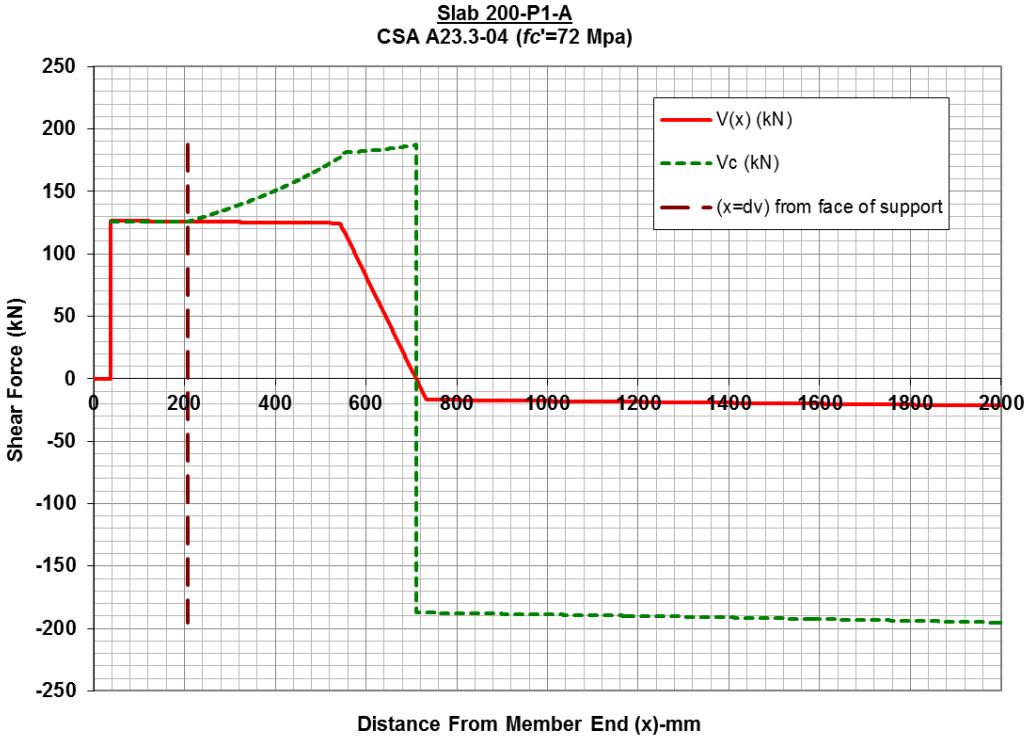


Figure (5.13): CSA code predicted shear resistance of slab 200-P1-A

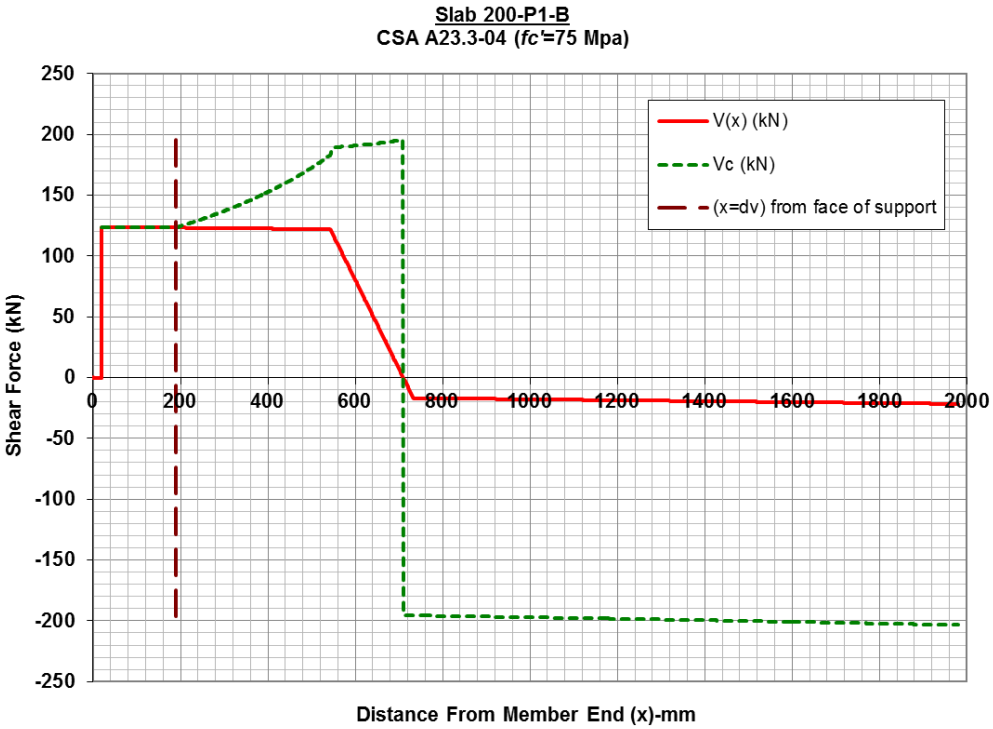


Figure (5.14): CSA code predicted shear resistance slab 200-P1-B

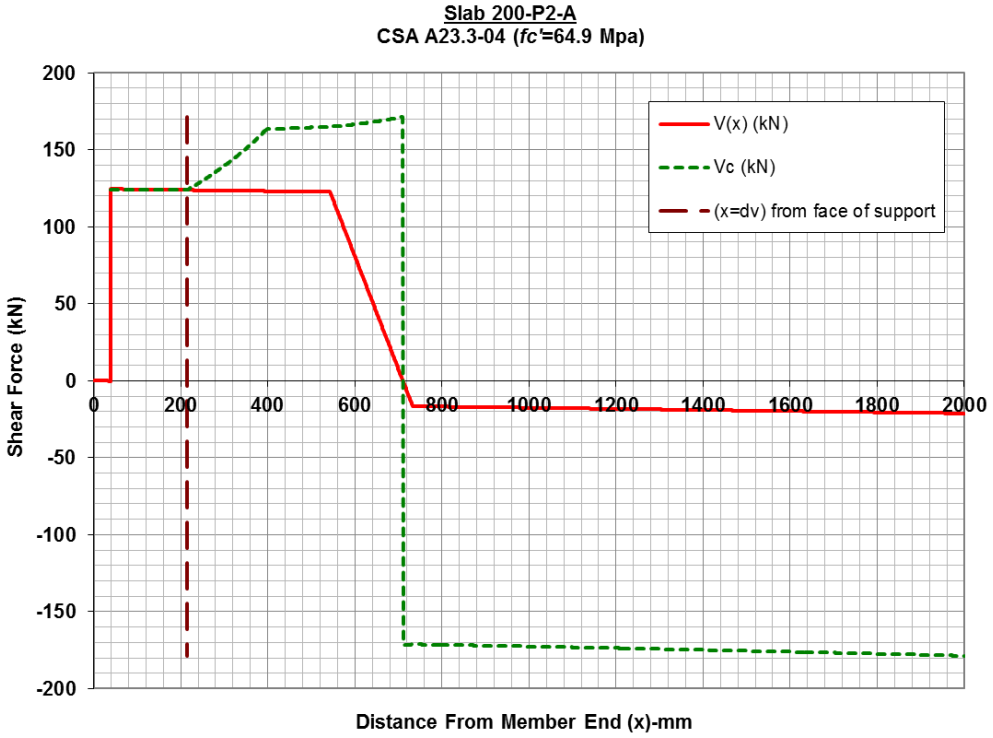


Figure (5.15): CSA code predicted shear resistance slab 200-P2-A

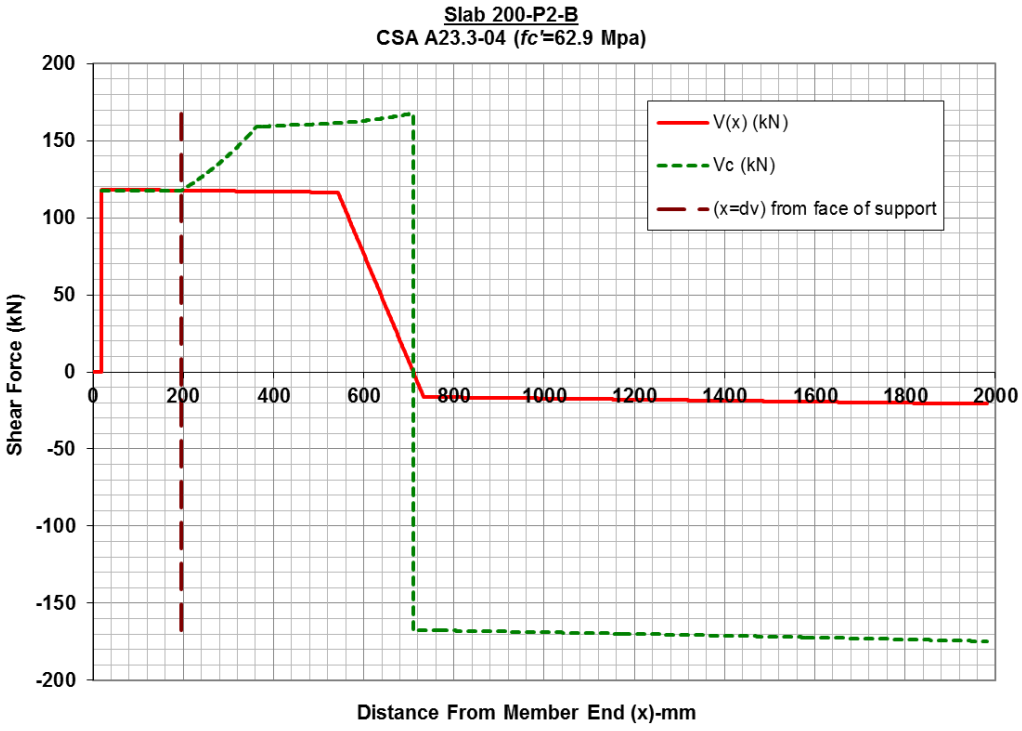


Figure (5.16): CSA code predicted shear resistance slab 200-P2-B

#### *5.2.2.2. Shear resistance diagrams for Series-250 slabs*

The variables that should be discussed in this series are void shape and bearing length. Although it appears as if there has been an influence for void shape in this series for example between capacity of slabs 250-P1-A and 250-P2-A, that is actually must have resulted from deviation in effective web thickness and depth since in Expression 3.7 $V_c$ is a function of $(b_w d_v)$. The sum of minimum web thicknesses and effective depth for Slab 250-P1-A were 338 mm and 186.8 mm, while for slab 250-P2-A these values were 259 mm and 198.2 mm. This makes the code-predicted shear resistance for slab 250-P2-A lower. Moreover, these predictions were totally opposite to the trend of the experimental observed results as shown in Table (5.2); slab 250-P1-A (non-circular) found to resist more shear forces than 250-P2-A (circular). Same as discussed in previous series, the code predictions have showed reduction in shear capacity as result of reduced bearing length. When capacity of slab 250-P1-A is compared with 250-P1-B the reduction was 5% and for slab 250-P2-A with 250-P2-B it was 4%.

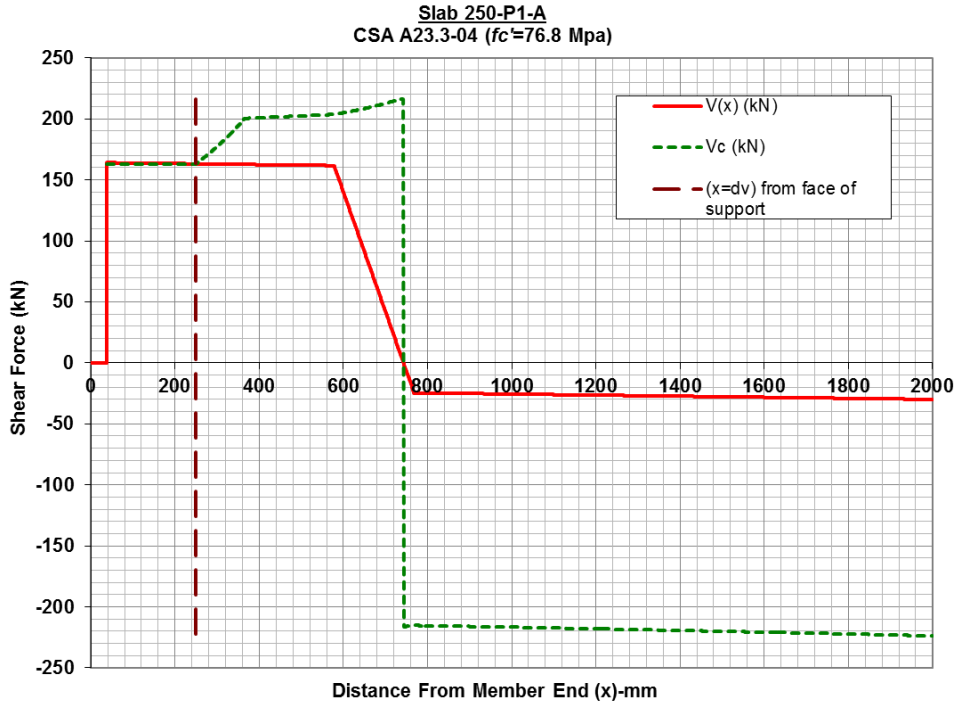


Figure (5.17): CSA code predicted shear resistance slab 250-P1-A

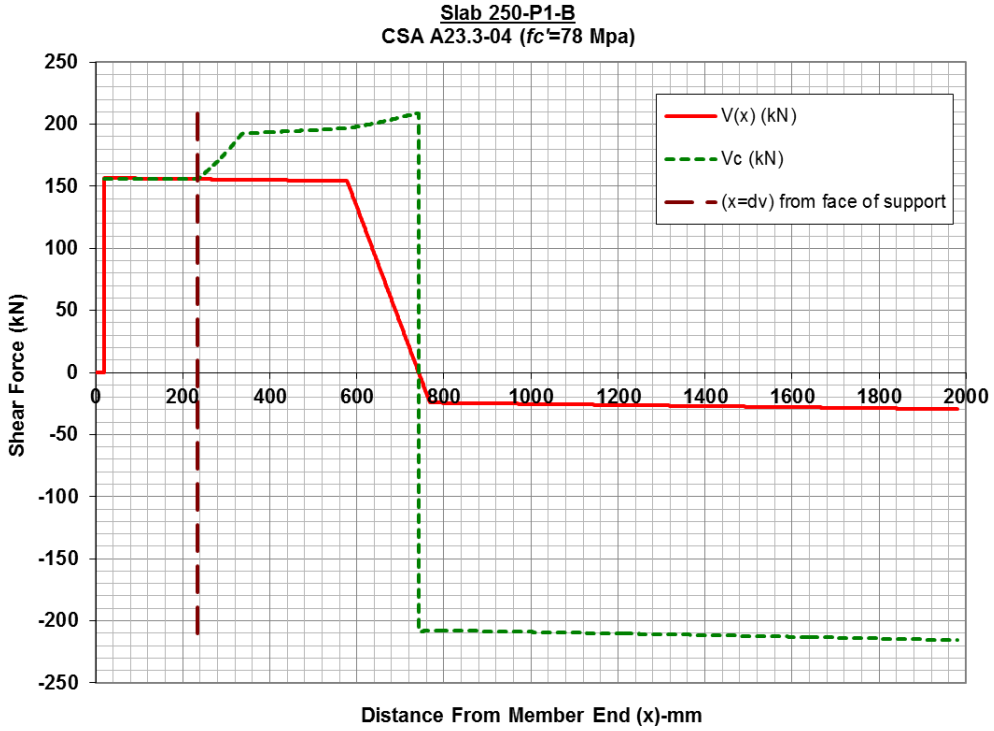


Figure (5.18): CSA code predicted shear resistance slab 250-P1-B

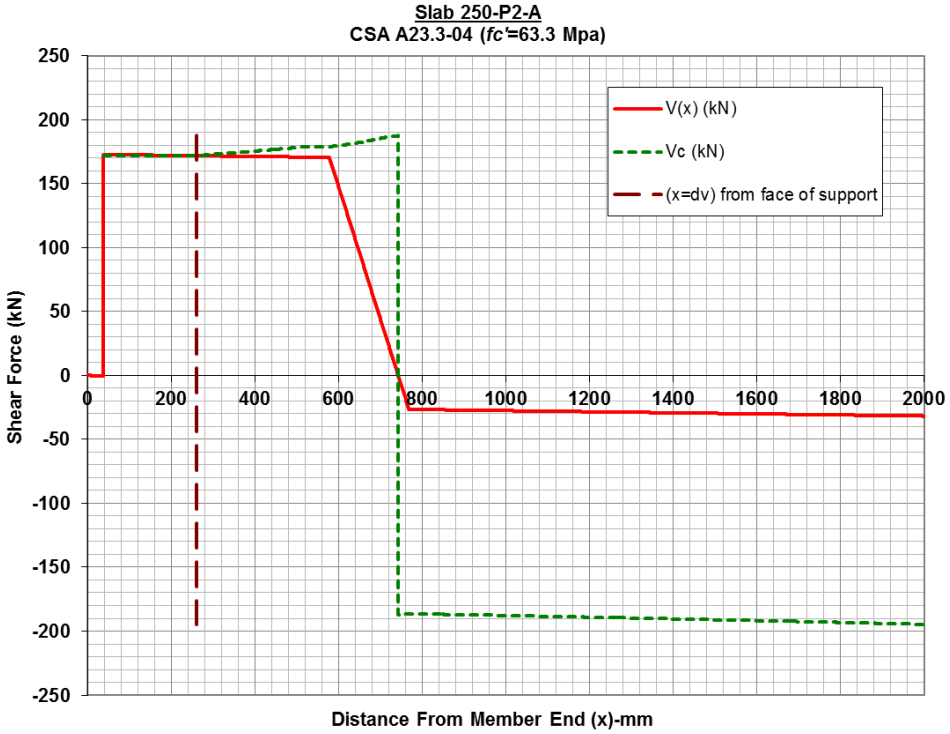


Figure (5.19): CSA code predicted shear resistance slab 250-P2-A

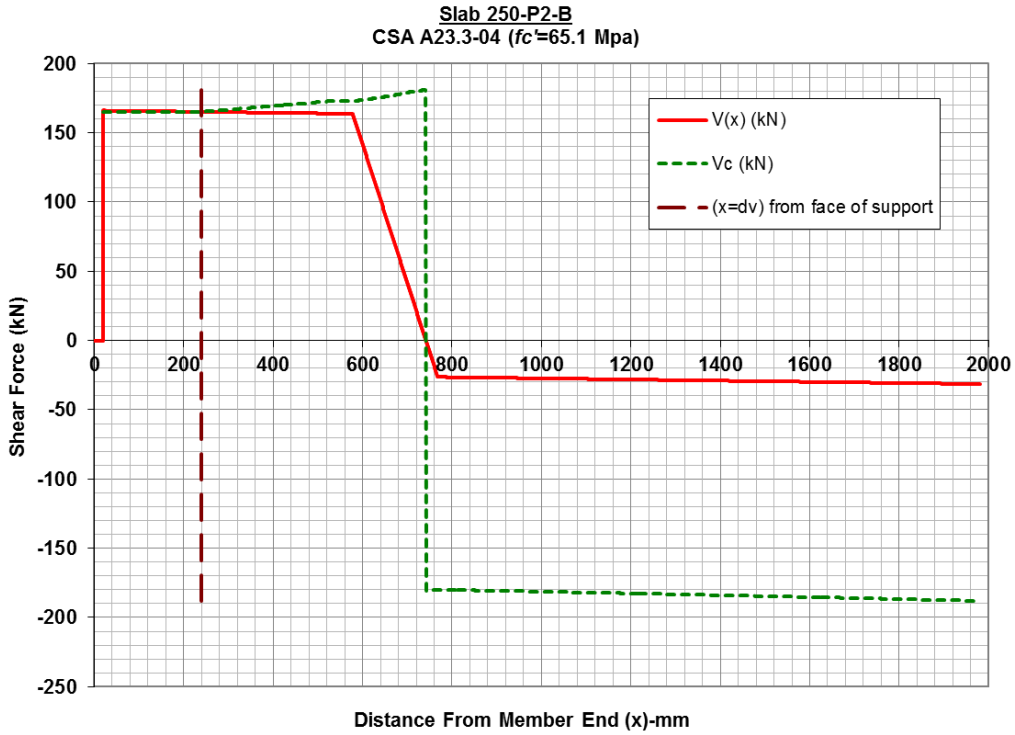


Figure (5.20): CSA code predicted shear resistance slab 250-P2-B

### *5.2.2.3. Shear resistance diagrams for Series-300 slabs*

The only variable that should be discussed in this series is bearing length. However, the CSA code seems to predict almost no effect for bearing length on shear capacities in slabs of Serie-300. The reduction in shear resistance was very marginal for the slabs with the reduced bearing in comparison with those with the full bearing, for example capacity of slab 300-P1-A has been predicted to reduce only by 1% in slab 300-P1-B. Again, it is worth to mention that since there was a deviation in effective total web thicknesses between the slabs from different suppliers, the influence has reflected on the analysis results as well as on experimental results shown in Table (5.2).

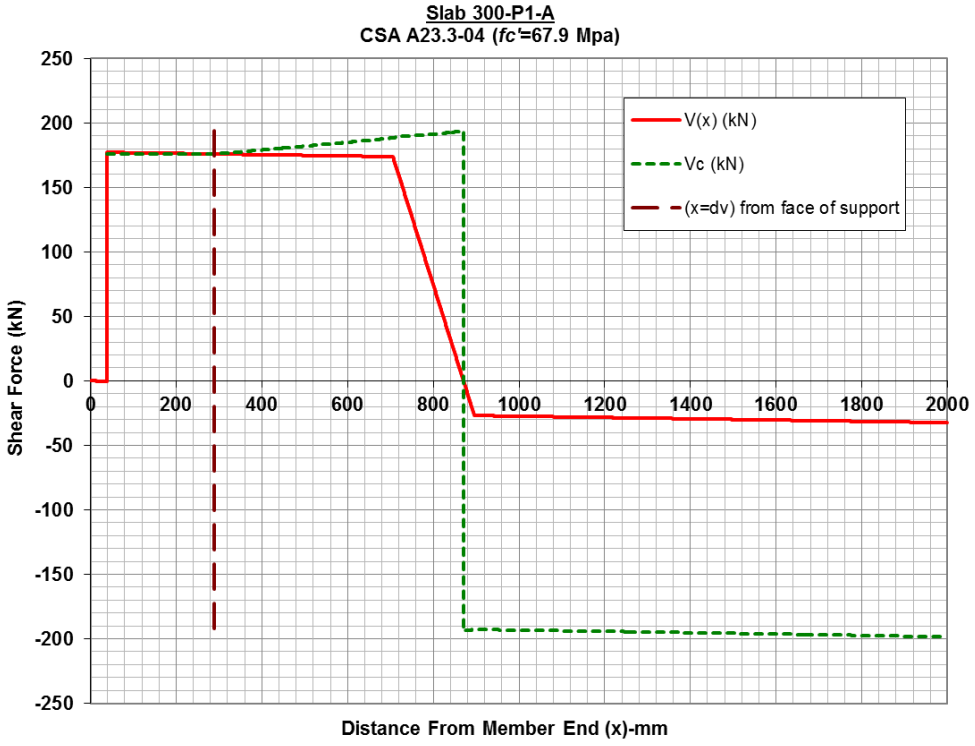


Figure (5.21): CSA code predicted shear resistance slab 300-P1-A

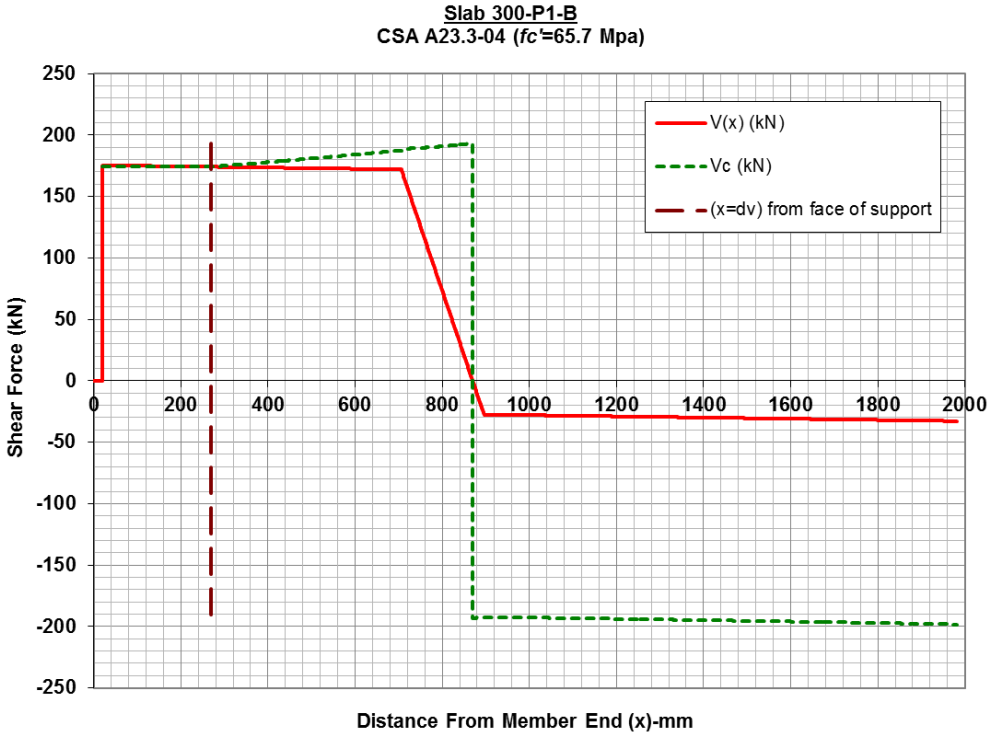


Figure (5.22): CSA code predicted shear resistance slab 300-P1-B

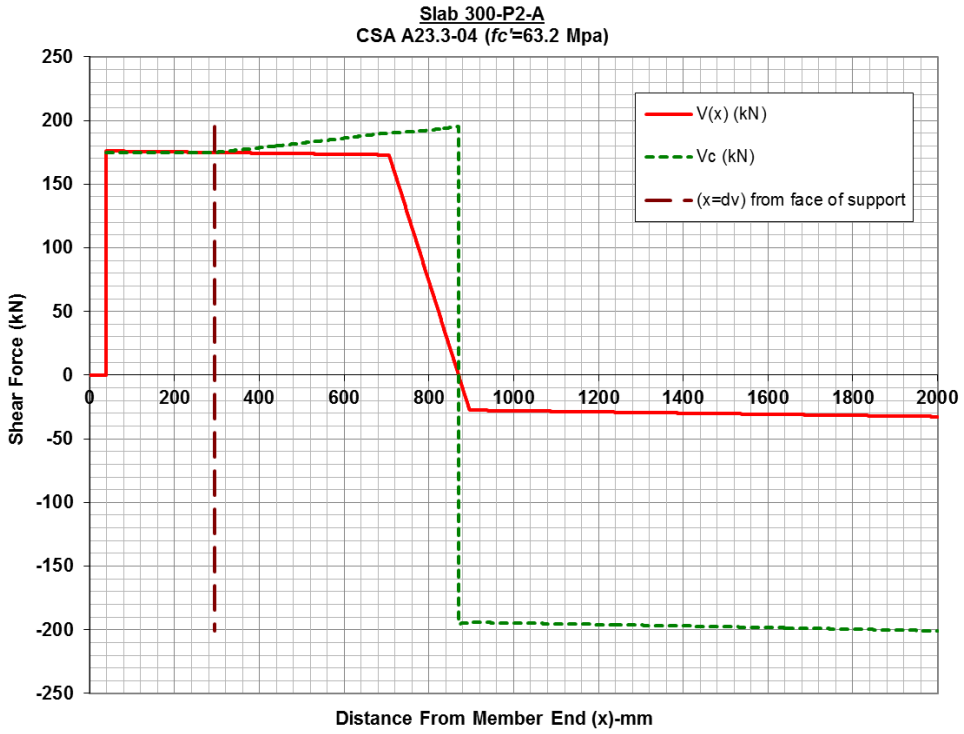


Figure (5.23): CSA code predicted shear resistance slab 300-P2-A

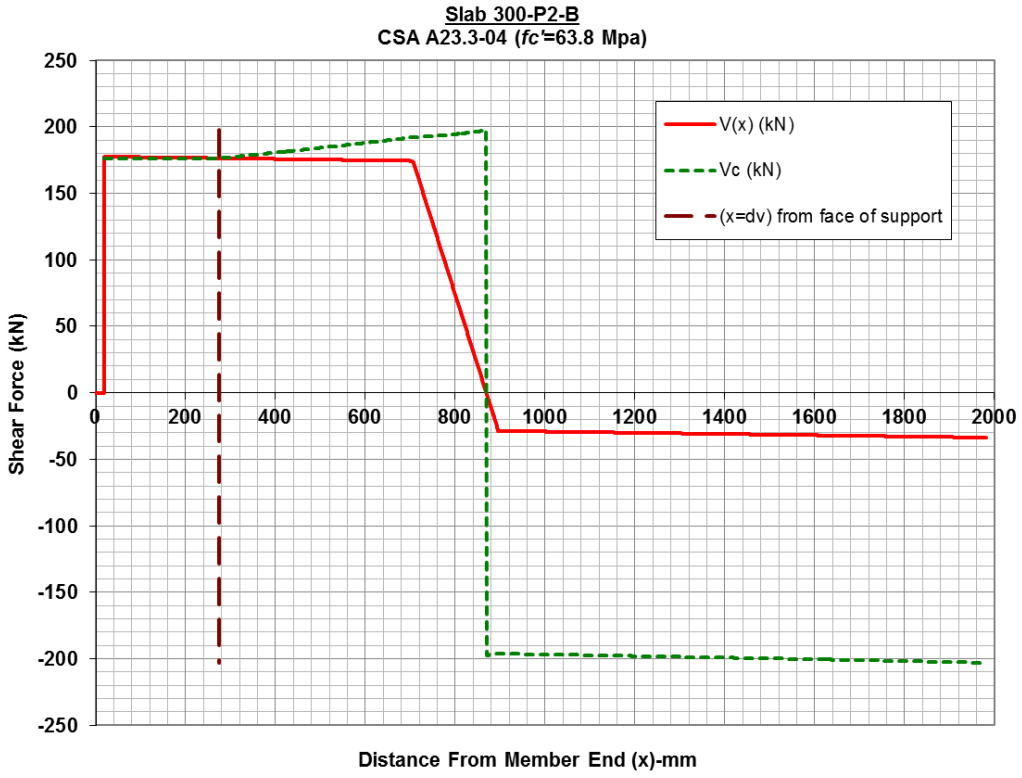


Figure (5.24): CSA code predicted shear resistance slab 300-P2-B

### *5.2.2.4. Comparison of CSA code predictions with experimental results*

Table (5.2) outlines the predicted values by the CSA code using both as-built (*Actual*) and as-designed (*Nominal*) slab cross sectional details. The table includes following information:

- *X-Sec Details* is an indication of the assumed slab cross section geometric properties during analysis by the considered code. Because of variation observed in slab dimensions between as-built (Actual) and as-designed (Nominal) it was preferred to check shear capacity using both.
- (*Pre. Failure Location*) denotes for the distance measured from loaded end of the slab to the critical section where failure is assumed to occur according to the considered code.

- *Vexp* is the calculated shear force at the *Pre. Failure Location* due to effect of applied ultimate *P-test* plus self-weight of the slab unit.
- *P-pre* is the code estimated maximum value for a vertical line load that the slab could resist before shear failure. It is applied at the same shear span used for *P-test* during the experiments.
- *Vc-pre* is the code predicted shear capacity as calculated at the *Pre. Failure Location* according to expressions of the considered code. It was subscripted by *c* since the shear resistance of PHC slabs are solely dependent on concrete contribution.
- *Vexp/Vc-pre* is the ratio of experimentally observed shear capacity to the code predicted shear resistance. This ratio was used as a measure for level of accuracy of the predicted values using code provisions. If the ratio is more than unity, that implies an under-estimation of slab shear capacities by the considered code.

Table (5.2): Summary of shear capacity analysis performed on tested slabs using CSA code

| | | Exp. Results | | CSA A23.3 Predictions | | | |
|---|---|---|---|---|---|---|---|
| Slab ID | X-Sec Details | P-test (kN) | Vexp (kN) | P-pre (kN) | Pre. Failure Location (mm) | Vc-pre (kN) | Vexp/Vc-pre |
| 200-P1-A | Actual | 235.52 | 206.15 | 140.67 | 208 | 125.84 | 1.64 |
| | Nominal | | 205.463 | 133.7 | 209 | 119.237 | 1.72 |
| 200-P1-B | Actual | 196.29 | 172.35 | 138 | 189 | 123.27 | 1.40 |
| | Nominal | | 171.523 | 129.21 | 190 | 114.97 | 1.49 |
| 200-P2-A | Actual | 227.03 | 198.79 | 138.5 | 214 | 123.84 | 1.61 |
| | Nominal | | 197.98 | 130.68 | 209 | 116.40 | 1.70 |
| 200-P2-B | Actual | 186.98 | 164.04 | 132 | 196 | 117.71 | 1.39 |
| | Nominal | | 163.317 | 125.48 | 190 | 111.48 | 1.46 |
| 250-P1-A | Actual | 351.35 | 302.22 | 185.44 | 250 | 163.16 | 1.85 |
| | Nominal | | 301.096 | 178.95 | 251 | 156.58 | 1.92 |
| 250-P1-B | Actual | 350.8 | 299.98 | 177.8 | 234 | 155.78 | 1.93 |
| | Nominal | | 298.971 | 172.68 | 232 | 150.50 | 1.99 |
| 250-P2-A | Actual | 244.92 | 212.64 | 196.32 | 261 | 171.91 | 1.24 |
| | Nominal | | 211.82 | 172.38 | 248 | 151.02 | 1.40 |
| 250-P2-B | Actual | 222.7 | 192.99 | 189.28 | 239 | 165.13 | 1.17 |
| | Nominal | | 192.21 | 170.1 | 229 | 148.30 | 1.30 |
| 300-P1-A | Actual | 318.81 | 274.75 | 199.72 | 289 | 175.85 | 1.56 |
| | Nominal | | 273.45 | 185.89 | 292 | 163.07 | 1.68 |
| 300-P1-B | Actual | 263.89 | 228.15 | 198.51 | 269 | 174.08 | 1.31 |
| | Nominal | | 227.03 | 192.68 | 273 | 168.13 | 1.35 |
| 300-P2-A | Actual | 346.68 | 296.92 | 199.6 | 294 | 174.81 | 1.70 |
| | Nominal | | 296.52 | 200.27 | 293 | 174.98 | 1.69 |
| 300-P2-B | Actual | 223.8 | 194.26 | 202.15 | 275 | 176.36 | 1.10 |
| | Nominal | | 193.76 | 198.71 | 274 | 173.02 | 1.12 |
| | | | | | Mean Value | | 1.49 |
| | | | | | Standard deviation | | 0.27 |

From Table (5.2), it was found that mean value of (*Vexp/Vc-pre*) for CSA code based on analysis with *Actual* details was found to be 1.49 and the standard deviation of (*Vexp/Vc-pre*) was 0.27. This implies that the CSA code tends to under-predict shear capacity of PHC slabs with medium prestressing level by approximately 49% when compared to experimental results.

Furthermore, comparison of values in column *Vexp* and in column *Vc-pre* shows that CSA code predictions for effect of void shape was totally opposite to experimental observation in both Series-200 and Series-250. The experiments showed a higher capacity for non-circular voided slabs, 250-P1 and 200-P1, than their counterparts' 250-P2 and 200-P2 with circular voids.

The effect of reduced bearing length on predicted shear capacities by CSA code was not as significant as it was on experimental results. In other words, the CSA code prediction method found to be less sensitive to the change in support bearing length. The amount of reduction in predicted capacities due to reduced bearing length in all specimens generally ranged from 1% to 5%.

### 5.2.3. ACI code

The concrete shear resistance ($V_c$) according to ACI code is classified into two types and the ultimate shear capacity is the lesser one. The first type is web-shear failure ($V_{cw}$), which is not a function of the applied load (*P-test*), and therefore, it does not require iteration. However, the second type, flexural-shear ($V_{ci}$), is proportional to applied load, *P-test*. For reference, the expressions of $V_{cw}$ and $V_{ci}$ are stated here again.

$$V_{cw} = (0.29\lambda\sqrt{f_c'} + 0.3f_{pc})b_w d_p \qquad [3.15]$$

$$V_{ci} = 0.05\lambda\sqrt{f_c'}\, b_w d_p + V_d + \frac{V_i M_{cre}}{M_{max}} \geq 0.17\lambda\sqrt{f_c'}\, b_w d \qquad [3.12]$$

Expression 3.12 implies that values of $V_{ci}$ , $V_i$ and $M_{max}$ are unknown if the applied *P-test* was not given, where $V_i$ and $M_{max}$ are both derived from *P-test*. So, similar to the approach used in spreadsheets of CSA code, a criterion for failure whenever shear force ($V_i + V_d$) becomes equal

to shear resistance ($V_c = V_{cw}$ or $V_{ci}$) at any point between the load and the specified shear critical section from face of support was applied. Therefore, the *P-test* was increased until first failure point was identified where $V_c = (V_i + V_d)$ and the corresponding *P-test* value is recorded as the predicted failure load.

For all tested slabs, the shear-force and code-predicted shear-resistance diagrams by the ACI code are presented in Sections 5.2.3.1 to 5.2.3.3 using as-built cross section properties and actual concrete compressive strength.

The shear diagrams include the following information:

- $V_{(x)}$ represents the total shear force at any given distance from the loaded end of the slab. It includes effects of both the *P-test*, that will cause shear failure, and self-weight of member.
- $V_c$ is the code-predicted shear resistance estimated using the governing value of the web-shear or flexure-shear equations, as outlined in Section 3.4.2.
- The line ($x = h/2$ from face of support) represents location of the shear critical section as specified by the code from the support at the loaded end of the slab.

#### *5.2.3.1. Shear resistance diagrams for Series-200 slabs*

The variables that should be discussed in this series are void shape and bearing length. The ACI code, like CSA code, does not account for the effect of void shape. However, the variation noticed in the predicted shear capacity of some specimens (for example, slabs 200-P1-A and 200-P2-A) was actually due to difference in as-built web widths.

Regarding the effect of reduced bearing length, the amount of reduction in shear capacity predicted by the ACI code for slabs with reduced bearing length was very small. This can be

observed in the comparison between results presented in Table (5.3). It can be seen that specimen 200-P1-B (with high concrete strength) had higher web-shear capacity than slab 200-P1-A with full bearing length. Since all the slabs in this series had the same web-thickness, the difference in the results reported in Table (5.3) could be attributed to the variation in concrete strength. For reference, actual concrete strength for each tested slabs was outlined in Appendix B. Considering the CSA code predictions as control, the difference between shear capacities predicted by the two codes (ACI & CSA codes) was found to range from 11% to 41% for slabs in Series-200. ACI was less conservative but a little closer to experimental shear capacities.

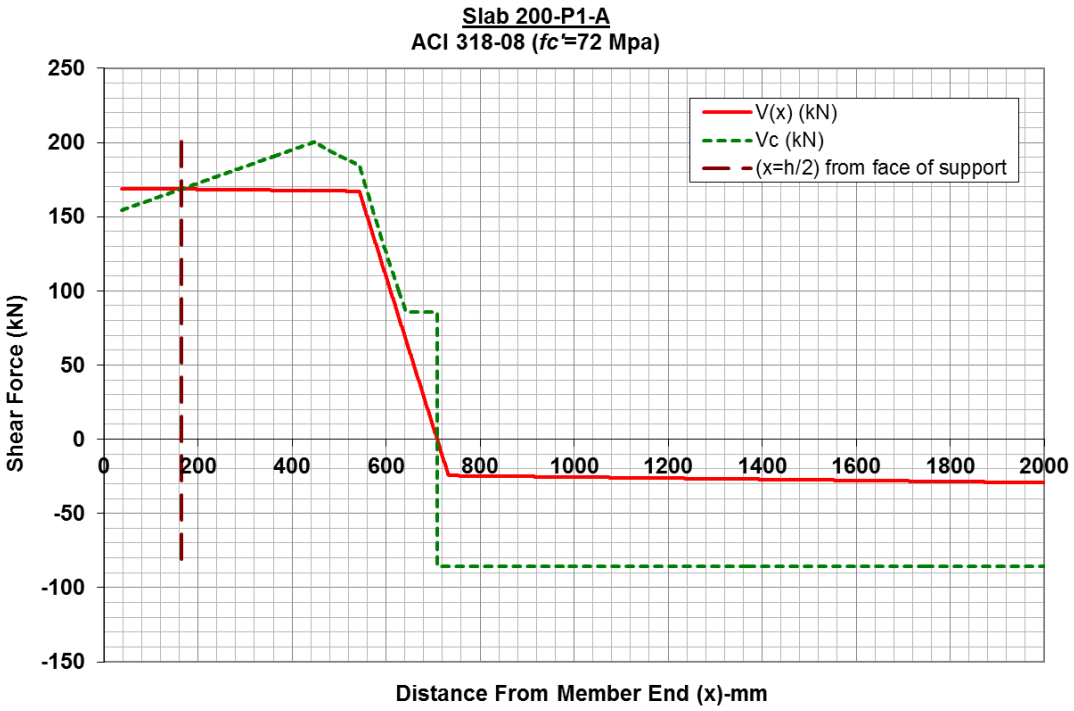


Figure (5.25): ACI code predicted shear resistance slab 200-P1-A

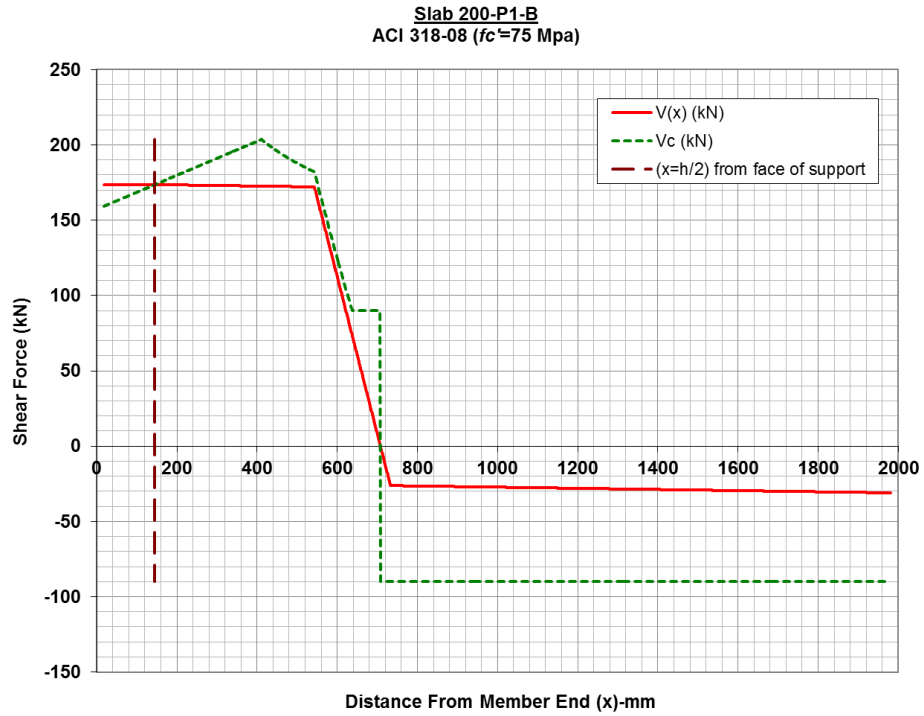


Figure (5.26): ACI code predicted shear resistance slab 200-P1-B


Figure (5.27): ACI code predicted shear resistance slab 200-P2-A

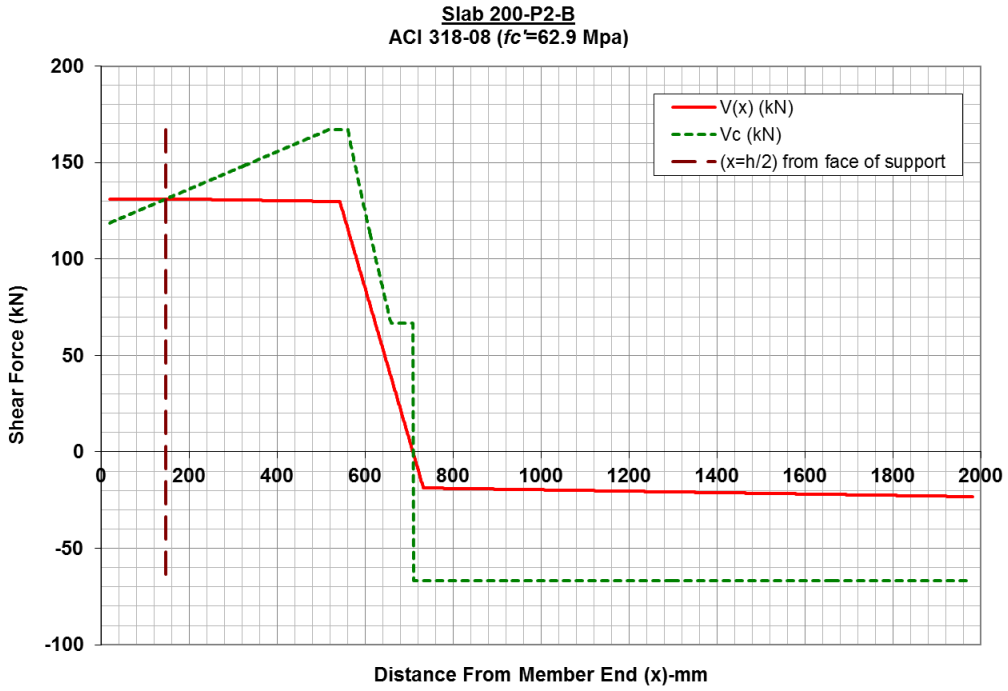


Figure (5.28): ACI code predicted shear resistance slab 200-P2-B

### *5.2.3.2. Shear resistance diagrams for Series-250 slabs*

The shear capacity predicted by ACI code for slab 250-P1-B with reduced bearing dropped by 4% compared to its counterpart slab 250-P1-A with full bearing. Similarly, the shear capacity of slab 250-P2-B was reduced by 3% compared to slab 250-P2-A. The difference between the shear capacities predicted by ACI & CSA codes for Series-250 was not consistent. This is because ACI code was less conservative in predicting non-circular slabs (250-P1-A and 250-P1-B) while more conservative than CSA code in prediction of circular ones (250-P2-A & 250-P2-B). Generally speaking, the difference between predictions of the two codes ranged from 8% to 25% in this series.

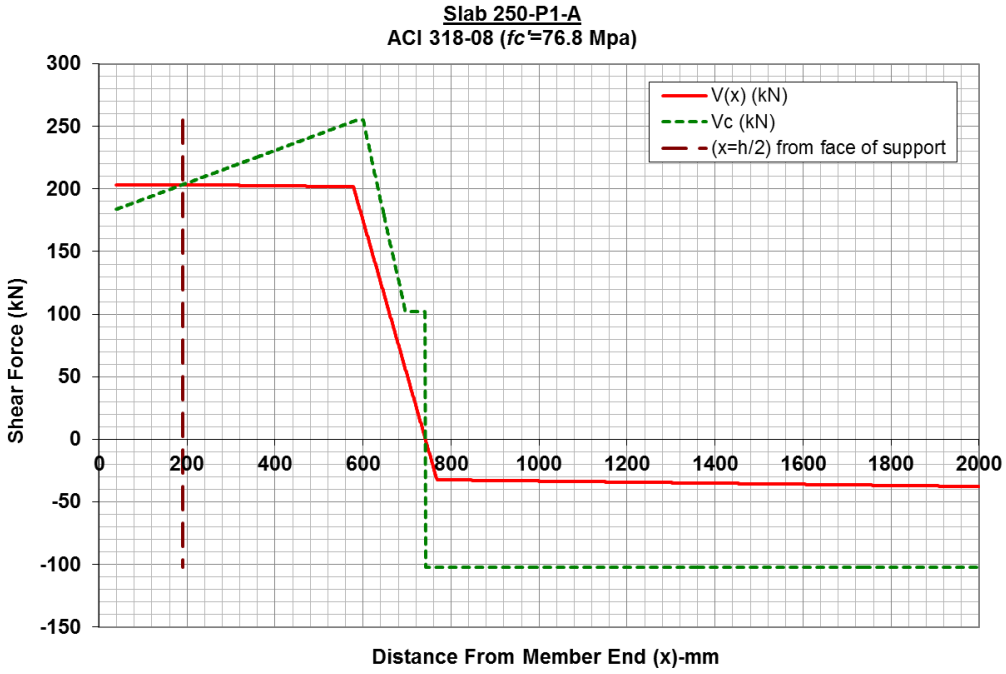


Figure (5.29): ACI code predicted shear resistance slab 250-P1-A

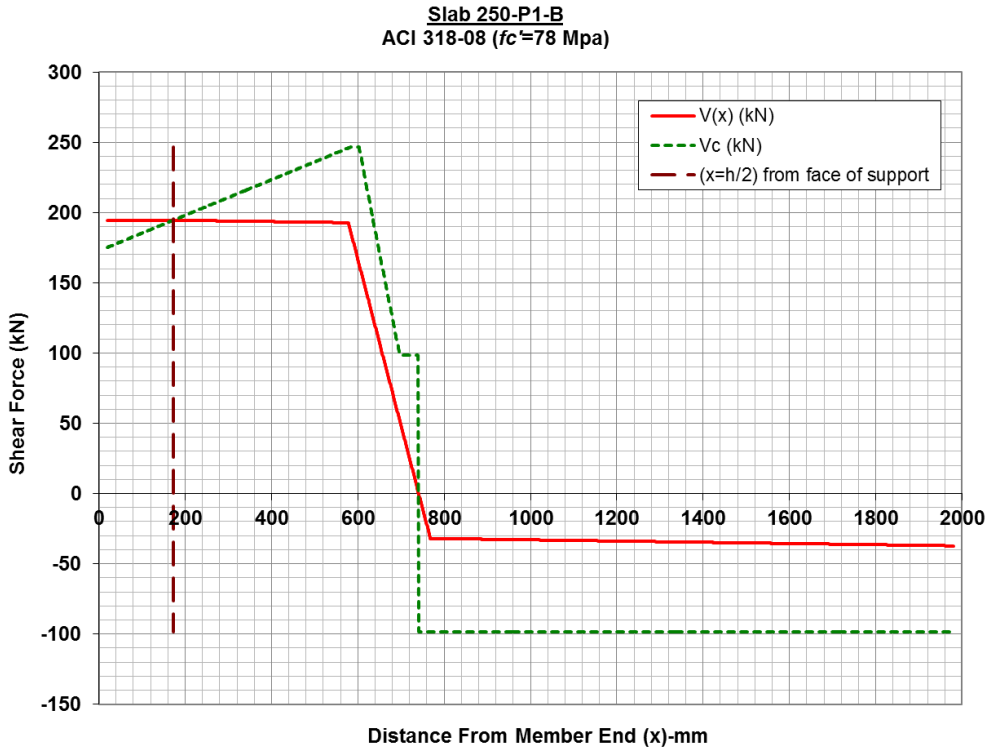


Figure (5.30): ACI code predicted shear resistance slab 250-P1-B

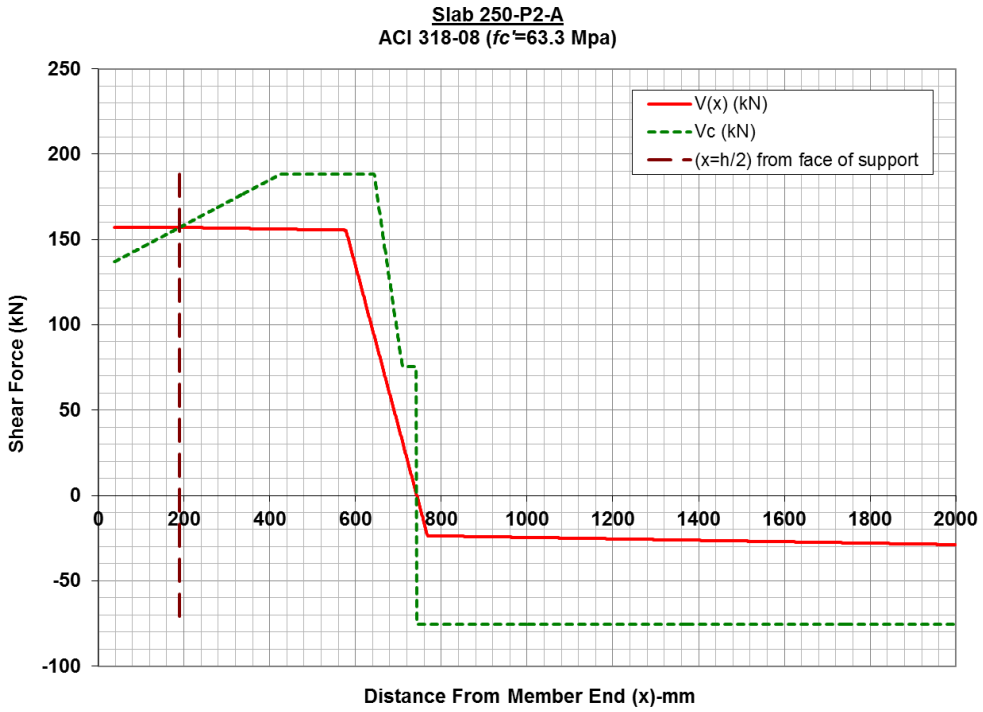


Figure (5.31): ACI code predicted shear resistance slab 250-P2-A

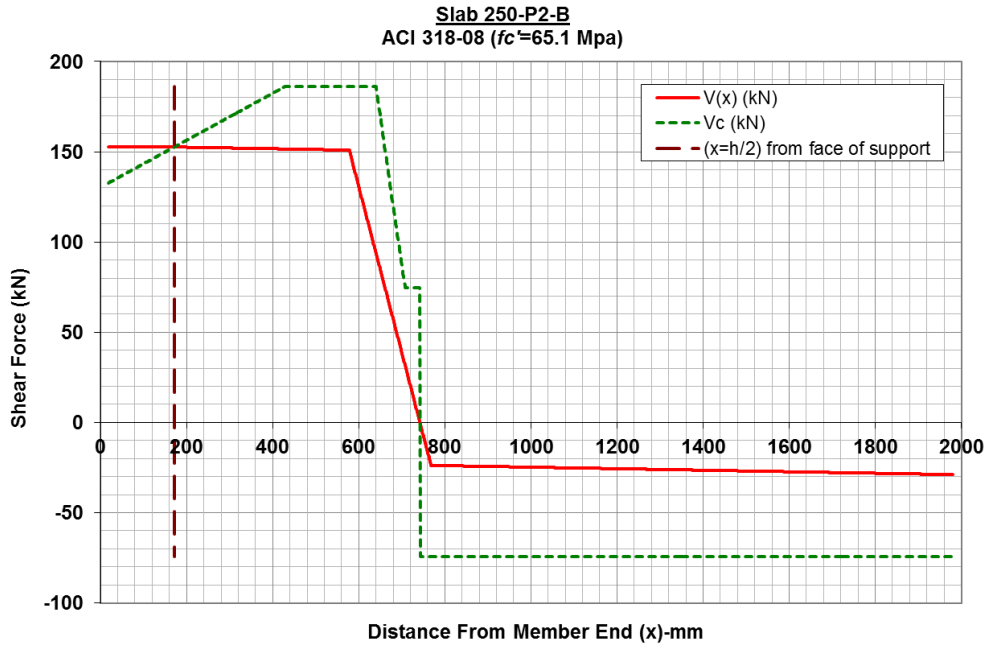


Figure (5.32): ACI code predicted shear resistance slab 250-P2-B

### *5.2.3.3. Shear resistance diagrams for Series-300 slabs*

It can be seen in Figure (5.33) and Figure (5.34) that there is a 7% reduction in shear capacity due to reduced bearing length in slab 300-P1-B compared to slab 300-P1-A. However, that reduction percentage in the predicted capacities is several times smaller than the actual reductions happened in experimental results of the same slabs as stated in Section 5.1.4.2.

It is worth to mention that accuracy levels for the ACI and CSA codes predictions were close to each other in Series-300. The difference was ranging from only 2% to 6%. Nevertheless, the ACI code's prediction was more conservative than the CSA code predicted values in case of slabs 300-P1-B, 300-P2-A, and 300-P2-B. It was less conservative than the CSA code only in case of slab 300-P1-A.

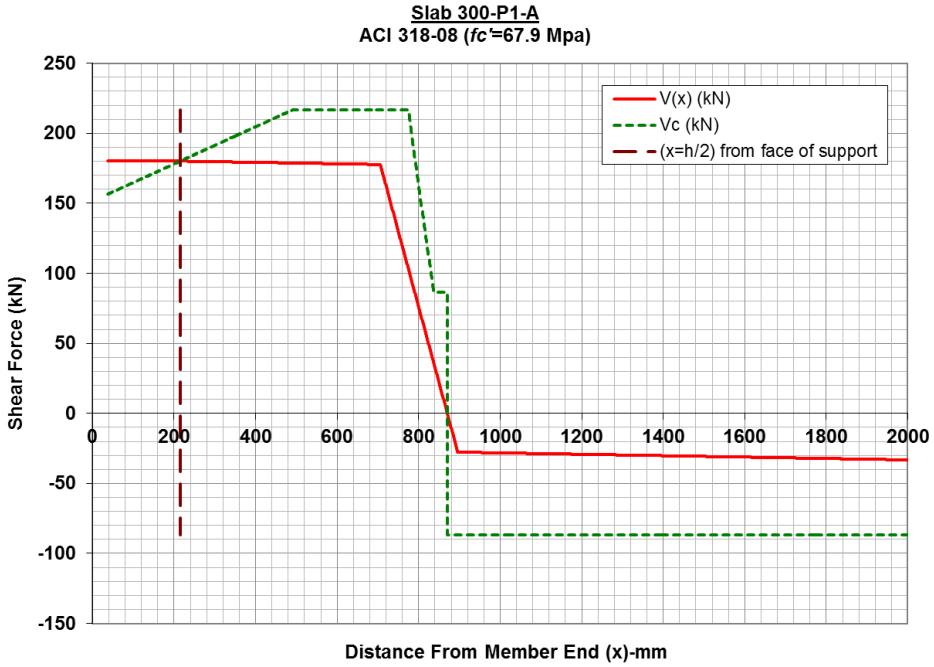


Figure (5.33): ACI code predicted shear resistance for slab 300-P1-A

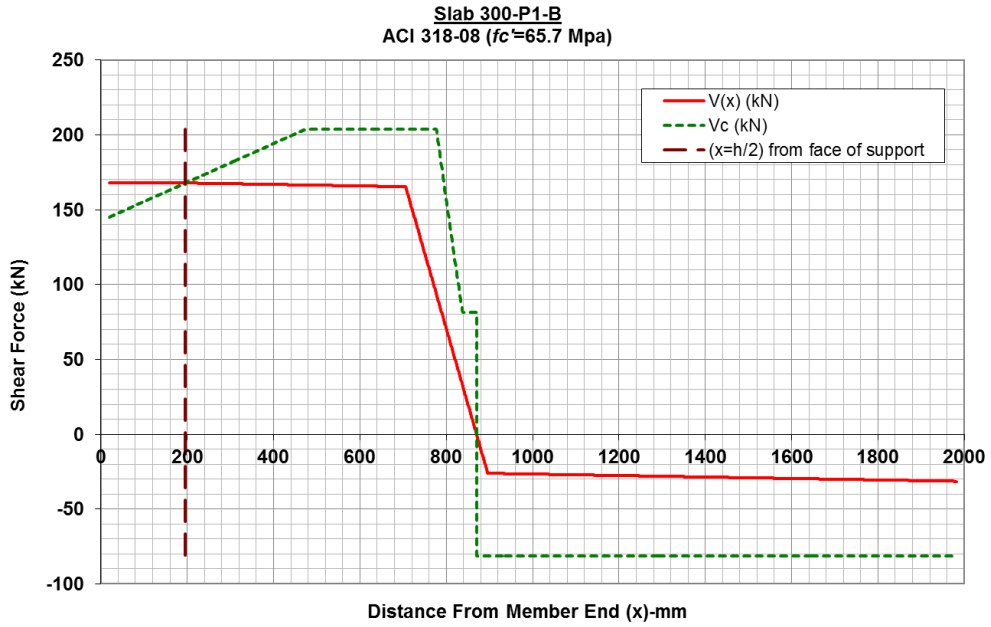


Figure (5.34): ACI code predicted shear resistance slab 300-P1-B

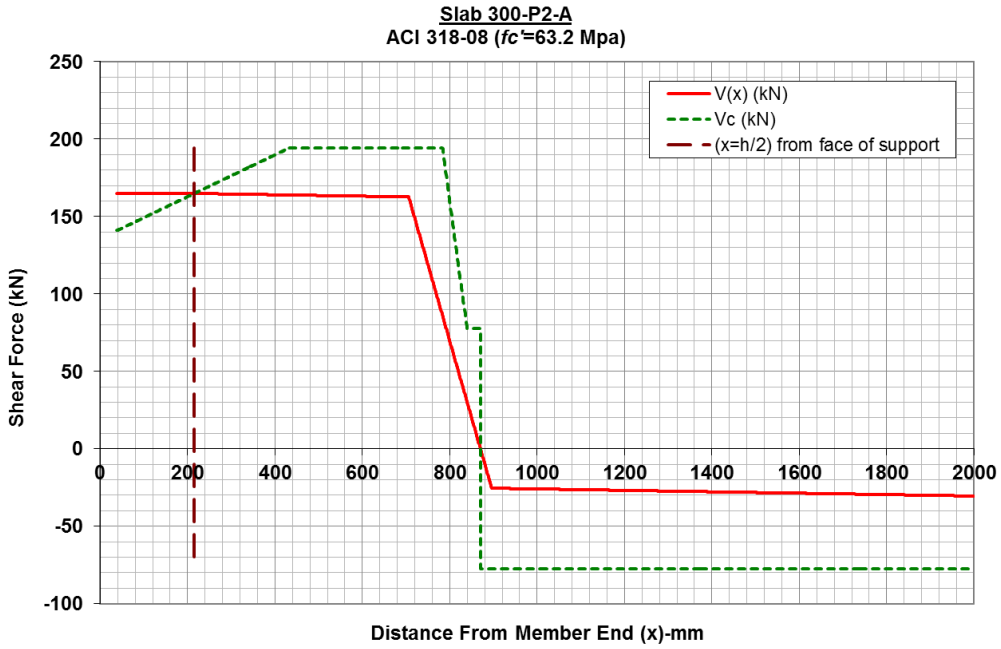


Figure (5.35): ACI code predicted shear resistance slab 300-P2-A

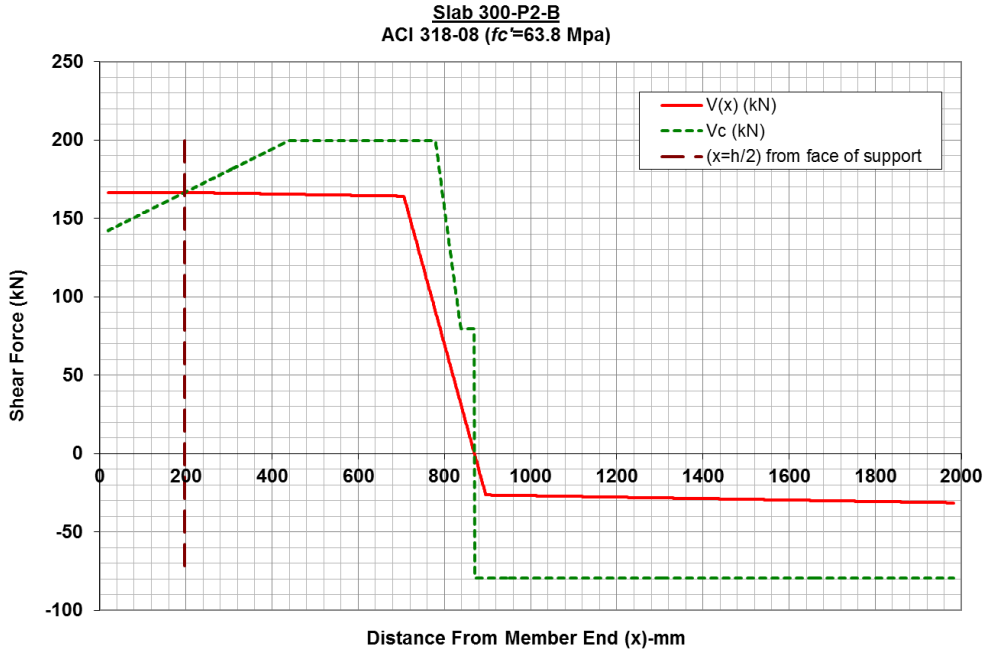


Figure (5.36): ACI code predicted shear resistance slab 300-P2-B

### *5.2.3.4. Comparison of ACI code predictions with experimental results*

Table (5.3) outlines the analysis results by the ACI code using both *Actual* and as-designed *Nominal* slab cross sectional details. The table includes same type of information introduced in Section 5.2.2.4. Since the ACI code predicts the mode of shear failure with the shear capacity, additional columns for comparison with experimental were added to the table as following:

- (*Exp. Failure Mode*) and (*Pre. Failure Mode*), respectively, denotes for experimentally attained and code predicted modes of shear failures. The experimental modes of failure were identified based on the observations during experiments and in light of the definitions discussed in Sections 2.2.1 & 2.2.2 for each mode.

Table (5.3): Summary of shear capacity analysis performed on tested slabs using ACI code

| | | Exp. Results | | | ACI 318-08 Predictions | | | | |
|---|---|---|---|---|---|---|---|---|---|
| Slab ID | X-Sec Details | P-test (kN) | Vexp (kN) | Exp. Failure Mode | P-pre (kN) | Pre. Failure Location (mm) | Vc-pre (kN) | Pre. Failure Mode | Vexp/Vc-pre |
| 200-P1-A | Actual | 235.52 | 206.317 | Flexural | 190.93 | 164 | 168.563 | Web-shear | 1.22 |
| | Nominal | | 205.612 | | 165.21 | 165 | 146.192 | | 1.41 |
| 200-P1-B | Actual | 196.29 | 172.522 | Flexural & Flexural-shear | 197.6 | 145 | 173.627 | Web-shear | 1.00 |
| | Nominal | | 171.672 | | 166.59 | 146 | 146.637 | | 1.17 |
| 200-P2-A | Actual | 227.03 | 198.967 | Web-shear | 156.41 | 166 | 139.173 | Web-shear | 1.43 |
| | Nominal | | 198.124 | | 139.36 | 165 | 123.890 | | 1.60 |
| 200-P2-B | Actual | 186.98 | 164.211 | Web-shear | 147.76 | 148 | 131.170 | Web-shear | 1.25 |
| | Nominal | | 163.458 | | 135.8 | 146 | 120.333 | | 1.36 |
| 250-P1-A | Actual | 351.35 | 302.487 | Flexural-shear | 233.21 | 190 | 203.454 | Web-shear | 1.49 |
| | Nominal | | 301.323 | | 209.13 | 190 | 182.101 | | 1.65 |
| 250-P1-B | Actual | 350.8 | 300.249 | Flexural-shear | 223.92 | 172 | 194.491 | Web-shear | 1.54 |
| | Nominal | | 299.198 | | 208.73 | 171 | 180.774 | | 1.66 |
| 250-P2-A | Actual | 244.92 | 212.944 | Web-shear | 178.26 | 190 | 157.073 | Web-shear | 1.36 |
| | Nominal | | 212.041 | | 156.9 | 188 | 138.270 | | 1.53 |
| 250-P2-B | Actual | 222.7 | 193.279 | Web-shear | 173.92 | 171 | 152.619 | Web-shear | 1.27 |
| | Nominal | | 192.429 | | 156.7 | 169 | 137.405 | | 1.40 |
| 300-P1-A | Actual | 318.81 | 275.115 | Web-shear | 204.44 | 215 | 180.148 | Web-shear | 1.53 |
| | Nominal | | 273.783 | | 193.82 | 216 | 169.996 | | 1.61 |
| 300-P1-B | Actual | 263.89 | 228.510 | Web-shear | 190.5 | 196 | 167.816 | Web-shear | 1.36 |
| | Nominal | | 227.358 | | 188.56 | 197 | 165.047 | | 1.38 |
| 300-P2-A | Actual | 346.68 | 297.276 | Web-shear | 187.2 | 215 | 164.874 | Web-shear | 1.80 |
| | Nominal | | 296.860 | | 189.48 | 216 | 166.358 | | 1.78 |
| 300-P2-B | Actual | 223.8 | 194.621 | Web-shear | 189.75 | 197 | 166.472 | Web-shear | 1.17 |
| | Nominal | | 194.101 | | 187.77 | 197 | 164.314 | | 1.18 |
| | | | | | | | Mean Values | | 1.37 |
| | | | | | | | Standard Deviation | | 0.21 |

In Table (5.3), the mean value of (*Vexp/Vc-pre*) using *Actual* details was found to be 1.37 and the standard deviation of (*Vexp/Vc-pre*) was 0.21. This implies that the ACI code was also, in

general, more likely tending to under-predict shear capacity of the PHC slabs having medium prestressing levels by about 37%. This is a little more efficient than the CSA code.

The table also has showed that the code-predicted mode of failures by the ACI code were in agreement with experimental observations except in the cases of non-circular void slabs in Series-200 and Series-250 which fail in flexural modes. The impact of reduced bearing length on predicted shear capacities by ACI code was also not as great as it had been on experimental results outlined in Column "*Vexp"* of the table. The amount of reduction in predicted capacities by the code in Column "*Vc-pre"* between full bearing and reduced bearing specimens ranged from only 3% to 7%. Nevertheless, the code surprisingly predicted increase in capacity of few cases of slabs despite the reduced bearing length.

### 5.2.4. EN 1168 code

The concrete shear resistance ($V_{Rd,c}$) according to EC2 code, as discussed in Chapter 3, is classified into two types. The first type, cracked by bending (flexural-shear resistance) is calculated using Expression 3.18 from EC2 code in which $V_{Rd,c}$ is not a function of the applied vertical load (*P-test*). The second type, un-cracked shear (web-shear resistance) is calculated using Expression 3.25 given in EN 1168 in which $V_{Rd,c}$ is a function of the applied *P-test* since the value of $\sigma_{cp}(y)$ is derived from applied loads. However, there was no need to calculate the cracked shear type since all tested specimens were governed by un-cracked shear capacity. This can be seen in Table (5.4) where the predicted load values at which the critical sections were supposed to crack in flexural (*P-crack*) were several times higher than the predicted load (*P-test*) that causes diagonal web shear crack. For reference, the expressions for both types of shear resistance are restated below.

$$V_{Rdc} = \left[ C_{Rd,c} k (100 \rho_l f_{ck})^{1/3} + k_1 \sigma_{cp} \right] b_w d \qquad [3.18]$$

$$V_{Rdc} = \frac{I \cdot b_w(y)}{S_c(y)} \left[ \sqrt{(f_{ctd})^2 + \sigma_{cp}(y) \cdot f_{ctd}} - \tau_{cp}(y) \right] \qquad [3.25]$$

The above Expression 3.25 implies that values of $V_{Rdc}$, and $\sigma_{cp}(y)$ are unknown unless the applied *P-test* was found. Moreover, the shear critical section is not directly specified by the code; therefore, the position of the critical point is an additional parameter in this code that needs to be predicted.

To find the value of predicted web-shear capacity for each slab according to this code, certain trial points were selected as a potential position for the critical point; using an educated guess and following recommendation of the code as outlined in Section 3.4.4. Next, all sectional properties were determined for each of the assumed positions. The critical of those assumed positions would be the one resulting in the lowest shear resistance calculated by Expression 3.25. Then, the *P-test* in the spreadsheet was adjusted until both the calculated shear resistance at the *x* section, where the critical point was located, and the shear force due to all applied loads calculated at the same section become equal.

Both shear-force and code-predicted shear-resistance diagrams by the EN 1168 code are presented in Sections 5.2.4.1 to 5.2.4.3 for all tested slabs in this program using as-built cross section details and actual estimated concrete compressive strengths.

The shear diagrams include the following information:

- $V_{(x)}$ represents the total shear force at any given distance from loaded end of the slab. It includes effects of both the *P-test*, that will cause the shear failure, and self-weight of member.
- $V_{Rd,c(y)}$ is the code-predicted shear resistance estimated using the expression for un-cracked shear, as outlined in Section 3.4.4.
- The line at distance $l_x$ from the slab end represents the distance of the section were critical point for shear resistance is located according to the guidelines mentioned earlier.

#### *5.2.4.1. Shear resistance diagrams for Series-200 slabs*

There was a noticeable and consistent effect for void shape on this code's predictions for slabs in Series-200. The predicted un-cracked shear capacities of 200-mm slabs from provider 2, which were with noncircular voids, were approximately 20% higher than their counterparts with circular voids. Also, the reduction in shear capacities that resulted from reducing the bearing length has ranged from 3% to 7% with respect to the capacity of the slabs of the same series tested with full bearing length.

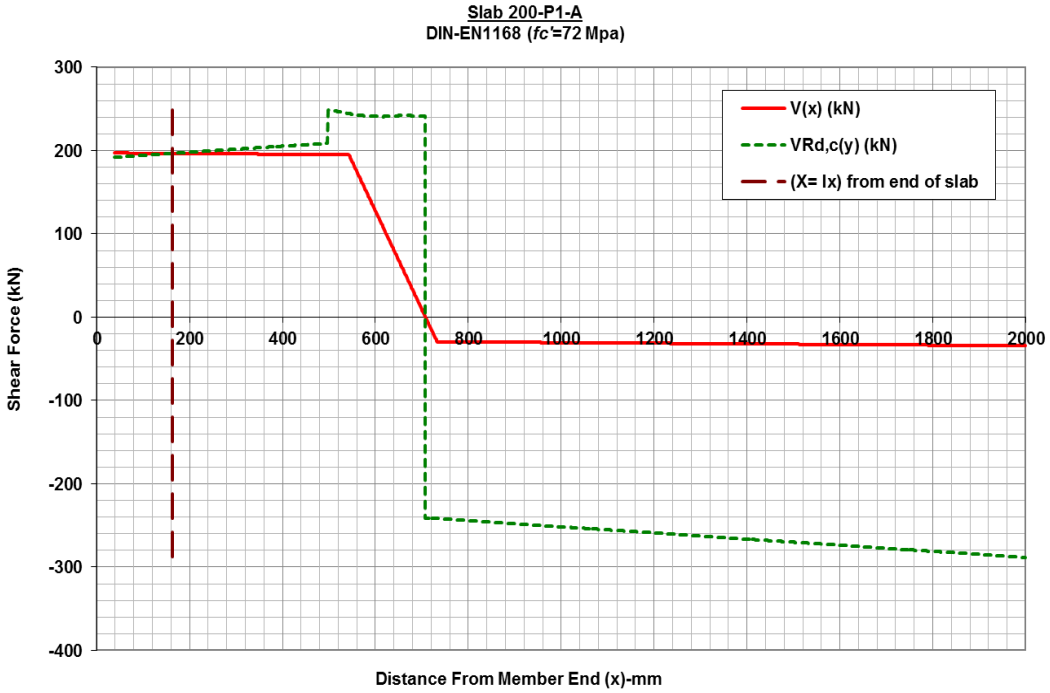


Figure (5.37): EN 1168 code predicted shear resistance slab 200-P1-A

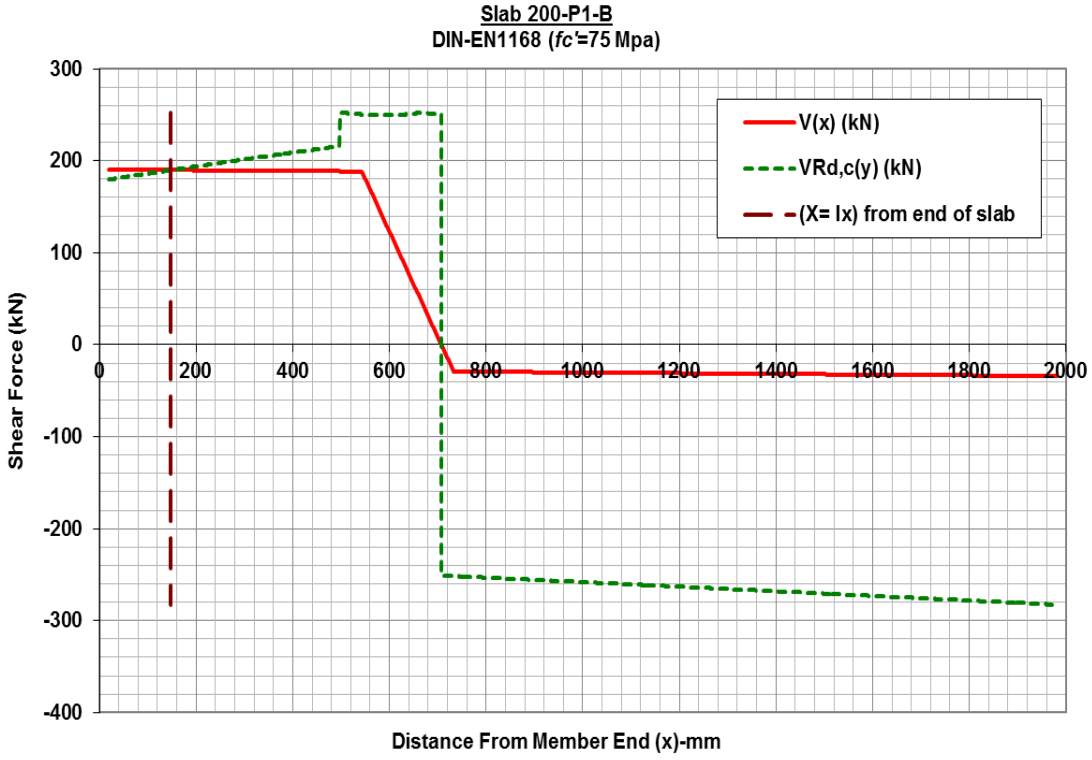


Figure (5.38): EN 1168 code predicted shear resistance slab 200-P1-B

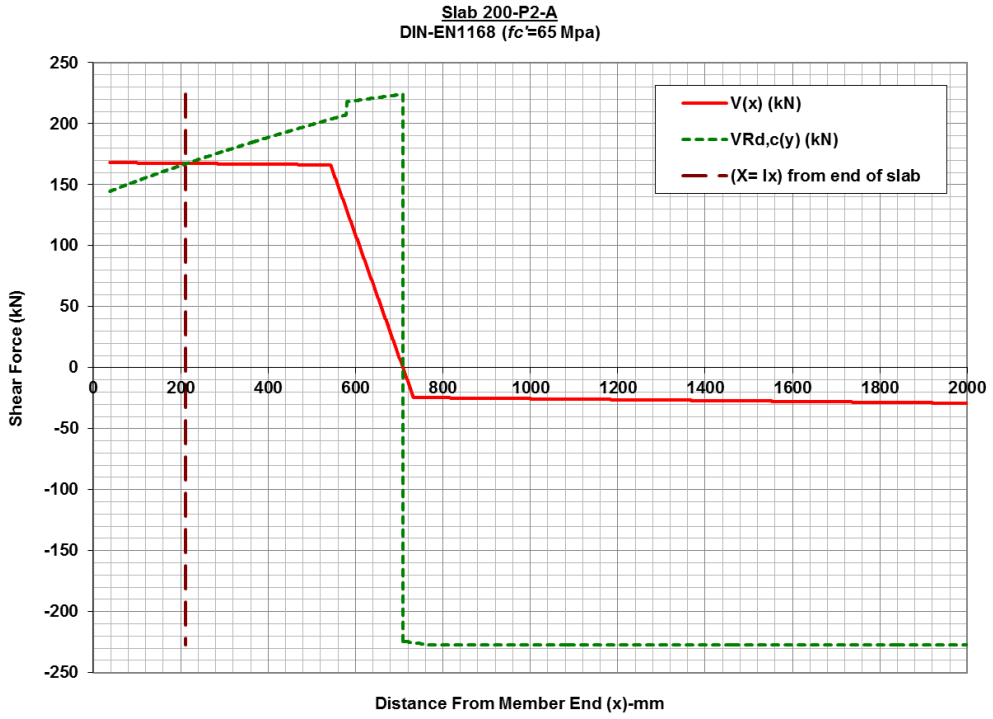


Figure (5.39): EN 1168 code predicted shear resistance slab 200-P2-A

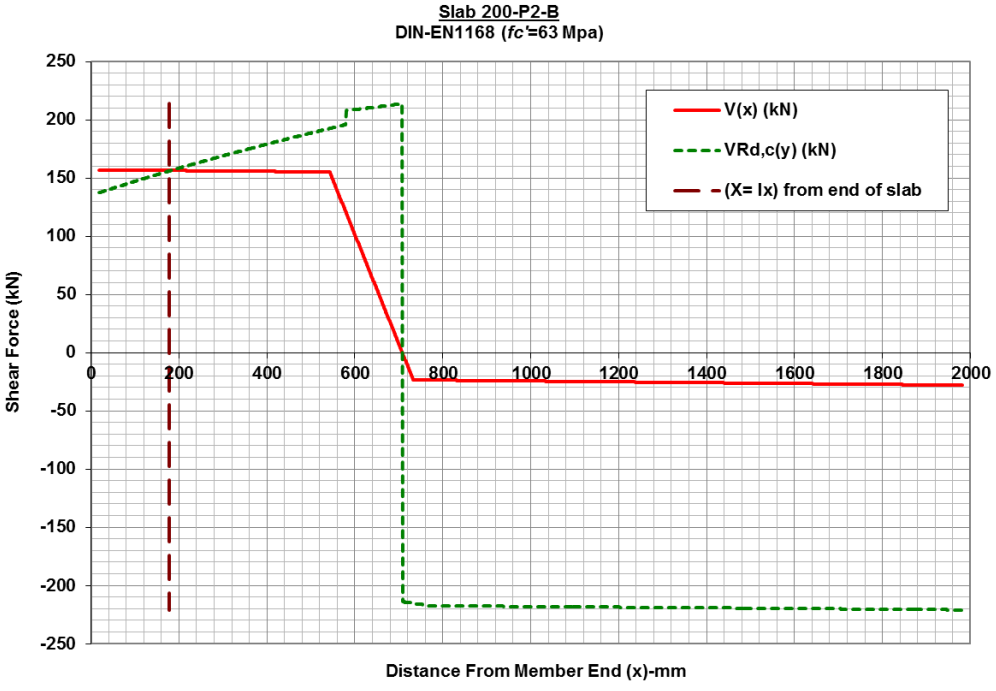


Figure (5.40): EN 1168 code predicted shear resistance slab 200-P2-B

### *5.2.4.2. Shear resistance diagrams for Series-250 slabs*

The influence of noncircular void shapes in Series-250 was more than it was in Series-200. The apparent reason for this behaviour was discussed earlier in Section 5.1.4.1. The average increase in predicted shear capacity by EN 1168 for 250-mm slabs with noncircular voids found to be 25% with reference to the corresponding circular ones. Moreover, the negative effect of reduced bearing length in this series ranged from 4% to 8%.

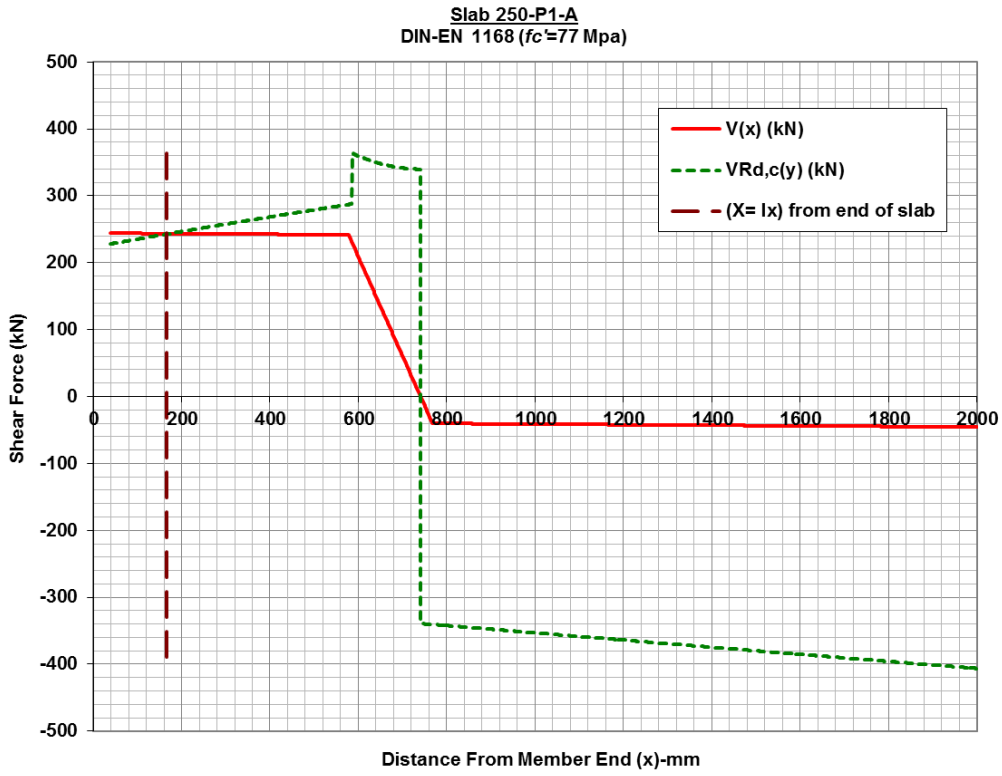


Figure (5.41): EN 1168-08 code predicted shear resistance slab 250-P1-A

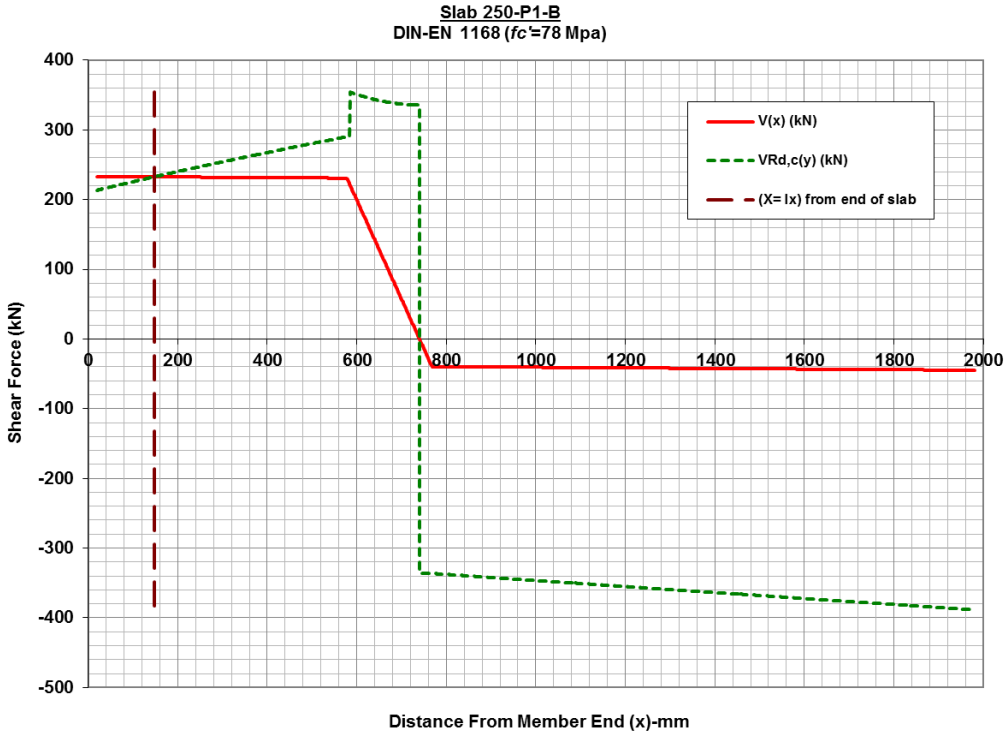


Figure (5.42): EN 1168 code predicted shear resistance slab 250-P1-B

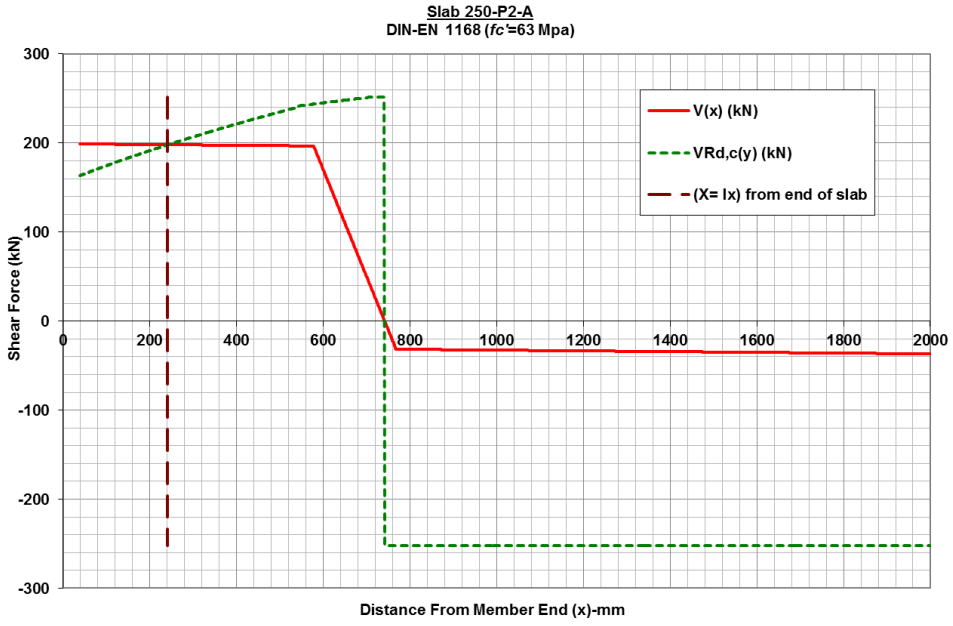


Figure (5.43): EN 1168 code predicted shear resistance slab 250-P2-A

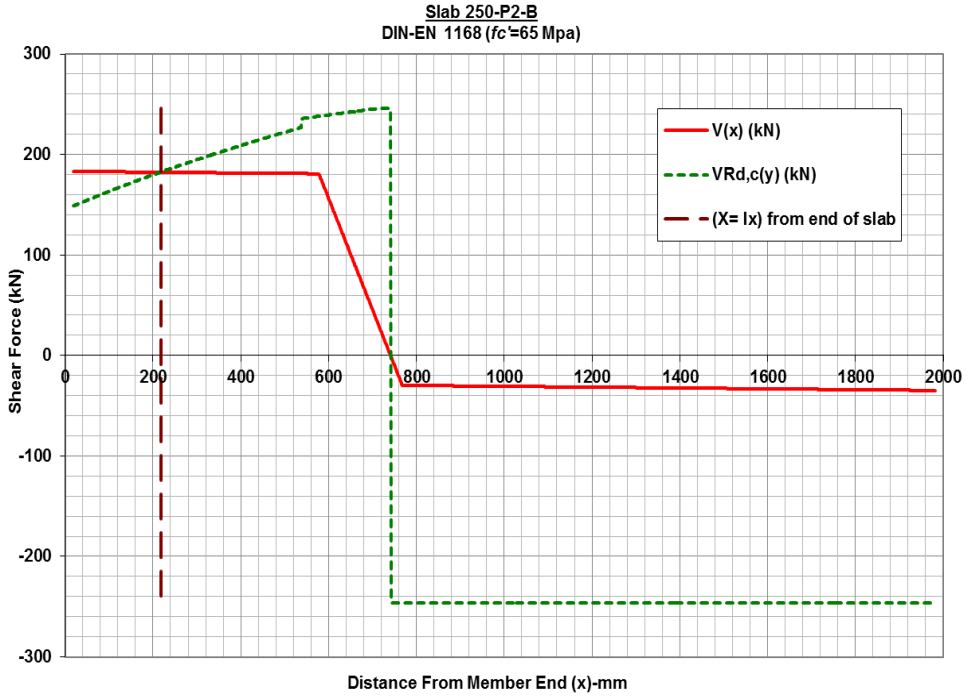


Figure (5.44): EN 1168 code predicted shear resistance slab 250-P2-B

### *5.2.4.3. Shear resistance diagrams for Series-300 slabs*

The predicted shear capacity for slab 300-P2-B was 1% lower than the capacity of slab 300-P2-A while prediction of slab 300-P1-B has showed a reduction of about 9% compared to the capacity of slab 300-P1-A. Again, these reduction percentages due to effect of bearing length are smaller than observed reduction in experimentally observed capacities.

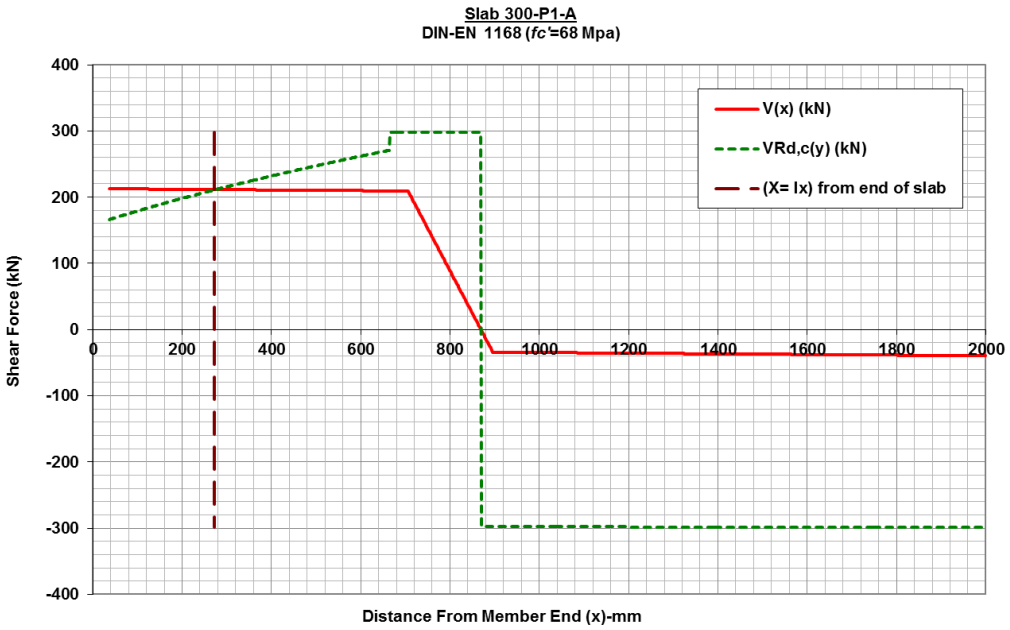


Figure (5.45): EN 1168 code predicted shear resistance slab 300-P1-A

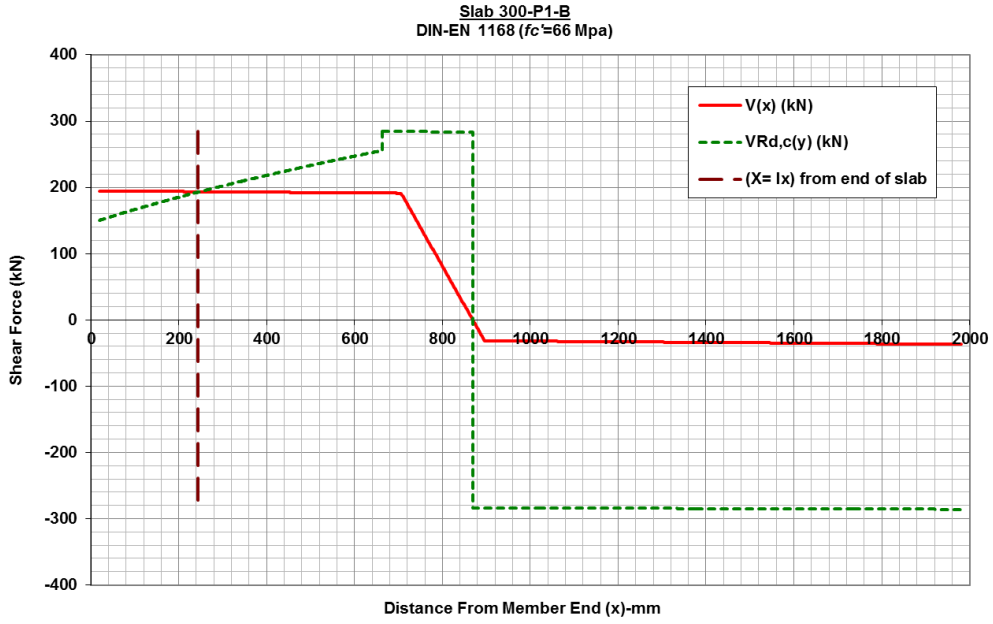


Figure (5.46): EN 1168 code predicted shear resistance slab 300-P1-B

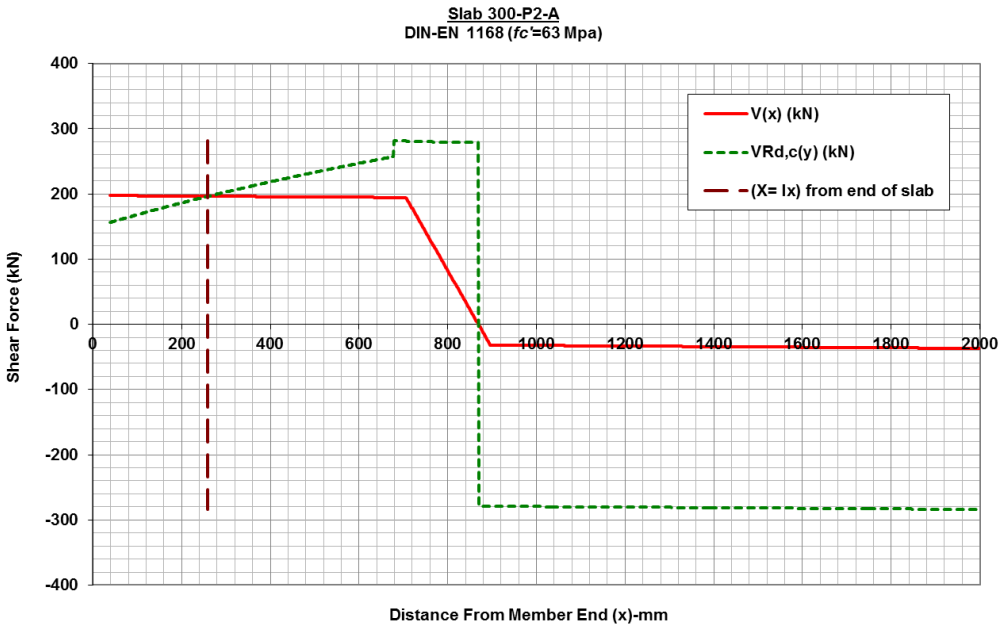


Figure (5.47): EN 1168 code predicted shear resistance slab 300-P2-A

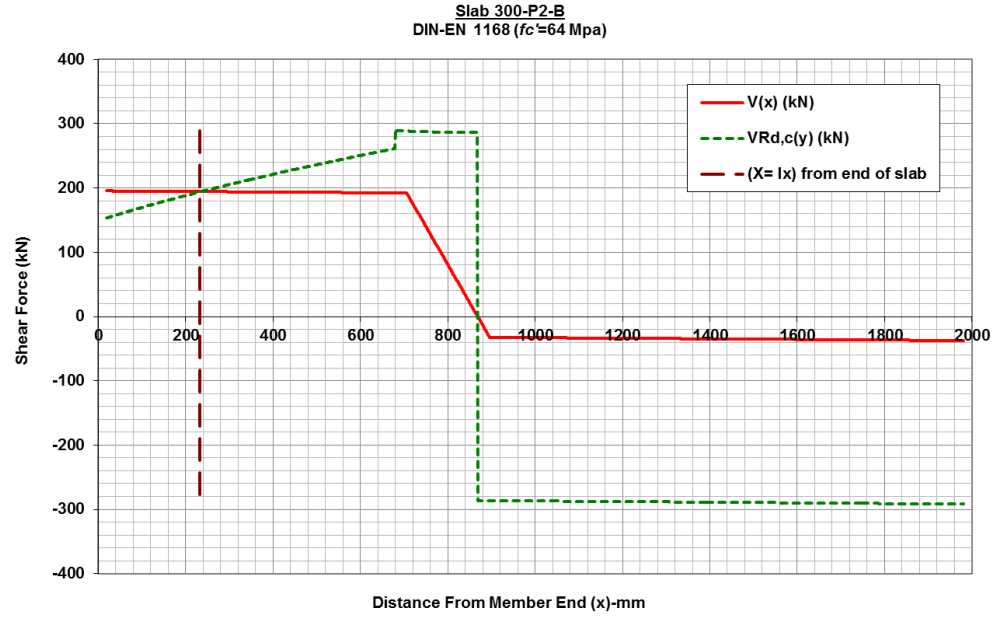


Figure (5.48): EN 1168 code predicted shear resistance slab 300-P2-B

#### *5.2.4.4. Comparison of EN 1168 code predictions with experimental results*

Table (5.4) below is a summary of the analysis results by the EN 1168 code using both as-built and as-designed slab cross sectional details. The table includes similar type of information introduced in Sections 5.2.2.4 and 5.2.3.4, in addition to one more term defined as following:

- *P-crack* is the minimum predicted machine load that would cause a flexural crack on the bottom surface of the slabs within the critical zone; the zone between the support and the identified shear critical section for web-shear resistance.

Table (5.4): Summary of shear capacity analysis performed on tested slabs using EN 1168 code

| | | Exp. Results | | | DIN EN-1168-08 Predictions | | | | | |
|---|---|---|---|---|---|---|---|---|---|---|
| Slab ID | X-Sec Details | P-test (kN) | Vexp (kN) | Exp. Failure Mode | P-crack (kN) | P-pre (kN) | Pre. Failure Location (mm) | Vc-pre (kN) | Pre. Failure Mode | Vexp/Vc-pre |
| 200-P1-A | Actual | 235.5 | 206 | Flexural | 377 | 223.9 | 163 | 196 | Web-shear | 1.05 |
| | Nominal | | 206 | | | 189 | 159 | 166 | | 1.24 |
| 200-P1-B | Actual | 196.3 | 173 | Flexural & Flexural-shear | 359 | 216.9 | 148 | 190 | Web-shear | 0.91 |
| | Nominal | | 172 | | | 186.5 | 134 | 163 | | 1.05 |
| 200-P2-A | Actual | 227.0 | 199 | Web-shear | 299 | 190 | 210 | 167 | Web-shear | 1.19 |
| | Nominal | | 198 | | | 166 | 206 | 146 | | 1.36 |
| 200-P2-B | Actual | 187.0 | 164 | Web-shear | 301 | 177.9 | 178 | 156 | Web-shear | 1.05 |
| | Nominal | | 163 | | | 161 | 181 | 141 | | 1.16 |
| 250-P1-A | Actual | 351.4 | 302 | Flexural-shear | 663 | 281 | 166 | 243 | Web-shear | 1.24 |
| | Nominal | | 301 | | | 235 | 158 | 204 | | 1.48 |
| 250-P1-B | Actual | 350.8 | 300 | Flexural-shear | 638 | 269.5 | 148 | 233 | Web-shear | 1.29 |
| | Nominal | | 299 | | | 228.5 | 133 | 197 | | 1.52 |
| 250-P2-A | Actual | 244.9 | 213 | Web-shear | 488 | 227.5 | 240 | 198 | Web-shear | 1.08 |
| | Nominal | | 212 | | | 309.5 | 239 | 266 | | 0.80 |
| 250-P2-B | Actual | 222.7 | 193 | Web-shear | 465 | 209.8 | 218 | 182 | Web-shear | 1.06 |
| | Nominal | | 192 | | | 303 | 214 | 259 | | 0.74 |
| 300-P1-A | Actual | 318.8 | 275 | Web-shear | 624 | 242.5 | 272 | 211 | Web-shear | 1.30 |
| | Nominal | | 274 | | | 234 | 279 | 203 | | 1.35 |
| 300-P1-B | Actual | 263.9 | 228 | Web-shear | 608 | 221.8 | 244 | 193 | Web-shear | 1.18 |
| | Nominal | | 227 | | | 227.5 | 254 | 197 | | 1.15 |
| 300-P2-A | Actual | 346.7 | 297 | Web-shear | 620 | 225.5 | 259 | 196 | Web-shear | 1.51 |
| | Nominal | | 297 | | | 230.5 | 279 | 200 | | 1.49 |
| 300-P2-B | Actual | 223.8 | 194 | Web-shear | 609 | 223.8 | 232 | 194 | Web-shear | 1.00 |
| | Nominal | | 194 | | | 226.5 | 254 | 196 | | 0.99 |
| | | | | | | | | Mean Values | | 1.16 |
| | | | | | | | | Standard Deviation | | 0.17 |

In Table (5.4) mean value of (*Vexp/Vc-pre*) based on analysis with *Actual* details was found to be 1.16 and the standard deviation of (*Vexp/Vc-pre*) was 0.17. Those statistic values indicate that

the performance of EN 1168 code in prediction of shear capacity of PHC slabs was quite remarkable for the range of parameters covered in the experimental program. The code generally was conservative by only 16%, and in many cases it has successfully predicted almost exact shear capacities found from the experiments. However, the code overestimated the capacity of a number of slabs resulting in less conservative predictions. Therefore, it is reasonable to call the web-shear capacity expression in EN 1168 the most efficient and consistent among the three codes used for analysis in this research program.

The size effect could be investigated on slabs from the second supplier (P2) as the only variable was the thickness of the units. Values of *Vc-pre* for these specimens in the table have indicated increasing trend relatively with the increased thickness. When the amount of increase in slabs thickness was 25% (between Series-200 and Series-250), *Vc-pre* has increased by 18% and when the thickness was increased by 50% (between Series-200 and Series-300), the predicted shear resistance has increased by 21%.

# CHAPTER 6: FINITE ELEMENT MODELING

## 6.1. General

Finite element modeling (FEM) is a very useful and economic tool to study the complex behaviour of structural elements such as shear resistance of PHC slabs. It was observed during the literature review that FEM helped researchers (Yang 1994; Wolanski 2004; Cheng and Wang 2010) to derive very important conclusions about effect of parameters, which were not covered in laboratory experiments. As a result, this part of the research program was dedicated to the nonlinear analysis using three-dimensional FEM to simulate the laboratory tests. The finite element software package, Mechanical APDL (ANSYS, 2010), was used for this purpose. Using the provided structural features in that package, a model for PHC slabs was constructed and used to conduct a parametric study that is presented in the next chapter.

In ANSYS, models can be created using a typed command input or the graphical user interface. It is worth to mention that the software has no "undo" option; consequently, errors in modeling could be quite challenging to recover while with command approach, editing is as simple as editing any text. In addition, some of the capabilities of the software were only available in commands setup; as a result, the author preferred the command approach to save time and storage space.

This chapter presents details of procedures followed in constructing the FEM model. This includes discussion of type of elements used for simulation of different components of the PHC slabs, constitutive model for each element, meshing, boundary conditions, and how the solution was controlled. Finally, the model was verified against the laboratory results.

## 6.2. Material Properties and Element Types

### 6.2.1. Concrete

The concrete was simulated using an element type called SOLID65. It is a three dimensional solid element that is capable of taking into account the nonlinear elasto-plastic characteristics of concrete. Also, it has the ability to simulate plastic deformations, crushing, cracking and even shear transfer at cracks interface. The geometry of the element is defined by eight corner nodes with three translational degrees of freedom (UX, UY, and UZ) at each node. To avoid any contradiction between local axes of the elements and the global axes of the model, node numbers have to be input in a certain order. So, according to the node names used in Figure (6.1), the element would be defined in the following node order: (I, J, K, L, M, N, O, P) or (2, 4, 3, 1, 6, 8, 7, 5).

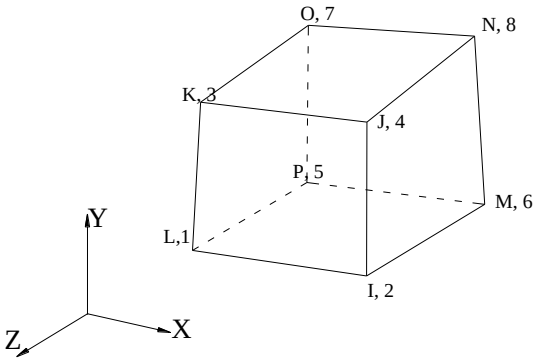


Figure (6.1): Element SOLID 65 (reproduced from user manual of ANSYS 2010)

The most used constitutive model with SOLID 65 by previous researchers was based on the model for concrete developed by William and Warnke (1974). That constitutive model requires three sets of parameters to be identified for concrete as follows:

a) Set 1 (linear isotropic material properties)

For the elastic zone in concrete behaviour which extends till a stress level about 0.4 $f_c^{'}$, linear elastic material properties are required. In the developed model a 0.17 value was assumed for the Poisson's ratio and the modulus of elasticity ($E_c$) was calculated from the empirical equation below, which was given in Table (3.1) of EC2 as follows:

$$E_c = 22\left[ f_c^{'}/10 \right]^{0.3} = \quad (GPa) \qquad [6.1]$$

Where, $f_c^{'}$ is in concrete compressive strength in MPa.

b) Set 2 (nonlinear material curve)

In here, the nonlinear stress-strain curve of concrete is approximated with a multi-linear curve; this was achieved by choosing the Von-Mises failure criterion in the software. The type of concrete used in PHC slabs production is usually high strength concrete ( $f_c^{'}$ >50 MPa) and the strain at peak stress ($\varepsilon_{c1}$) for high strength concrete would be larger than that of normal strength concrete which usually happens at 0.002. On the contrary, as high strength concrete tend to be less plastic the descending branch of its curve is shorter and its ultimate strain at failure is smaller than ultimate strain of normal concrete. An appropriate stress-strain relationship for non-linear structural analysis that considers all those mentioned characteristics of high strength concrete was provided in Clause 3.1.5 of EC2 code and Clause C3.1.5 of the Commentary Eurocode 2 (2008). This relationship was used in the constructed FEM of this research program. The expressions used to calculate the points on the stress-strain ($\sigma_c$ - $\varepsilon_c$) curve for concrete

elements are outlined below. Also, in Figure (6.2) a plot of the concrete curve for FEM of slab 300-P1-A is shown as a sample.

The ascending branch of the curve (when $\varepsilon_c < \varepsilon_{c1}$ ) is determined from following:

$$\sigma_c = \left( \frac{k\eta - \eta^2}{1 + (k-2)\eta} \right) f_c^{'} \qquad [6.2]$$

$$\varepsilon_c = \eta \cdot \varepsilon_{c1} \qquad [6.3]$$

$$k = 1.05 E_c \frac{\varepsilon_{c1}}{f_c^{'}} \qquad [6.4]$$

However, the descending branch of the curve (when $\varepsilon_c > \varepsilon_{c1}$ ) is given as follows:

$$\sigma_c = \frac{f_c^{'}}{\left[ 1 + \{(\eta_1 - 1)/(\eta_2 - 1)\}^2 \right]} \qquad [6.5]$$

$$\varepsilon_c = \eta_1 \cdot \varepsilon_{c1} \qquad [6.6]$$

$$\eta_2 = (\varepsilon_{c1} + \varepsilon_{c0}) / \varepsilon_{c1} \qquad [6.7]$$

Where,

- $\varepsilon_c$ and $\sigma_c$ are the calculated values of strain and stress of any point on the curve.
- $\varepsilon_{c1}$ is the compressive strain at peak stress, at $f_c^{'}$, as estimated from Expression [6.8].
- $\varepsilon_{cu1}$ is the ultimate compressive strain and its value for high strength concrete is determined from Expression [6.9].
- $\varepsilon_{co}$ is an additional parameter used for the descending branch and its value is dependent on the value of $f_c^{'}$, as given in Table (6.1) below.

$$\varepsilon_{c1} = \frac{0.7}{1000}(f_c^{'})^{0.31} < 0.0028 \qquad [6.8]$$

$$\varepsilon_{cu1} = \frac{(2.8 + 27\left[(98 - f_c^{'})/100\right]^4)}{1000} \quad \text{for} \quad f_c^{'} \geq 50 \text{ MPa} \qquad [6.9]$$

Table (6.1): Values of $\varepsilon_{co}$ adopted from commentary Euro code 2 (2008)

| $f_c^{'}$ (MPa) | 50 | 60 | 70 | 80 | 90 |
|---|---|---|---|---|---|
| $\varepsilon_{co}$ | $0.807\text{x}10^{-3}$ | $0.579\text{x}10^{-3}$ | $0.338\text{x}10^{-3}$ | $0.221\text{x}10^{-3}$ | $0.070\text{x}10^{-3}$ |

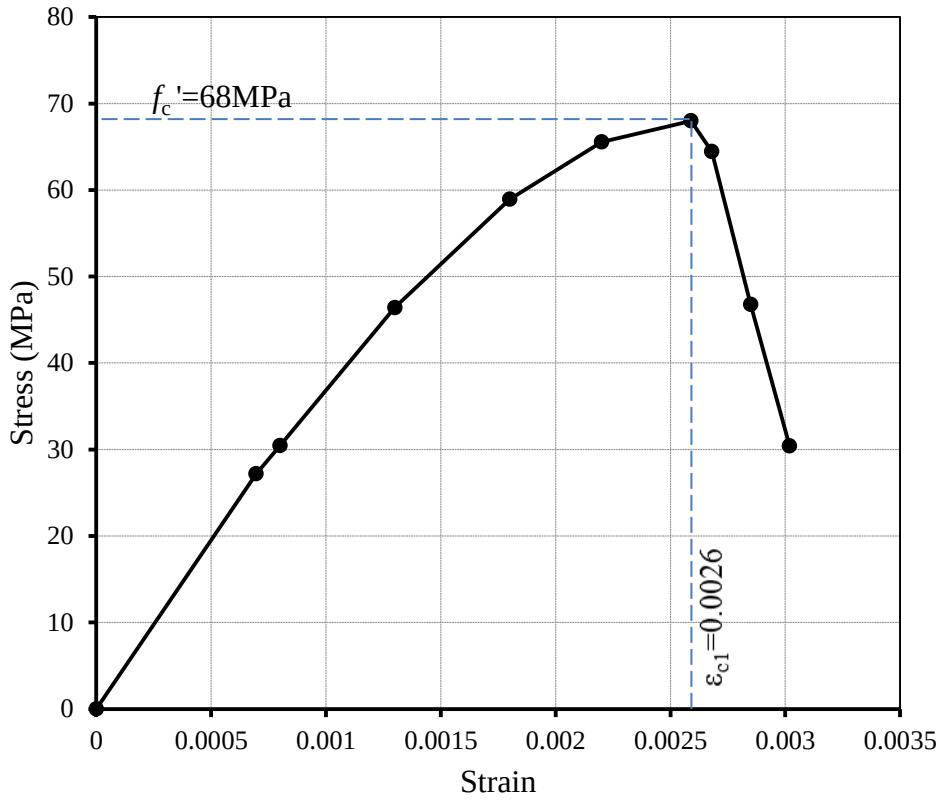


Figure (6.2): Stress-strain curve for concrete elements used in FEM

c) Set 3 (complementary constants and coefficients)

Beside the behaviour of concrete under compression, there are a group of additional parameters that need to be specified for SOLID 65 to simulate concrete behaviour with other types of loading. The most relevant parameters for the shear loading are as follows.

- *C1* = Shear transfer coefficient at open crack lines
- *C2* = Shear transfer coefficient at closed crack lines
- *C3* = Uniaxial tensile strength of concrete
- *C4* = Uniaxial crushing strength of concrete

Values of *C1* and *C2* coefficients could ranges from 0.0 (shear transfer is not allowed simulating a very smooth interface) to 1.0 (full shear transfer is possible at cracks which simulates a very rough interface condition). For the PHC slab model in this study, C1 and C2 were taken 0.3 and 0.95, respectively, as recommended by Cheng and Wang (2010).

One of the disadvantages to mention about performance of the SOLID 65 element is related to its extra sensitive reaction to stress concentration which leads to conversions issues due to prematurely crushing of the elements in areas around the support locations, and ends of strands in case of PHC slab models. This behaviour was also pointed out by all previous researchers who used ANSYS and the most suggested solution was to "turn off" the crushing feature of the SOLID 65 elements by putting -1 as a value for *C4*.

### 6.2.2. Reinforcement

The prestressing strands of the PHC slabs were modeled using an element type called LINK180. This is a 3-D truss element that is capable of resisting axial compression and tension forces but not moment. It has characteristics of plasticity, large deflection, and large strain deformations. The geometry of the element is defined by node numbers at its both ends (I and J), as shown in Figure (6.3). Also, the cross-sectional area which would represent area of the strands is the additional required information to define geometry of the element.

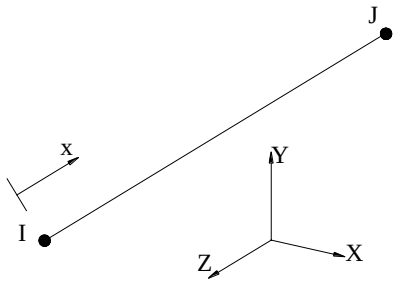


Figure (6.3): LINK180 element (reproduced from user manual of ANSYS 2010)

The definitions of material properties of LINK180 elements are outlined below in two sets.

a) Set 1 (linear isotropic material properties)

It consists of modulus of elasticity ($E_p$) and Poisson's ratio for the strands, which were taken as 28,500 ksi (196,500MPa) and 0.2, respectively.

b) Set 2 (Nonlinear material curve)

The prestressing strands do not have identifiable yielding point like in case of regular mild steel and no strain hardening exist before rupture. The multi-linear curve option (MISO) was useful again to define stress-strain curve of prestressing strand elements in this research. Coordinates for each point on the curve were derived using the equations found in PCI Manual for the Design of HC Slabs (PCI, 2007) for low relaxation strands of grade 270 ksi (1860 MPa) which have been summarised below and also plotted in Figure (6.4).

For the elastic segment of the curve when ($\varepsilon_p < 0.0086$), stress in the LINK180 element ($f_p$) is calculated from the following linear equation:

$$f_p = 28,500\varepsilon_p \quad \text{(ksi)} \qquad [6.11]$$

While, for the plastic segment ($\varepsilon_p > 0.0086$), the stress in strand elements ($f_p$) is calculated from following expression:

$$f_p = 270 - \frac{0.04}{(\varepsilon_p - 0.007)} \text{ (ksi)} \qquad [6.12]$$

Where $f_p$ and $\varepsilon_p$ are the strand stress (MPa) and corresponding strain at any arbitrary point on the curve.

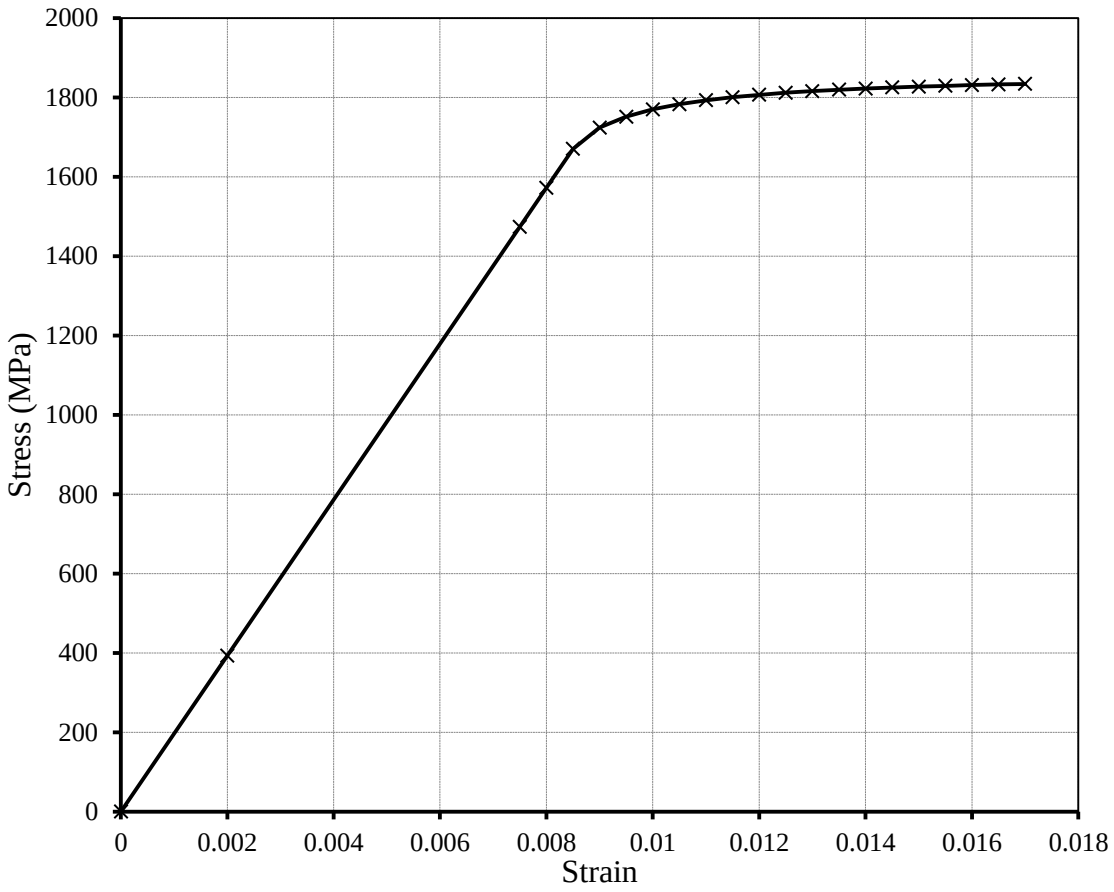


Figure (6.4): Stress-strain curve for strand elements used in FEM

c) Set 3 (initial stress state)

The most useful feature of the LINK180 element with respect to PHC slabs was the initial state capability that could be specified by the user to simulate the prestressing force. This was achieved by the *INISTATE* command. The strain had to be specified in the direction of the local axis that extends along length of the element; that is, in x-direction as illustrated in Figure (6.3). For this research, an amount of initial strain equal to 0.00568 which is corresponding to 1116 MPa (0.60 of ultimate 1860 MPa) on each strand was specified. This stress was transferred to the surrounding concrete elements by the end of first loading step.

### 6.2.3. Steel bearing plates

The support plates and flange of the loading beam were simulated by an eight node solid element, SOLID45. The geometry of this element is similar to SOLID65 except that it does not crack or crush. So, using SOLID45 prevents convergence problems, which occur at loading or reaction points when directly applied onto concrete elements.

Material properties of these steel elements were assumed to be linear-elastic. Consequently, modulus of elasticity and Poisson's ratio were the only essential properties to be specified in this research, which were taken as 200 GPa and 0.3, respectively.

### 6.2.4. Reinforcement-concrete interface

When location of the reinforcement would matter for the overall response of the model, the reinforcement elements are usually modeled discretely and joined with the concrete elements at the shared nodes, in case of perfect bond assumption. However, when bond-slip relationship is a crucial in the overall behaviour of the structural member such as the case of PHC slabs, the reinforcement will be connected to the shared concrete nodes via spring elements. In other

words, one end of the spring will be attached to concrete and the other end to the reinforcement element. Indeed, addition of springs would not cause any change in node locations or size of the elements but it requires a duplication of nodes along the line of reinforcement with a different numbering.

In this research, the bond-slip relationship between the strands and concrete was modeled with COMBIN39 element. This is a non-linear spring element with 1-D, 2-D, or 3-D options. For the purpose of this research, uniaxial tension-compression (1-D) setting was selected to simulate bond-slip only in longitudinal direction. The geometry of the element is defined by 2 preferably coincident nodes, I and J.

The second input data required from the user, for COMBIN39 to function, is the bond force-deflection curve which is calculated for each bar diameter by multiplying values in bond stress-slip curve with area of the considered strand. The bond stress-slip model for this research, shown in Figure (6.5), was adopted from Clause 3.1 of CEB-FIP Model code (CEB-FIP 1990).

The ascending branch of the bond stress-slip curve ($s \leq s_1$) was calculated from following expression:

$$\tau = \tau_{\max}\left(\frac{s}{s_1}\right)^{\alpha} \qquad [6.12]$$

Where, $\tau$ and $s$ are the bond stress (MPa) and the corresponding slippage (mm), respectively, of any point on the curve. In Expression 6.12, the term $\tau_{\max}$ is the maximum bond strength taken as $2.0\sqrt{f_c^{'}}$. While, $\alpha$ is a coefficient that ranges from 0.0 (constant bond stress till slippage) to 1.0

(linearly increasing bond stress till slippage), taken as 0.4 in this research. While, $s_1$ is called the characteristic slip value and it was assumed as 1.0 mm in the adopted model.

The descending branch of the curve ($s > s_1$) is supposed to be linear up to a minimum bond stress of $\tau_f = 0.15\tau_{max}$. However, as the prestressing strands are similar to smooth wires rather than ribbed surface bars and since the verified model did not perform well when descending branch was used; consequently it was assumed that $\tau_f = \tau_{max}$ at maximum slip, $s_3 = 3.0mm$ in the model.

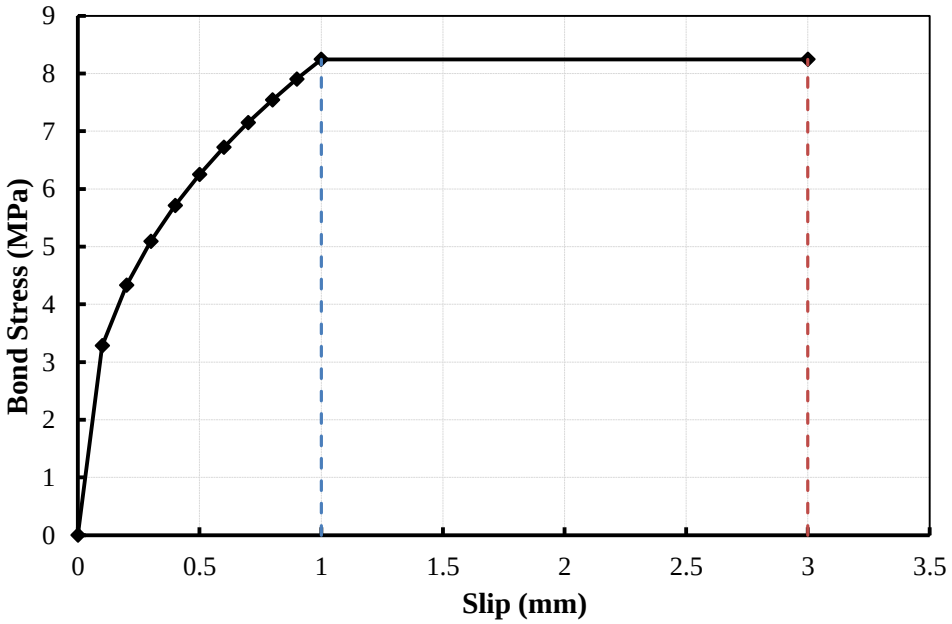


Figure (6.5): Bond stress-slip curve used for COMBIN39 elements

## 6.3. Model Geometry and Boundary Conditions

The cross section of the test specimens were symmetric about the vertical axis passing through center of area. This enabled the reduction of model size in order to cut down solution time and save storage disk space. As a result, only half width of the specimen was modelled with full length, as shown in Figure (6.6).

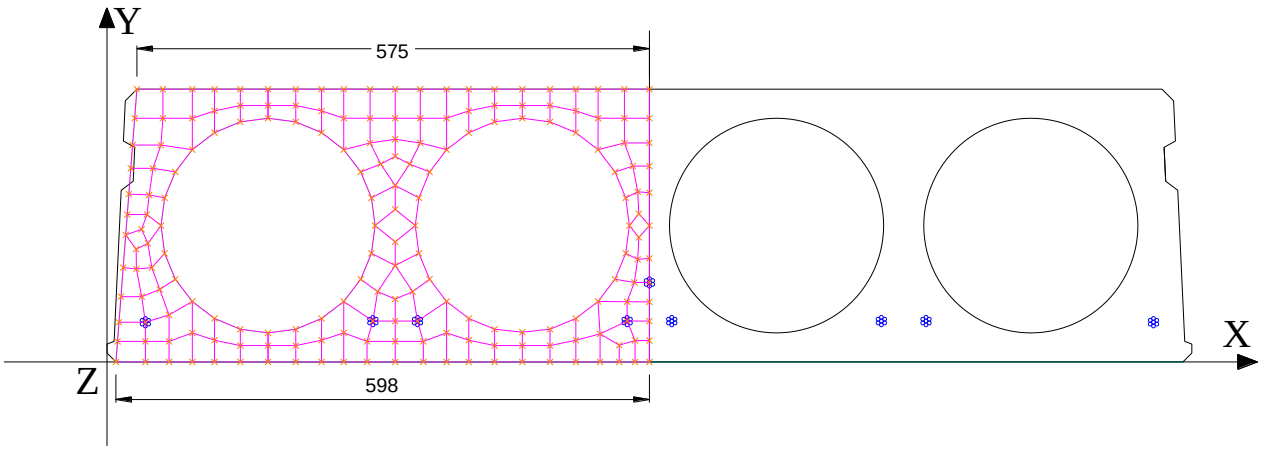


Figure (6.6): Meshing and view of the simulated portion from the full section of 300 mm slab

In the model, the z-axis was set along the longitudinal direction of the slab, the x-axis in the same horizontal plane, and the y-axis in the vertical plane. This means the cross section of the model is laid on x-y plane as shown in Figure (6.6). The nodes were numbered orderly even though it was time-consuming but was necessary to easily find any specific location or entity on the model as required. The curved edges of the PHC slabs at the corners of webs and around voids were simulated as the nominal profile of the real specimens with the advantage of allowable flexibility in geometry of SOLID65 elements. Figure (6.7) below shows an isometric full view of the FEM.

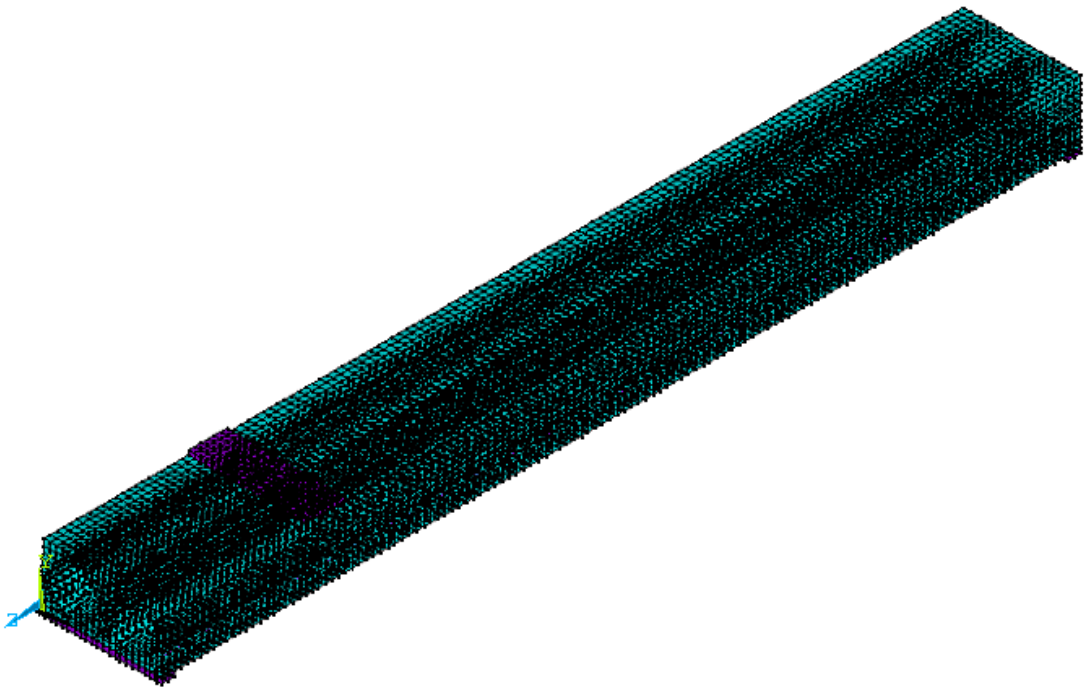

Figure (6.7): Full view of the geometry for the FEM

To simulate the same boundary conditions of the test specimens, all nodes located on the plane of symmetry were restrained from displacement in the direction of x-axis. Also to simulate the pin support at the loaded side of the model, the nodes along the centre line of the support plate were restrained in z and y directions. However, for a roller support condition on the other side, the nodes on the center line of the support plate were restrained only in y-direction, as shown in Figure (6.8). It is worth to mention that the technique to restrain displacement of any of those discussed nodes in the specified directions is achieved by just setting a magnitude of displacement equal to zero.

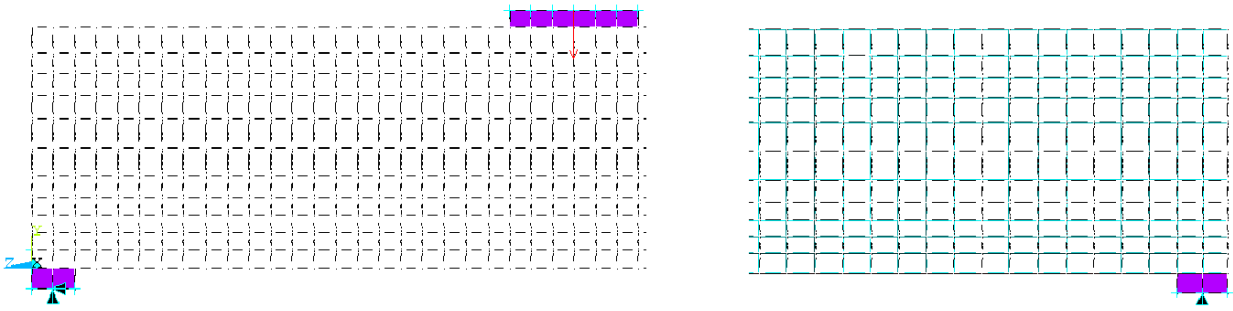

Figure (6.8): Boundary conditions of support plates in the FEM

## 6.4. Solution Control

The nonlinear analysis was performed in a number of loading steps. The purpose of the first loading step was to transfer the prestressing effect from the jacked/stressed strands to the surrounding concrete section; following the construction sequence of PHC slab. This loading step eventually causes the camber along length of the slab. In fact, all results obtained from the first load step were not required for the analysis and were offset from final results. The following loading steps simulated the gradual application of a vertical concentrated line load as performed during tests to cause the shear failure. Load increments of 1.0 kN was used until failure was reached.

In this study, the convergence criterion was based on force. The tolerance limit was set as 2% during only the first load step to ease the solution. However, after the first loading step a 1% limit was specified to the program. The solution of the model was terminated when convergence difficulties observed in the solution after web shear cracking load level has passed.

## 6.5. Model Verification

The FEM which has been introduced with details in the previous sections was proved to simulate web shear behaviour of PHC slabs in this section by comparing the results obtained from the model against physical experimental results. The goal was to ensure that the elements, material

models, constants, convergence criteria ...etc. utilized in the developed model were all suitable to simulate the subject matter of this study. The model was verified against all experimental results in the present research. The model showed reasonable consistency in simulating the behaviour of tested slabs. A comparison between FEM and experimental results is presented in the following sections. Two specimens that represent the two phases of the project (300-P1-A and 300-18-A) were selected to be illustrated in this chapter.

The readings of instrumentation that were used during the tests at specific locations on the specimens were used as base for comparison. That included load-strain relationship for concrete and strand elements and also load-deflection response. However, the most significant index in the comparison for web-shear behaviour was the cracking load which can be implied from the load-strain or load-deflection diagrams; it is the load level at which the strains and the deflection surge with almost no change in magnitude of the applied load.

### 6.5.1. Phase 1 slabs - slab 300-P1-A

Figures (6.9 to 6.12) present load versus normal strain relationships for two webs of slab 300-P1-A as obtained from the physical tests and the FEM. It can be seen that the FEM was able to predict the behaviour of the webs in very similar way like the tested slab. The stiffness of both web strain results agreed very well with experimental measurements. Also, it can be seen from the figures that the model has predicted the cracking load as 264kN for edge-web and 262kN for mid-web, while the corresponding experimental cracking loads were 275kN and 255kN, respectively. That implies deviation of predictions by the verified model was not more than 4% from experimental observations.

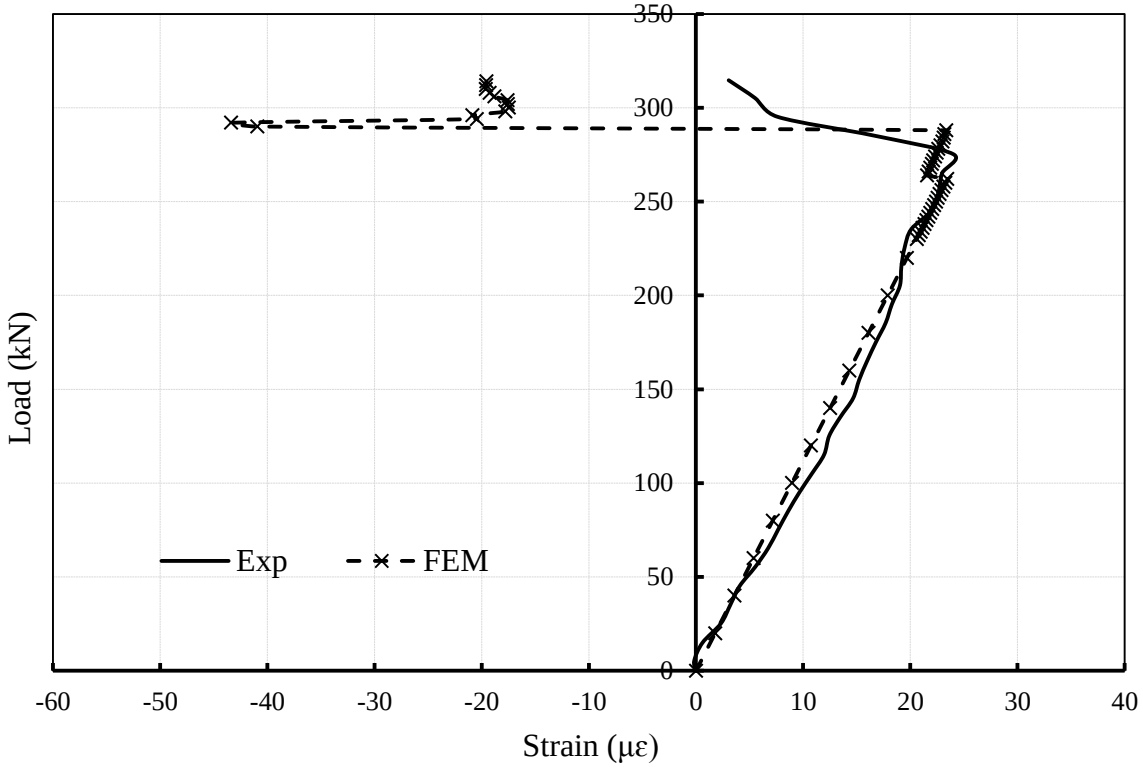


Figure (6.9): Concrete strains in edge-web of slab 300-P1-A at 438 mm from its loaded end

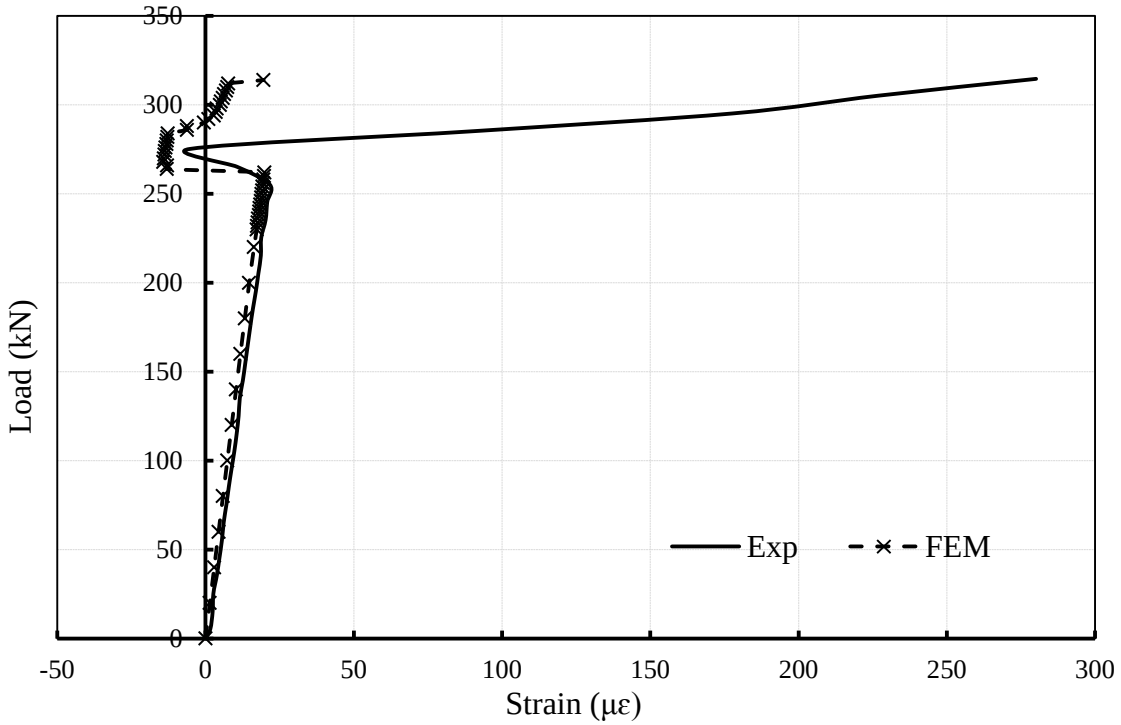


Figure (6.10): Concrete strains in mid-web of slab 300-P1-A at 438 mm from its loaded end

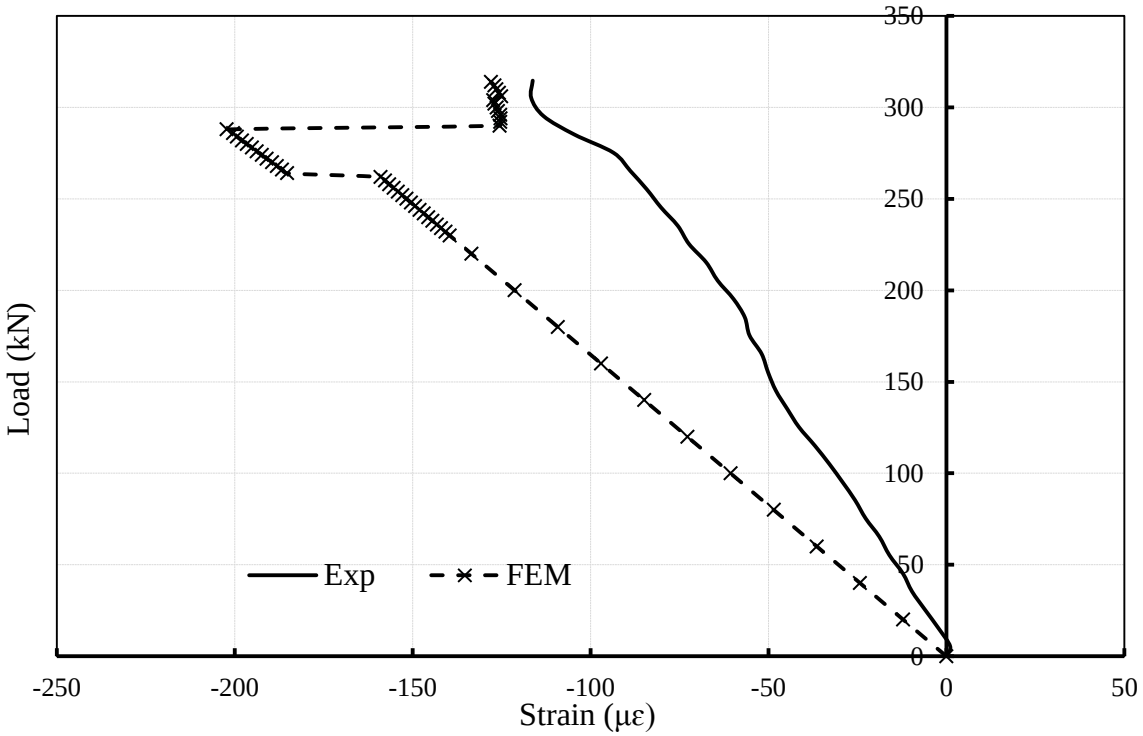


Figure (6.11): Concrete strains on top of edge-web of slab 300-P1-A at 438 mm

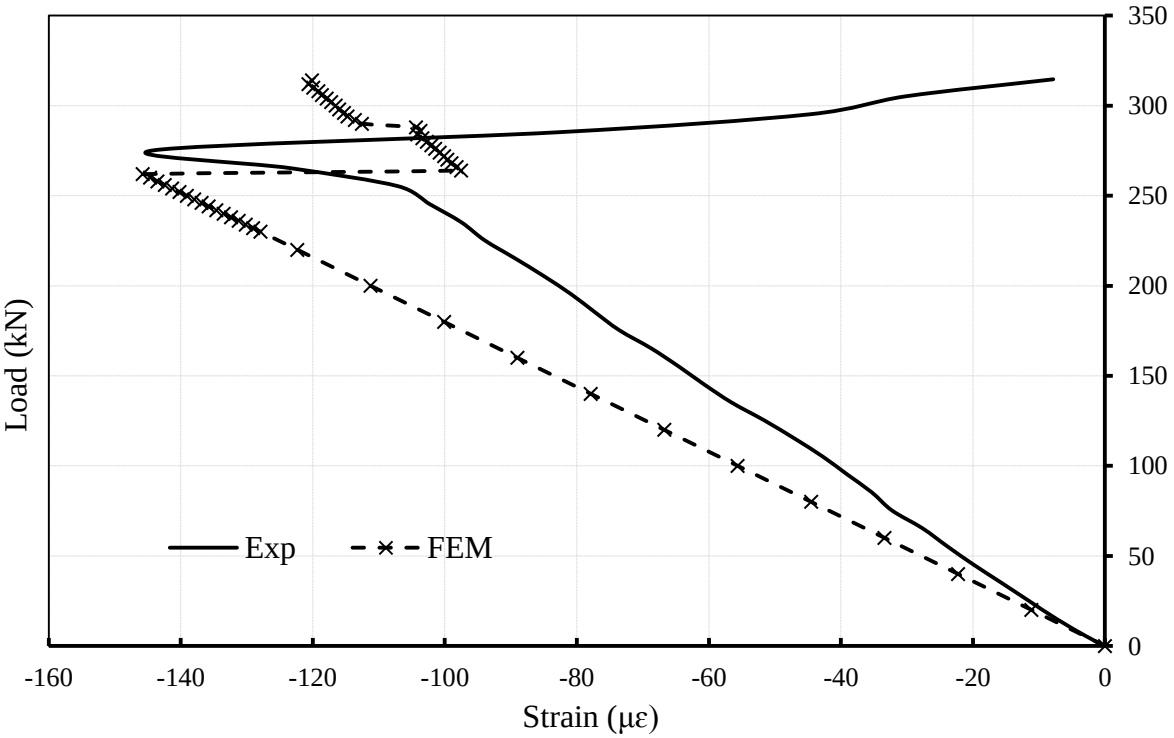


Figure (6.12): Concrete strains on top of mid-web of slab 300-P1-A at 438 mm

Moreover, the strains on the reinforcement elements as predicted in FEM was compared against experimentally measured values; Figures (6.13 and 6.14) below are showing that. The trend of both curves showed good agreement and response of the strand elements used in FEM compared to the physical experiment. Furthermore, FEM strains in both locations indicated the same cracking loads discussed earlier for concrete of webs and likewise in the experiment no sign of rupture or yielding was observable.

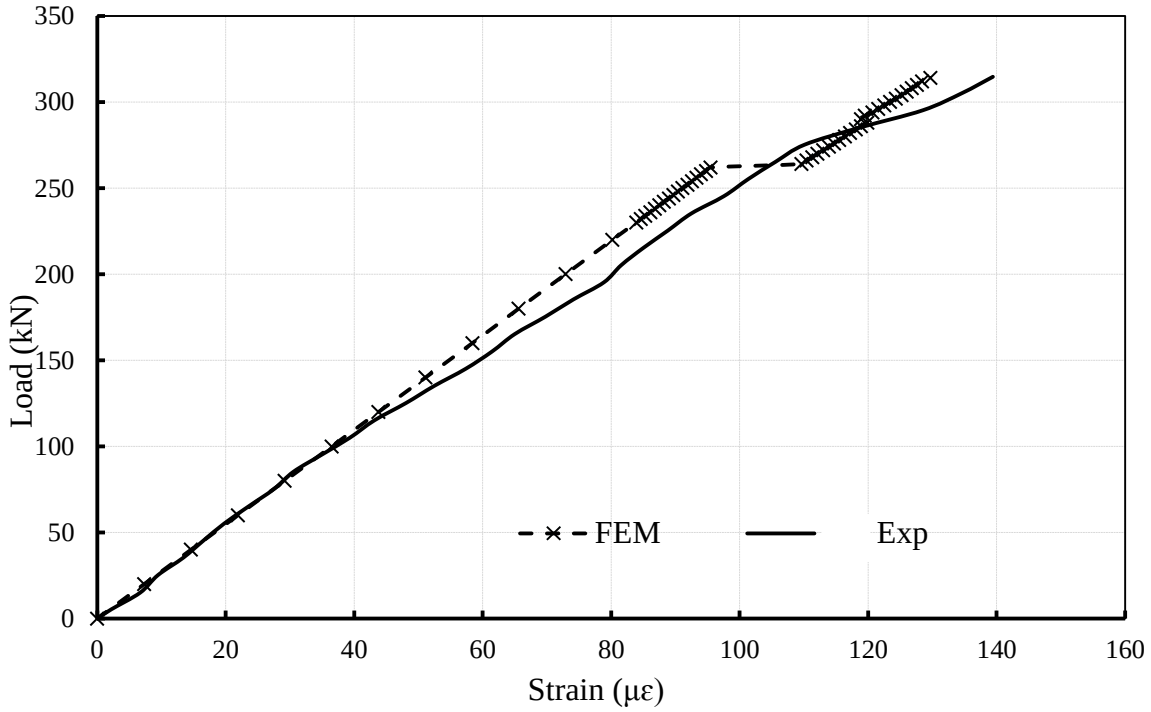


Figure (6.13): Strains in strand of edge-web of slab 300-P1-A at 438 mm

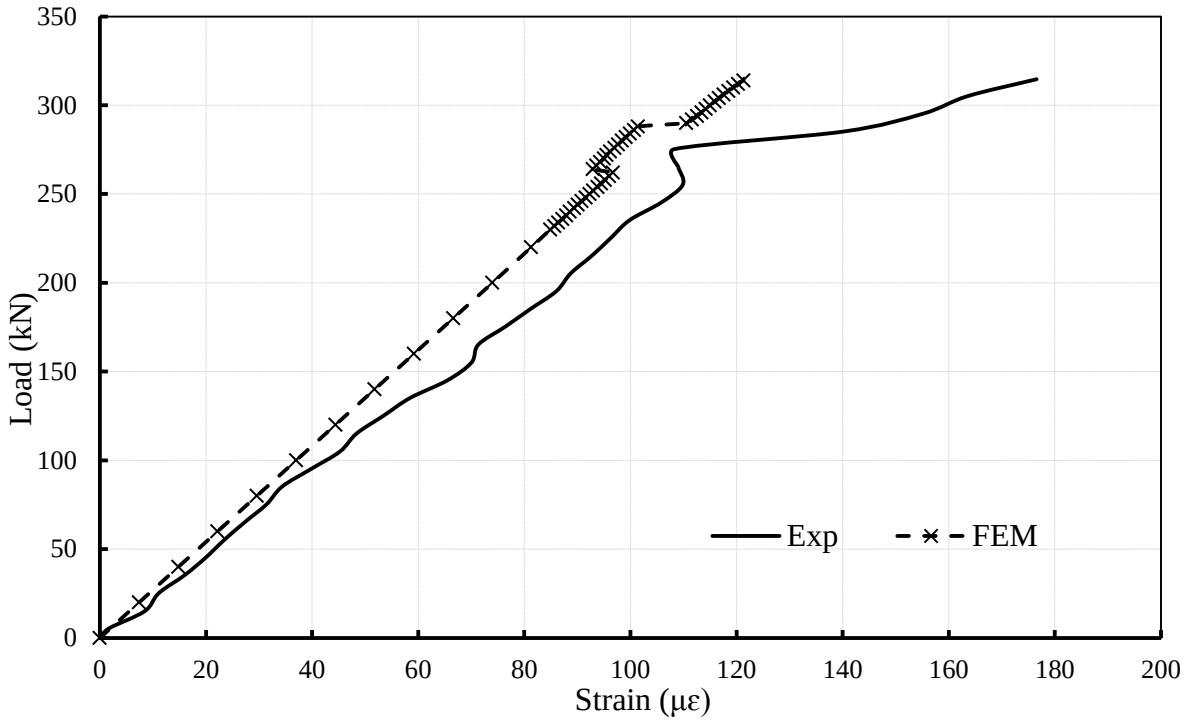


Figure (6.14): Strains in strand of mid-web of slab 300-P1-A at 438 mm

### 6.5.2. Phase 2 slabs - slab 300-18-A

It is claimed by some researchers that the load-deflection relationship is usually the most credible evaluation criterion for the performance of a finite element model since it represents the overall behaviour of specimens during tests. It was mentioned in Chapter 4 that no load-deflection data was available for any of the specimens tested within this study. However, for sake of further justification the developed model was verified in this section using an experimental result of slab 300-18-A which had load-deflection data. This experiment was performed in the previous phase of the same research program by Truderung (2011). The notation 18 used for ID of the specimen refers to strand code number. Actually that indicates the highest standard level of prestressing produced by the same supplier (P1) used in this study.

Figure (6.15) shows the load-deflection relationships at the mid span of slab 300-18-A as obtained from FEM against and as measured experimental one. It can be seen that the pattern of both curves was very similar and the FEM was able to simulate the load-deflection of the slab with almost same stiffness.

The comparison of cracking load for this specimen was made from Figures (6.17 and 6.18) which are presenting strains in concrete of the web. The numerical model has slightly captured the cracking load higher on the top surface of the slab but it was predicted as 200kN from web strains which was close to the 185kN observed from experimental results. Hence, the deviation in the predicted cracking load by the FEM for this specimen could be estimated as 8%. Moreover, it is worth to point out that the model was capable to capture compressive strains in Figure (6.16) likewise in experimental results for the web section at 117 mm, which is a very close zone to the support where struts might have formed.

In Figure (6.19) the load-strain variation in a strand of the mid web also demonstrated the same cracking load value for the numerical model and demonstrated good agreement in the trend of results from the model and the experiment.

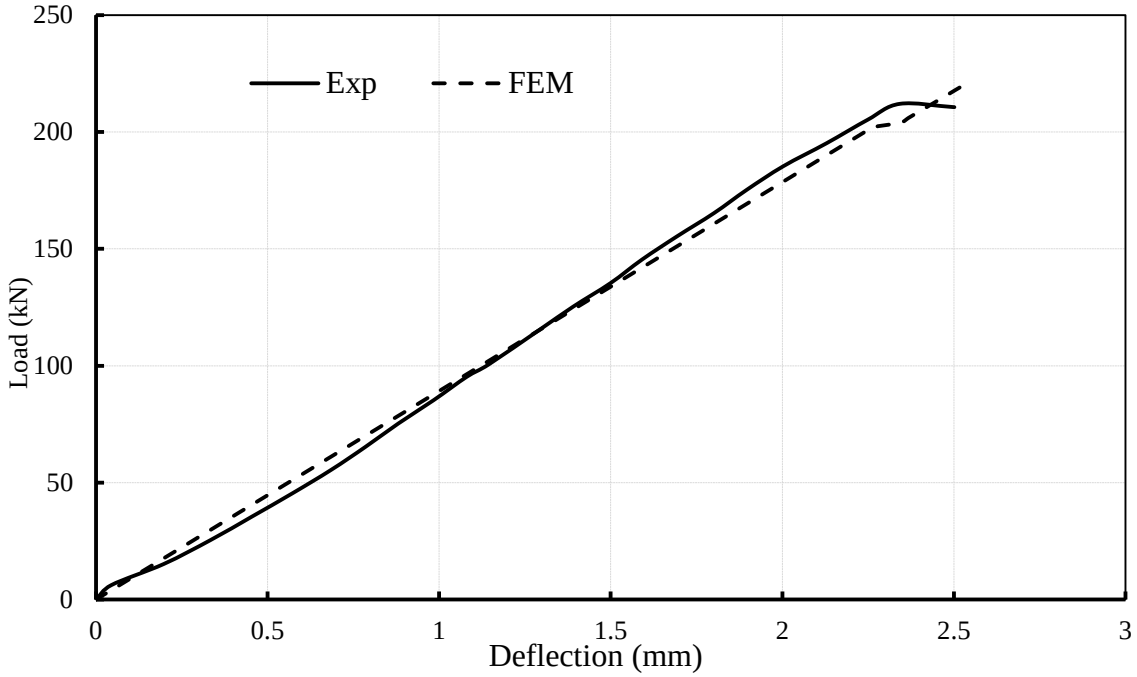


Figure (6.15): Load-deflection of slab 300-18-A at its mid span

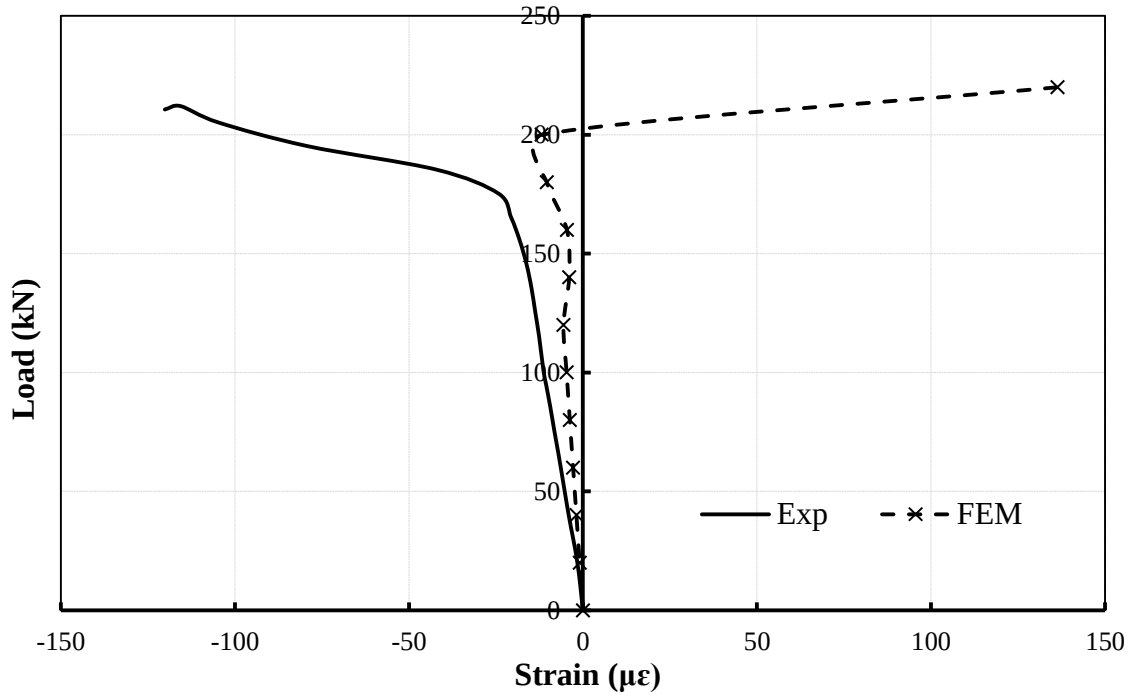


Figure (6.16): Concrete strains measured by SG on mid-web of slab 300-18-A at 117 mm from its loaded end

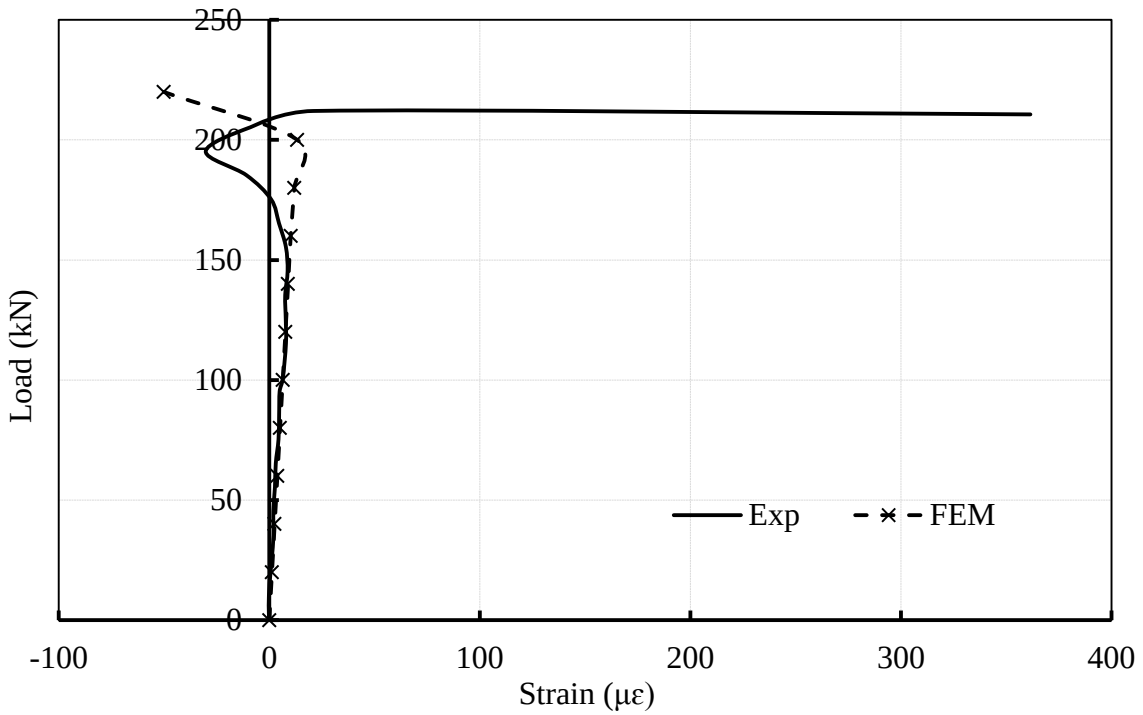


Figure (6.17): Concrete strains on mid-web of slab 300-18-A at 438 mm from its loaded end

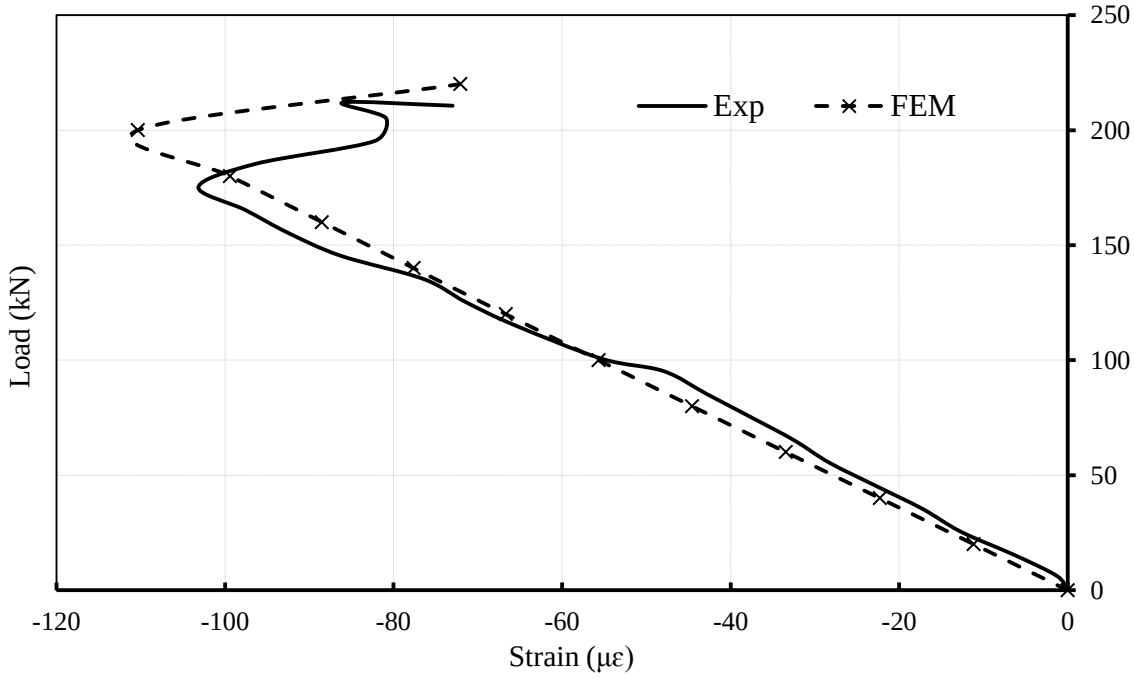


Figure (6.18): Concrete strains on top mid-web of slab 300-18-A at 438 mm from its loaded end

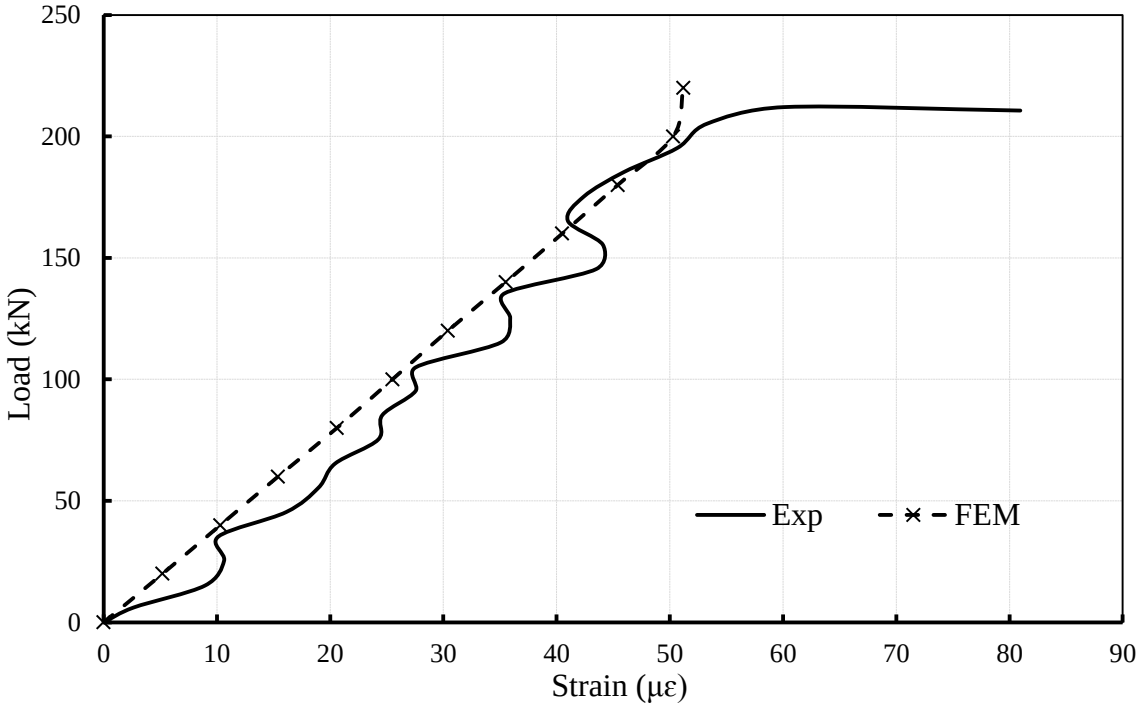


Figure (6.19): Strains in strand of mid-web of slab 300-18-A at 438 mm

### 6.5.3. Summary

The FEM discussed in this chapter showed good agreement to the compared experimental strain and deflection results. It is a general practice found among researchers to consider accuracy of predictions from a numerical model acceptable if the percentage of difference between the results of the model and the experimental results within a 10% limit. Therefore, it is concluded that the developed FEM for this research is suitable for use in further parametric study, which is the subject of the next chapter

# CHAPTER 7: PARAMETRIC STUDY

## 7.1. General

This chapter presents the results of the parametric study conducted using the constructed finite element model as presented in Chapter 6. The study investigates the effect of two key parameters that are expected to influence the shear capacity of PHC slabs. Those two parameters are the level of pretressing imposed on slabs cross section and the shear span of the simply-supported slabs.

The model used in this parametric study had the same geometric details, concrete and strand material properties of the model that was presented to simulate specimen 300-P1-A in Section 6.5.1.

The studied variables were altered with a wide range to practically cover the effect of the parameter on the shear behaviour of the PHC slabs. Outputs from model solutions were compared in terms of load-strain relationships for concrete and strands at the middle of the shear span as well as load-deflection behaviour. The following sections outline these results and the discussion for the investigated parameters.

## 7.2. Level of Prestressing

The web shear resistance equations of ACI and CSA codes, which presented in Chapter 3, are predicting a constant increase in shear capacity of PHC slabs with increase in amount of prestressing force in the cross section. However, this prediction is worth further investigation in this research. The level of prestressing was presented through the area of the prestressing strands ($mm^2$) while keeping the effective prestressing at 60% of ultimate strength of 1860 MPa.

Currently available levels of prestressing in the market for PHC produced by the first supplier (P1) ranges from 275 $mm^2$ (CODE 2) to 1335 $mm^2$ (CODE 18) and for slabs produced by the second supplier (P2) ranges from 495 $mm^2$ (Pattern No.1) to 1335 $mm^2$ (Pattern No. 10) according to the technical brochure of each provider. Consequently, the examined level of prestressing in this parametric study was selected to range from 274 $mm^2$ (0.31%) to 2374 $mm^2$ (2.66%) with an increment of 350 $mm^2$. These different levels of prestressing were simulated by changing the size of the strands while keeping number of the strands in the cross section same (9 strands).

The results of this parametric study showed a significant effect of level of prestressing. That effect on load-strain curves for concrete in the webs is shown in Figure (7.1). It can be seen that the webs failed in extremely brittle and sudden way when level of prestressing was increased to very high levels. This was identified since no significant plastic strains were observed after cracking load.

Figure (7.2) shows the load-strain curves for a concrete element on the top surface of the slab at the same section of the web elements. It can be seen from the figure that value of the load at the web shear cracking has degraded with increased level of prestressing. This finding supports the fundamental concept of Yang's (1994) and EN1168 code's web shear design methods which suggest that the development/variation in transferring prestressing force within the critical zone could cause a negative shear effect that need to be accounted for in web shear resistance predictions.

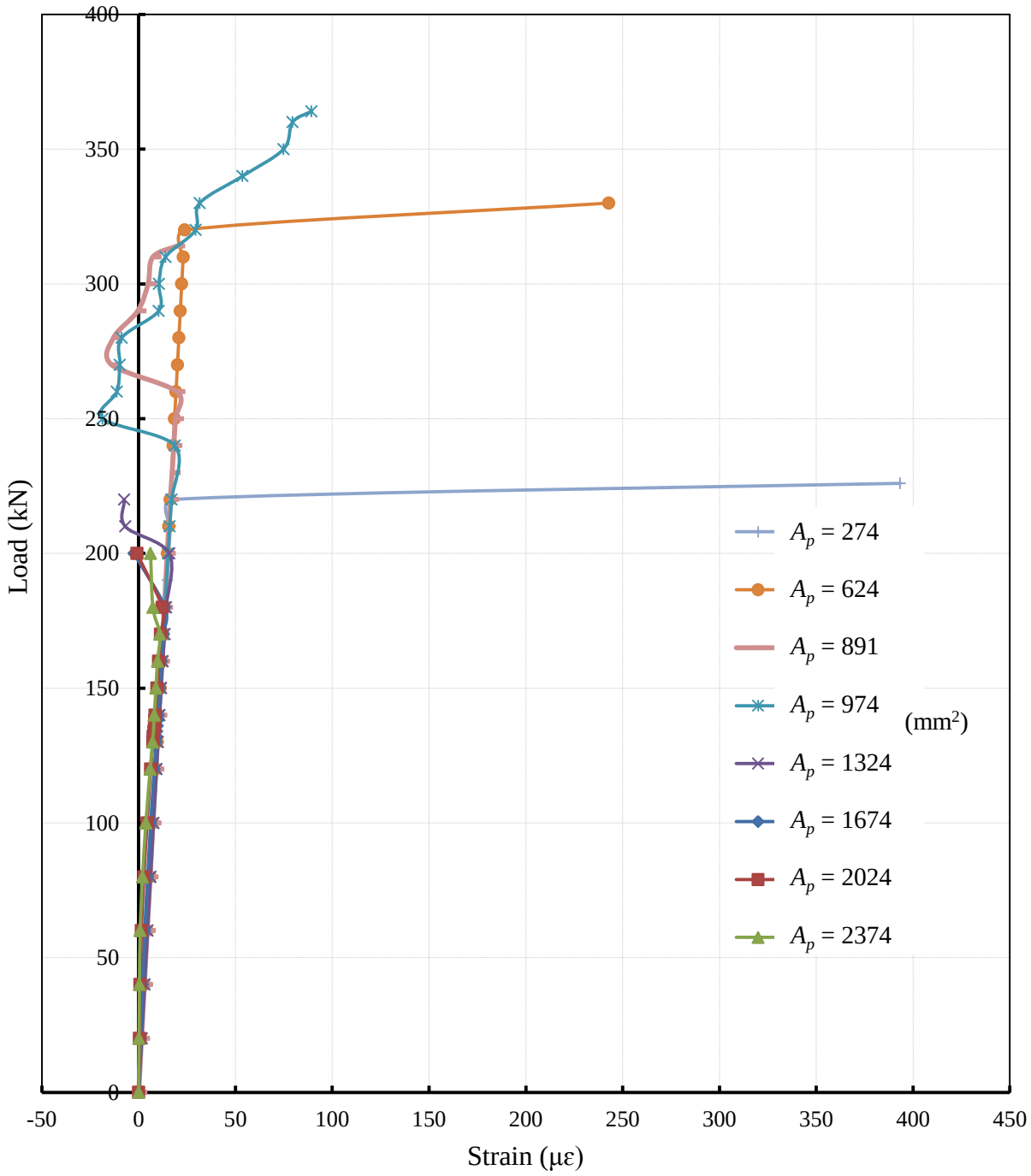


Figure (7.1): Strains in concrete element within the shear critical zone of at centroid level of mid-web

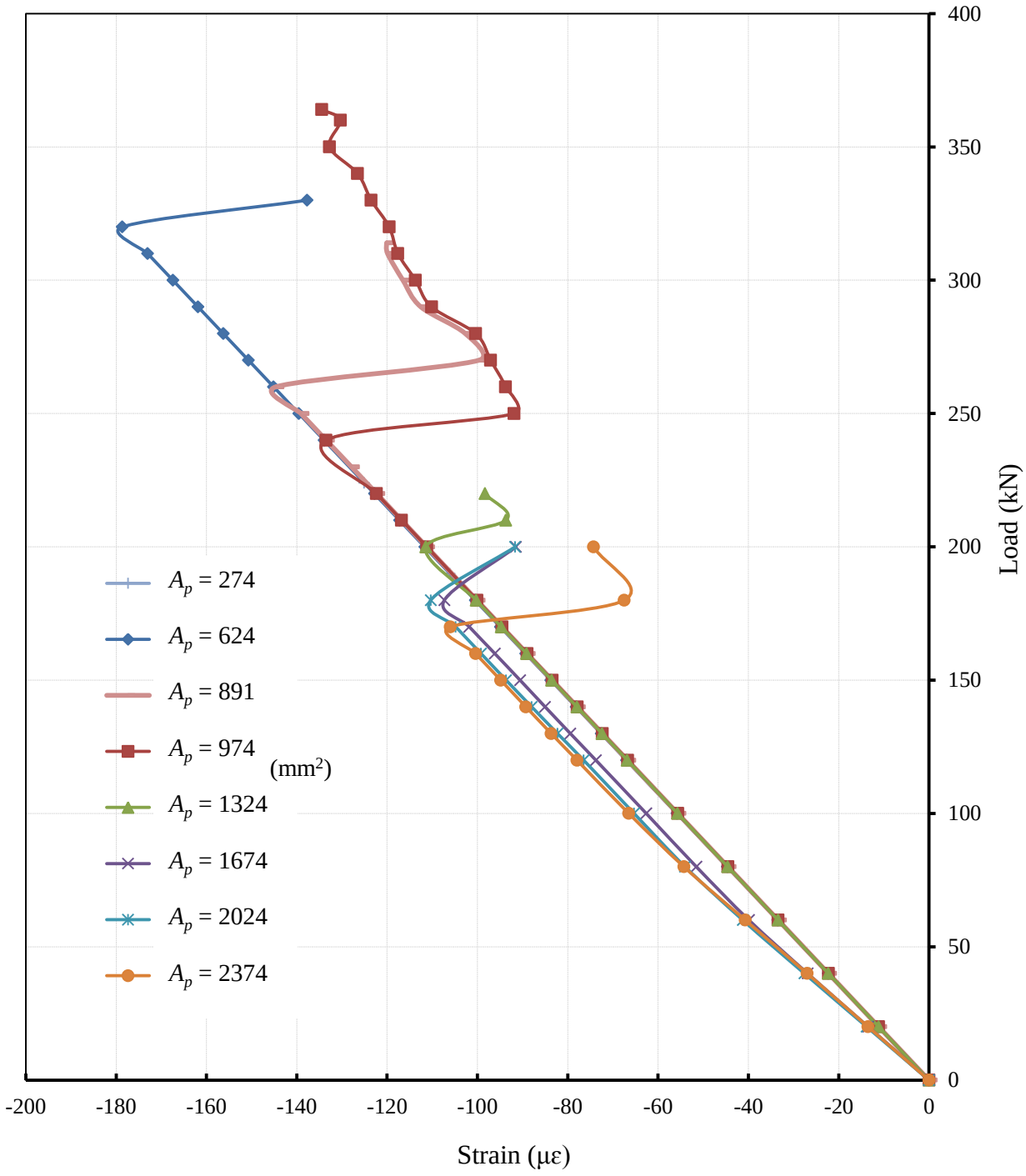


Figure (7.2): Strains in concrete element at the top surface of slab along mid-web

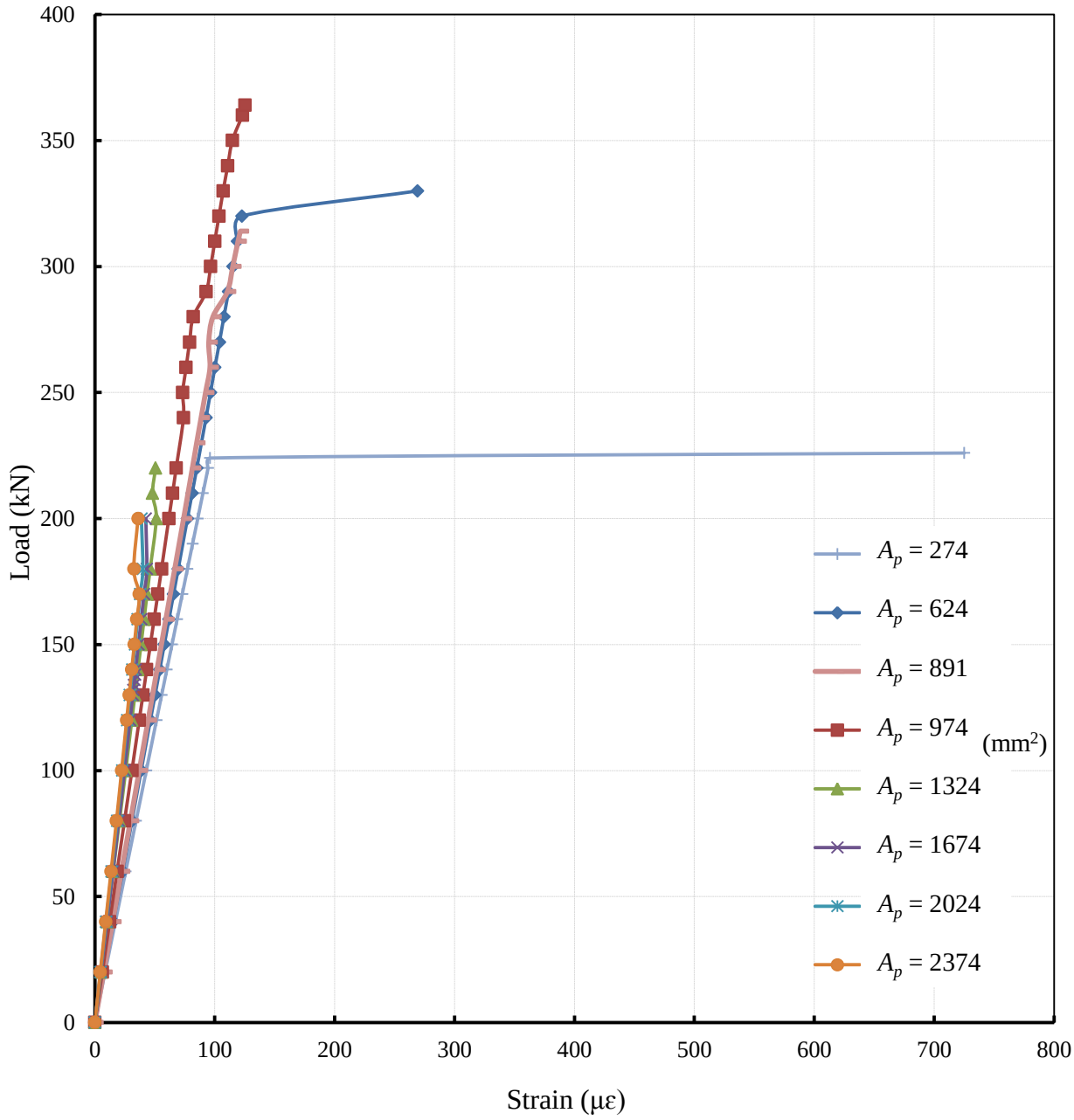


Figure (7.3): Strains in LINK180 element within the shear critical zone in a middle strand

In Figure (7.3), load-strain curves of a strand element at the shear critical zone are presented. It should be noted that the maximum strain in the strand element at ultimate load of the model with lowest prestressing level ($A_p$ = 274 mm$^2$) was more than 14,000 $\mu\varepsilon$ ; however, for sake of clarity, only portion of the plastic strain was presented in the figure. This observation implies that

strands of that model with lowest level of prestressing were ruptured which indicates a flexural or flexural- shear mode of failure for $A_p$ = 274 mm$^2$. It is worth recalling that the strand elements were expected to rupture at a tensile strain value of 20,000 $\mu\varepsilon$; nevertheless, this does not account for the initial amount of prestressing strain applied on the strands in the FEM which was 5680 $\mu\varepsilon$. Therefore, it can be concluded that level of prestressing as expected did also affect the modes of failure in this parametric study.

In Figure (7.4), the stiffness of load-deflection curves was not affected by level of prestressing at all. This is in good agreement with the expected behaviour since prestressed members are crack free elements with almost uniform stiffness across the span. Consequently, the deflections would be mainly dependent on stiffness of concrete which did not change during this parametric study.

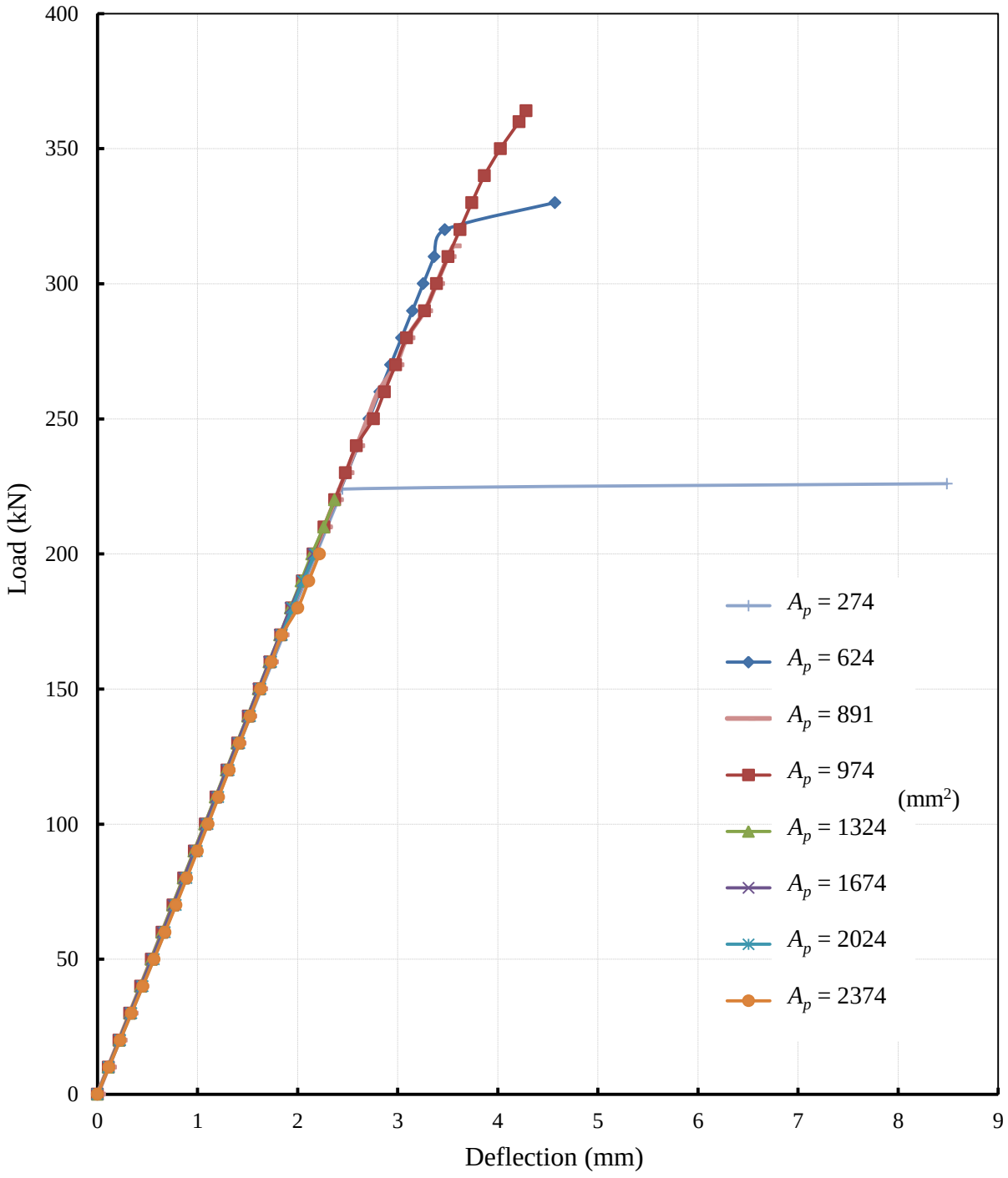


Figure (7.4): Load-Deflection at mid-span

In summary, Figure (7.5) presents ultimate failure loads of the slab at the different levels of prestressing examined in this study. It can be observed that the capacity of the slab has decreased

by 41% when level of prestressing was higher than 974 $mm^2$ (1.09%). In addition, the highest capacities were observed when prestressing levels ranged between 274 $mm^2$ (0.31%) and 1324 $mm^2$ (1.48%). Although using prestressing levels higher than 974 $mm^2$ (1.09%) could be necessary for long span requirements of the PHC units in certain projects, yet according to the results of this parametric study, it is recommended not to exceed the level of prestressing beyond 1.09% when possible. Moreover, the maximum practiced/standard level of prestressing used by both suppliers was found to be efficient according to the findings of this parametric study.

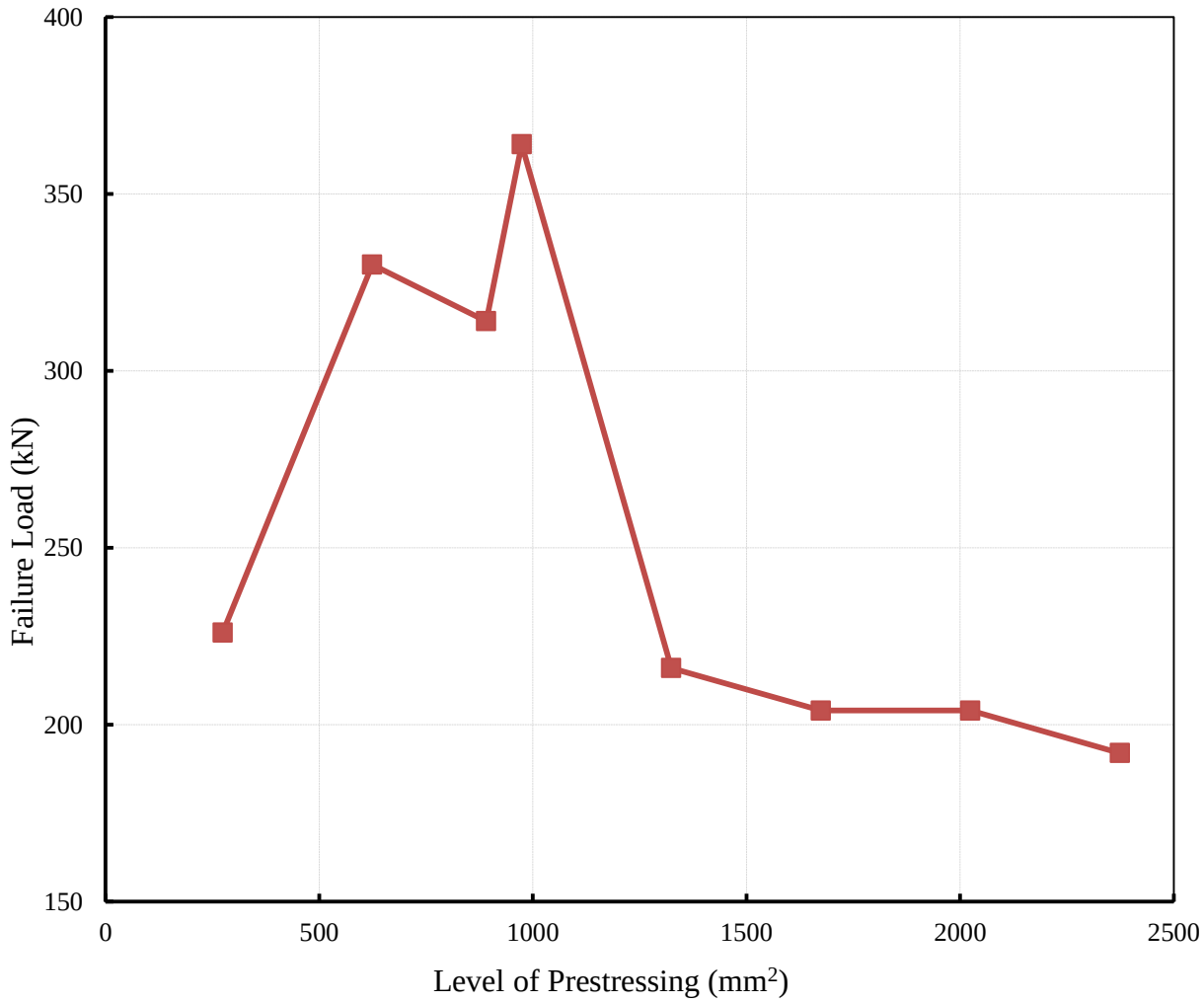


Figure (7.5): Summery of the effect of prestressing level

### 7.3. Shear Span

As discussed earlier in the literature review, there is a lack of research data about the critical shear span for the minimum diagonal shear resistance (web-shear capacity) of PHC slabs. Bartlett and MacGregor (2000) and Kani (1966) pointed out that the diagonal shear cracks are most critical when the shear span to depth ratio is around 2.5. However, this conclusion was derived from experimental work on regularly non-prestressed reinforced beams which could have different behaviour from PHC slabs. The main difference is due to the fact that reinforcement in PHC slabs is prestressed, which generates a negative effect on the shear capacity in the transfer zone in addition to absence of shear reinforcement. Some results were extracted from the parametric study performed by Yang (1994) on I-shaped single web FEM which simulated a non-circular voided PHC slab model of 400-mm thickness. Few other data found in Cheng and Wang (2010) for the effect of shear span in 200-mm PHC slabs with circular voids. There was no data found regarding effect of shear span on 300-mm thick slabs with circular voids, which what this study is investigating.

Since the effect of shear span was not investigated in the experimental phase of this study, the verified FEM was utilized for this purpose. This investigation was performed by changing the location of the applied vertical line load in the model. The shear span ($a$) is defined as the distance from the center line of the support plate close to the load to the center line of the loading plate. The shear span was related to the average depth of strands ($d$ = 255 mm) by the shear span to depth ratio ($a/d$). Different $a/d$ ratios, ranged from 1.0 to 5.0, were investigated. The load-stain results from this parametric study were presented for concrete and prestressing strands located at the middle of the shear span. Moreover, load-deflection results were also plotted at the mid-point of the slab.

Figure (7.6) shows curves for load versus strain in the longitudinal direction of the middle web at the centroid of the slab. For *a/d* ratios less than 2.0, it was observed that before cracking the load increased without significant increase in the tensile strains. However, when *a/d* was more than 2.0 significant tensile strains developed. The reason behind this could be that normal stresses from bending moment were higher in case of longer shear spans which shifted the neutral axis to a higher level than the slab mid-height.

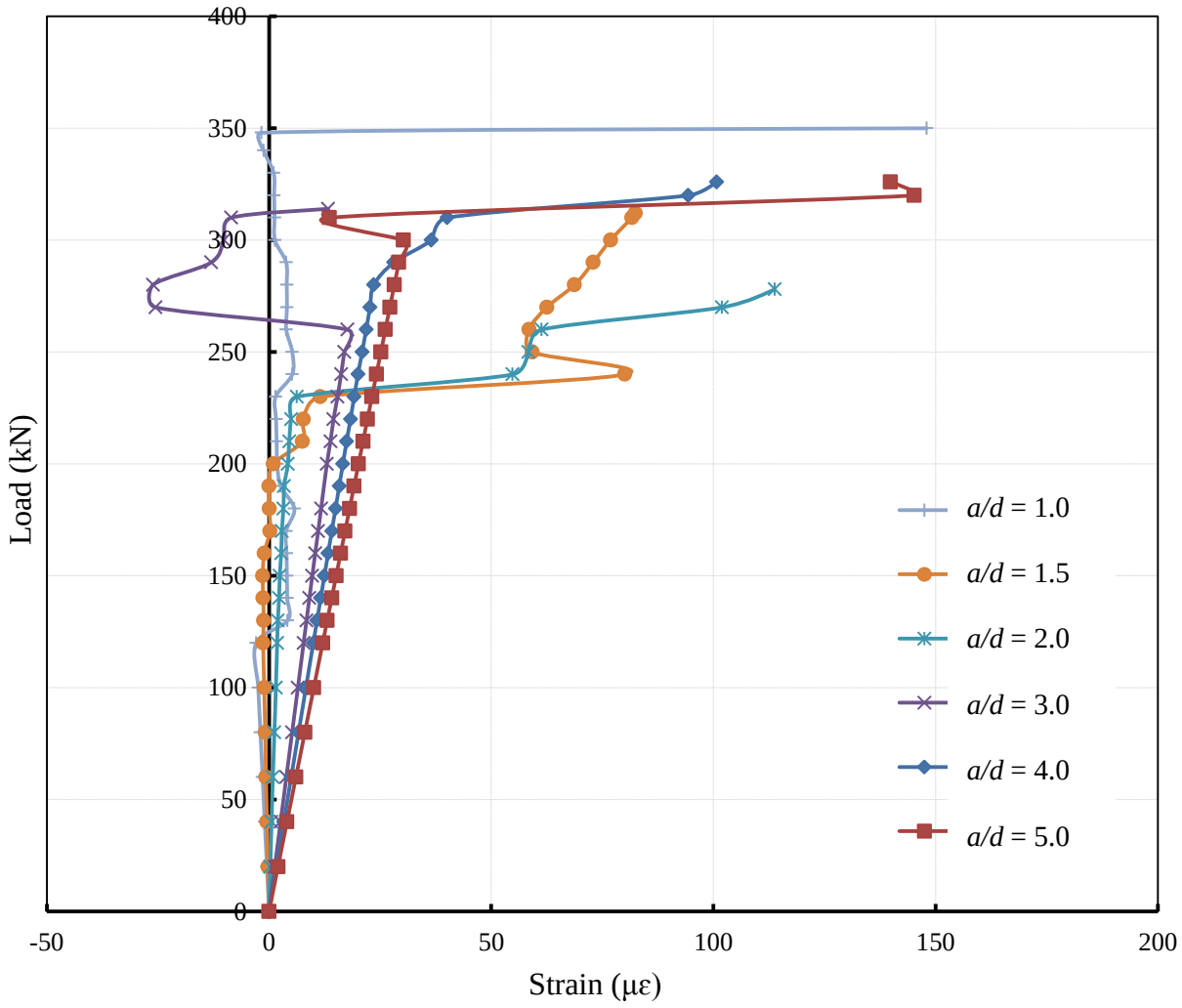


Figure (7.6): Strains in concrete element within the shear critical zone of at centroid level of mid web

High compressive strains in concrete observed in Figure (7.7) on the top surface of the slab in case of *a/d* = 5.0 and 4.0 indicate flexural-shear failure mode with *a/d* ratios more than 4.0. This is further strengthened by the observed high tensile strains on the prestressing reinforcement illustrated in Figure (7.8). Nonetheless, strain values are far from the compressive failure strain of concrete and rapture strain of strands which is an indication that the ultimate failure of the slab was due to anchorage loss of the strands.

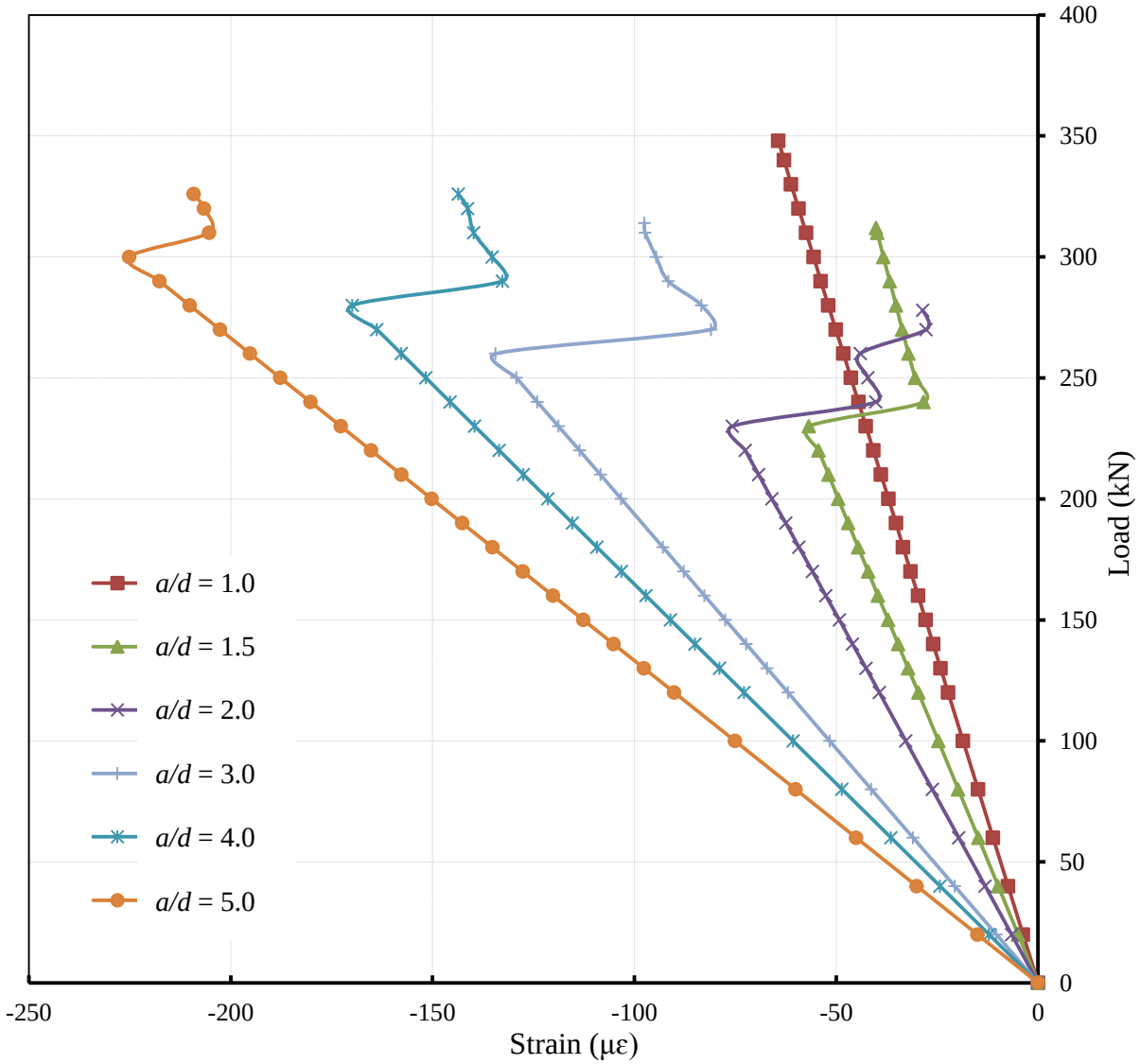


Figure (7.7): Strains in concrete element at the top surface of slab along mid-web

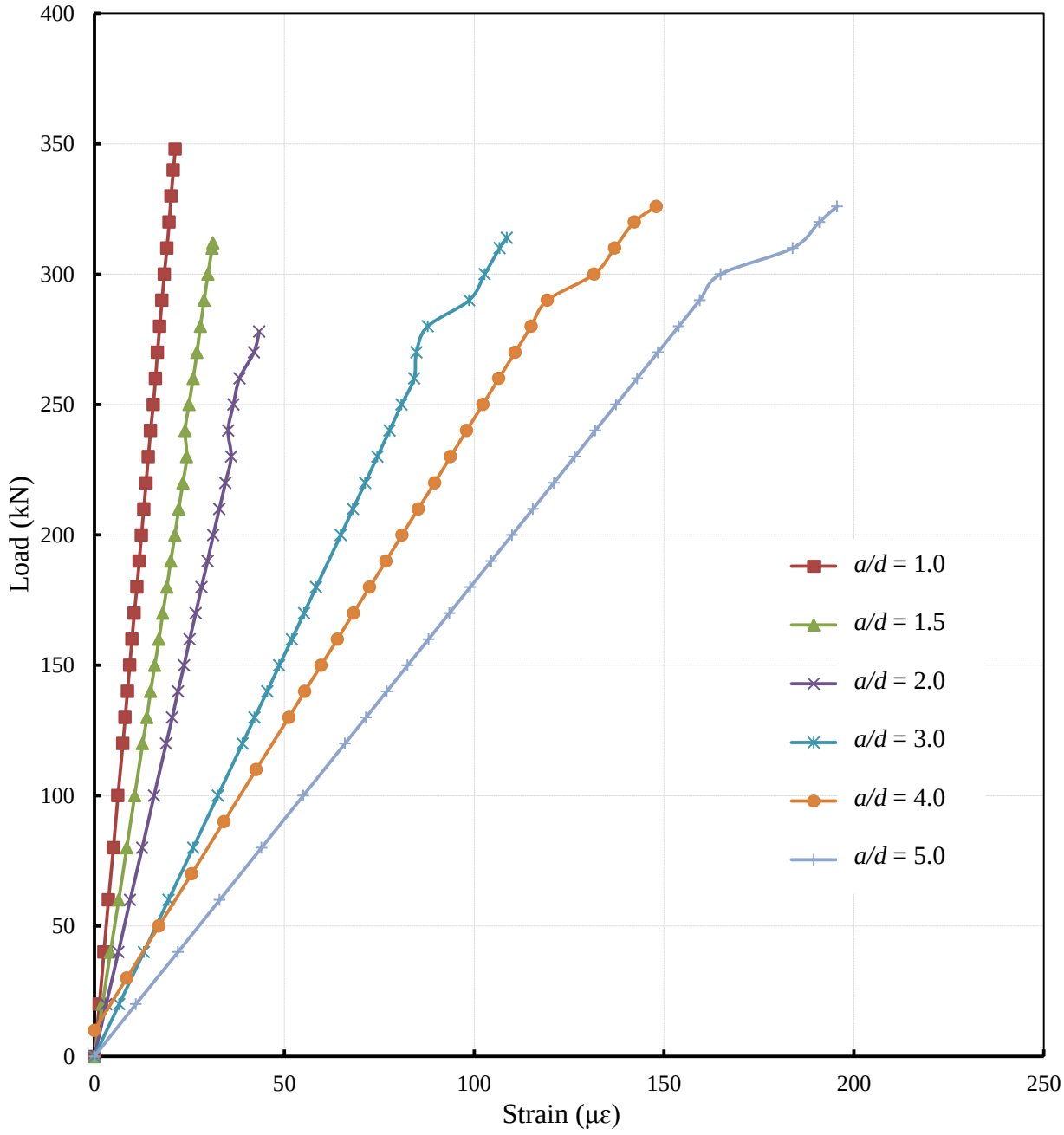


Figure (7.8): Strains in LINK180 element within the shear critical zone in a middle strand

The load-deflection graphs for the slab at the mid-span are shown in Figure (7.9). As expected, the deflection increased with increasing the shear span. The cracking load can be easily identified on the curves in case of flexural-shear failures (*a/d* = 4.0 and *a/d* = 5.0).

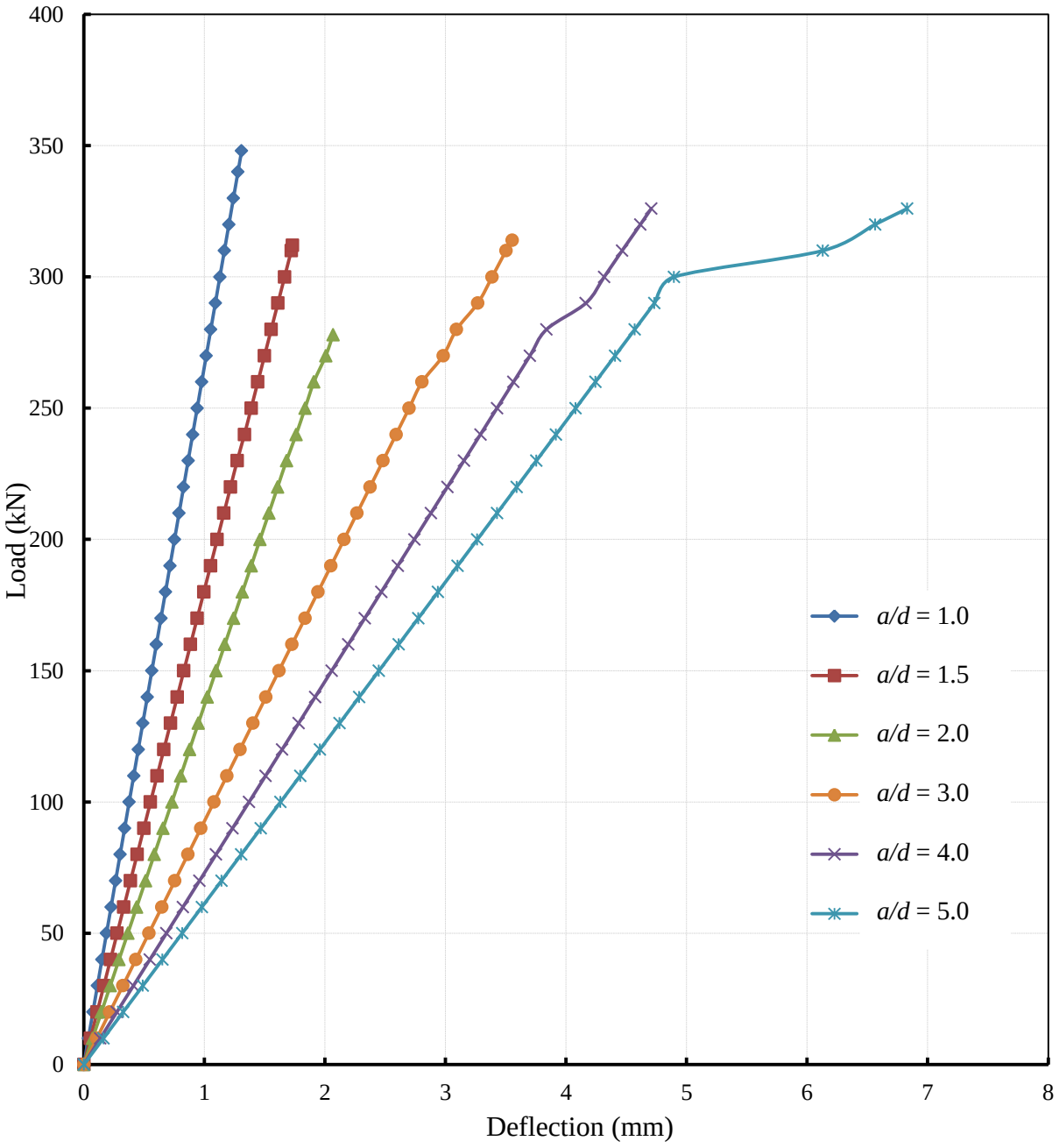


Figure (7.9): Load-Deflection at mid-span of FEM

Figure (7.10) presents ultimate failure loads versus the *a/d* ratio. The observed trend from the results for the effect of shear span on the capacity of the considered type of slab was in agreement with that reported by Yang (1994) in Figure (2.4). Therefore, according to the results of this conducted parametric study, it can be suggested that the most critical shear span for the simulated 300-mm PHC slab with circular voids is at *a/d* equal to 2.0. Since the slab appeared to have higher shear capacity with *a/d* values smaller than 2.0, the increase in the shear capacity was 25% in case of $a/d = 1.0$. On the other hand, application of the load at a $a/d > 4.0$ would be less critical as flexural-shear or even flexural failure would govern the mode of failure. Moreover, the capacity was 17% higher in case of *a/d* = 4.0 and 5.0, which appeared to fail due to flexural-shear.

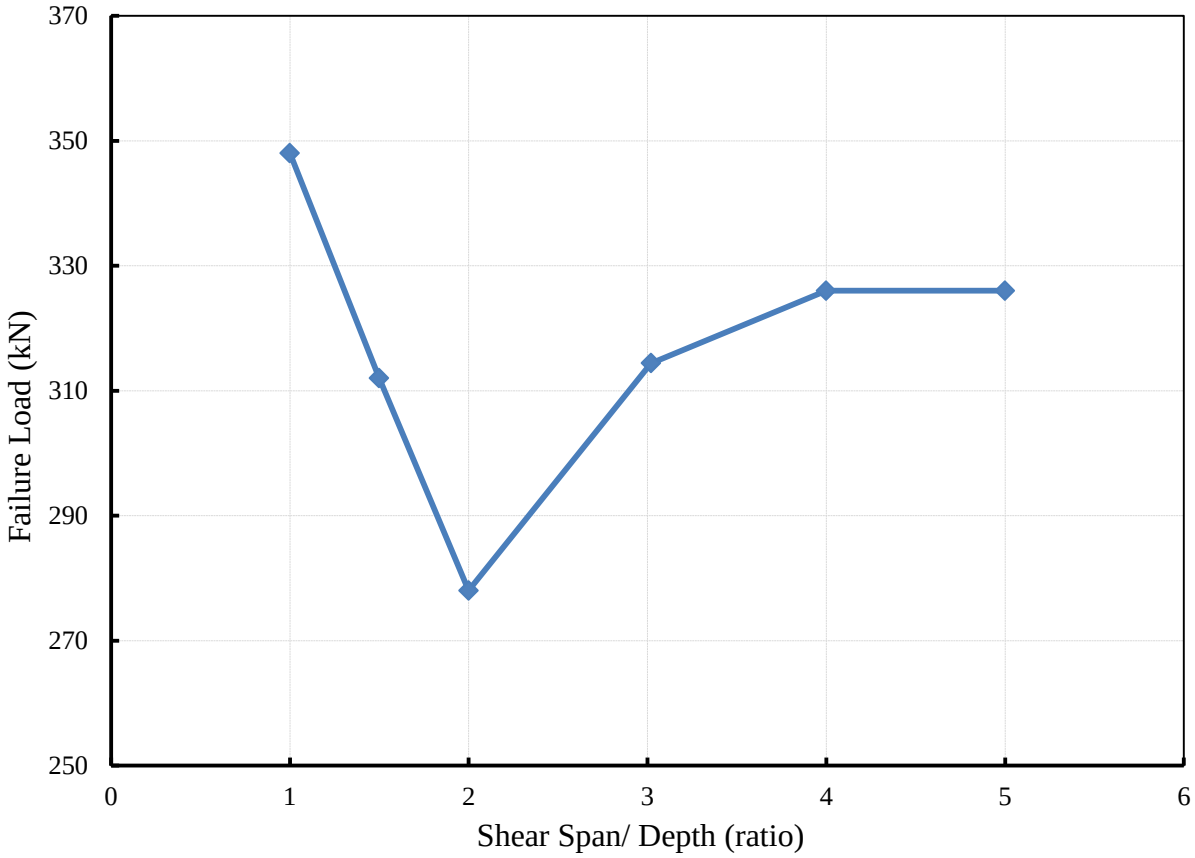


**Figure (7.10): Summery of findings from *a/d* studyCHAPTER 8: SUMMARY, CONCLUSIONS AND FUTURE WORK**

## 8.1. Summary

This research program was an effort to investigate challenges in predicting shear capacity of PHC slabs, especially web-shear capacity. The study consisted of two phases, experimental and numerical investigation. The study resulted in a number of findings about the effect of the studied parameters on the shear resistance of PHC slabs which contributes to the refinement of the shear design method exist in current CSA A23.3 code. The experimental phase included full scale testing of twelve PHC slab units from two different suppliers. The test set-up and load configuration was according to the standardized shear test method provided in Annex J of the European EN-1168 Code. Three series of slab thicknesses were tested in this program (Series-

200, Series-250, and Series-300). Void shape and length of bearing were also investigated. The main objective from this phase was to evaluate the validity and accuracy of formulas and equations provided in the Canadian, American, and European codes to calculate the ultimate shear capacity of PHC slabs. The experimental results of this phase were compared to code predictions for shear capacity of the tested specimens.

In the numerical phase of this research, a finite element model was constructed using ANSYS software. The model was verified against the experimental results. The main objective of this phase was to investigate and evaluate the effect of key parameters known to affect the shear capacity of PHC slabs. The parametric study in this phase investigated the influence of two variables. The first variable was the level of prestressing applied on the cross section while the second variable was the shear span.

## 8.2. Conclusions

Findings from this research project are summarised in the following sections.

### 8.2.1. Conclusions from the experimental study

1. The majority of the tested PHC slabs from all three series have failed due to diagonal web-shear except in the case of slabs with non-circular void shape from Series-250 and 200. The observed mode of failure for these slabs was classified as flexural-shear or flexural.
2. Based on the experimental results, reducing the bearing length from 63 mm to 38 mm resulted in a reduction of 9 to 35% in shear capacity of PHC slabs. However, in the case of 250-mm thick slabs with non-circular void shape, the effect of reducing the bearing

length was insignificant (less than 1.0%). Moreover, reducing the bearing length appeared to cause inclined shear cracks to form closer to the end of the slab.

3. The general shear provisions of the CSA code was found to be very conservative when compared with the experimental results in this study. The ratio of experimental-to-predicted shear capacity ranged from 1.10 to 1.93 with mean and standard deviation of 1.49 and 0.27, respectively. Moreover, it is worth to mention that the CSA code did not over predict the shear capacity of any tested slab in this study. In other words, it was always very conservative (uneconomic). The most conservative predictions were for Series-250 mm slabs with non-circular voids.

4. The ratio of experimental-to-predicted shear capacities by the ACI code ranged from 0.99 to 1.80 with a mean value of 1.37 and standard deviation of 0.21. This is better than the CSA code, yet conservative. However, the ACI code failed to predict the actual mode of failure for the tested slabs with non-circular void shape. ACI predicted the mode of failure to be web-shear while it was flexural shear.

5. The web-shear capacity equations of the European code (EN 1168) were found to give the most accurate and consistent predictions among the considered codes in this study. The experimental-to-predicted capacities by this code ranged from 0.91 to 1.51.

6. Load-strain data measured over the webs of the tested specimens and on strands indicated that the shear failure of the PHC slabs under force controlled type of loading could be extremely brittle even in some cases of flexural-shear mode. That mainly results from the slippage of the stands instantly when the crack lines reach the reinforcement.

### 8.2.2. Conclusions from the numerical modeling

Based on results from the FEM constructed in this research project, the following conclusion can be drawn.

7. The constructed FEM using ANSYS software was able to simulate the behaviour of the disturbed critical shear zone in PHC slabs within a reasonable accuracy. The predicted load-strain results agreed well with the corresponding experimental data (less than 10%).
8. High level of prestressing was found to be an advantage for shear resistance of PHC slabs. A prestressing level by a reinforcement ratio higher than 1.1% (974 $mm^2$) has increased the shear capacity by 41%. Moreover, a reinforcement ratio less than 0.7% (624 $mm^2$) was not sufficient as the shear capacity was found to decrease again beyond that level. Therefore, the recommended range of prestressing level (prestressing reinforcement ratio) for the considered slab geometry in the FEM study was found to be from 624 $mm^2$ (0.7%) to 974 $mm^2$ (1.1%). Consequently it is recommended to use the medium strand codes/patterns produced by the two PHC slab suppliers used in this research especially for structural cases where high concentrated line loads are expected.
9. From load-strain results of the FEM, it was observed that increasing level of prestressing did also increase brittleness of the shear failure in PHC slabs as the load-strain for web and strand elements showed less plastic behaviour after shear cracking in the cases of prestressing levels higher than 974 $mm^2$ (1.1%).
10. For the 300-mm modelled slabs with circular voids, a value of 2.0 was found to be the most critical shear span to depth ratio.
11. With values of shear span-to-depth ratios smaller than 2.0, signs of arching action were observed on the load-strain response from the FEM analysis and the ultimate failure

capacity was high. The shear capacity of a slab loaded with a line load applied at a distance equal to the depth of the slab was 25% higher than the failure of that with *a/d* = 2.0. On the other hand, with shear span-to-depth ratios higher than 3.0, flexural-shear modes started to govern the failure, which is known to be less critical than web-shear mode in PHC slabs.

## 8.3. Future Work

Based on the findings and conclusions of the current study, the following recommendations are made for future research.

1. The conservative results in shear predictions by the Canadian code for the tested slabs in this research program suggests that modification should be made in the equations of the code or perhaps adopting a new method similar to that used in the European code as it showed better predictions.
2. The number of tested specimens was not enough to adequately investigate the effect of different void shape profiles on the shear behaviour of PHC slabs. Therefore, additional experiments are needed for further investigation.
3. The results obtained from the developed FEM in this study are encouraging to investigate a wider range of the contested parameter in addition to the effect of other key parameters on shear capacity of PHC slabs such as different currently-used void shape profiles, slab sizes and different load configurations.
4. The FEM should be extended to investigate other geometric variables for the shape of voids as it could be helpful to identify the optimum PHC slab profiles in shear resistance.

5. The transfer length for prestressing strands in PHC slabs is a significant point that is not well covered and requires further research work which also could result into a standard bond-slip model for the strands to use in future numerical studies.

# REFERENCES

ACI Committee 318. (2005). "Building Code Requirements for Structural Concrete (ACI 318-89) and Commentary (ACI 318R-05)," American Concrete Institute, Farmington Hills, Michigan.

ACI Committee 318. (2008). "Building Code Requirements for Structural Concrete (ACI 318-08) and Commentary (ACI 318R-08)," American Concrete Institute, Farmington Hills, Michigan.

Anderson, A. R. (1976). "Shear Strength of Prestressed Concrete Beams," Technical Bulletin 76-B11/B12, Concrete Technology Associates, Tacoma, WA, Nov., 45 p.

Anderson, R. G. (1987). "Web Shear Strength of Prestressed Concrete Members," Technical Bulletin 85-B1, Concrete Technology Associates, Tacoma, WA, March, 38 p.

ANSYS (2010) ANSYS Release 13.0 Finite Element Analysis System, SAS IP, Inc.

Becker, R. J. and Buettner, D. R. (1985). "Shear Tests of Extruded Hollow Core Slabs," PCI Journal, Vol. 30, No.2, pp. 40-54.

Bertagnoli, G. and Mancini, G. (2009). "Failure Analysis of Hollow-Core Slabs Tested in Shear," Lausanne, fib, Structural Concrete, Journal of the fib, Vol. 10, No.3, September, pp. 139-152.

Canadian Precast/Prestressed Concrete Institute (CPCI). (2007). "Design Manual," 4th Edition, Canadian Precast/Prestressed Concrete Institute, Ottawa, ON, Canada.

Canadian Standard Association (CSA). (2004). "Design of Concrete Structures," CAN/CSA-A23.3-04, Canadian Standards Association, Rexdale, ON, Canada.

CEB-FIP. (1990). "Model code for concrète structures." comite Européen du béton, Paris France.

Cheng, S. and Wang, X. (2010). "Impact of Interaction between Adjacent Webs on the Shear Strength of Prestressed Concrete Hollow-Core Units", PCI Journal, Vol. 55, No. 3, pp. 46-63.

CTC (2007). Precast, Prestressed Hollow Core Slabs: Design Criteria & Span-Load Charts. Concrete Technology Corporation. Manufacturers of Prestressed Concrete, Tacoma, Washington.

CTE-73-B4 (1973), Performance of Double Tees Without Web Reinforcement. Concrete Technology Associates, Tacoma, Washington.

Deutsche Norm. (2005) . "Eurocode 2: Design of Concrete Structures – Part 1-1: General Rules and Rules for Buildings," DIN EN 1992-1-1-05, CEN-European Committee for Standardization, Brussels, Belgium.

Deutsche Norm. (2008). "Precast Concrete Products–Hollow Core Slabs (includes Amendment A1:2008)." DIN EN 1168-08, CEN-European Committee for Standardization, Brussels, Belgium.

Elliott, Kim S. (2000). Research and development in precast concrete framed structures. John Wiley and Sons, University Park, Nottingham.

fib (2003). Seismic design of precast concrete building structures. The International Federation for Structural Concrete, Lausanne, Switzerland.

Hawkins, N. M., Kuchma, D. A., Mast, R. F., Marsh, M. L. and Reineck, K. H. (2005) "Simplified Shear Design of Structural Concrete Members", National Cooperative Highway Research Program, Transportation Research Board, Washington, D.C.

Hawkins, N. M. and Ghosh, S. K. (2006). "Shear Strength of Hollow-Core Slabs", PCI Journal, Vol. 51, No. 1, pp. 110-114.

Kani, G. N. J. (1966). "Basic Facts Concerning Shear Failure," Journal of the American Concrete Institute, Title No. 63 32, June, September, pp. 675-692.

Macgregor, J. G. and Bartlett, F. M. (2000). "Reinforced Concrete Mechanics and Design," First Canadian Edition, Prentice Hall Canada Inc., Toronto, ON, Canada.

Micallef, P. (2005). "Assessment of Shear Capacity of Pre-stressed Hollow Core Floor Units in the Local Construction Industry," Faculty of Architecture and Civil Engineering, University of Malta, June, 7 p.

Pajari, M. (2005). "Resistance of Prestressed Hollow Core Slabs Against Web Shear Failure," Research Notes 2292, VTT Building and Transport, Kemistintie, Finland, April, 69 p.

Pajari, M. (2009). "Web Shear Failure in Prestressed Hollow Core Slabs," Rakenteiden Mekaniikka (Journal of Structural Mechanics), Vol. 42, No. 4, pp. 207-217.

Palmer, K. D. and Schultz, A. E. (2010). "Factors Affecting Web-Shear Capacity of Deep Hollow-Core Units", PCI Journal, Vol. 55, No. 2, pp. 123-146.

Pisanty, A. (1992). "The Shear Strength of Extruded Hollow-Core Slabs", Materials and Structures, RILEM, France, 25, 7 p.

Precast/Prestressed Concrete Institute (PCI). (2007). "Design Handbook," 6th Edition, Precast/Prestressed Concrete Institute, Chicago, IL.

Truderung, K. A. (2011). "Shear Capacity of Dry-Cast Extruded Precast/Prestressed Hollow-Core Slabs," M.Sc. Thesis, Department of Civil Engineering, University of Manitoba, Winnipeg, Manitoba.

Vecchio, F. J., and Collins, M. P. (1986). "The Modified Compression Field Theory for Reinforced Concrete Elements Subjected to Shear," Journal of the American Concrete Institute, V. 83, No. 2 (March-April): pp. 219-231.

Walraven, J. C. and Mercx, W. P. M. (1983). "The Bearing Capacity of Prestressed Hollow Core Slabs," Heron, Vol. 28, No. 3, 46 p.

Willam, K.J. and Warnke, E.P. (1974), "Constitutive Model for Triaxial Behaviour of Concrete," Seminar on Concrete Structures Subjected to Triaxial Stresses, International Association of Bridge and Structural Engineering Conference, Bergamo, Italy, 174.

Wolanski, A. J. (2004). "Flexural Behavior of Reinforced and Prestressed Concrete Beams using Finite Element Analysis," M.Sc. Thesis, Marquette University, Milwaukee, Wisconsin.

Yang, L. (1994). "Design of Prestressed Hollow Core Slabs with Reference to Web Shear Failure," Journal of Structural Engineering, ASCE, V. 120, No. 9, pp. 2675-2696.

# NOTATIONS

$a$: shear span

$a_g$: specified nominal maximum size of coarse aggregate

$A$: area of the whole cross-section

$A_c$: area of the concrete cross-section

$A_{ct}$: area of concrete on flexural tension side of member

$A_c(y)$: area above the level of critical point height ($y$)

$A_i$: fictive cross-section surface, whole area of PHC slab's cross-section excluding area of voids

$A_p$: area of prestressing tendons

$A_s$: area of longitudinal reinforcement on the flexural tension side of the member

$b_w$: minimum effective web width, smallest width of the cross-section in the tensile area, width of the cross-section at the centroidal axis, total web width of all webs at the smallest section

$b_w(y)$: web width at height $y$

$Cp_t(y)$: factor taking into account the position of the considered tendon layer

$d$: distance from extreme compression fibre to centroid of longitudinal tension reinforcement

$d_b$: strand diameter

$d_p$: distance from extreme compression fibre to centroid of prestressing steel

$dN_p/d_x$: gradient of effective prestress force in strands along their transfer length

$d_v$: effective shear depth

$d'$: distance between centroid of $A_c(y)$ and the centroid of the whole section as illustrated in Figure 3.1

$e$: vertical distance between centroid of prestressed strands and centroid of whole cross-section

$E_{ct}$ or $E_c$: modulus of elasticity of concrete

$E_p$: modulus of elasticity of prestressing tendons

$E_s$: modulus of elasticity of non-prestressed reinforcement

$f_b(x)$: flexural stress on bottom face of the PHC slab unit at the considered section

$f_{bpt}$: bond strength of concrete

$f_{pu}$: ultimate tensile strength of strands

$f_c'$: specified compressive strength of concrete

$f_{cd}$: design value of concrete compressive strength

$f_{ck}$: characteristic compressive cylinder strength of concrete at 28 days

$f_{ct}$: concrete tensile strength, characteristic tensile strength of concrete

$f_{ctd}$: design value of concrete tensile strength

$f_{ctk}$: characteristic axial tensile strength of concrete

$f_{pc}$: compressive stress in concrete (after allowance for all prestress losses) at the centroid of the cross-section resisting externally applied loads, or at the junction of the web and flange, when the centroid lies within the flange.

$f_{pe}$: compressive stress in concrete due to effective prestress forces only (after allowance for all prestress losses) at the extreme section fibre, where tensile stress is caused by externally applied loads

$f_{po}$: stress in prestressing tendons when strain in the surrounding concrete is zero

$f_{se}$: effective stress in the prestressing tendons after allowance for all prestressing losses

$h$: overall thickness or height of member

$I$: moment of inertia of section about centroidal axis, second moment of area of cross-section

$k$: size factor

$l_d$: development length of prestressing strands

$l_t$: transfer length of prestressing strands

$l_x$: distance of section considered from the starting point of the transmission length, distance of the considered point on the line of failure from the starting point of the transmission length (= $x$)

$l_{pt}$: basic general transfer length

$l_{pt2}$: upper bound value of the transmission length of the prestressing element

$M_{cre}$: moment causing flexural cracking at section due to externally applied loads

$M_{Ed}$: bending moment due to vertical load

$M_f$: moment due to factored loads

$M_{max}$: maximum factored moment at section due to externally applied loads

$M_{sw}(x)$: moment due to self-weight

$M_{Ptest}(x)$: moment due to applied external test load

$N_{Ed}$: axial force in the cross-section due to the loading or prestressing

$N_f$: factored axial load normal to the cross-section occurring simultaneously with $V_f$, including effects of tension due to creep and shrinkage

$N_p$: effective prestress force in strands

$n$: number of tendon layers

$P_{m,t}(x)$: effective prestress force in all tendons of the PHC slab unit at time $t$ after jacking and distance ($x$) from end of the slab

$P_t(l_x)$: prestressing force in the considered tendon layer at distance $l_x$

$s$: slippage in strand element at any bond stress $\tau$

$s_1$: characteristic slip value

$s_3$: final slippage of strand element at $\tau_f$

$S_b$: bottom section modulus

$S_c(y)$: first moment of area above height $y$ and about the centroidal axis

$s_z$: crack spacing parameter dependent on crack control characteristics of longitudinal reinforcement

$s_{ze}$: equivalent value of $s_z$ that allows for influence of aggregate size

$V_c$: shear resistance attributed to the concrete, nominal shear strength provided by the concrete

$V_{ci}$: nominal shear strength provided by concrete when diagonal cracking results from combined shear and moment

$V_{cw}$: web-shear resistance of the concrete, nominal shear strength provided by concrete when diagonal cracking results from high principal tensile stress in web

$V_d$: shear force at section due to un-factored dead load

$V_{Ed}$: design value of the shear force

$V_f$: factored shear force

$V_i$: factored shear force at a section due to externally applied loads occurring simultaneously with $M_{max}$

$V_p$: component in the direction of the applied shear of the effective prestressing force, vertical component of effective prestress force at section

$V_r$: factored shear resistance

$V_{Rdc}$: design value for the shear resistance of a member without shear reinforcement

$V_s$: shear resistance provided by shear reinforcement, nominal shear strength provided by shear reinforcement

$V_u$: factored shear force

$v_{min}$: minimum value of shear stress resistance for concrete

$Y_c$: height of the centroidal axis

$Yp_t$: height of the position of the considered tendon layer

*(y)*: height of the critical point on the line of failure

*y'*: height from bottom of slab unit to centroid of area above critical point level, as illustrated in Figure 3.1

$y_t$: distance from centroidal axis of gross section, neglecting reinforcement, to tension face

$\alpha$ : coefficient for curve of bond-slip model

$\alpha_l$ : factor that accounts for method of prestressing release

$\alpha_2$ : factor that accounts for type of tendons

$\beta$ : factor accounting for shear resistance of cracked concrete, angle, ratio or coefficient, angle between bottom surface of hollow-core slab and line from centre of support to critical point

$\gamma_c$ : partial factor for concrete, factor of safety

$\varepsilon_c$ : strain in concrete due to compressive stress, $\sigma_c$

$\varepsilon_{co}$ : a factor to account for the special descending branch in stress-strain curve of high strength concrete

$\varepsilon_{c1}$ : compressive strain at peak stress, $f_c^{'}$

$\varepsilon_{cu1}$: ultimate compressive strain in concrete at failure

$\varepsilon_x$: longitudinal strain at mid-depth of the member due to factored loads

$\varepsilon_p$: strain in strand elements due to any tensile stress, $f_p$

$\theta$: angle of inclination of diagonal compressive stresses to the longitudinal axis of the member

$\lambda$: factor to account for low-density concrete

$\rho_l$: flexural tensile reinforcement ratio

$\sigma_{cp}$: compressive stress in the concrete from axial load or prestressing

$\sigma_{cp}(y)$: concrete compressive stress at height *y* of the considered section

$\sigma_N$: average concrete compressive stress in the cross-section, average stress due to fully transferred prestressing force in the ultimate state

$\sigma_{m,t}$: stress in concrete just at release of prestressing strands

$\eta_{P1}$: coefficient that accounts for type of tendons

$\eta_1$: coefficient that accounts for bond quality

$\tau$: shear stress, bond stress at strand and concrete interface

$\tau_{cp}(y)$:concrete shear stress due to transmission of prestress at height *y* of the considered section

$\tau_f$: residual bond stress in strand element after max slippage has occurred

$\tau_{\max}$: bond strength of strands to concrete elements

$\phi$ : strength reduction factor, diameter of tendons

$\phi_c$ : resistance factor for concrete

# APPENDIX A:

# AS-BUILT SLABGEOMETRY

## (200-P1-A) SLAB GEOMETRY

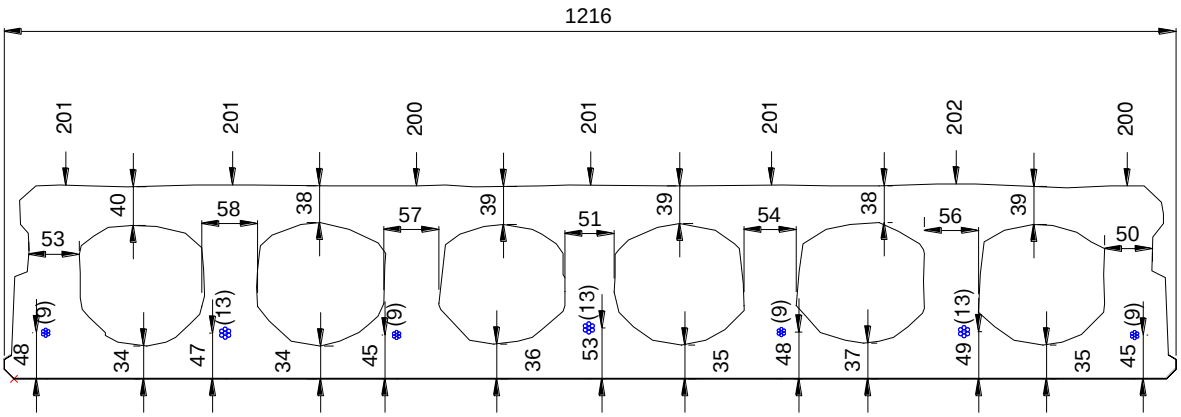


AVG. HEIGHT -> 201 mm  TOTAL WEB WIDTH -> 379 mm  TEST DATE CAMBER -> (10 mm)

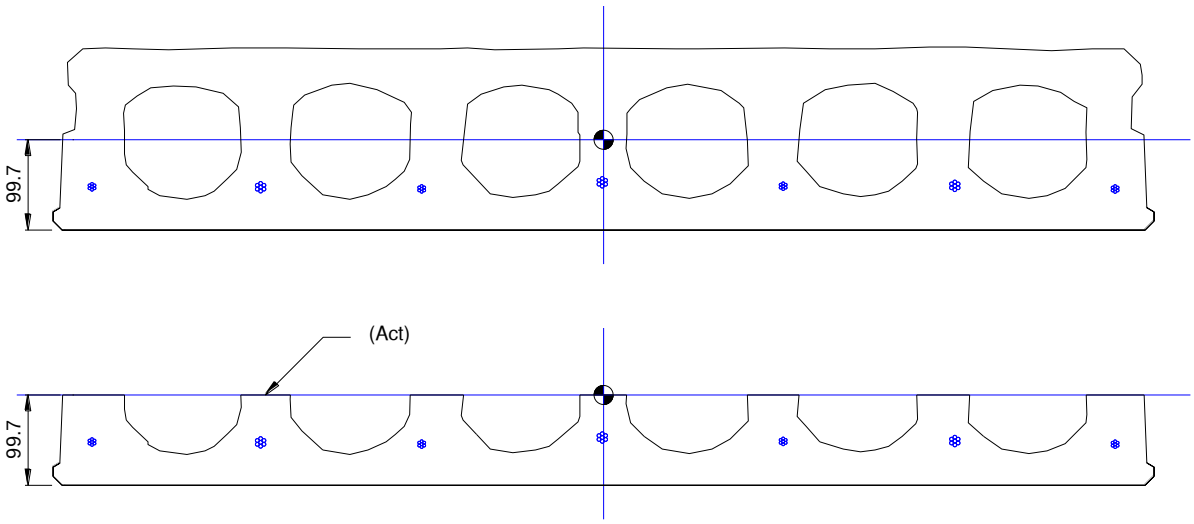


GROSS AREA BELOW N/A (Act) -> 78568 mm2

## (200-P1-B) SLAB GEOMETRY

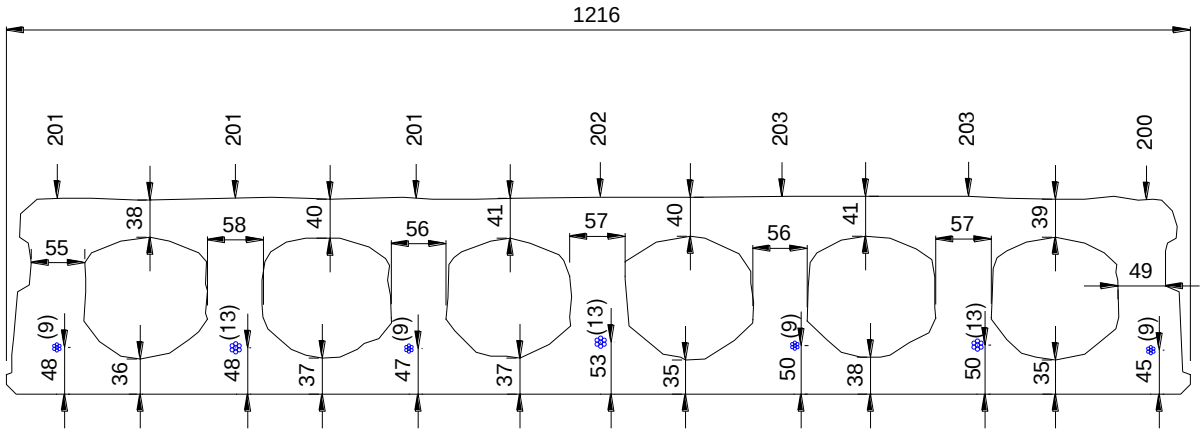


AVG. HEIGHT -> 202 mm  TOTAL WEB WIDTH -> 388 mm  TEST DATE CAMBER -> (6 mm)

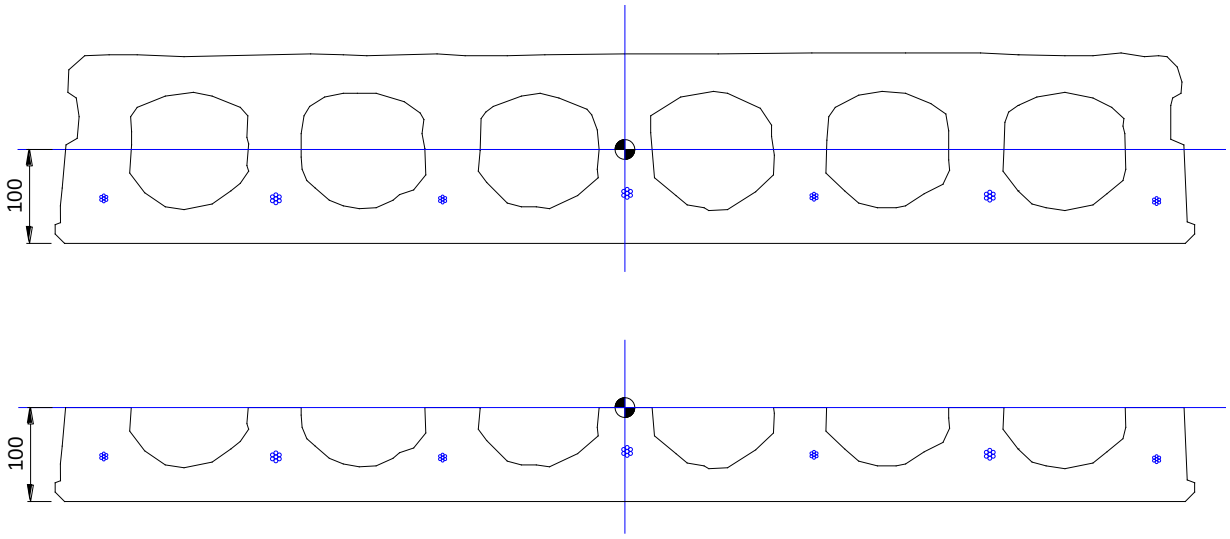


GROSS AREA BELOW N/A (Act) -> 80381 mm2

(200-P2-A) SLAB GEOMETRY

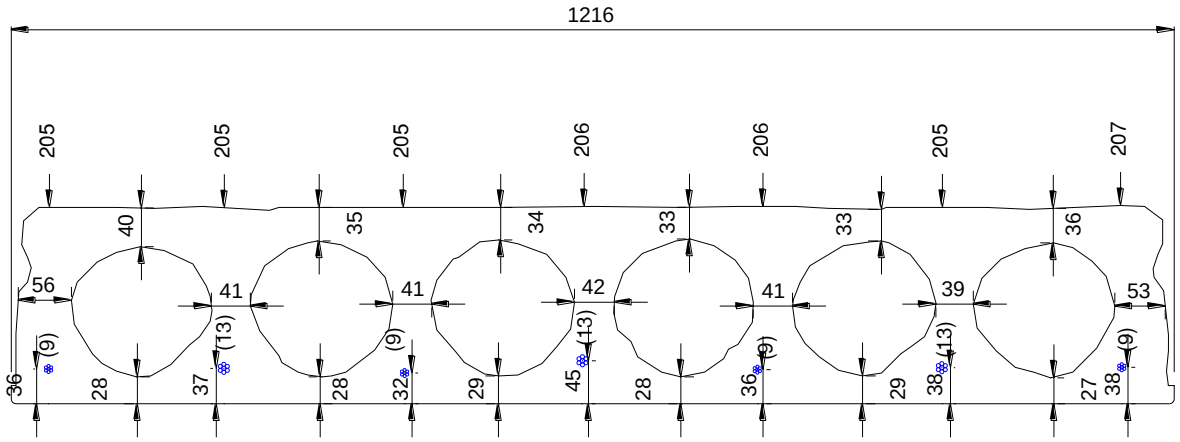


AVG. HEIGHT -> 206 mm  TOTAL WEB WIDTH -> 313 mm  TEST DATE CAMBER -> (6 mm)

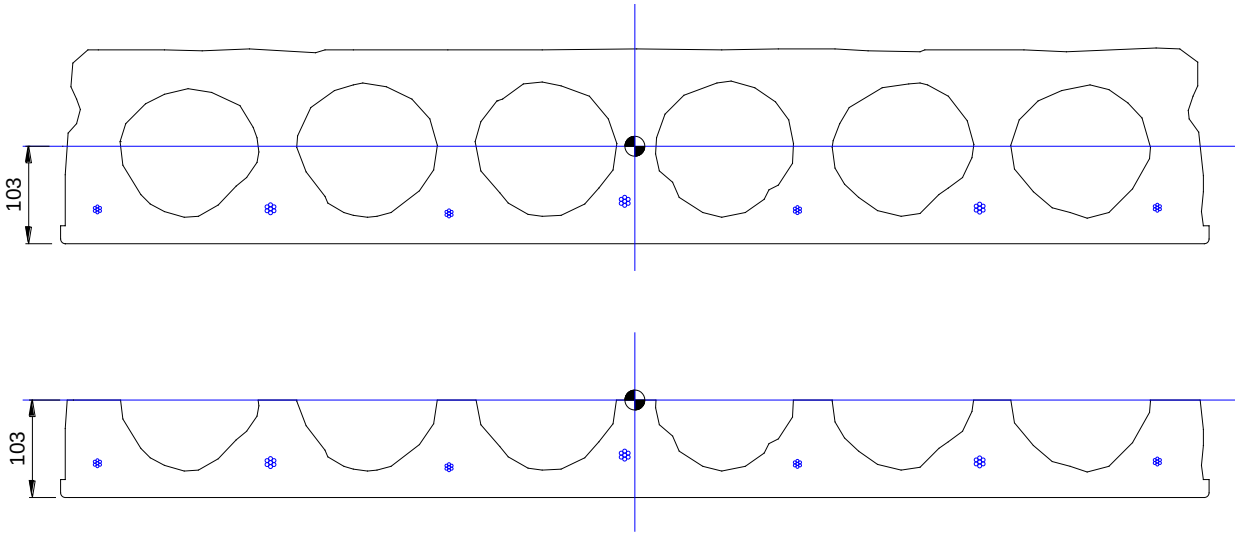


GROSS AREA BELOW N/A (Act) -> 75554 mm2

(200-P2-B) SLAB GEOMETRY

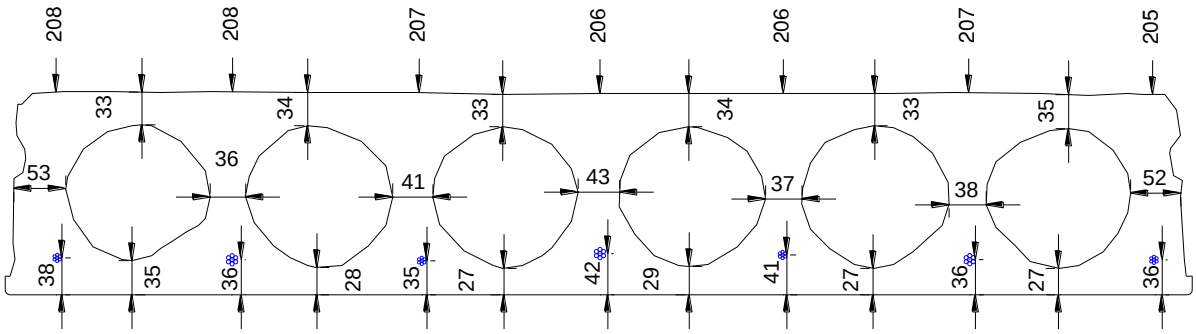


AVG. HEIGHT -> 207 mm

TOTAL WEB WIDTH -> 300 mm

TEST DATE CAMBER -> (8 mm)

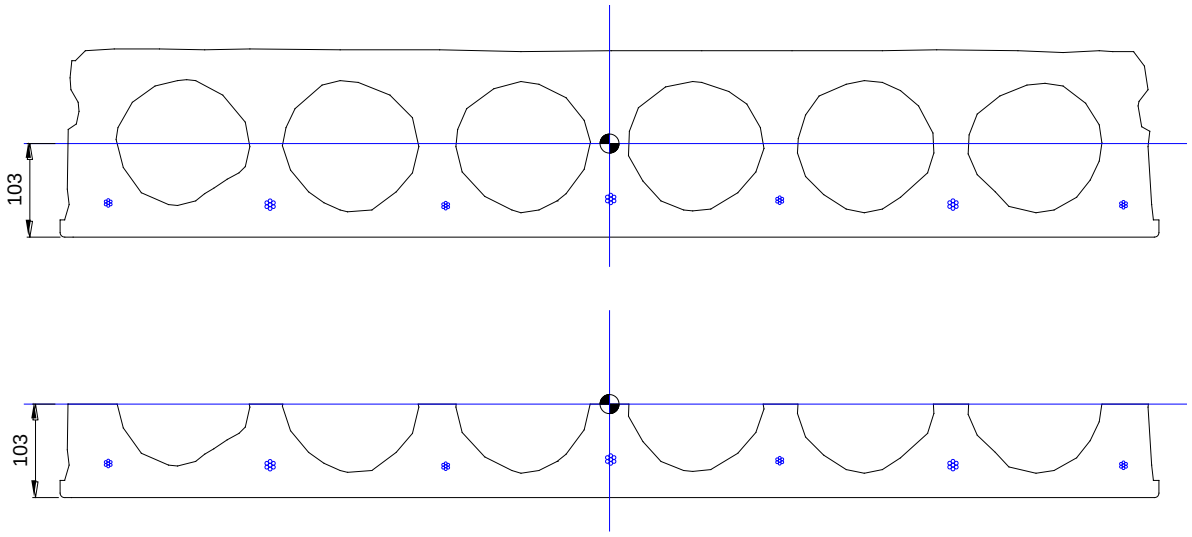


GROSS AREA BELOW N/A (Act) -> 74839 mm2

(250-P1-A) SLAB GEOMETRY

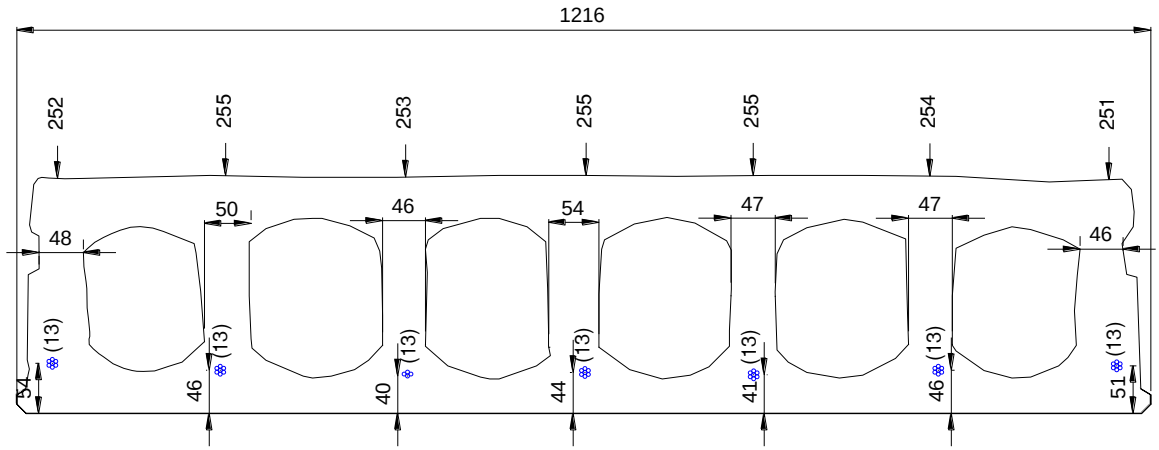


AVG. HEIGHT -> 254 mm

TOTAL WEB WIDTH -> 338 mm

TEST DATE CAMBER -> (6 mm)

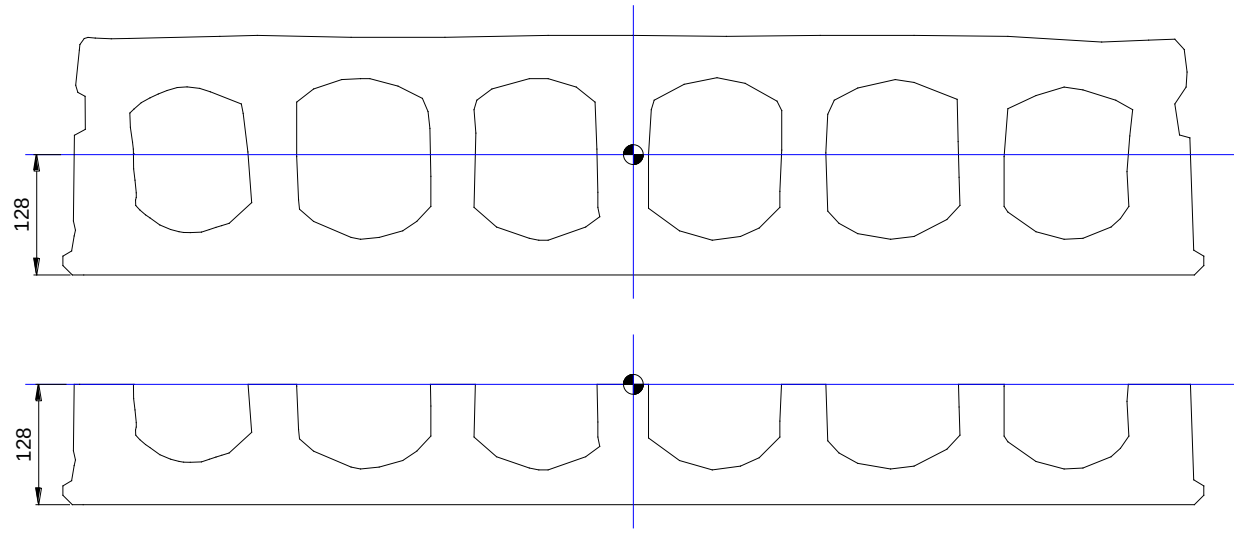


GROSS AREA BELOW N/A (Act) -> 89601 mm2

(250-P1-B) SLAB GEOMETRY

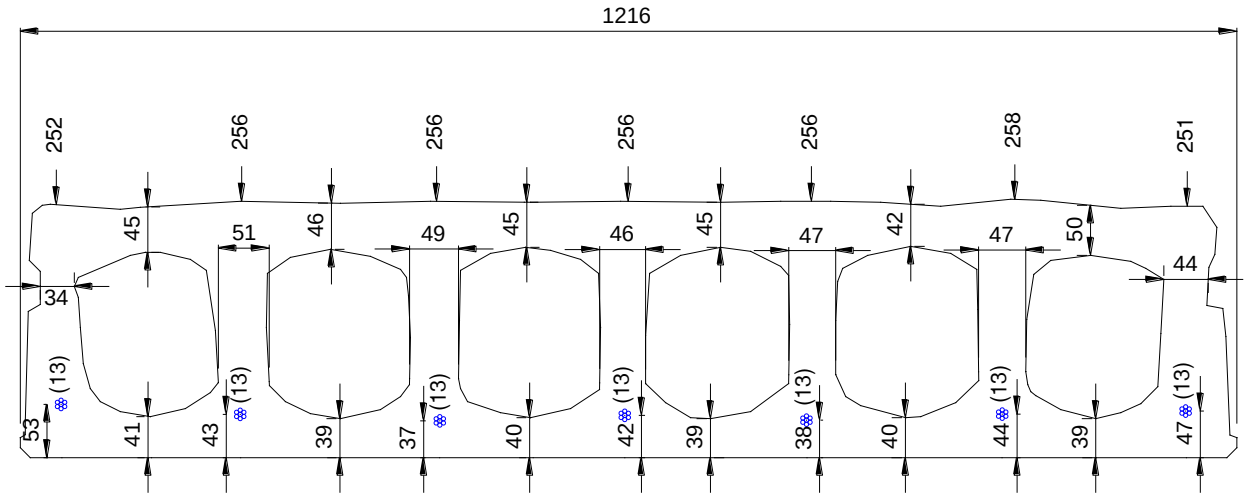


AVG. HEIGHT -> 255 mm

TOTAL WEB WIDTH -> 318 mm

TEST DATE CAMBER -> (8 mm)

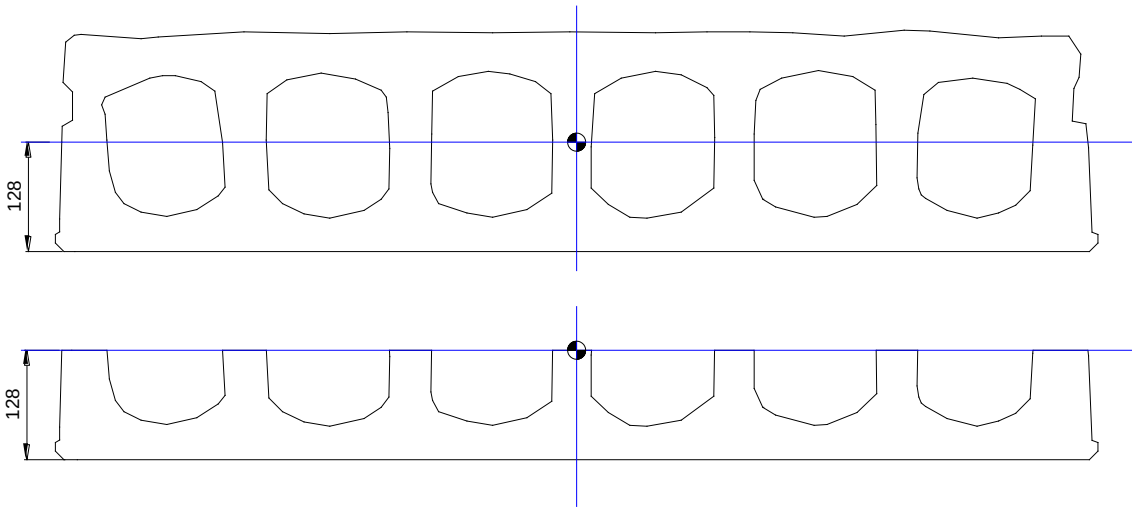


GROSS AREA BELOW N/A (Act) -> 89249 mm2

(250-P2-A) SLAB GEOMETRY

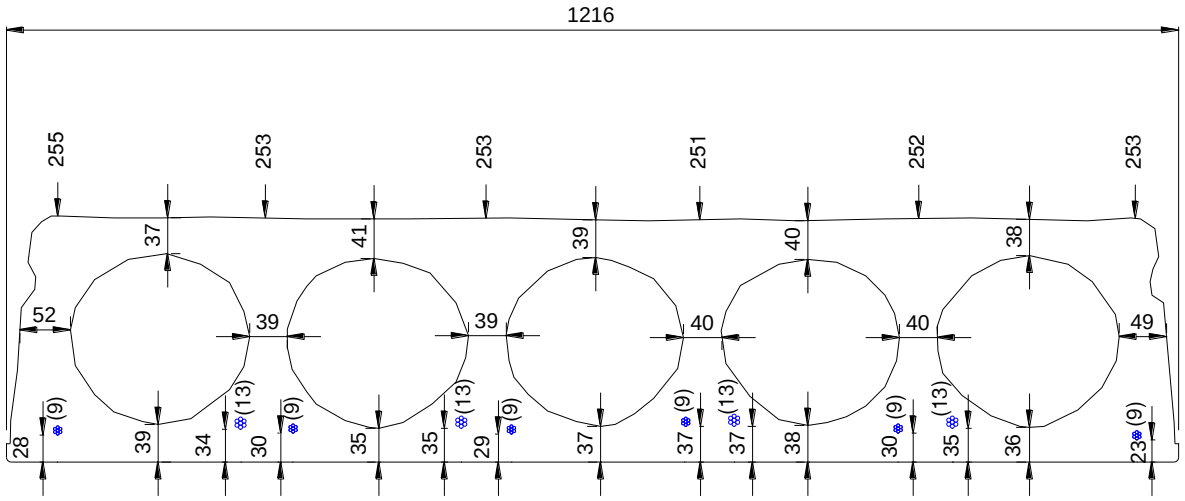


AVG. HEIGHT -> 253 mm

TOTAL WEB WIDTH -> 259 mm

TEST DATE CAMBER -> (10 mm)

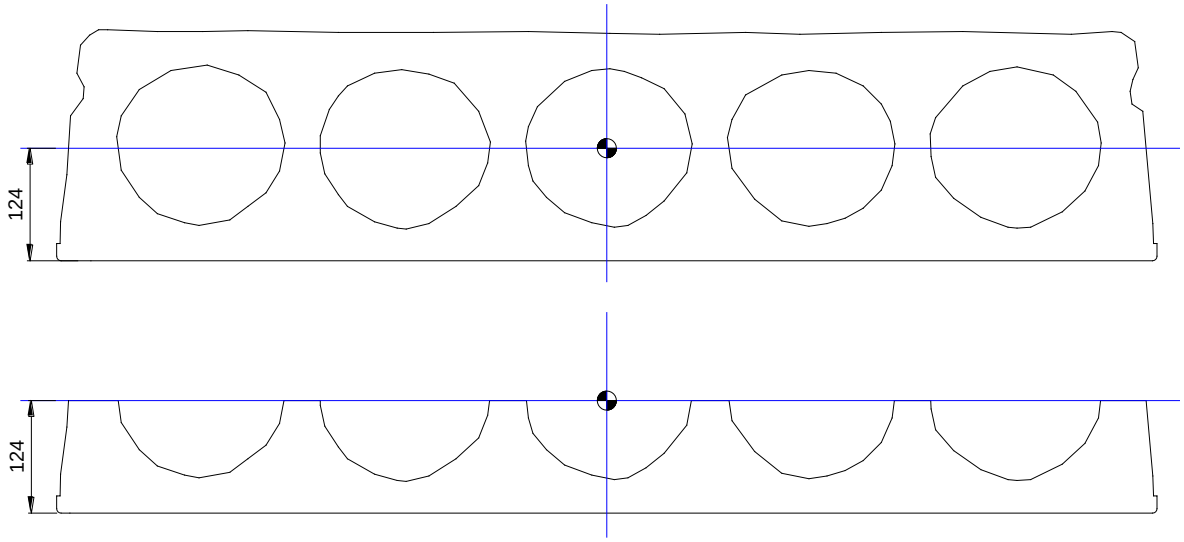


GROSS AREA BELOW N/A (Act) -> 89189 mm2

(250-P2-B) SLAB GEOMETRY

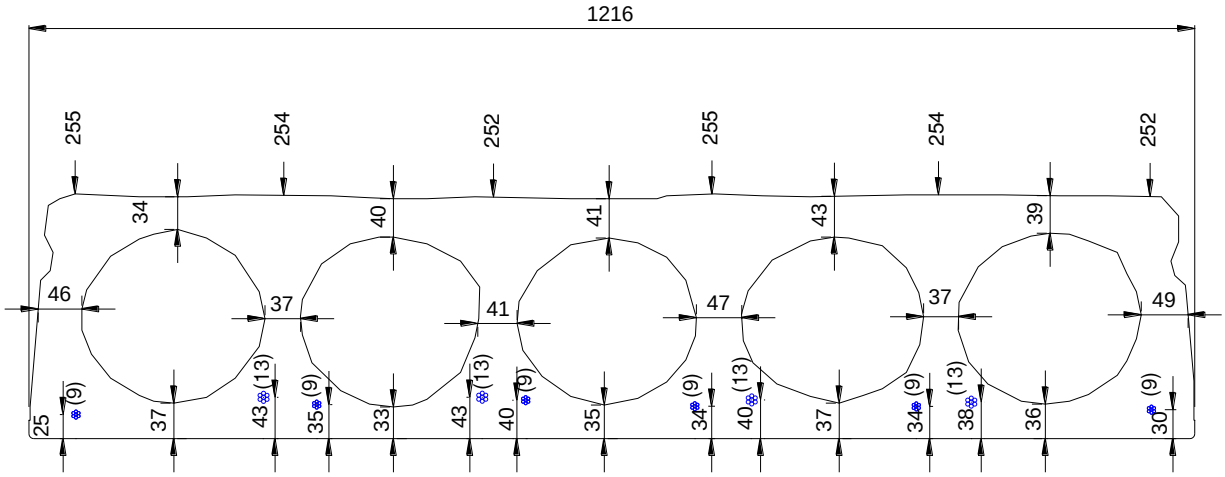


AVG. HEIGHT -> 254 mm  TOTAL WEB WIDTH -> 257 mm  TEST DATE CAMBER -> (10 mm)

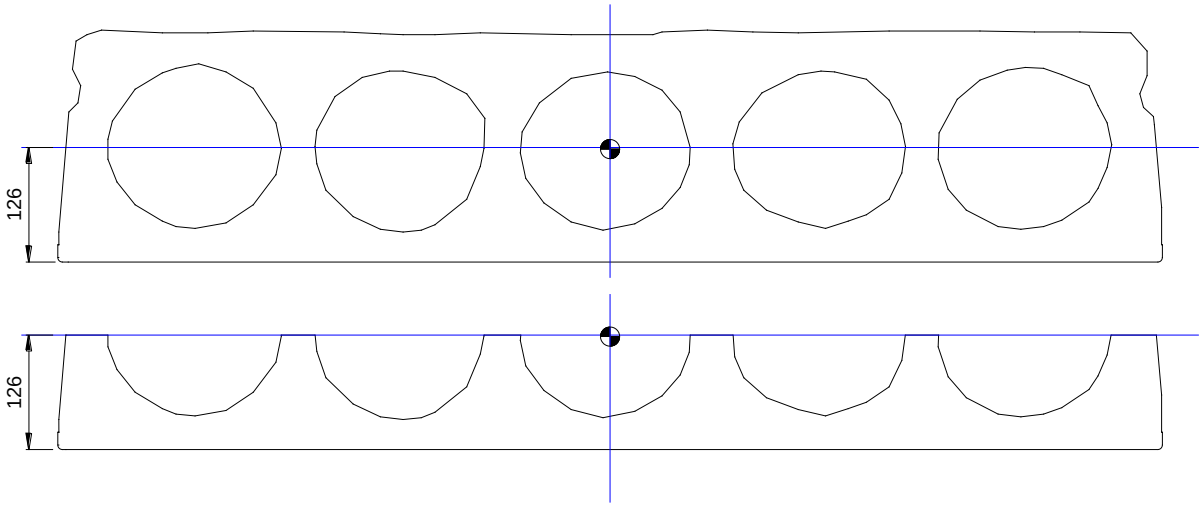


GROSS AREA BELOW N/A (Act) -> 86970 mm2

(300-P1-A) SLAB GEOMETRY

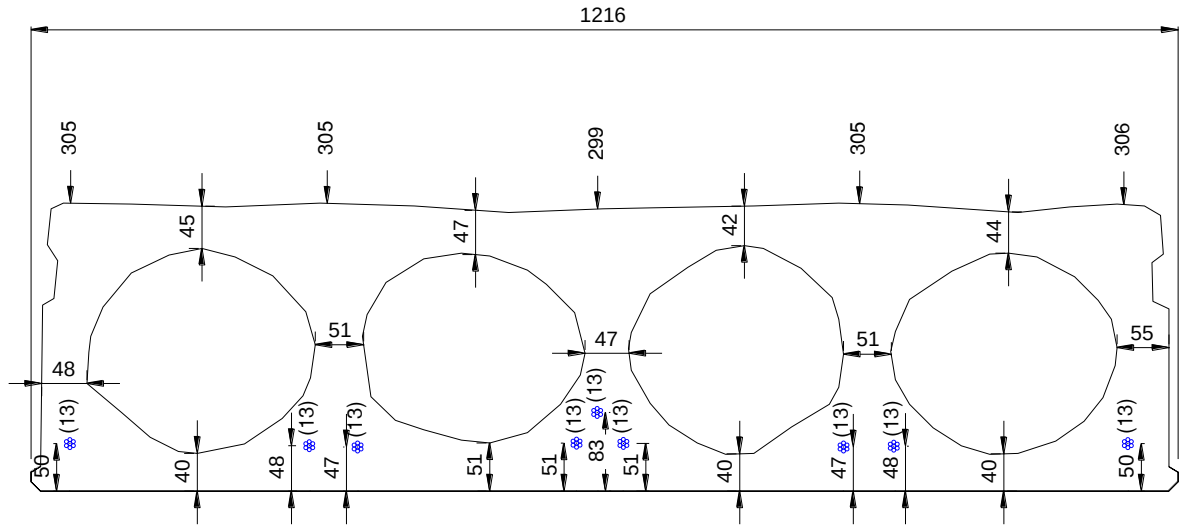


AVG. HEIGHT -> 304 mm TOTAL WEB WIDTH -> 252 mm TEST DATE CAMBER -> (12mm)

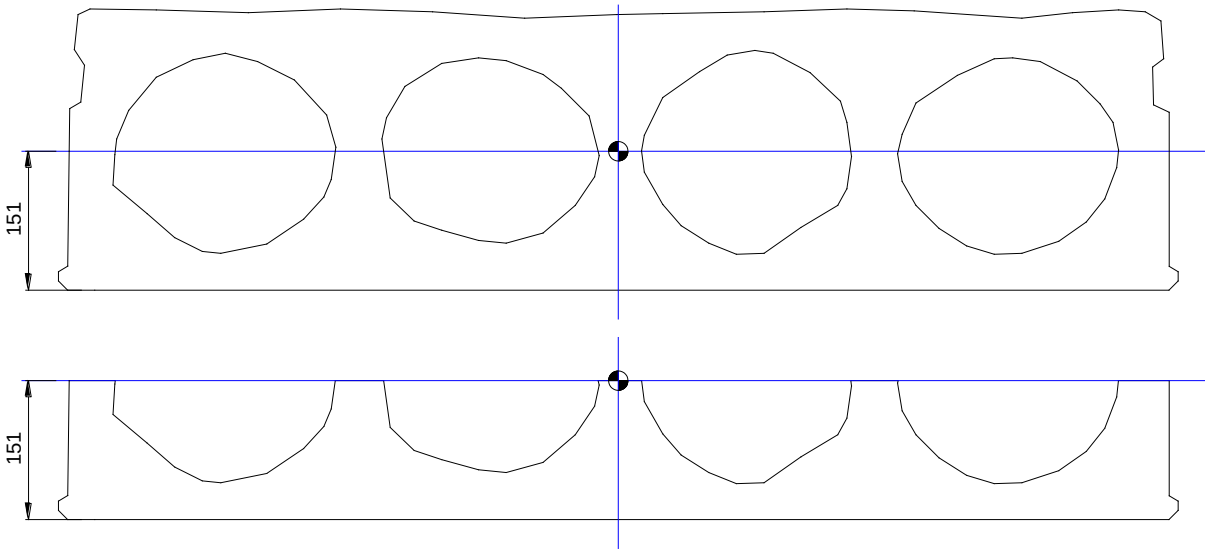


GROSS AREA BELOW N/A (Act) -> 103107 mm2

(300-P1-B) SLAB GEOMETRY

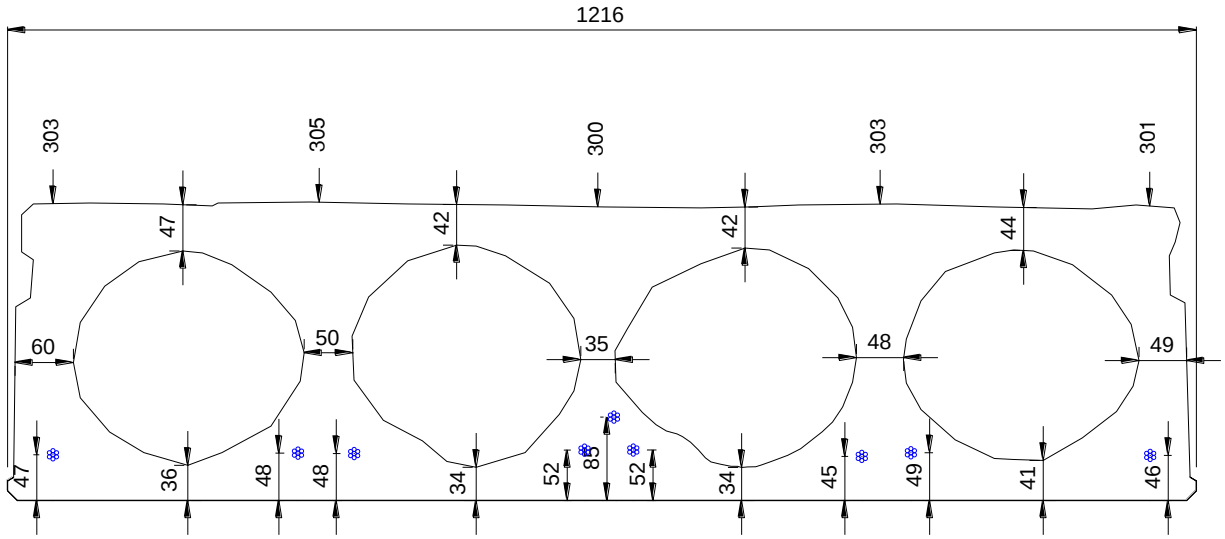


AVG. HEIGHT -> 302 mm

TOTAL WEB WIDTH -> 242 mm

TEST DATE CAMBER -> (12 mm)

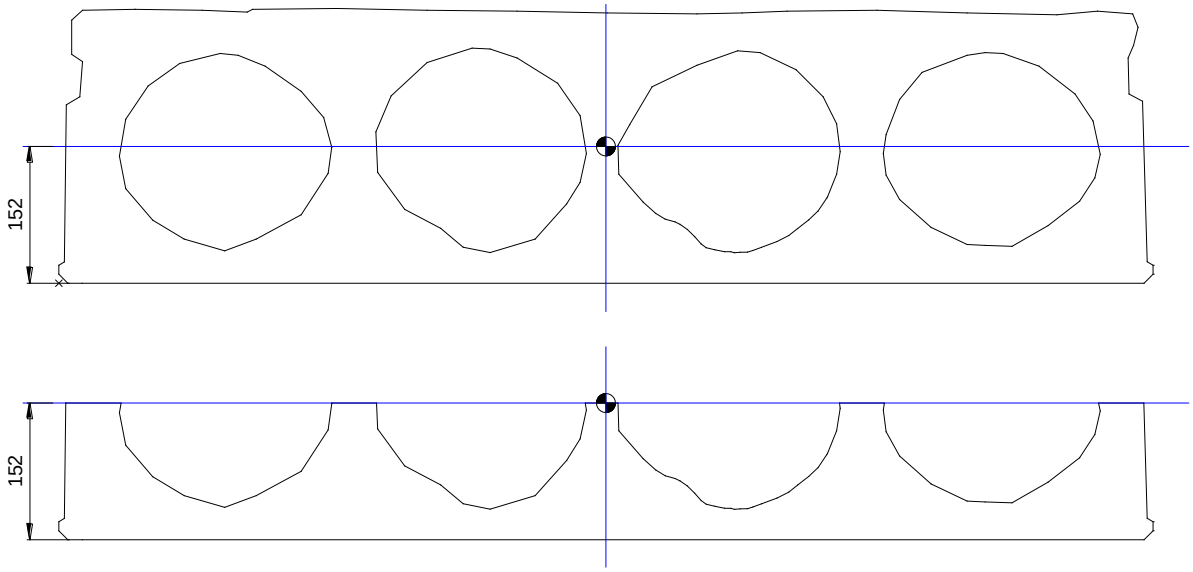


GROSS AREA BELOW N/A (Act) -> 100356 mm2

(300-P2-A) SLAB GEOMETRY

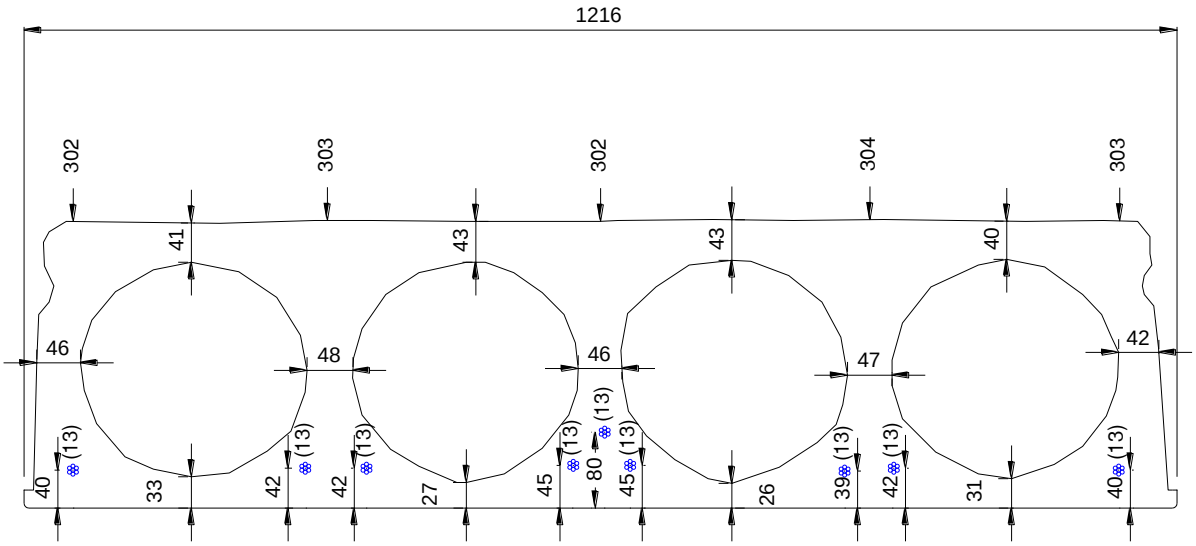


AVG. HEIGHT -> 303 mm

TOTAL WEB WIDTH -> 229mm

TEST DATE CAMBER -> (11 mm)

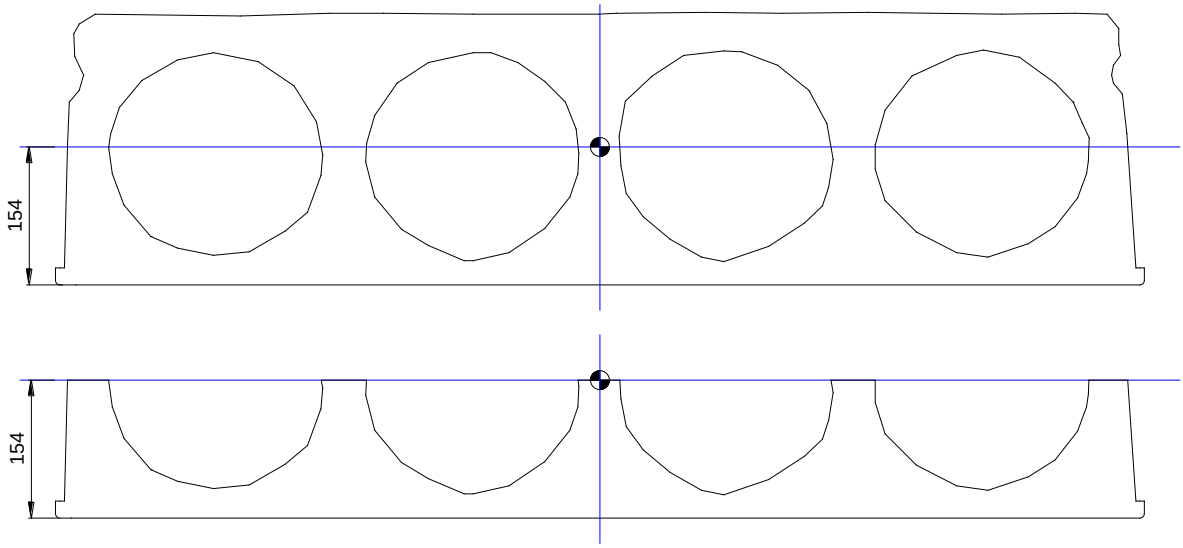


GROSS AREA BELOW N/A (Act) -> 91837 mm2

(300-P2-B) SLAB GEOMETRY

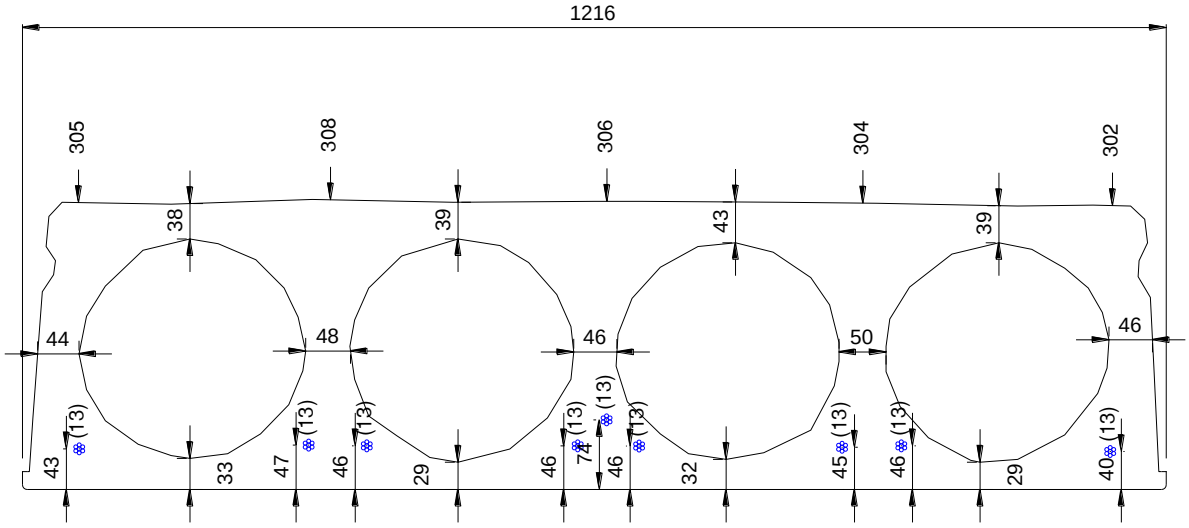


AVG. HEIGHT -> 305 mm

TOTAL WEB WIDTH -> 234 mm

TEST DATE CAMBER -> (15 mm)

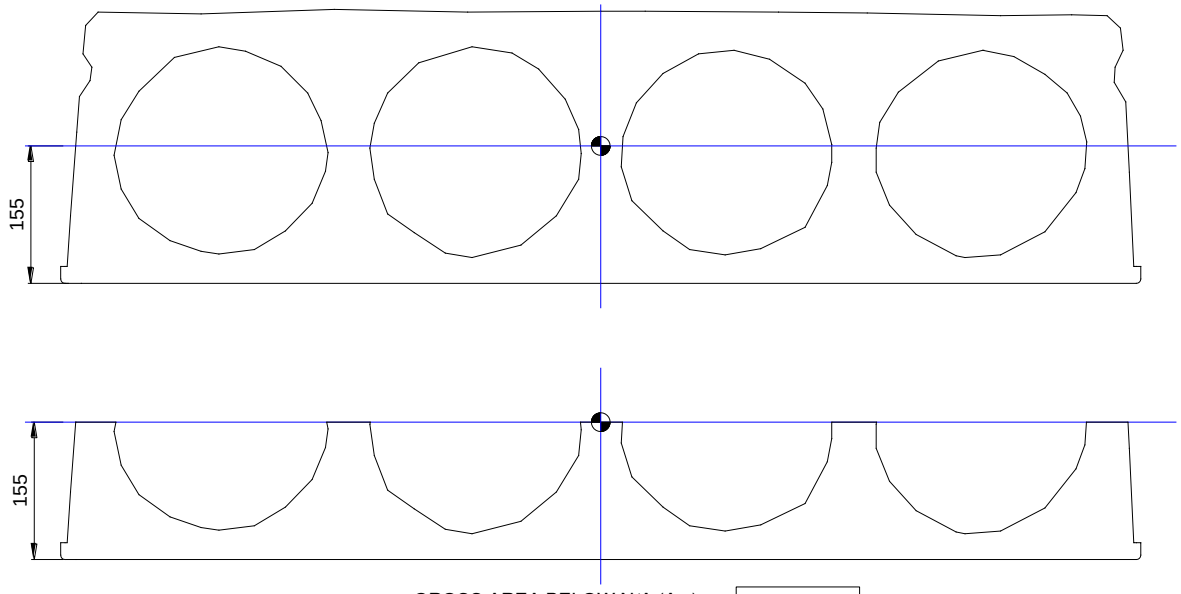


GROSS AREA BELOW N/A (Act) -> 93141 mm2

# APPENDIX B:

# CONCRETE CYLINDER TEST RESULTS

| Slab ID | Cylinder's Age at Testing | Measured Avg. Strength(MPa) |
|---|---|---|
| 200-P1-A | 27 hrs. | 35.2 |
| | 28 days | 63.7 |
| | 96 days (test date) | 72.0 |
| 200-P1-B | 27 hrs. | 35.2 |
| | 28 days | 63.7 |
| | 106 days (test date) | 74.8 |
| 200-P2-A | 21.3 hrs. | 27.6 |
| | 28 days | 63.2 |
| | 100 days (test date) | 64.9 |
| 200-P2-B | 21.3 hrs. | 27.6 |
| | 28 days | 63.2 |
| | 111 days (test date) | 62.9 |
| 250-P1-A | 24 hrs. | 41.7 |
| | 28 days | 68.7 |
| | 91 days (test date) | 76.8 |
| 250-P1-B | 24 hrs. | 41.7 |
| | 28 days | 68.7 |
| | 99 days (test date) | 78.0 |
| 250-P2-A | 20 hrs. | 30.3 |
| | 28 days | 67.3 |
| | 96 days (test date) | 63.3 |
| 250-P2-B | 20 hrs. | 30.3 |
| | 28 days | 67.3 |
| | 107 days (test date) | 65.1 |
| 300-P1-A | 21 hrs. | 34.1 |
| | 28 days | 57.7 |
| | 81 days (test date) | 67.9 |
| 300-P1-B | 21 hrs. | 34.1 |
| | 28 days | 57.7 |
| | 60 days (test date) | 65.7 |
| 300-P2-A | 19 hrs. | 32.5 |
| | 28 days | 56.0 |
| | 115 days (test date) | 63.2 |
| 300-P2-B | 19 hrs. | 32.5 |
| | 28 days | 56.0 |
| | 101 days (test date) | 63.8 |

- Average concrete strength for specimens from P1 = 73 MPa
- Average concrete strength for specimens from P2 = 64 MPa

# APPENDIX C:

# ACTUAL STRAND PROPERTIES

| Slab ID | 200-P1 | 200-P2 | 250-P1 | 250-P2 | 300-P1 | 300-P2 |
|---|---|---|---|---|---|---|
| Date Cast | May 11/10 | May 5/10 | May 11/10 | May 5/10 | May 10/10 | May 5/10 |
| Strands | | | | | | |
| (13mm) Strands Pack # T2C17 | | | 3 | | | |
| (13mm) strands Pack # T5C13 | | | 2 | | | |
| (13mm) strands Pack # T5C20 | | | 2 | | | |
| (13mm) strands Pack # T1C26 | | | | | 3 | |
| (13mm) strands Pack # T2C2 | 2 | | | | 3 | |
| (13mm) strands Pack # T3C10 | 1 | | | | 3 | |
| (9mm) Strands Pack # 384-14 | 2 | | | | | |
| (9mm) strands Pack # 383-6 | 2 | | | | | |
| total no. of strands used | 7 | 0 | 7 | 0 | 9 | 0 |

| Strands | E-Value Mpsi | E-Value (MPa) | Ultimate Load (lbs) | Ultimate Load (kN) | Strand Area (mm2) | Ultimate Strength (MPa) | Design Strength (MPa) |
|---|---|---|---|---|---|---|---|
| (13mm) Strands Pack # T2C17 | 29 | 199948 | 43646 | 194.1 | 98.7 | 1967 | 1860.0 |
| (13mm) strands Pack # T5C13 | 28 | 193053 | 43871 | 195.1 | 98.7 | 1977 | 1860.0 |
| (13mm) strands Pack # T5C20 | 29 | 199948 | 44321 | 197.1 | 98.7 | 1997 | 1860.0 |
| (13mm) strands Pack # T1C26 | 28.1 | 193743 | 43871 | 195.1 | 98.7 | 1977 | 1860.0 |
| (13mm) strands Pack # T2C2 | 28.3 | 195122 | 43871 | 195.1 | 98.7 | 1977 | 1860.0 |
| (13mm) strands Pack # T3C10 | 28.7 | 197880 | 44321 | 197.1 | 98.7 | 1997 | 1860.0 |
| (9mm) Strands Pack # 384-14 | 29 | 199948 | 24073 | 107.1 | 51.6 | 2075 | 1860.0 |
| (9mm) strands Pack # 383-6 | 29 | 199948 | 23848 | 106.1 | 51.6 | 2056 | 1860.0 |

# APPENDIX D:

# PHOTOS OF TESTED SPECIMENS

Photos of **HC 200-P1-A** (Flexural Failure)

Photos of **HC 200-P1-B (**Flexural & Flexure-Shear Failure)

Photos of **HC 200-P2A** (Web-Shear Failure)

Photos of **HC 200-P2-B** (Web-Shear Failure)

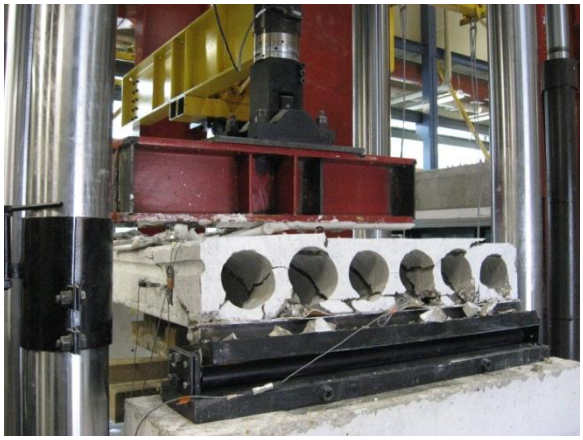

Photos of **HC 250-P1A** (Flexural-Shear Failure)

Photoes of **HC 250-P1-B** (Flexural-Shear Failure)

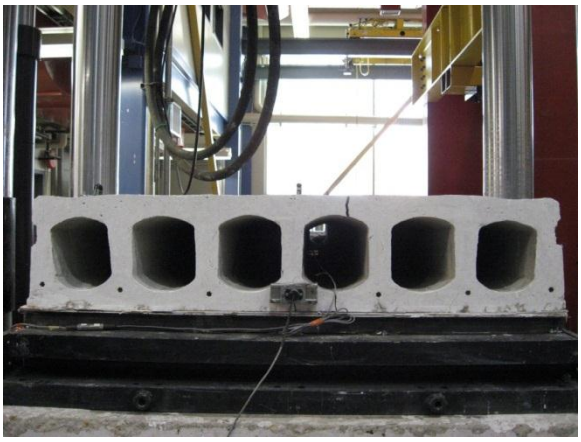

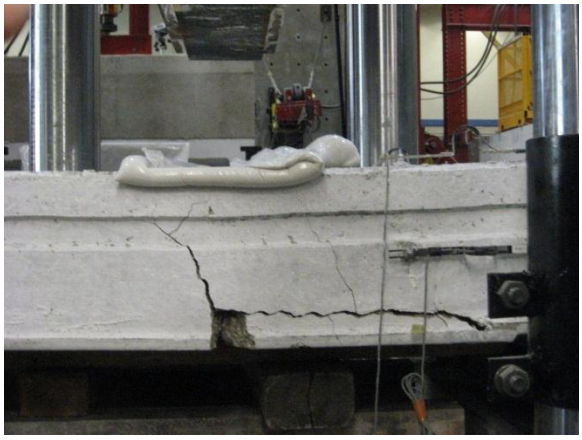

Photoes of **HC 250-P2A** (Web-Shear Failure)

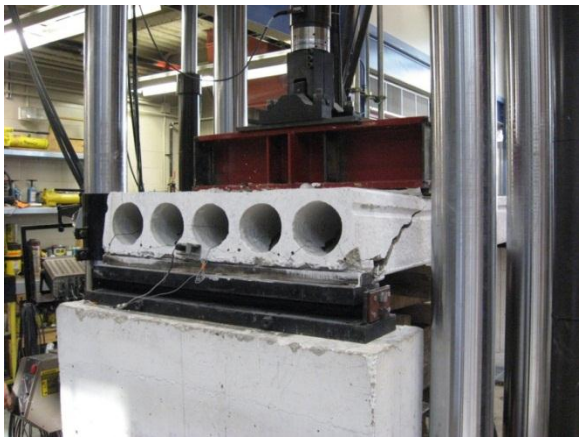

Photoes of **HC 250-P2-B (**Web-Shear Failure)

Photoes of **HC 300-P1-A (**Web-Shear Failure)

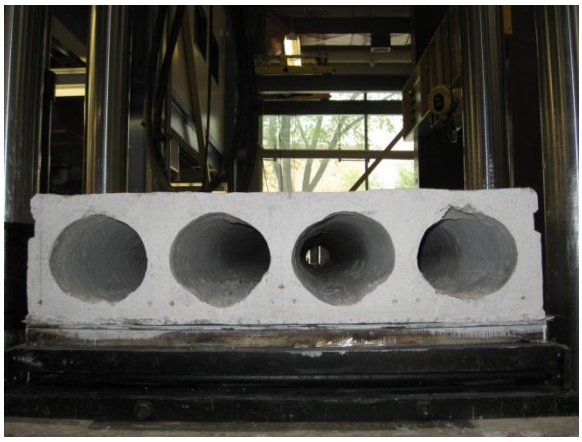

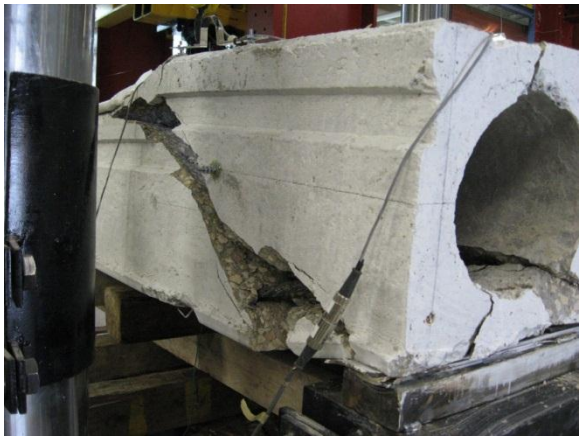

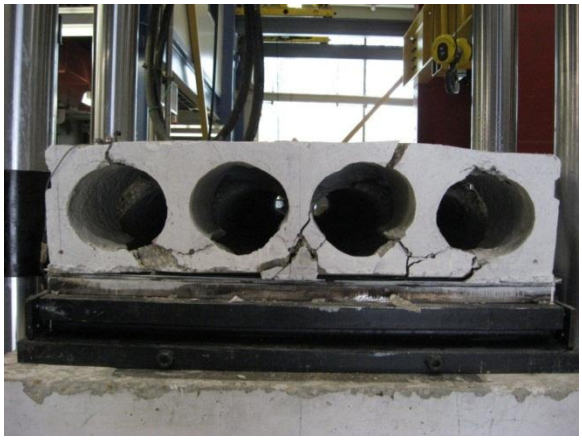

Photoes of **HC 300-P1B** (Web-Shear Failure)

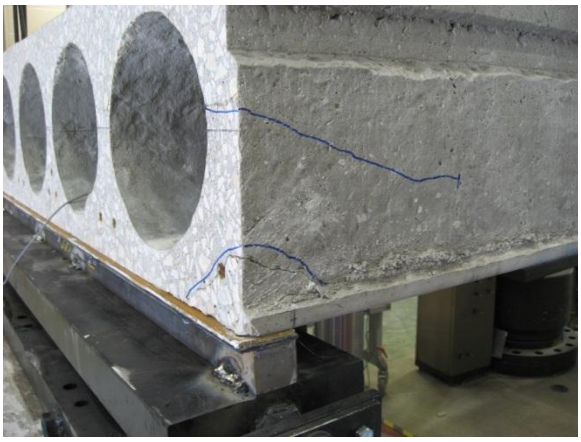

Photoes of **HC 300-P2A** (Web-Shear Failure)

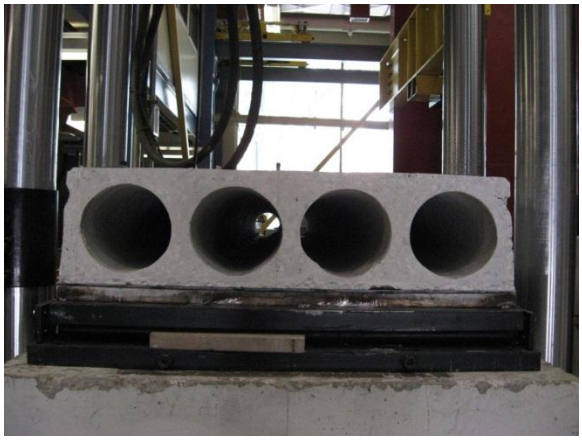

Photoes of **HC 300-P2-B (**Web-Shear Failure)